Doctoral Dissertation

博士論文

Comprehensive detection and spatio-temporal distributions of deep low-frequency earthquakes in volcanic areas all over Japan

(日本全国の火山地域で発生する深部低周波地震の網羅的検出と時空間分布)

A Dissertation Submitted for Degree of Doctor of Philosophy

December 2019

Department of Earth and Planetary Science,
Graduate School of Science, The University of Tokyo

令和元年１２月 博士(理学) 申請

東京大学大学院理学系研究科地球惑星科学専攻

Ryo Kurihara

栗原　亮

Abstract

Deep low-frequency (DLF) earthquakes occur at depths of roughly 30 km in which regular crustal earthquakes rarely occur. The dominant frequencies of DLF earthquakes are about 1−10 Hz, which are lower than those of regular earthquakes with similar magnitudes. There are two types of DLF earthquakes; tectonic DLF earthquakes occur along the subducting plate interface and inland DLF earthquakes occur near active volcanoes or active faults. DLF earthquakes near volcanoes are considered to be affected by fluid in the lower crust because they often occur in or around of low-velocity anomalies. However, the generating mechanisms of DLF earthquakes and relationship with the surrounding structure are still unknown because hypocenters of DLF earthquakes do not have a good resolution due to their weak signals. In this study, I focus on the inland DLF earthquakes beneath volcanoes in order to reveal the structures in which DLF earthquakes occur and the relationship between DLF earthquakes and volcanic activities.

The relationship between activities of DLF earthquakes and surface volcanic activities such as eruptions was discussed so far because we have observed many DLF earthquakes beneath active volcanoes. For example, DLF earthquakes were observed before the 1986 eruptions of Izu-Oshima volcano and 1991 eruptions of Pinatubo volcano. Recent studies also showed increases of DLF earthquakes before the eruptions in Klyuchevskoy volcano in Russia and Hakone volcano in Japan. However, the number of observations of DLF earthquakes associated with volcanic activities is small and the relationship between DLF earthquakes and volcanic activities is still unknown in many volcanoes. Although the Japan Meteorological Agency (JMA) observe DLF earthquakes in Japan and construct the catalog of DLF earthquakes, the catalog does not completely cover entire activity of DLF earthquakes due to their weak signals and DLF earthquakes associated with eruptions have not been observed from the JMA catalog. Besides, detailed spatial and temporal evolution of DLF earthquakes has not been constrained even in the volcanoes in which DLF earthquakes associated with eruptions have been observed.

To reveal detailed activities of DLF earthquakes, I applied following three analyses to DLF earthquakes occurring in 52 regions all over Japan. The first analysis is the network correlation coefficient method for the precise relocation of hypocenters of DLF earthquakes. The second analysis is the classification of DLF earthquakes into some groups in each region based on waveform correlation of every earthquake pair. Third, more DLF earthquakes were detected from continuous velocity seismograms of high-

sensitivity seismograph network (Hi-net) operated by National Research Institute for Earth Science and Disaster Resilience (NIED) between April 2004 and December 2018 based on the matched filter technique. Combining the results of the three analyses, I revealed hypocentral distributions and activities of DLF earthquakes.

Relocation analysis revealed that hypocenters of DLF earthquakes concentrate into some small isolated groups with separations of several kilometers in the vertical direction in most regions. For example, DLF earthquakes occur in four groups with the intervals of 5 km between 20 and 35 km depths in Hijiori, northeastern part of Japan, even though the JMA catalog showed vertically continuous distribution. As for quantifying temporal activity patterns of DLF earthquakes, I defined the swarm ratio for each group of all regions and generally classified the activity patterns into two types; episodic and constant occurrences. In many regions, only constant occurrences of DLF earthquakes were observed, on the other hand, 12 regions included groups that show episodic occurrences of DLF earthquakes. Episodic DLF earthquakes have similar waveforms, magnitudes distribution with high b-values, and low maximum magnitudes compared to constant DLF earthquakes. These results suggest that episodic DLF earthquakes may repeatedly occur in the concentrated similar smaller-scale sources and constant DLF earthquakes may occur in different sources closely located.

DLF earthquakes associated with volcanic activities were observed in five volcanoes. In Kirishima, which is one of the most active volcanoes in Japan, activation of DLF earthquakes at a depth of approximately 25 km was observed between December 2009 and September 2011, in which subplinian eruptions of Shinmoe-dake occurred. Such a two-year activation in DLF seismicity was well correlated with crustal deformation caused by the volume change of a magma reservoir at a depth of 8 km. The waveforms and hypocenters of DLF earthquakes during the activation period were different from those during other periods. Although the hypocenters of activated DLF earthquakes and not activated DLF earthquakes are close to each other within 0–5 km, temporal activity patterns of those DLF earthquakes were clearly different. The activated DLF earthquakes were characterized by the waveforms with lower dominant frequencies and deeper hypocentral locations compared to DLF earthquakes during the other period. The DLF earthquakes can be divided into four types and the activated types were switched at the transitions of the eruption styles. Besides, the waveforms and hypocenters of DLF earthquakes associated with the 2018 eruptions were different from those associated with

the 2011 eruptions. These results suggest that DLF earthquakes could be triggered by various fluid paths those are altered by the eruptive process. The fluid paths of the 2018 eruptions might be different from those of the 2011 eruptions.

Activations of DLF earthquakes associated with volcanic activities were also observed in other four volcanoes, Meakan, Sakurajima, Ontake, and Hakone. In Meakan and Sakurajima, DLF earthquakes correlated with volcanic activities occurred only in some limited groups and other groups of DLF earthquakes show constant occurrences or episodic occurrences with no correlation with eruptions or crustal deformations. In addition, DLF earthquakes associated with eruptions had low dominant frequencies, similar to those in Kirishima. Time-lags between activations of DLF earthquakes and eruptions are a few hundred days in Kirishima and Meakan, while a phreatic eruption occurred after only 20 days from the activation of DLF earthquakes at the 2014 eruption of Ontake. As a result, the five volcanoes in which associations of DLF earthquakes with eruptions were divided into two categories based on activities of DLF earthquakes and time-lags between activations of DLF earthquakes and surface activities of the volcanoes.

As a result of this study, a model of structure around hypocenters of DLF earthquakes is proposed. In previous model, DLF earthquakes distribute in or around of low-velocity anomalies on a scale of about 10 km. However, the discrete distributions of DLF earthquakes suggest that DLF earthquakes occur on a scale corresponding to heterogeneities of 0–5 km. One of possible candidates of such heterogeneities is formed by sill-like magma discussed in petrological studies instead of a volumetric magma body. Furthermore, different spatio-temporal distributions of DLF earthquakes in each group suggest that they are triggered by fluid flow through many paths forming a complicate network in the lower crust. Although it is difficult to predict eruptions based on the monitoring of DLF earthquakes at this moment, the accuracy of predictions of eruptions may be improved by a more comprehensive analysis of DLF earthquakes.

Contents

1. General Introduction

1.1. Deep low-frequency earthquakes

Most of all crustal regular earthquakes occur at depths shallower than 15 km. On the other hand, earthquakes with predominant frequencies of 1–10 Hz, which is lower than those of similar-size regular earthquakes, are often observed at a depth of roughly 30 km and are called as “deep low-frequency (DLF) earthquakes” or “deep long-period (DLP) earthquakes” (Figure 1.1). In this study, these earthquakes are called DLF earthquakes. In Japan, Japan Meteorological Agency (JMA) has observed the DLF earthquakes and recorded in the JMA unified earthquake catalog (Katsumata & Kamaya, 2003; Figure 1.2). The depths of DLF earthquakes are roughly equivalent to the depths of Moho discontinuities; however, they sometimes extend from 10 to 50 km (Kosuga et al., 2017; Ukawa, 2007). In this study, DLF earthquakes are defined as low-frequency earthquakes in the JMA catalog.

DLF earthquakes are classified into two types; one occurs along the subducting plate interfaces and the other occurs in inland regions near volcanoes and active faults. DLF earthquakes at the subducting plate interfaces are called as “tectonic” DLF earthquakes (e.g. Aso et al., 2013). They were observed within low-frequency tremor called non-volcanic tremor (Obara, 2002), which is interpreted as a superposition of successive occurrences of tectonic DLF earthquakes. On the other hand, inland DLF earthquakes, which occur far from the subducting plates, have been observed in volcanic regions before the discovery of tectonic DLF earthquakes (e.g. Hasegawa & Yamamoto, 1994; Suzuki, 1992). DLF earthquakes were also observed where there are no active volcanoes and plate boundaries (Aso et al., 2011; Aso & Ide, 2014). These DLF earthquakes are supposed to occur near Quaternary volcanoes (Aso & Ide, 2014) or deep extensions of active faults (Katoh et al., 2018; Ohmi et al., 2004). Aso & Ide (2014) defined these DLF earthquakes as “semi-volcanic” DLF earthquakes. In this study, DLF earthquakes in active volcanic regions are mainly focused and DLF earthquakes at active faults are included in analyses to compare the DLF earthquakes in different locations.

Compared to regular earthquakes, it is difficult to detect and locate DLF earthquakes. The magnitudes of most DLF earthquakes in the JMA catalog are approximately 0–1. Therefore, the detection of DLF earthquakes is difficult and the catalog does not completely include whole DLF earthquakes. Besides, it is difficult to locate the hypocenters of DLF earthquakes because the arrival phases of P and S waves

are unclear. Therefore, errors of hypocentral locations may be larger than those of regular earthquakes.

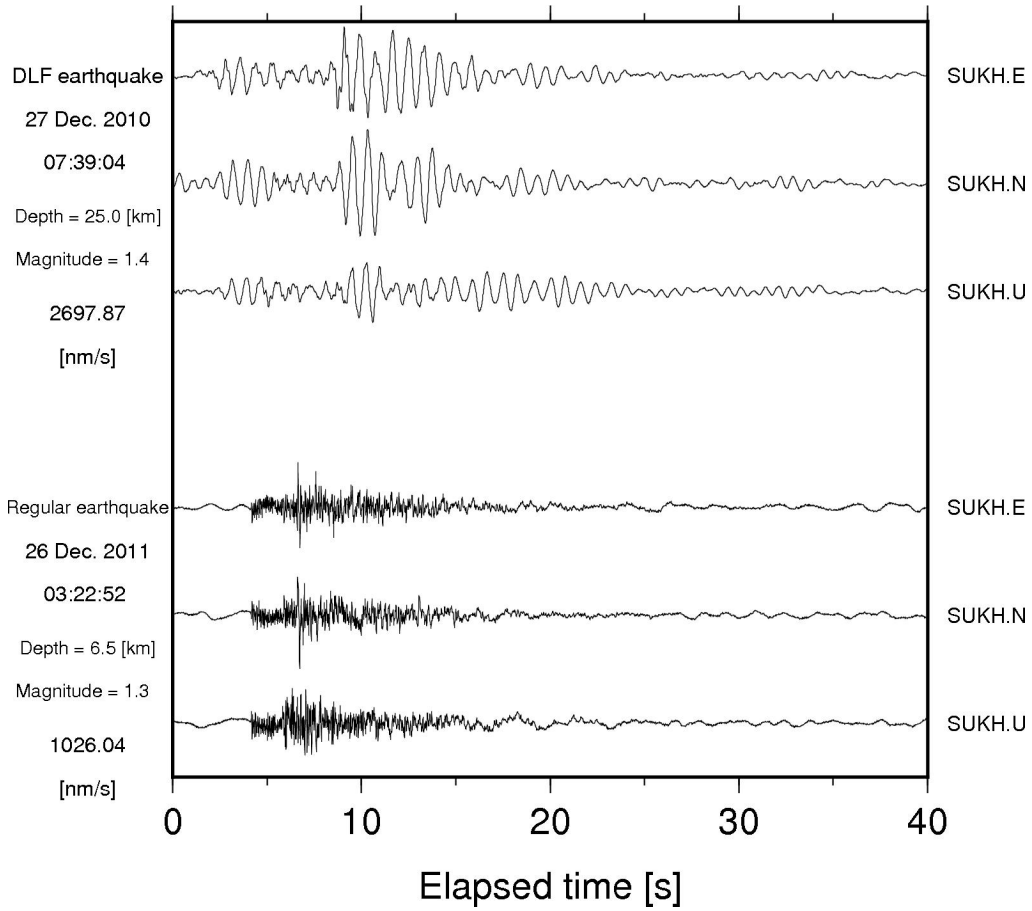

Figure 1.1 Three components velocity waveforms of a DLF earthquake and a regular earthquake observed at the N.SUKH station near Kirishima. Three waveforms for each earthquake correspond to the east-west, north-south, and up-down components from the top. Depths and magnitudes are referred to from the catalog of JMA. All waveforms are normalized by the maximum amplitudes of each earthquake written on the left. A bandpass filter is not applied to the waveforms.

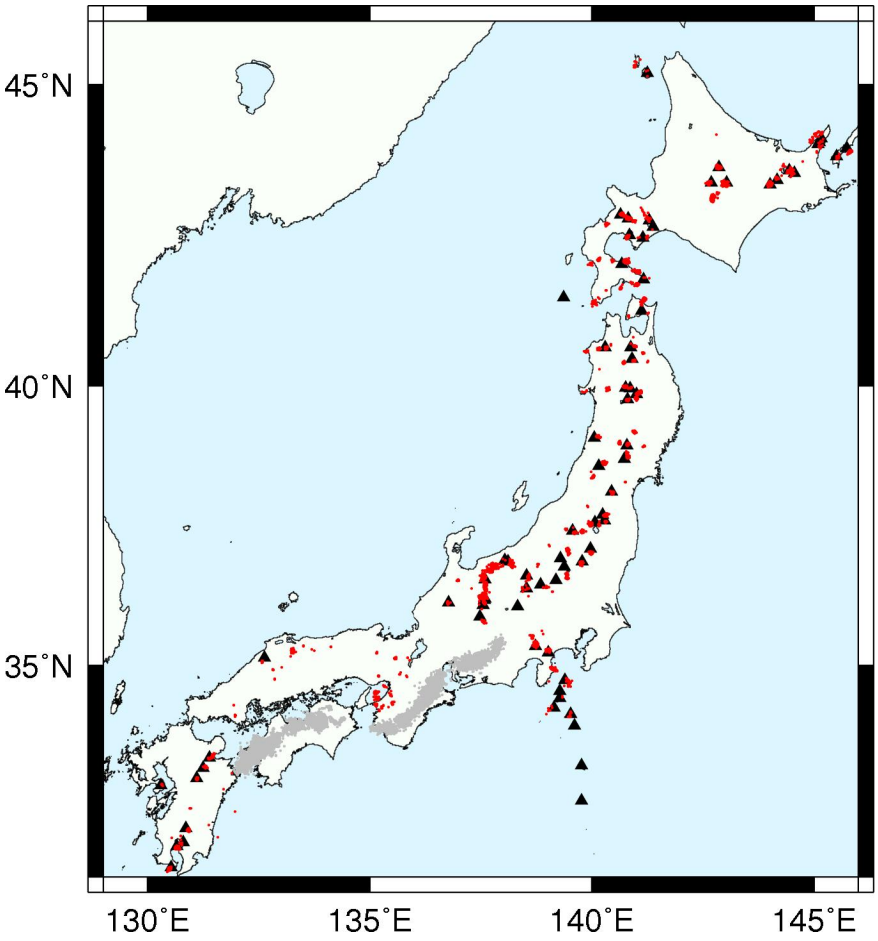

Figure 1.2 Distribution of DLF earthquakes in Japan. Grey dots show the distribution of tectonic DLF earthquakes in the Nankai subduction zone, red dots show the distribution of inland DLF earthquakes. Hypocenter locations are referred to from the JMA catalog. Solid triangles show the summits of volcanoes based on the active volcano catalog of JMA (Japan Meteorological Agency, 2013).

1.2. Relationship between DLF earthquakes and volcanic activities

DLF earthquakes near volcanoes can be a key to understand the physical processes of volcanic activities, including eruptions because some studies showed the relationship between DLF earthquakes and eruptions. Ukawa & Ohtake (1987) reported that a DLF earthquake at a depth of about 30 km occurred before the 1986 eruption of Izu-Oshima volcano. DLF earthquakes also occurred before the 1991 eruption of Pinatubo volcano, Philippines (White, 1996). Shapiro et al. (2017) and Frank et al. (2018) showed the relationship between DLF earthquakes and long-period earthquakes near the

surface with eruptions beneath the Klyuchevskoy volcano group at Kamchatka, Russia. DLF earthquakes also increased before phreatic eruptions of Hakone volcano in Japan at the 2015 eruptions (Yukutake et al., 2019). Written in above, DLF earthquakes sometimes preceded before the eruptions. Combining results of petrological studies with the geophysical observations, DLF earthquakes with deep magma intrusions are thought to occur before eruptions (White & McCausland, 2019).

Although DLF earthquakes may be an important factor to predict eruptions, observations of DLF earthquakes associated with eruptions are still limited. Thus, the relationship between DLF earthquakes and volcanic activities is still unknown in many other volcanoes; for example, Takahashi & Miyamura (2009) analyzed DLF earthquakes all over Japan based on the JMA catalog and concluded that DLF earthquakes do not correspond to surface volcanic activities such as eruptions. The number of DLF earthquakes in a volcano does not correlate with the activity level of the volcano. In the JMA catalog, DLF earthquakes have constantly been observed and we cannot find any associations of DLF earthquakes with volcanic activities. Besides, differences of hypocenters or waveforms of the DLF earthquakes between during eruption and during other periods have not been fully investigated.

1.3. Geophysical and petrological properties around sources of DLF earthquakes

The relationship between distributions of DLF earthquakes and underground structure is very important to understand the mechanism of DLF earthquake. Hasegawa & Yamamoto (1994) showed that DLF earthquakes occur not just beneath the summits of volcanoes but about 10 km horizontally far from the summits. Because DLF earthquakes are often distributed in and around the low-velocity anomalies from tomography studies, DLF earthquakes are supposed to be related to fluid in the lower crust (e.g. Hasegawa et al., 2005; Nakajima, 2017; Shiina et al., 2018). Hypocenters of DLF earthquakes relocated using 3-D velocity models also show clear relations to the low-velocity anomalies (Niu et al., 2018; Yu et al., 2018). However, detailed distributions of DLF earthquakes are still unclear because it is difficult to pick the arrival time of P and S waves due to their weak amplitudes and unclear onsets. Besides, resolutions of seismic tomography are not so high in the depths of DLF earthquakes. The relationship between DLF earthquake and fluid flow has been also suggested in studies of DLF earthquakes.

Hensch et al. (2019) suggested that migration of magma or magmatic fluid may be related to DLF earthquakes and DLF earthquakes may occur with a recharge of a magma chamber. Hotovec-Ellis et al. (2018) showed the relationship between fluid flow and DLF earthquakes from the seismicity of regular earthquakes at Mammoth Mountain, California, USA.

The low-velocity anomalies imaged by travel-time seismic tomography do not directly mean that there is a large mass of fluid. “Magma reservoirs” are supposed to be composed of “Crystal mush” and “Magma chambers” (Bachmann & Bergantz, 2008; Tomiya, 2016). “Crystal mush” includes many crystals and melts. “Magma chambers” are filled with eruptible magma, therefore this region is supposed to be mainly filled by fluid. In the lower crust, petrological studies suggested that sill-like magmas may intrude into multiple depths instated of the existence of large magma chambers (Annen et al., 2006; Cashman et al., 2017; Geshi, 2016). Magma sills in the multiple depths may be required to explain various chemical properties of igneous rock. In the depths of intruded magma, partial melting of basalt ascending from the mantle and surrounding rocks may occur (Annen et al., 2006).

1.4. Focal mechanisms of DLF earthquakes

Focal mechanisms of DLF earthquakes were obtained in some volcanoes. In Mt. Iwate volcano, northeastern Japan, focal mechanisms of DLF earthquakes were generally described by a superposition of compensated linear vector dipole (CLVD) and double couple components (Nakamichi et al., 2003). DLF earthquakes often have large amounts of CLVD components, compared to the regular earthquakes. The amounts of CLVD components were 3 to 72 per cents in Mt. Iwate volcano. The result suggests that DLF earthquakes occur associated with fluid movements. However, the focal mechanisms are widely varied even in the analyzed nine DLF earthquakes, therefore the mechanisms of DLF earthquakes are still in discussion. Various focal mechanisms of DLF earthquakes were also reported in Zao volcano, northeastern Japan (Oikawa et al., 2019).

One of the models of occurrence mechanisms of DLF earthquakes is the cooling magma model (Aso & Tsai, 2014). In the model, a fracture in an intruded magma is first triggered by thermal stress and harmonic coda waves are radiated from resonance excited by the fracture. This model can explain the CLVD focal mechanisms. The width of intruded magma in which DLF earthquakes occur is estimated about 10–100 meters.

1.5. Influence of large stress change to DLF earthquakes

The Influence of external stress change for DLF earthquakes is one of the important topics because the focal mechanism may be revealed if DLF earthquakes are triggered by external stress change. Tectonic DLF earthquakes or tremor are well known to be triggered by dynamic stress change such as tidal stress and surface waves of teleseismic earthquakes (e.g. Kurihara et al., 2018; Miyazawa, 2005; Rubinstein et al., 2008). Dynamic triggering of volcanic DLF earthquakes by tidal stress was also reported in St. Helens, USA (Han et al., 2018).

Static stress change is also considered to affect the seismicity. Many source regions of inland DLF earthquakes which are the targets in this study are distributed in Tohoku district, which is near the hypocenter of the 2011 Tohoku earthquake (Mw 9.0). Near the surface of volcanoes in the Tohoku district, velocity reductions of seismic wave and volcanic subsidence were observed after the 2011 Tohoku earthquake (e.g. Brenguier et al., 2014; Takada & Fukushima, 2013). Besides, seismicity rate of crustal regular earthquakes were changed after the 2011 Tohoku earthquake (e.g. Yoshida et al., 2019). It was also reported that the number of DLF earthquakes increased and the focal mechanisms of DLF earthquakes changed in Zao after the 2011 Tohoku earthquake (Kosuga et al., 2017; Oikawa et al., 2019). However, it was only observed in Zao, even though DLF earthquakes were observed in many volcanoes of Tohoku district and the influence of the 2011 Tohoku earthquake was widely observed in the seismicity of regular earthquakes (e.g. Okada et al., 2011).

1.6. Purpose of this study

As mentioned above, spatio-temporal distributions of DLF earthquakes are still unclear in most volcanic areas. In this study, in order to understand distributions and activities of DLF earthquakes in Japan, I applied three analyses to continuously observed seismograms and then combined the results to construct comprehensive catalog of DLF earthquakes. First, I relocated hypocenters of DLF earthquakes in the JMA catalog using network correlation coefficient (NCC) method to investigate the detailed characteristics of the spatial distribution of DLF earthquakes accurately. Second, I developed the classification method based on waveform correlations and classified DLF earthquakes into some groups. Third, I detected more DLF earthquakes from continuously observed seismograms using the matched filter technique to reveal the temporal distributions of DLF earthquakes. Finally, I combined the results of the three analyses, so that I construct a comprehensive catalog of DLF earthquakes to investigate the distributions and activities of DLF earthquakes.

The catalog of DLF earthquakes was used to investigate the relationships between activities of DLF earthquakes and volcanic activities near the surface, which include eruptions, volcanic tectonic earthquakes, and crustal deformations. I focused on five volcanoes where eruptions or crustal deformations occurred in the analyzed period from 2004 to 2018. Besides, I also investigated the relationships between DLF earthquakes and large earthquakes using the 2011 Tohoku earthquake.

A comparison of DLF earthquakes in each volcano is one of the important topics of this study. I investigated the differences of seismicity and waveforms of DLF earthquakes in each region.

2. Data and Method

In this study, in order to understand distributions and activities of DLF earthquakes in Japan, I constructed new catalog of DLF earthquakes based on three analyses, relocation, classification and detection. I applied the three analyses for DLF earthquakes in the JMA catalog between Aril 2004 and December 2015 and merged the results for new catalog (Figure 2.1).

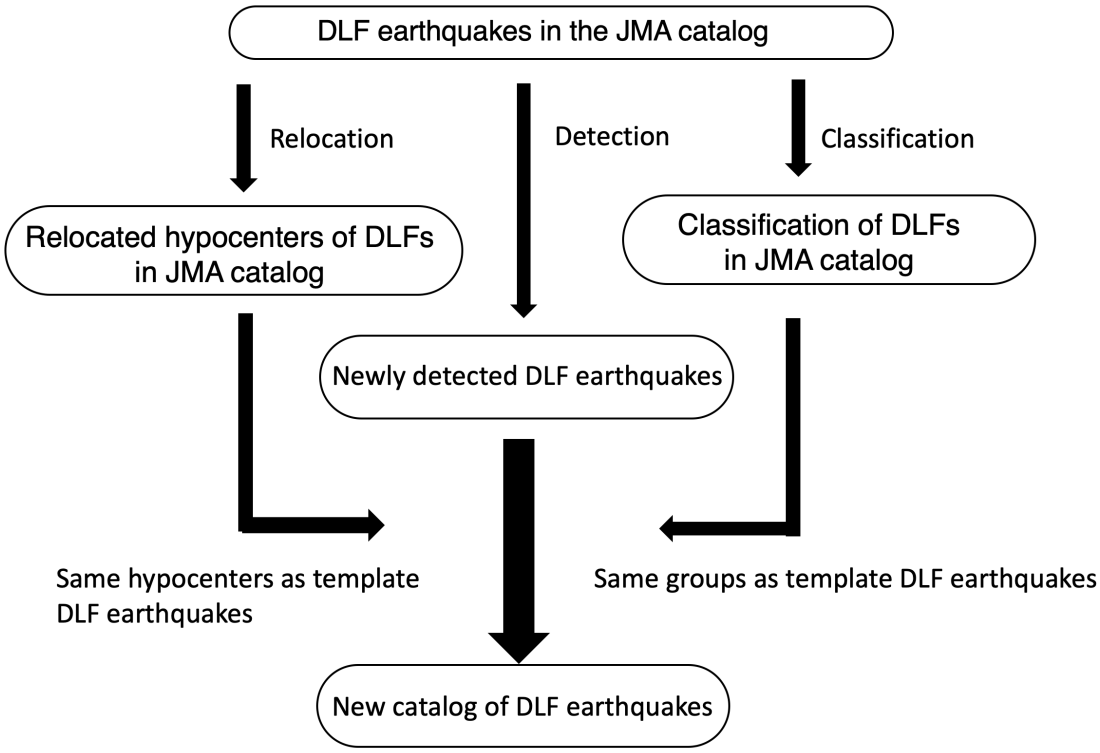

Figure 2.1 Flowchart of constructing the new DLF earthquakes.

2.1. Target regions of analyses

To comprehensively investigate activities of DLF earthquakes across Japan except for tectonic DLF earthquakes, I tried to analyze 82 DLF source regions which include not only volcanic regions but also regions near active faults. However, I discard some regions, where only less than 20 DLF earthquakes were detected in the JMA catalog between 2004 and 2015 or there are only less than 10 Hi-net stations within about 70 km from the target regions because it is difficult to statistically discuss activities of DLF earthquake in such regions. Finally, 52 regions were selected for analysis of this study including 49 volcanic regions (Figure 2.2–Figure 2.5, Table 2.1). The rest 3 regions are Shirakami (No.11) with non-volcanic mountains, Tanba (No.45) and east-Shimane

(No.46) with active faults. Names of the regions were named after volcanos or places such as towns or cities.

In this study, I used for main three analyses, relocation, classification, and detection, three-component velocity seismograms of the high-sensitivity seismograph network (Hi-net), operated by the National Research Institute for Earth Science and Disaster Resilience (NIED) (National Research Institute for Earth Science and Disaster Resilience, 2019; Okada et al., 2004) after applying a band-pass filter of 1–4 Hz. The target period of analysis is April 2004–December 2018. Because higher (> 4 Hz) frequency components show incoherent features, these filtered velocity seismograms were used in the analyses to stabilize the calculations. I used the maximum of 10 Hi-net stations for three analyses in each region (examples are illustrated in Figure 2.6).

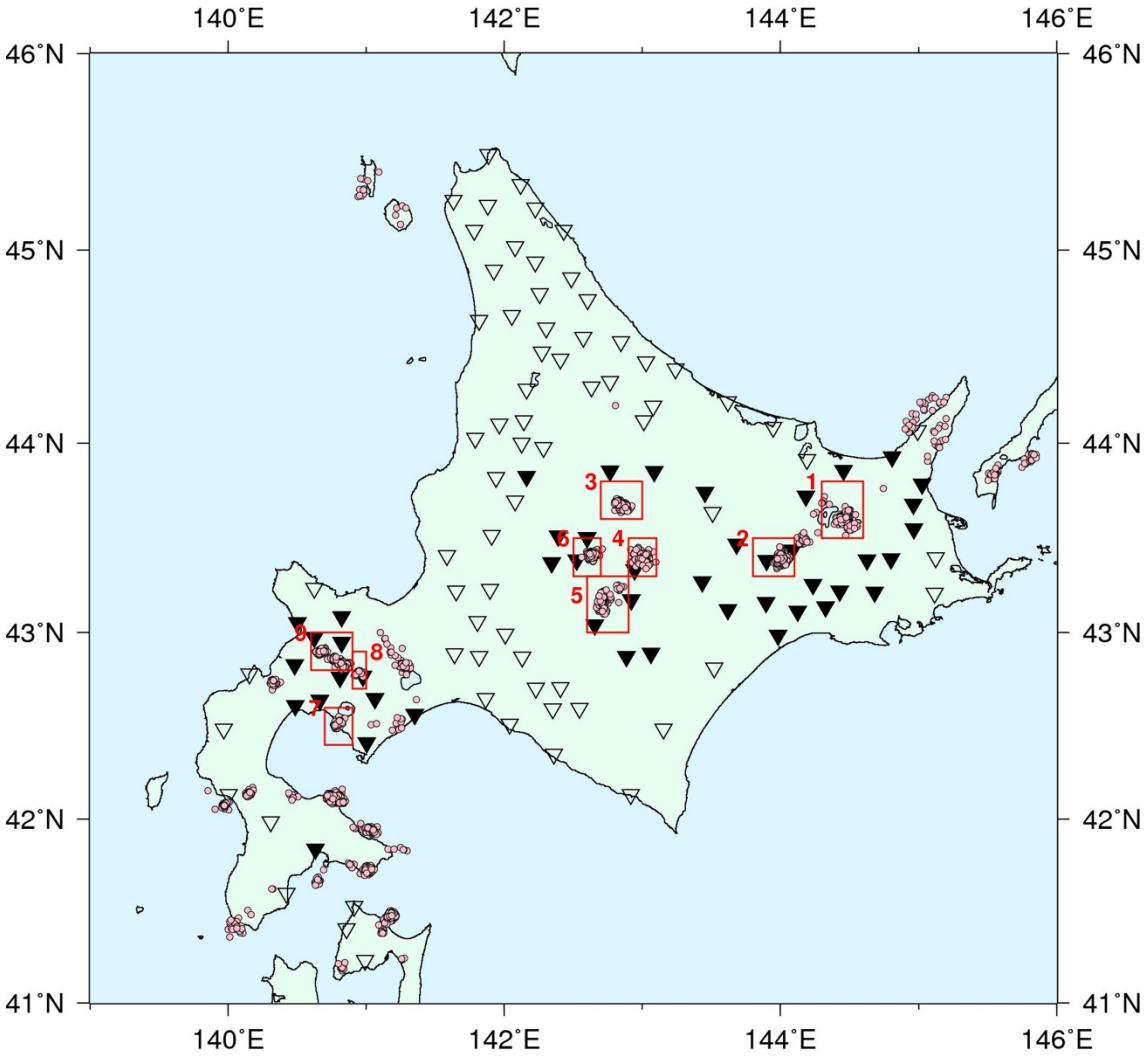

Figure 2.2 Distribution of target regions in the Hokkaido district. Red rectangles show the target regions of this study. The number near each adjacent red rectangle is the index of target regions (Table 2.1). Pink circles show the epicenters of DLF earthquakes in the JMA catalog from 2004 to 2015. Inverted triangles show the location of seismic stations in Hi-net. Black ones were used more than one target regions.

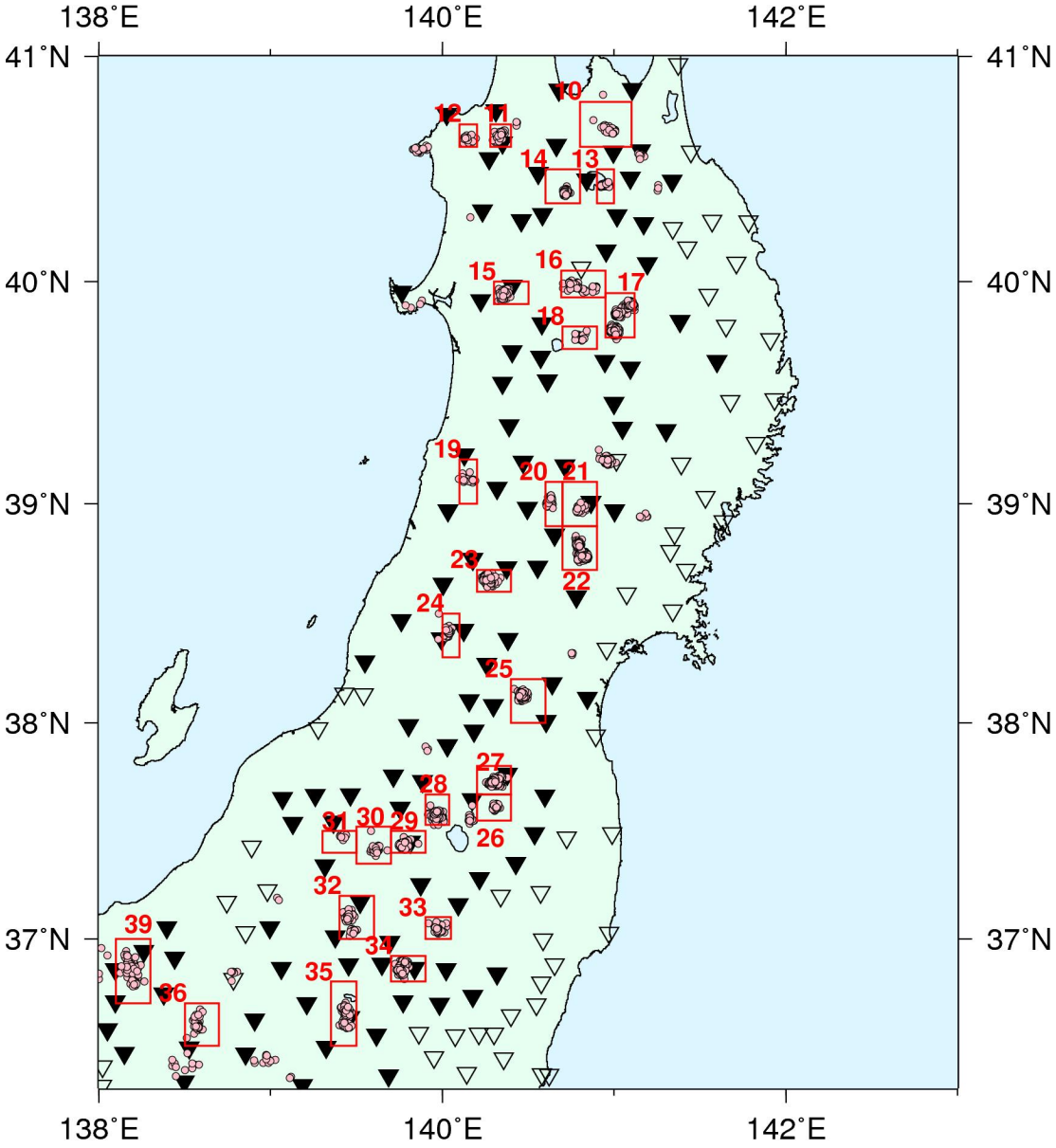

Figure 2.3 Distribution of target regions in the Tohoku district. Symbols are the same as Figure 2.2.

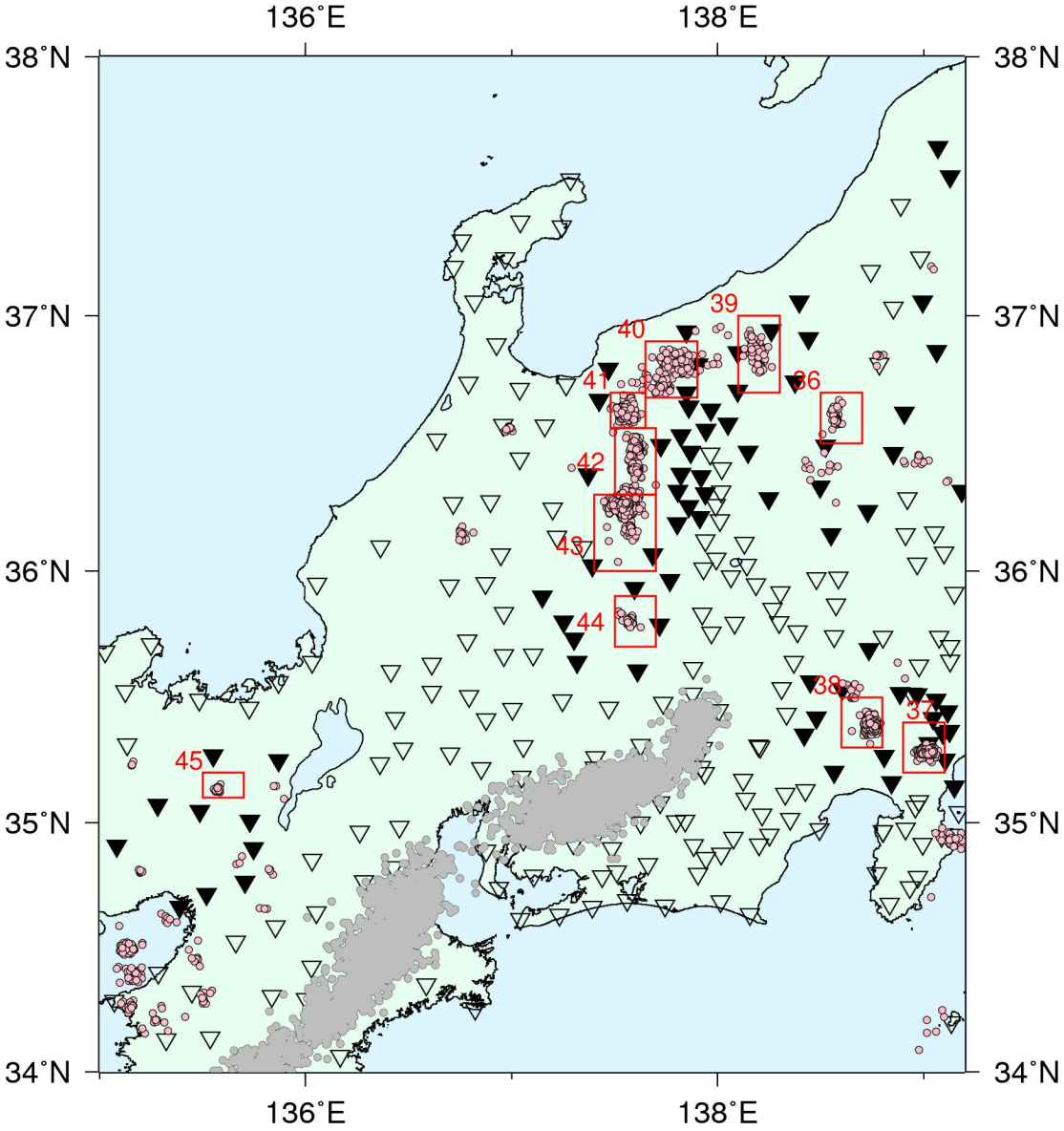

Figure 2.4 Distribution of target regions in Kanto and Chubu districts. Symbols are the same as Figure 2.2. Grey filled circles show the epicenters of tectonic DLF earthquakes occurring on the plate boundary.

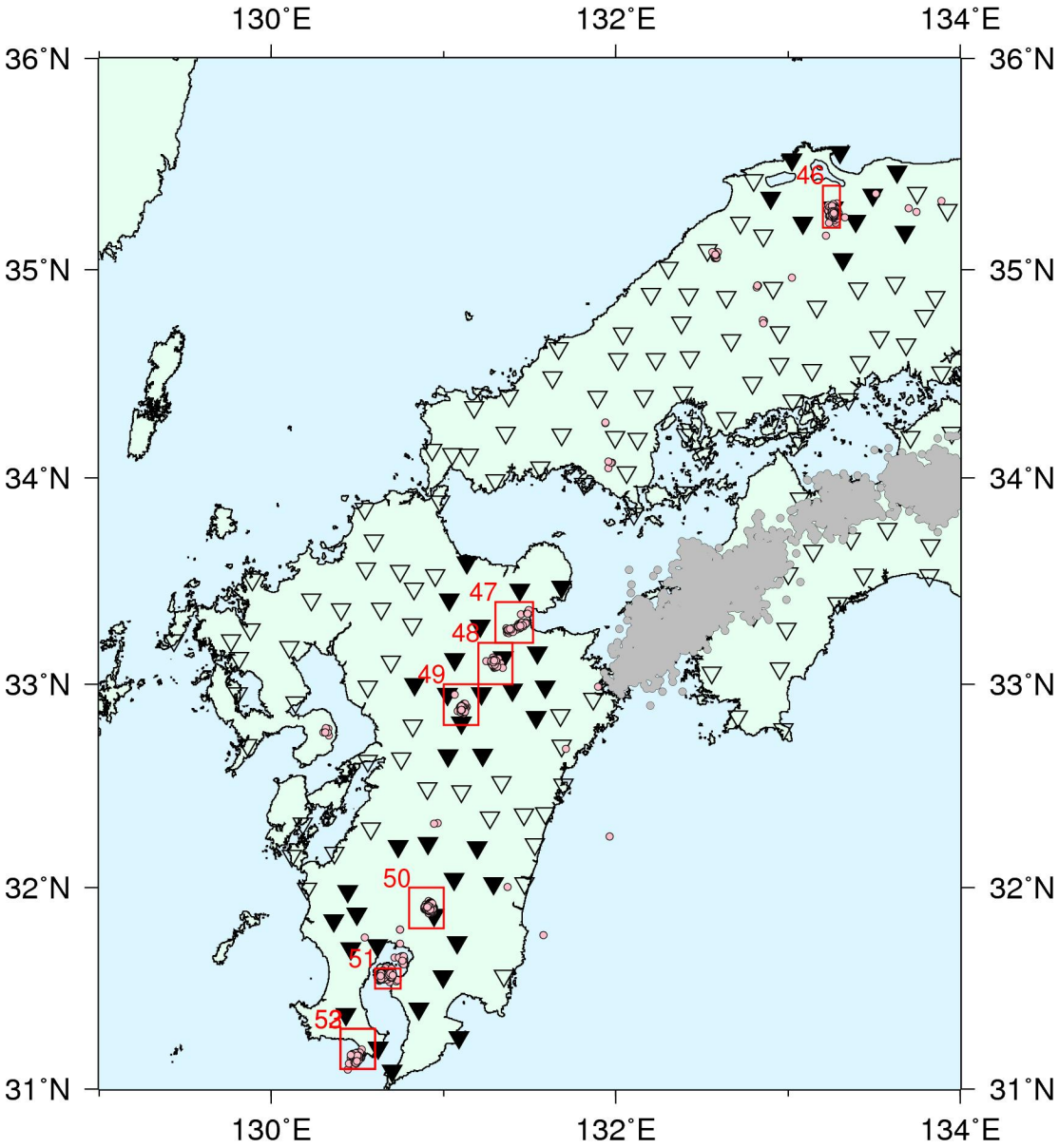

Figure 2.5 Distribution of target regions in Kyushu and Chugoku districts. Symbols are the same as Figure 2.2

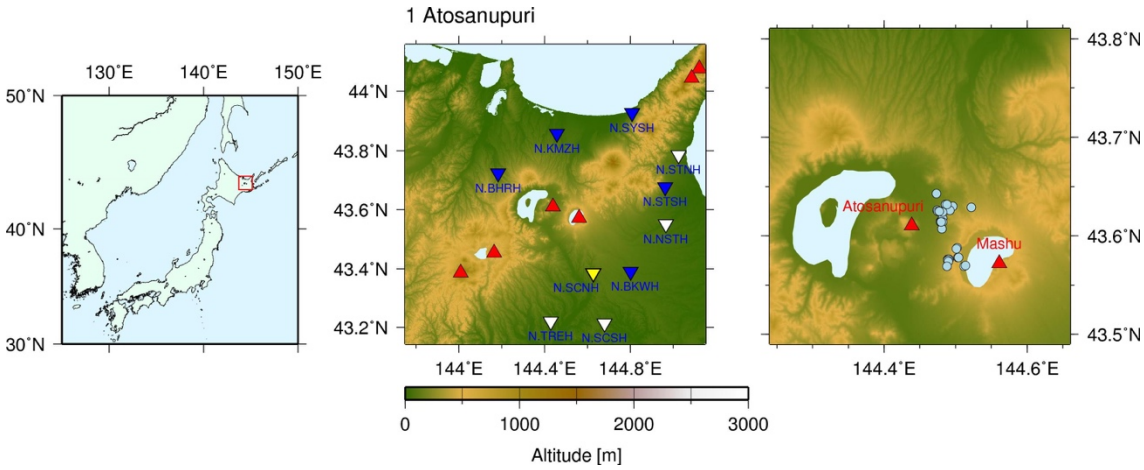

Figure 2.6 An example of maps of the target region, Atosanupuri. Three different scales of maps are illustrated in each panel. Inverted triangles in middle and right panels indicate the locations of Hi-net stations used for relocation, estimation of magnitude and detection (yellow), relocation and detection (blue) and used only for relocation (white). Stations plotted as white inverted triangles are also used for detection when one or two stations plotted as yellow or blue triangles are missing observations. Light blue circles in the right panel show the epicenters of DLF earthquakes obtained by the relocation in this study. Maps of other regions are illustrated in the Appendix (Chapter 10.1).

Table 2.1 List of target regions and the number of DLF earthquakes in the JMA catalog from April 2004 to December 2015. Volcanic activity rank is referred from Japan Meteorological Agency (2003) and Quaternary volcanoes are referred from Nakano et al. (2013). Rank A means most active volcanoes based on activities in last 100 years and 10000 years. Rank B means the next active volcanoes. Rank C means the least active volcanoes. If there are two active volcanoes in the region, both ranks are written in the same column.

District	Index	Region name	Number of DLFs	Volcanic activity
Hokkaido	1	Atosanupuri	191	C
	2	Meakan	1414	B
	3	Taisetsu	158	C
	4	Maruyama	145	C
	5	Tomamu	124	Near Tokachidake
	6	Tokachidake	367	A
	7	Usu	114	A
	8	Kimobetsu	30	Quaternary volcano
	9	Yotei-Niseko	231	C・C
Tohoku	10	Hakkoda	29	C
	11	Mt.Iwaki	43	B
	12	Shirakami	21	No volcano
	13	Towada-east	43	B
	14	Kosaka	75	
	15	Moriyoshi	99	Quaternary volcano
	16	Yakeyama-Hachimantai	78	B・C
	17	Mt.Iwate	605	B
	18	Akita-Komagatake	26	B
	19	Chokaisan	20	B
	20	Kurikoma-NW	44	B
	21	Kurikoma-center	90	
	22	Naruko	439	C
	23	Hijiori	147	C
	24	Asahidake	23	Near Hijiori

	25	Zao	170	B
	26	Azuma	407	B
	27	Adatara	53	B
	28	Bandai-west	138	B
	29	Aizu-Takada	98	Near Bandai and Numazawa
	30	Numazawa	44	C
	31	Mikagura	20	Quaternary volcano
	32	Hiuchigatake	77	C
Kanto	33	Nasu	82	B
	34	Mt.Takahara	264	C
	35	Nikko	161	C
	36	Kusatsu-Shirane	28	B
	37	Hakone	294	B
Chubu	38	Fuji	1366	B
	39	Myoko	90	C
	40	Shirouma	180	Quaternary volcano
	41	Tateyama	200	C
	42	Washiba-Kumonotaira	200	Quaternary volcano
	43	Yakedake	759	B
	44	Ontake	61	B
Kinki	45	Tanba	23	Active faults (Katoh et al., 2018)
Chugoku	46	East-Shimane	1126	Active faults (Ohmi & Obara, 2002) or Quaternary volcanos (Aso et al., 2013)
Kyushu	47	Beppu	71	B・C
	48	Kuju	44	B
	49	Aso	120	A
	50	Kirishima	275	B
	51	Sakurajima	401	A
	52	Kaimon	89	C

2.2. Network Correlation Coefficients method for hypocenter relocation

Detailed distributions of hypocenters are very important to discuss the activity of DLF earthquakes. However, it has been known that the locations of DLF earthquakes in the JMA catalog have large errors, especially in the depths. Therefore, the relocation of the hypocenters of DLF earthquakes is necessary.

In this study, to reduce the hypocentral errors in the JMA catalog, I applied the network correlation coefficient (NCC) method (Ohta & Ide, 2011). In this method, I calculated NCC for each pair of DLF earthquakes to search for relative locations. NCC is calculated by the following equation,

$$NCC\left(\Delta x,\Delta y,\Delta z,\Delta t\right) = \sum_{i,j} \frac{\sum_{\tau=-1.5\mathrm{s}}^{\tau=2.5\mathrm{s}} v_{i,j}\left(x_1,y_1,z_1,\tau\right)u_{i,j}\left(x_1+\Delta x,y_1+\Delta y,z_1+\Delta z,\tau+\Delta t\right)}{\sqrt{\sum_{\tau=-1.5\mathrm{s}}^{\tau=2.5\mathrm{s}} {v_{i,j}}^2\left(x_1,y_1,z_1,\tau\right)}\sqrt{\sum_{\tau=-1.5\mathrm{s}}^{\tau=2.5\mathrm{s}} {u_{i,j}}^2\left(x_1+\Delta x,y_1+\Delta y,z_1+\Delta z,\tau+\Delta t\right)}} \quad \cdot\cdot\cdot (2.1)$$

where, $u_{i,j}$ and $v_{i,j}$ show the velocities of target and reference earthquakes of the *i*-th station and the *j*-th component, respectively. The longitude, latitude, and depth of the reference event are represented by x_1, y_1, and z_1, respectively. The parameter τ shows the time from arrival time of P wave for vertical component and S wave for two horizontal components. τ is changed with intervals of 0.01 seconds which are the same as the sampling rate 100 Hz. Four-seconds time window was used same as original study (Ohta & Ide, 2011). I used three-component seismograms at the nearest 10 stations in all regions. Arrival times measured by JMA are basically used. When arrival time is not estimated in the station, theoretical arrival time of first motion was calculated. The 1D velocity structure of JMA2001 (Ueno et al., 2002) was used to evaluate theoretical arrival time. I searched maximum NCC value with changing Δx, Δy, Δz, and Δt. The parameters Δx and Δy are changed in 10 km with 200 m intervals. Depth difference Δz is changed from 0 km to 50 km with intervals of 200 m. The time difference Δt is changed between plus 1 second and minus 1 second every 0.04 seconds. After getting the

relative locations of each pair, the inversion problem is solved to get final results with minimizing Akaike's Bayesian information criterion (Akaike, 1980). When the maximum NCC is smaller than 6 times of the standard deviation of NCCs calculated in each grid, the data are removed from the inversion. Some DLF earthquakes were not relocated because of this removement of the data.

Estimation of error in this method is difficult because this method consists of multiple calculation. Then, I applied the jackknife test (e.g. Tichelaar & Ruff, 1989)using 9 seismic observation stations, in other words, removing a station, in Chapter 10.2, in order to verify the accuracy of the results.

2.3. Two-stage classifications based on waveform correlations

I classified DLF earthquakes into some groups based on waveform correlations in all regions to investigate the activities of DLF earthquakes. While Kosuga et al. (2017) used waveform correlations of a station for grouping DLF earthquakes, I used summed correlation coefficients (CCs) of 3 components in 6 stations to adjust the condition for the matched filter technique, introduced in the next section. In order to adopt many volcanoes, where different numbers of DLF earthquakes were detected, I used the following method including two stages of classification (Figure 2.7; Figure 2.8).

First, I calculated summed CCs between each pair of DLF earthquakes in the JMA catalog using the following equation,

$$CC(p,q) = \underset{\Delta t}{\mathrm{Max}} \left(\sum_{i,j} \frac{\sum_{\tau=-2.5\mathrm{s}}^{\tau=2.5s} u_{i,j}\left(t_{i,j}^{p}+\tau+\Delta t\right) v_{i,j}\left(t_{i,j}^{q}+\tau\right)}{\sqrt{\left(\sum_{\tau=-2.5\mathrm{s}}^{\tau=2.5s} {u_{i,j}}^{2}\left(t_{i,j}^{p}+\tau+\Delta t\right)\right)\left(\sum_{\tau=-2.5\mathrm{s}}^{\tau=2.5s} {v_{i,j}}^{2}\left(t_{i,j}^{q}+\tau\right)\right)}} \right) \quad \cdot\cdot\cdot (2.2).$$

Here, p and q show the label of earthquakes, respectively. $u_{i,j}$ and $v_{i,j}$ show the j-th component velocities of the earthquakes *p* and *q* obeserved at *i*-th statio*n*, respectively. $t_{i,j}^{p}$ and $t_{i,j}^{q}$ show the times from the origins of the reference and target earthquakes to arrivals of S wave at the *i*-th station. The parameter Δt means the shift of time-lags to fit the phases of two earthquakes. The value of Δt was selected between minus 1 second and plus 1 second with the interval of every 0.01 seconds and the

maximum value is selected as $CC(p,q)$. The time shift was applied to earthquake p with fixed earthquake q, $CC(p,q)$ is not equal to $CC(q,p)$. Therefore, I use the average value of $CC(p,q)$ and $CC(q,p)$ in the following analysis. I define $CC_2(p,q)$ as the average value.

$$CC_2(p,q) = \frac{CC(p,q) + CC(q,p)}{2} \qquad \cdots (2.3)$$

When the value of $CC_2(p,q)$ is over the threshold, then earthquakes p and q are classified into the same group. The value of the threshold is 5.5, while the maximum value of $CC_2(p,q)$ is 18.0 when the waveforms are the same in three components of six stations. Even if $CC_2(p,r)$ is lower than the assumed threshold, earthquakes p and r are classified into the same group, when both $CC_2(p,q)$ and $CC_2(q,r)$ are over the threshold. These procedures were repeated until all earthquakes were classified into any group. After classification, the groups are named as Group 1, Group 2, Group 3, ・・・, in decreasing order of the number of DLF earthquakes in the group. By using this method, the DLF earthquakes in the JMA catalog were classified. The DLF earthquake detected by the matched filter technique was classified into the same group of the template earthquake which detected it.

The method written above could roughly classify DLF earthquakes. For example, in Hijiori (No.23), 123 DLF earthquakes were classified into 5 major groups including three or more earthquakes and 24 DLF earthquakes were classified into minor groups including only one or two DLF earthquakes (Figure 2.9). However, the classification was not enough in some regions such as Meakan (No.2) and Tokachidake (No.6) (Figure 2.10, Figure 2.12). In those regions, there are striped patterns of high CC values in Groups 1 and 2. They show the possibility of further detailed classification. Therefore, I classified DLF earthquakes into further detailed groups using $CC_2(p,q)$ as

the second-stage classification.

In the second-stage of classification, I divided all groups of the first-stage classification which include three or more DLF earthquakes (Label "α" in Figure 2.7). The average value of CC_2 in the group G_i is calculated as

$$\overline{\mathrm{CC}_2\_\mathrm{group}}\left(G_i\right)=\frac{1}{n^2}\sum_{p\subset G_i}\sum_{q\subset G_i}\mathrm{CC}_2\left(p,q\right) \quad \cdot\cdot\cdot (2.4).$$

Here, *n* is the number of DLF earthquakes in the group.

Next, the earthquake which have maximum $\overline{\mathrm{CC}_2}\left(p\right)$ defined by the following equation are selected.

$$\overline{\mathrm{CC}_2}\left(p\right)=\frac{1}{n}\sum_{q\subset G_i}\mathrm{CC}_2\left(p,q\right) \qquad \cdot\cdot\cdot (2.5)$$

Here, the earthquake of number 1 in the group is defined as the earthquake p which have the largest $\overline{\mathrm{CC}_2}\left(p\right)$. The earthquake of number 2 is defined as the earthquake to have the largest $\mathrm{CC}_2\left(2,1\right)$. The earthquake of number 3 is defined as the earthquake to have the largest $\mathrm{CC}_2\left(3,1\right)+\mathrm{CC}_2\left(3,2\right)$. In this way, the earthquakes are selected in series from remained earthquakes in the group to maximize the value $\widetilde{\mathrm{CC}_2}\left(m\right)$, defined by the following equation.

$$\widetilde{CC_2}\left(m\right)=\frac{1}{m-1}\sum_{q=1}^{m-1}CC_2\left(m,q\right) \qquad \cdot\cdot\cdot (2.6)$$

Here, *m* and *q* show the label of DLF earthquakes. When the $\widetilde{CC_2}\left(m_1\right)$ is smaller than the average value of CC in the group of the first-stage classification, $\overline{\mathrm{CC}_2\_\mathrm{group}}\left(G_i\right)$, the earthquakes labeled as between 1 and (m_1-1) are classified into the group $G_{i.1}$ and earthquakes labeled as after m_1 are classified into the next group $G_{i.2}$. For second group

or more latter group, I used substitute equation (2.7) for equation (2.6)

$$\widetilde{CC_2}(m) = \frac{1}{m - m_1} \sum_{q=m_1}^{m-1} CC_2(m,q) \qquad \cdots (2.7)$$

Same as the above process, the remaining earthquakes in the group G_i were classified into the groups of the second-stage classification and when the values of $\widetilde{CC_2}(m)$ is smaller than $\overline{\mathrm{CC_2\_group}}(G_i)$ then, the new second-stage group was set. However, in the Meakan (No.2), Fuji (No.37) and east-Shimane (No.46), $\overline{\mathrm{CC_2\_group}}(G_i)$ was not a good threshold because there are over 1000 DLF earthquakes in the JMA catalog. Then, I set variable threshold values to classify DLF earthquakes in the best way (Table 2.2). After the second-stage classification, subdivided groups were obtained (Figure 2.11, Figure 2.13). In this study, the groups of the results of the second-stage classification are written as Group *i.j*, in which *i* shows the label of the first-stage classification and *j* shows the label of the second-stage classification. When a group of the first-stage classification includes only one or two DLF earthquakes (Label "β" in Figure 2.7), the group is written as Group *i.*

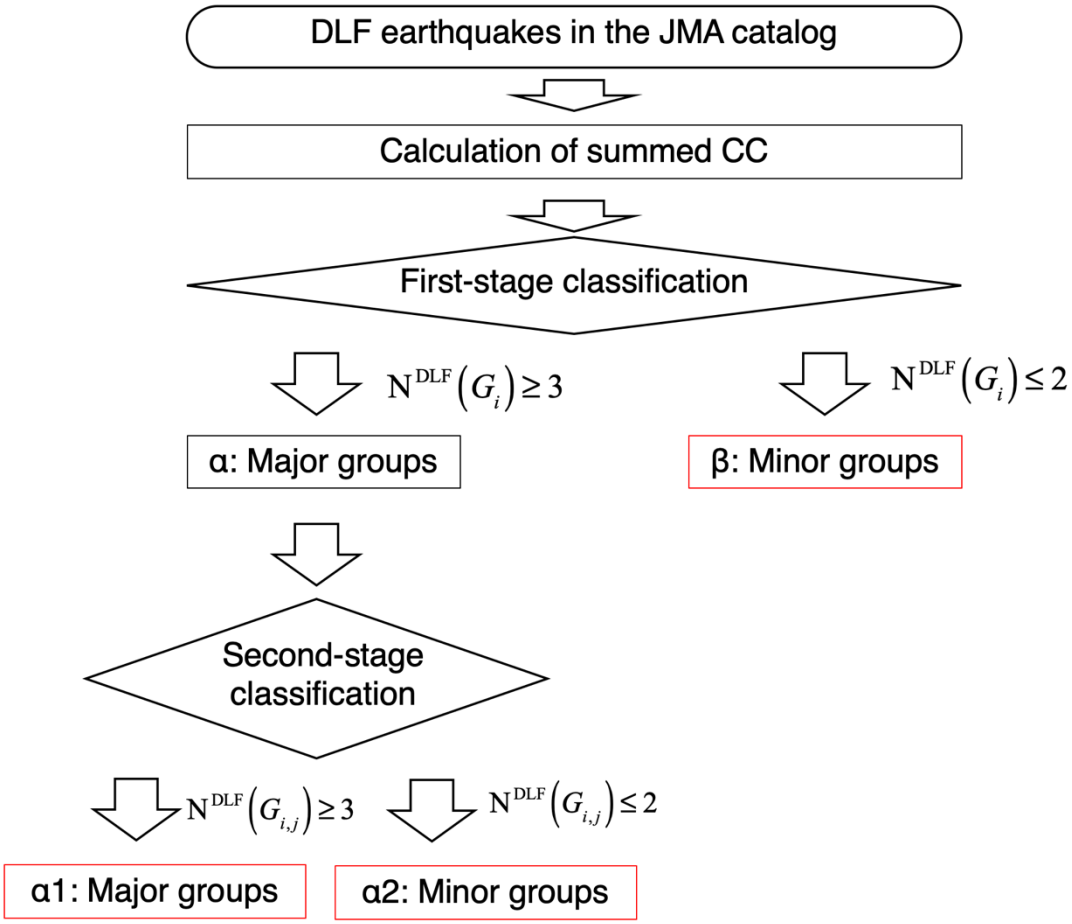

Figure 2.7 The flow chart of the classifications. The final results are in the red boxes.

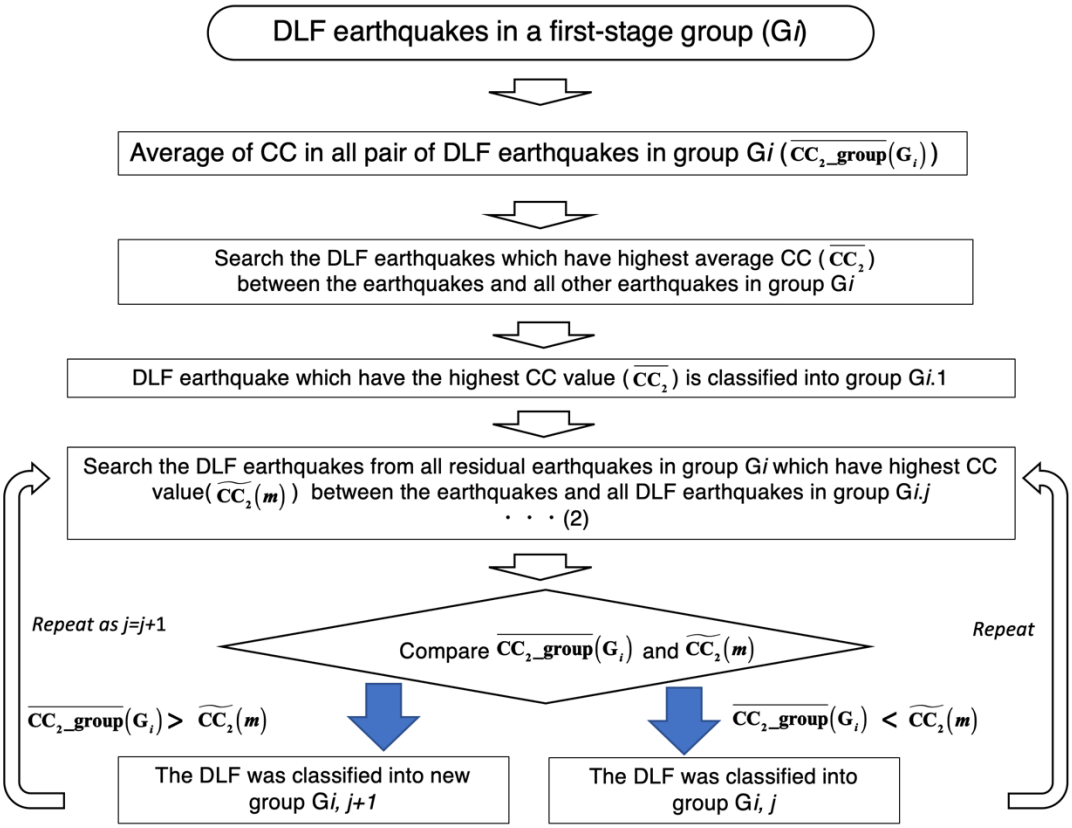

Figure 2.8 The flow chart of the second stage of the classification.

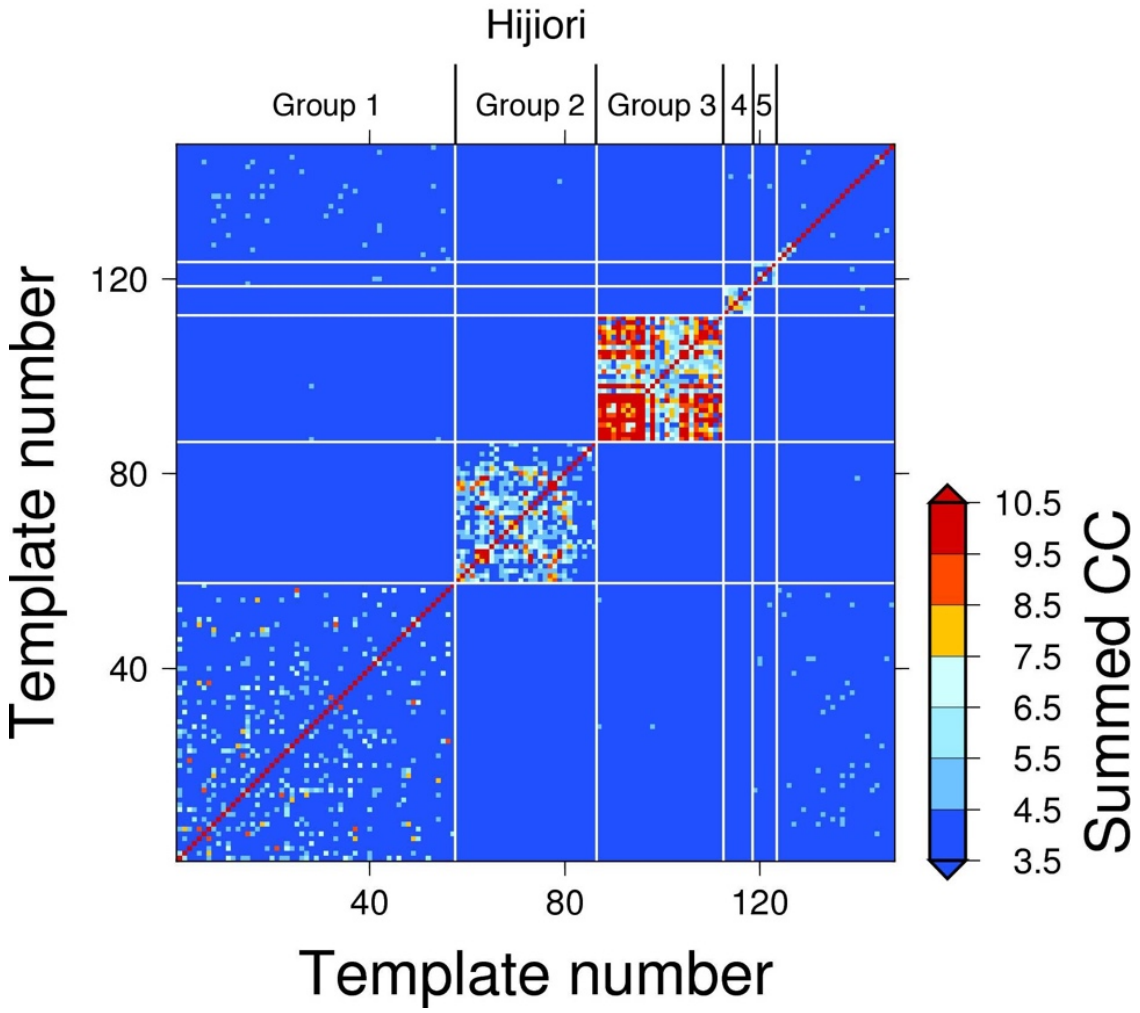

Figure 2.9 Summed CC values of each DLF earthquake pair in three components of six stations in Hijiori and the result of first-stage classification. White lines show the boundaries of the first-stage classification. The boundary lines are plotted when the groups include three or more DLF earthquakes.

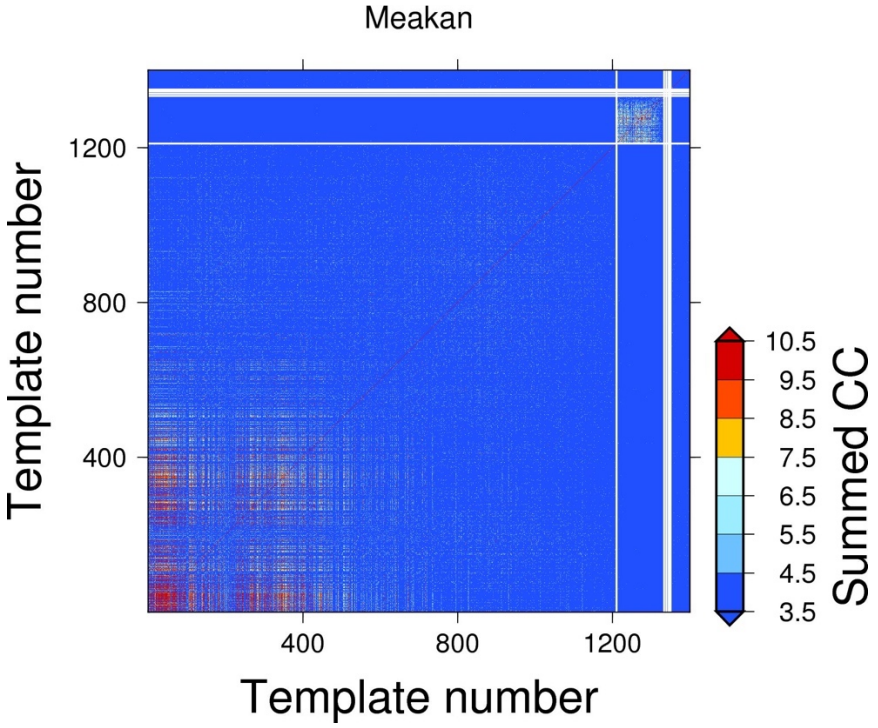

Figure 2.10. Same figure as Figure 2.9 but in Meakan.

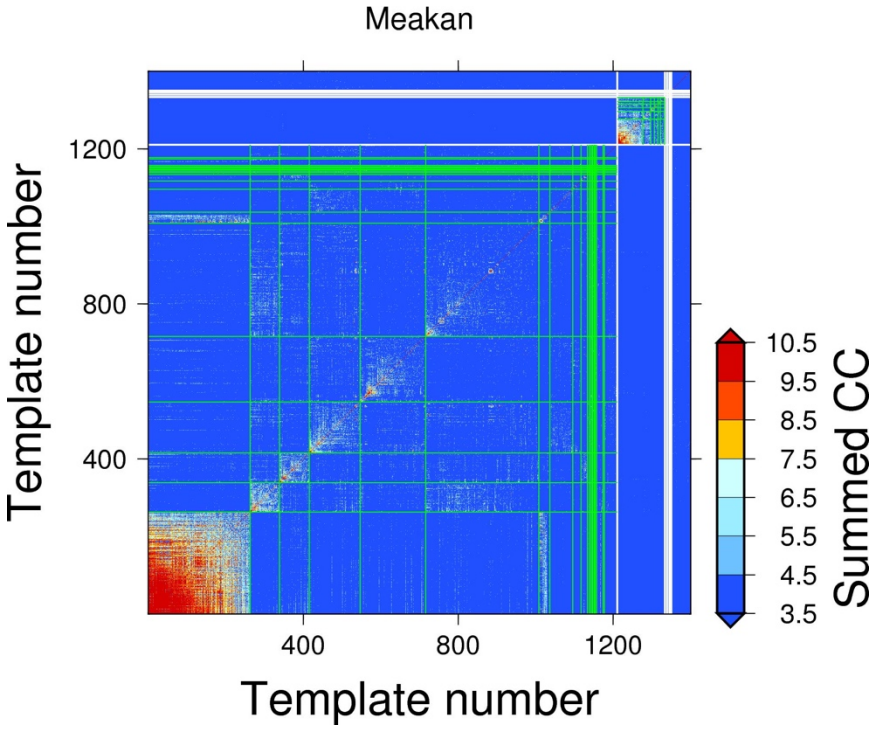

Figure 2.11 Summed CC values of each DLF earthquake pair in Meakan and the two-stages of classifications. White and green lines show the boundaries of the first-stage and the second-stage classifications, respectively. The boundary lines are plotted when the groups include three or more DLF earthquakes.

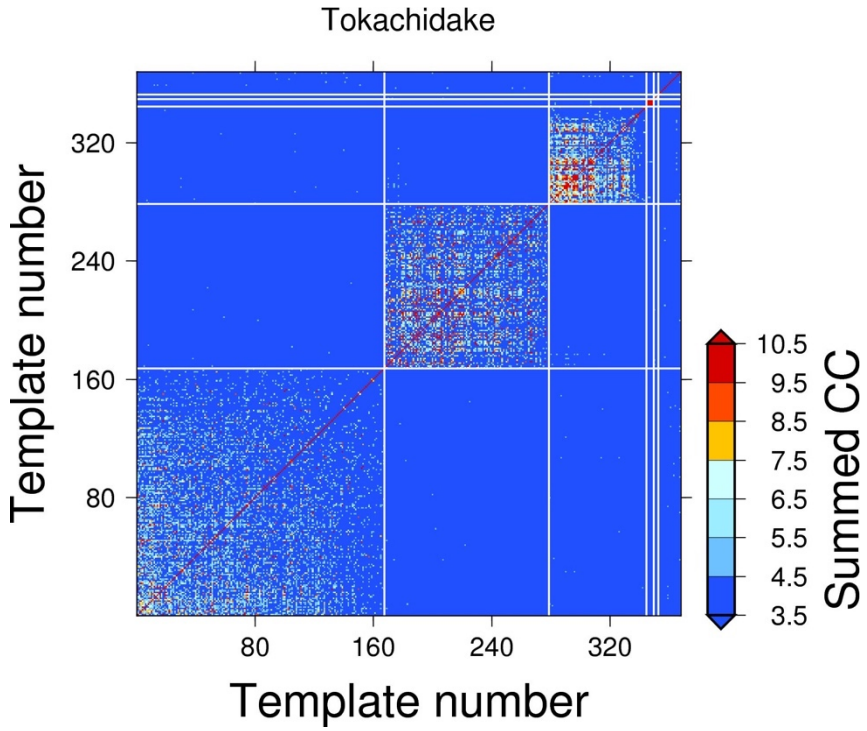

Figure 2.12 Same figure as Figure 2.9 but in Tokachidake.

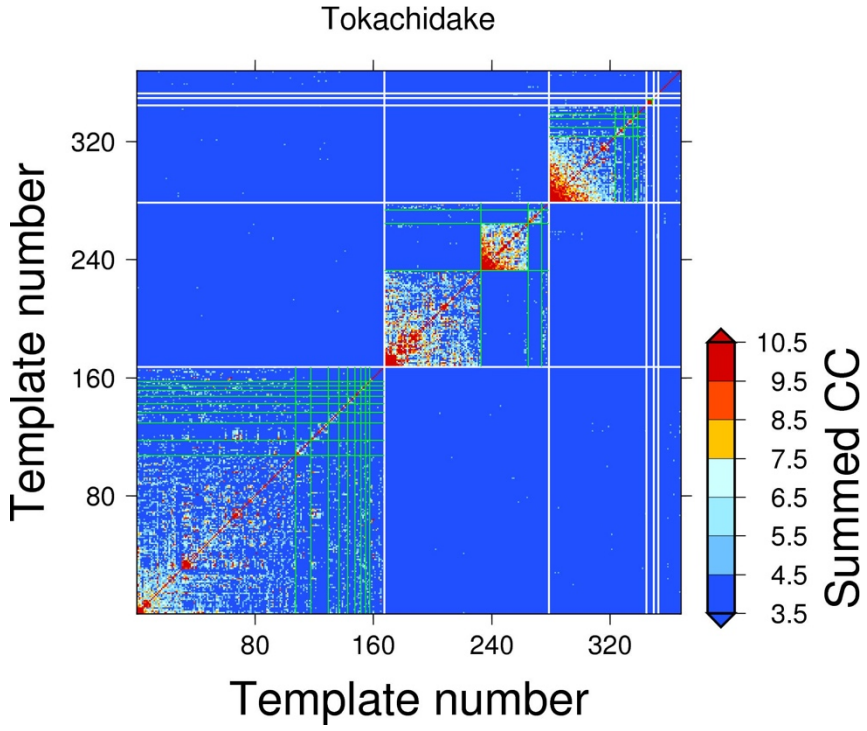

Figure 2.13 Same figure as Figure 2.11 but in Tokachidake.

Table 2.2 Threshold values used for the second-stage classification in Meakan, Fuji, and East-Shimane.

Boundary of groups	*i*.1– *i*.2	*i.2*– *i*.3	*i.3*– *i*.4	*i.4*– *i*.5	*i.4*– *i*.5	*i*.5–*i*.6 and follows
Meakan	5.0	4.5	4.0	3.5	3.0	2.5
Fuji	9.0	6.5	4.0	2.5	2.5	2.5
East-Shimane	9.0	7.0	5.0	3.0	2.5	2.5

2.4. Comprehensive detection of DLF earthquakes based on matched filter technique

To construct a comprehensive catalog of DLF earthquakes, including DLF earthquakes not listed in the JMA catalog, I applied the matched filter technique (MFT; Gibbons & Ringdal, 2006; Shelly et al., 2007) to continuous Hi-net seismograms. In this method, more DLF earthquakes are detected when the summed correlation coefficients (CCs) of waveforms between template earthquakes and continuous data of three components of six stations are higher than the detection threshold. Summed CCs are calculated by the following equation,

$$\mathrm{Summed\_CC}(t)=\sum_{i,j}\frac{\sum_{\tau=-2.5\mathrm{s}}^{\tau=2.5s}u_{i,j}\left(t+t_1(i,j)+\tau\right)v_{i,j}\left(t_1(i,j)+\tau\right)}{\sqrt{\left(\sum_{\tau=-2.5\mathrm{s}}^{\tau=2.5s}{u_{i,j}}^2\left(t+t_1(i,j)+\tau\right)\right)\left(\sum_{\tau=-2.5\mathrm{s}}^{\tau=2.5s}{v_{i,j}}^2\left(t_1(i,j)+\tau\right)\right)}} \quad \cdots (2.8).$$

Here, $v_{i,j}$ and $u_{i,j}$ show the velocities of template earthquakes and continuous data of the *i*-th station and the *j*-th component, respectively. $t_1(i,j)$ show the time from the origin of the template earthquake to the arrival of S-wave at the station. t means the time of continuous data. Different length of time window was used to verify the effect of time window in Chapter 10.3.

The analysis period ranges from April 2004 to December 2018. I first decimated the Hi-net data from 100 Hz to 12.5 Hz to reduce the computational cost. All DLF earthquakes in the JMA catalog from April 2004 to December 2015 in the region were used as templates except where the number of DLF earthquakes is over 200. In the region, 200 templates were selected with high signal to noise ratios (SN ratios) in a station (Yellow triangle of Figure 2.6). When the data of one or two seismic stations are missing for the target day, we add the same amount of data from the other stations that are used for relocation as well. Then, the maximum value of the summed correlation coefficients (CC) is always 18. The detection threshold of summed CC is set to 5.5, approximately equivalent to 11 times of median absolute deviations (MAD). This value is higher than that used for the analysis of tectonic DLF earthquakes (e.g., Shelly et al., 2007), to prevent false detection. After detection, I selected the one detected earthquake that has the highest summed CC in 10-seconds time-window to avoid multiple counting of one DLF

earthquake.

Regardless of our severe threshold, false detections sometimes occur because the number of stations is limited, and the SN ratios of waveforms are usually low. To reduce the false detections, I used two criteria of CCs and estimated magnitudes calculated based on template DLF earthquakes written in section 2.5. I distinguish detected DLF earthquakes from false detections based on the following procedures. First, I selected as DLF earthquakes only the detected events whose summed CCs are larger than 7.0. Next, I removed the detected events with large magnitudes because they may be caused by the surface waves of regular earthquakes. The threshold of the magnitudes was calculated based on the DLF earthquakes selected above. Events were recognized as false detection when the magnitudes of the events with summed CC between 5.5 and 7.0 are larger than the magnitude of the top 3% of DLF earthquakes, for example, the value is equal to magnitude 0.8 in Kirishima (No.50). Finally, to reduce false detections due to noise such as wind or microseisms, I calculated the spectral ratios of 0.5–1.0 Hz to 2.0–4.0 Hz. Then, I removed the events whose summed CCs are between 5.5 and 7.0 and spectrum ratios are less than 0.2. In other words, I removed the events with large energy on the 0.5–1.0-Hz band, which have lower dominant frequency compared to typical DLF earthquakes, 1.0–10.0 Hz. Furthermore, some templates in regions, such as Hakone (No.37) and Kuju (No.48), made many false detections. Therefore, the events detected by such templates were removed from the catalog.

2.5. Magnitude estimation of DLF earthquakes

Magnitude is one of the important parameters to discuss the sources and activities of DLF earthquakes. However, magnitudes of some DLF earthquakes are not determined in the JMA catalog. Besides, magnitudes of some DLF earthquakes in the JMA catalog may be incorrectly estimated due to differences in the depths in the JMA catalog. In order to compare magnitudes of DLF earthquakes in each region, I re-calculated magnitudes of DLF earthquakes using the results of the two-stages classification.

In each region and each group, I first calculated a and b values in the following equation using the least square method using the DLF earthquakes in the JMA catalog (e.g. Figure 2.14).

$$M_{\mathrm{JMA}} = a\log_{10}\left(\max\left(v(t)\right)\right) + b \qquad \cdots (2.9)$$

Here, $\max\left(v(t)\right)$ shows the maximum absolute value of velocity seismogram in east-west component of one station (yellow triangle of Figure 2.6) in the five seconds time-window same as MFT and M_{JMA} means the magnitude of DLF earthquakes in JMA catalog. Parameters *a* and *b* were calculated for the groups which include more than 10 DLF earthquakes in the JMA catalog. When there are less than 10 DLF earthquakes in the group in the JMA catalog, the average value of all groups in the region was used for estimation of magnitude.

Next, magnitude of detected events was calculated and those of the earthquakes in the JMA catalog were re-calculated using the equation (2.10).

$$M_{\mathrm{NEW}} = a\log_{10}\left(\max\left(v(t)\right)\right) + b \qquad \cdots (2.10)$$

$\max\left(v(t)\right)$ shows the maximum absolute value of velocity seismogram in one station. Parameters *a* and *b* were calculated in equation (2.9).

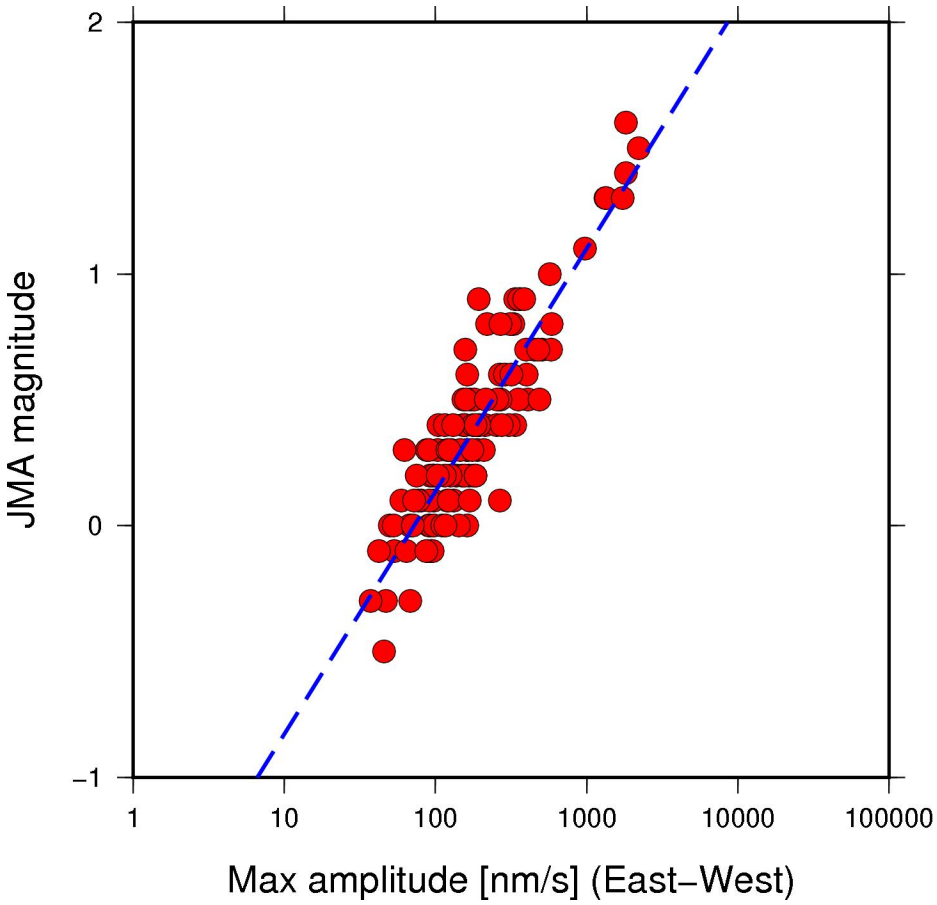

Figure 2.14 The relationship between maximum amplitude of velocity seismogram and JMA magnitude in Group 1.1 of Kirishima (No.50). Red circles show the maximum amplitudes and magnitudes of DLF earthquakes in the JMA catalog. Blue broken line shows the regression line used for estimation of the magnitude of DLF earthquakes in the new catalog.

3. Characteristics of activities of DLF earthquakes all over Japan

In this chapter, I show the results of the three analyses to discuss the characteristics of activities of DLF earthquakes all over Japan. As a result of the analyses, a complete catalog of DLF earthquakes was constructed in each region. As a result of relocation based on NCC method introduced in section 2.2, most DLF earthquakes in the JMA catalog were relocated, although a part of DLF earthquakes was excluded from the relocation. All DLF earthquakes in the JMA catalog were divided into some groups using the two-stages classifications introduced in section 2.3. 105,327 DLF earthquakes were detected by MFT introduced in section 2.4 and the earthquakes were recorded in the newly constructed catalog. The locations and classifications of DLF earthquakes in the new catalog are based on those of template DLF earthquakes. Finally, magnitudes of all DLF earthquakes in the new catalog were calculated based on the method in section 2.5.

In section 3.1, I introduce the spatial distributions of DLF earthquakes. Discrete distributions of DLF earthquakes are shown in each region. In section 3.2, I introduce an index “swarm ratio (SR)” which shows the ratio of swarm of DLF earthquakes in each group of each region and I classify episodic and constant occurrence of DLF earthquakes. Intervals, magnitude-frequency distributions and waveform characteristics of DLF earthquakes in each region are shown from section 3.3 to 3.5. Discussion based on the results and the summary of this chapter are written in section 3.6 and section 3.7, respectively.

After the analyses, activities of DLF earthquakes associated with volcanic activities were observed in Kirishima (No.50), Meakan (No.2), Sakurajima (No.51), Ontake (No.44), and Hakone (No.37), as written in Chapters 4 and 5.

3.1. Distribution of DLF earthquakes

As a result of relocation, discreate distributions of DLF earthquakes in vertical direction are seen in most regions all over Japan. For example, in Hijiori (No.23), DLF earthquakes were separately relocated into the four groups at depths of 20 km, 25 km, 30 km, and 35 km, while DLF earthquakes were continuously distributed in the vertical direction in the JMA catalog (Figure 3.1 and Figure 3.2). This distribution of the hypocenters mostly corresponds to the groups based on the classification. Groups 3, 2, and 4 at a depth of 25 km, 30 km, and 35 km, respectively are seen like as dots (Figure

3.1). This result suggests that hypocenters of DLF earthquakes are concentrated in some small spots, although the Group 1 at a depth of 20 km has a little width in the east-west direction. While DLF earthquakes in Group 1 show lower summed CC values between each pair of template earthquakes, DLF earthquakes in Groups 2 and 3 at depths of 30 and 25 km show higher summed CC values in each pair (Figure 3.3). These results suggest that very similar DLF earthquakes in Groups 2 and 3 repeatedly occurred in the same locations, while DLF earthquakes in Group 1 sometimes occurred at a little different location. As the results of the jackknife test, the same pattern in distribution of DLF earthquakes is obtained for in each sample using any nine stations (Chapter 10.2.1). The errors of the hypocenters are mostly less than 1 km based on the jackknife test.

In Nikko (No.35), the discrete distribution of DLF earthquakes was also observed (Figure 3.4 and Figure 3.5), although the intervals of depths were not equal. Group 1 and Group 4 were very close each other with a separation of shorter than 1 km, while there are seismic gaps of approximately 5 km in the depth of 30–35 km for Groups 4 and 2.

As the cases of Hijiori and Nikko, while depths of DLF earthquakes continuously distribute in the JMA catalog (Figure 3.6), discrete distributions of DLF earthquakes in depths are seen in most regions all over Japan in the new catalog (Figure 3.7). Most DLF earthquakes were separately distributed in depths of 10–40 km. Most DLF earthquakes are classified into 2–29 major groups (Table 3.1). The intervals of depths of the major groups are approximately 5 km in many regions such as Yotei-Niseko (No.9), Naruko (No.22) as like as Hijiori, while those are 10 km in Mt.Takahara (No.34) and 20 km in Mt.Iwate (No.17). Narrower intervals of depths approximately 1 km were observed in Nikko (No.35) and Sakurajima (No.51).

The depth of Moho discontinuity in each region approximately corresponds to the lower limit depth of DLF earthquakes. DLF earthquakes were mainly distributed between the depths of Moho discontinuity and D90. D90 is defined as the depth above which 90 % of regular crustal earthquakes occur and means the lower limit depth of crustal regular earthquakes. For example, depths of Moho discontinuity and DLF earthquakes in Kyushu district are shallower than those of other districts. On the other hand, there are DLF earthquakes deeper than 40 km in Chokaisan (No.19) and Ontake (No.44), despite the absence of DLF earthquakes in the depths of other regions.

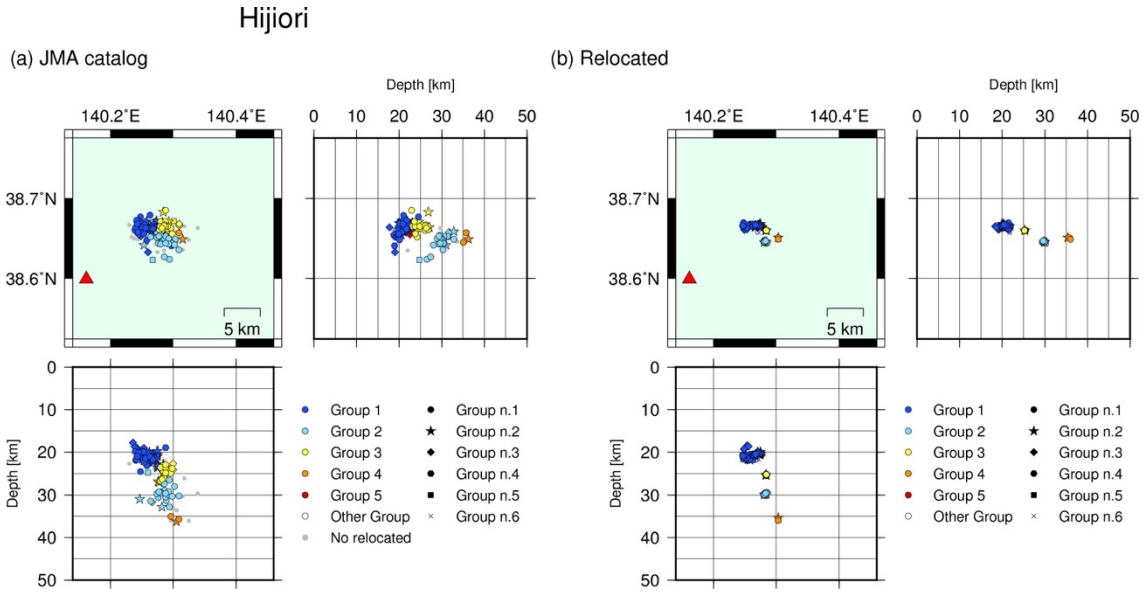

Figure 3.1 Three-dimensional hypocenter distribution of DLF earthquakes in Hijiori. (a) Hypocenter distribution of DLF earthquakes in the JMA catalog. Color and symbols corresponding to the group of first-stage and second-stage, respectively. (b) Hypocentral distribution of DLF earthquakes after the relocation.

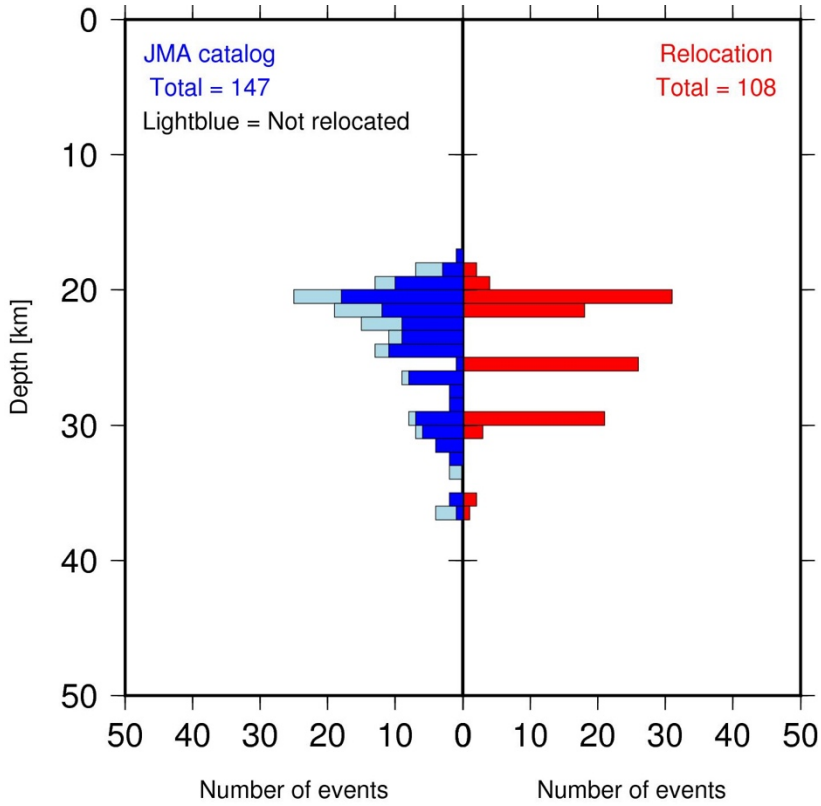

Figure 3.2 Depth distributions of DLF earthquakes in Hijiori in the JMA catalog on the left side and those after the relocation on the right side.

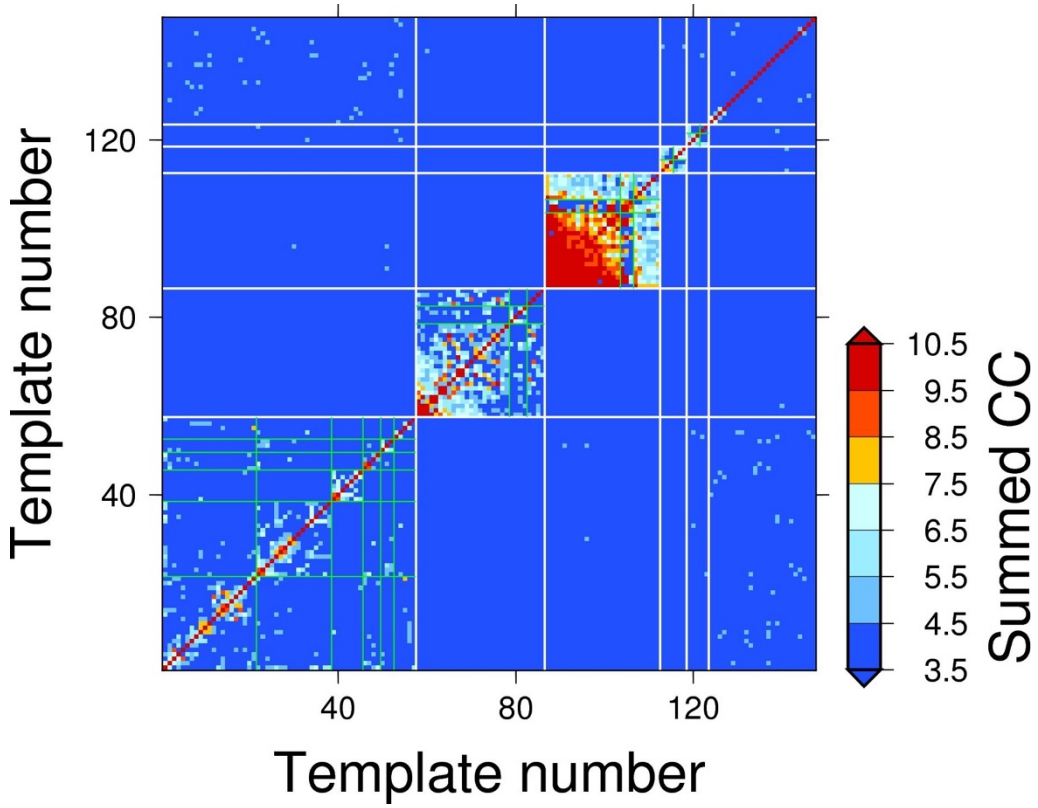

Figure 3.3 Same figure as Figure 2.11 but in Hijiori.

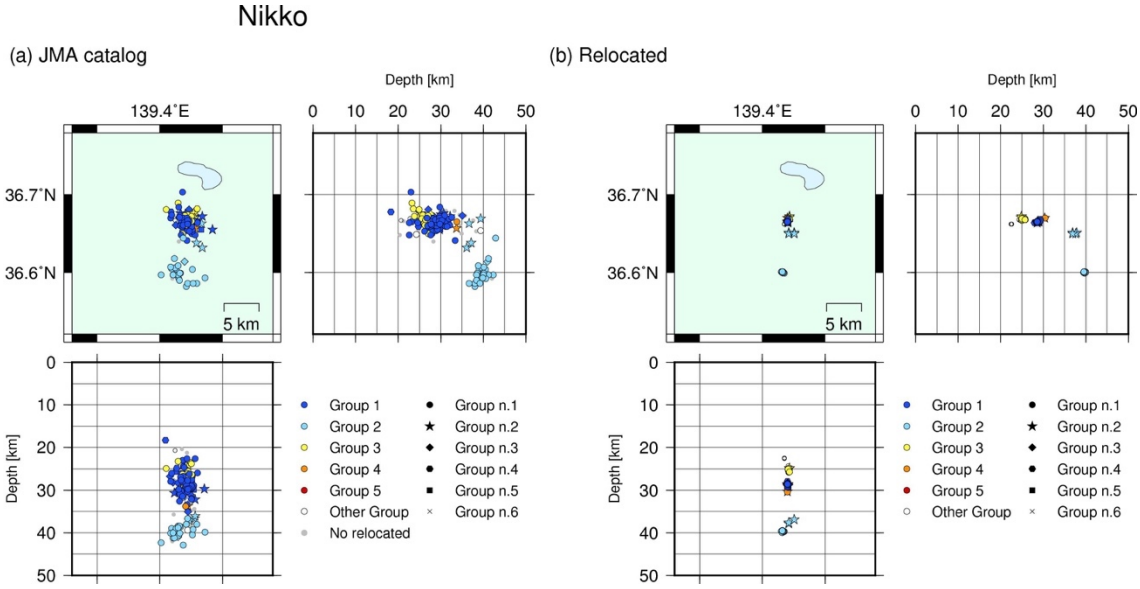

Figure 3.4 Same figure as Figure 3.1 but in Nikko.

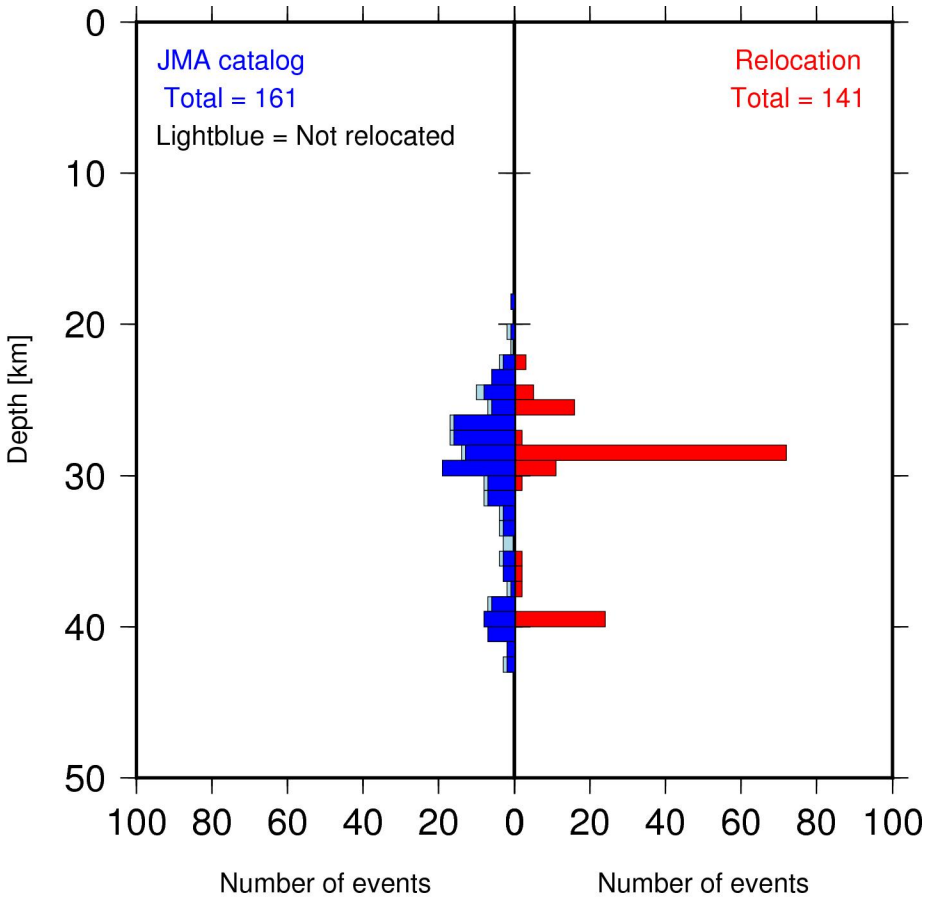

Figure 3.5 Same figure as Figure 3.2 but in Nikko.

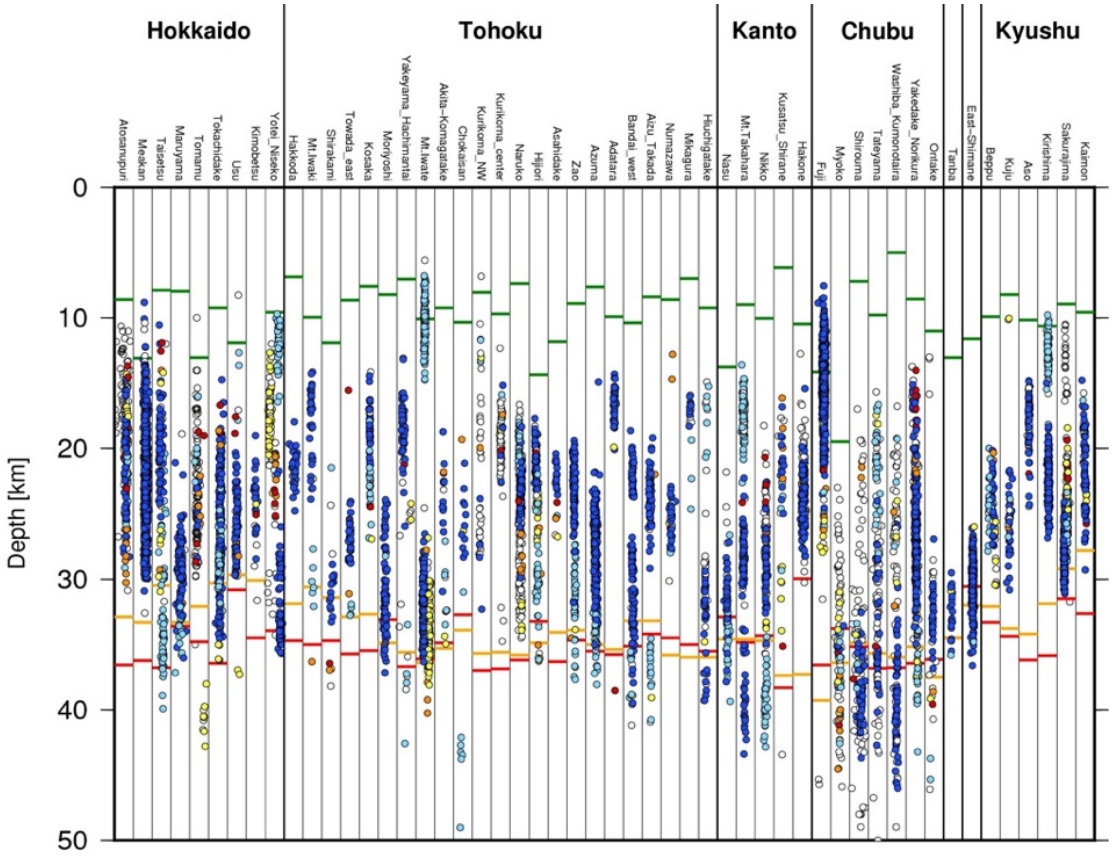

Figure 3.6 Depth distributions of DLF earthquakes in the JMA catalog in the 52 regions. Regions are aligned following the index number (Table 2.1). Horizontal axis in a bin corresponds to the longitude and vertical axis corresponds to the depths of DLF earthquakes. Colors correspond to the first-stage groups of the DLF earthquakes and the color is the same as Figure 3.1. Green lines show the depths of D90 in each region. D90 is calculated using the JMA catalog. Orange and red lines show the depths of Moho discontinuity in Katsumata (2010) and Matsubara et al. (2017), respectively. This figure is referred from (Ukawa, 2007).

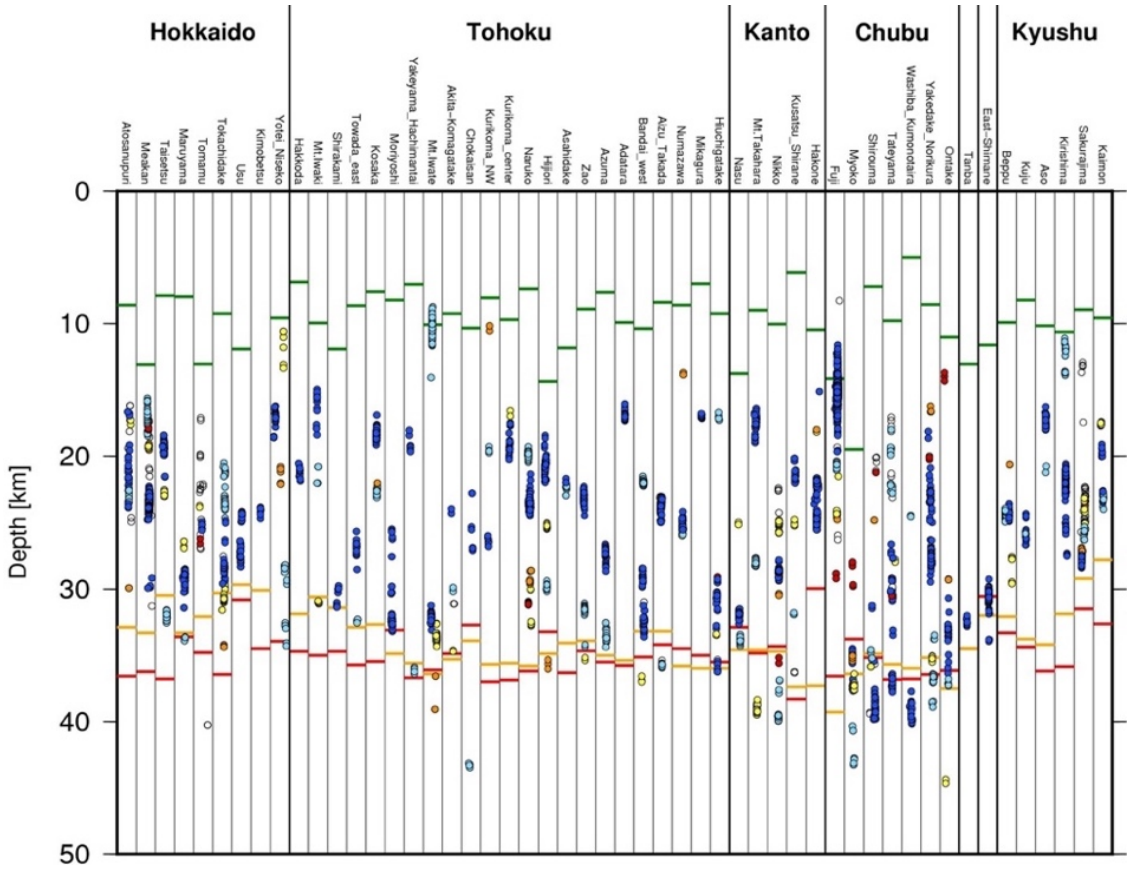

Figure 3.7 Depth distributions of DLF earthquakes in the relocated catalog at the 52 regions. Symbols are the same as Figure 3.6.

Table 3.1 Number of DLF earthquakes and groups into which DLF earthquakes were divided.

Regions	Number of DLFs (JMA)[1]	Number of DLFs (This study)[2]	Number of major groups (First-stage)[3]	Number of major groups (Two stages)[4]	Number of all groups (First-stage)[5]	Number of all groups (Two stages)[6]
Atosanupuri	191	1670	8	14	95	125
Meakan	1414	5508	5	29	67	130
Taisetsu	158	757	3	10	12	35
Maruyama	145	935	3	11	12	36
Tomamu	124	684	8	6	86	105
Tokachidake	367	1238	5	18	20	60
Usu	114	831	2	8	15	32
Kimobetsu	30	55	1	4	11	17
Yotei-Niseko	231	3077	5	15	47	77
Hakkoda	29	209	1	3	6	12
Mt.Iwaki	43	360	3	4	6	21
Shirakami	21	787	1	3	9	14
Towada-east	43	266	2	5	7	19
Kosaka	75	692	2	6	8	23
Moriyoshi	99	774	1	7	5	14
Yakeyama-Hachimantai	78	745	2	7	28	42
Mt.Iwate	605	3550	4	27	67	119
Akita-Komagatake	26	120	2	4	8	16
Chokaisan	20	408	2	4	6	12
Kurikoma-NW	44	101	3	4	13	26
Kurikoma-center	90	192	2	4	17	31
Naruko	439	747	6	24	92	158
Hijiori	147	1351	5	13	28	55
Asahidake	23	93	2	3	11	19
Zao	170	1901	2	9	10	34
Azuma	407	9911	2	11	7	69
Adatara	53	260	1	5	6	14

Bandai-west	138	2228	3	8	14	34
Aizu-Takada	98	605	3	6	12	27
Numazawa	44	449	3	5	10	21
Mikagura	20	75	2	3	5	11
Hiuchigatake	77	1085	2	7	12	23
Nasu	82	432	2	7	5	23
Mt.Takahara	264	1144	3	12	23	65
Nikko	161	5814	5	10	19	49
Kusatsu-Shirane	38	326	4	4	13	25
Hakone	294	3649	2	9	10	20
Fuji	1366	16183	6	15	26	72
Myoko	90	418	5	12	21	42
Shirouma	180	1103	4	10	47	67
Tateyama	200	511	5	10	43	70
Washiba-Kumonotaira	200	769	4	9	48	68
Yakedake	759	7255	5	16	35	80
Ontake	61	1501	5	5	9	26
Tanba	23	107	1	2	4	12
East-Shimane	1126	6156	2	9	5	20
Beppu	71	449	3	7	12	28
Kuju	44	1156	1	5	9	16
Aso	120	4562	2	5	22	36
Kirishima	275	2964	3	10	23	49
Sakurajima	401	8669	11	23	70	140
Kaimon	89	495	4	6	15	34

1) DLF earthquakes in the JMA catalog between April 2004 and December 2015
2) DLF earthquakes in the newly constructed catalog between April 2004 and December 2018
3) Number of the groups with label "α" in Figure 2.7
4) Number of the groups with label "α 1" in Figure 2.7
5) Number of the groups with label "α" and "β" in Figure 2.7
6) Number of the groups with label "α 1", "α 2", and "β" in Figure 2.7

3.2. Temporal activity patterns of DLF earthquakes in each group

As a result of the construction of the new catalog, not only spatial distribution of DLF earthquakes but also characteristic temporal activity patterns of DLF earthquakes were revealed. For example, typical activities of DLF earthquakes in each group were observed in Hijiori (No.23; Figure 3.8). In Groups 1.1 and 1.2 at a depth of approximately 20 km, DLF earthquakes constantly occurred from 2004 to 2018. In Group 3.1 at a depth of 25 km, DLF earthquakes episodically occurred in the period. Swarms of DLF earthquakes sometimes occurred with intervals of approximately one year. In Group 2.1 at a depth of 30 km and Group 4.2 at a depth of 35 km, DLF earthquakes mainly occurred between 2011 and 2015.

In order to compare temporal activity patterns of DLF earthquakes in each group of each region across Japan, I defined an index "swarm ratio (SR)", which indicates the ratio of swarms of DLF earthquakes as following.

$$SR = \frac{N^{\mathrm{Swarms}}}{N^{\mathrm{Total}}} \qquad \cdots (3.1)$$

N^{Total} shows the total number of DLF earthquakes in each group. N^{Swarms} shows the number of DLF earthquakes in swarms. In this study, swarms are defined when 10 or more earthquakes occur with the shorter interval from the former earthquake than the expected interval time of the group. The expected interval time was calculated by the division of analysis period, which is 14 years and nine months, by the total number of DLF earthquakes in the group.

As a result, SR values calculated for each group in each region are plotted in Figure 3.9–Figure 3.12. While there are both low SR groups and high SR groups in Hijiori (No.23), some regions include only groups with high SR values or only groups with low SR values. SR values larger than 0.7 were observed in 12 regions, Atosanupuri (No.1), Meakan (No.2), Hakkoda (No.10), Kosaka (No.14), Chokaisan (No.19), Hijiori (No.23), Nikko (No.35), Hakone (No. 37), Yakedake (No.43), Ontake (No.44), Kuju (No.48), and Aso (No.49). There is a weak tendency that SR in Tohoku district is low and SR in Chubu district is high. In other words, DLF earthquakes constantly occur in the Tohoku district and episodically occur in the Chubu district (Figure 3.10 and Figure 3.11). SR does not have any dependence on depth (Figure 3.13).

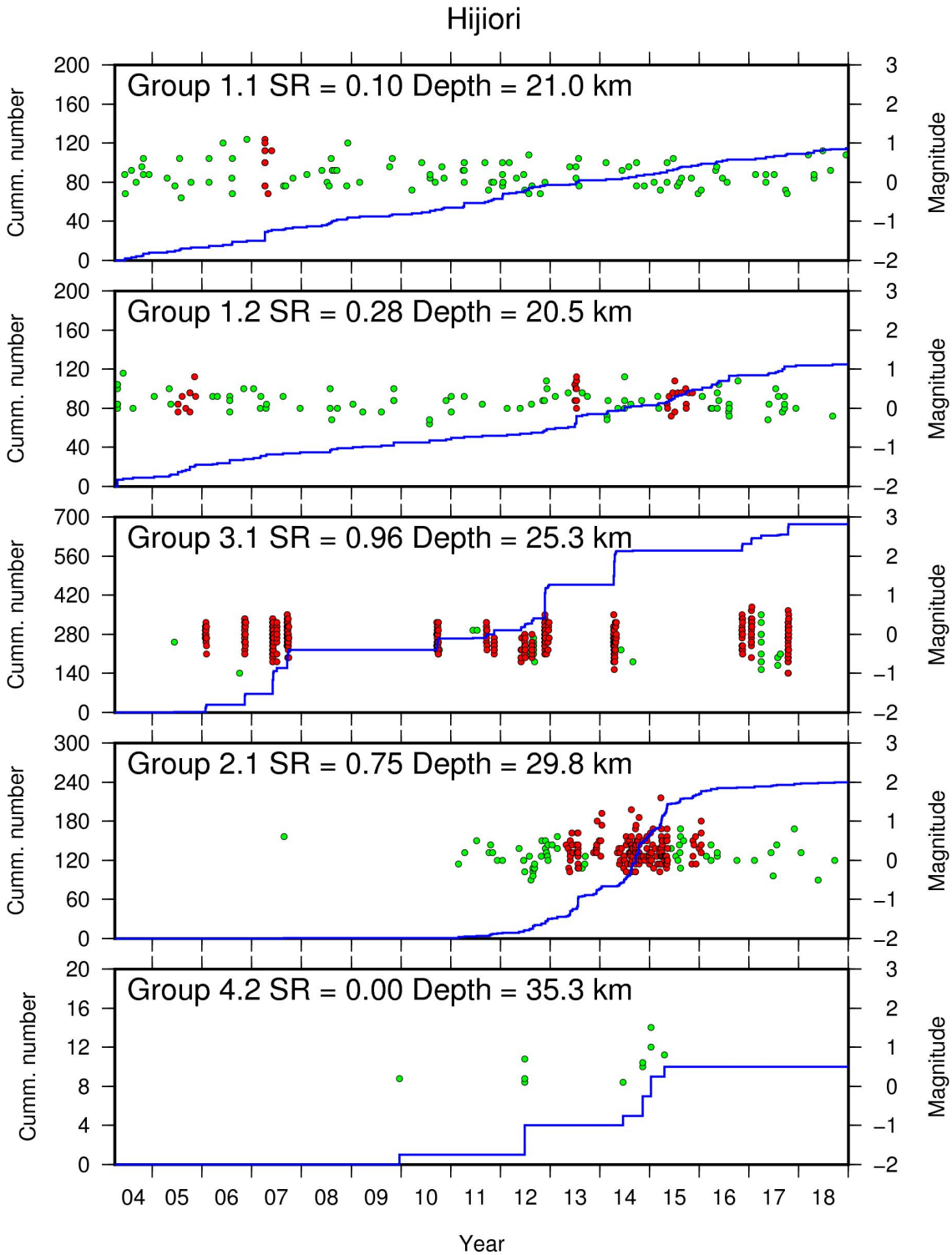

Figure 3.8 Cumulative number of DLF earthquakes from April 2004 and magnitude-time distributions in each group of Hijiori. Red circles show magnitudes of DLF earthquakes in swarms and green circles show those of DLF earthquakes not in swarms. Blue lines show cumulative numbers of DLF earthquakes (left axis). The four most major groups and Group 4.2 are plotted, and the groups are in order of depths.

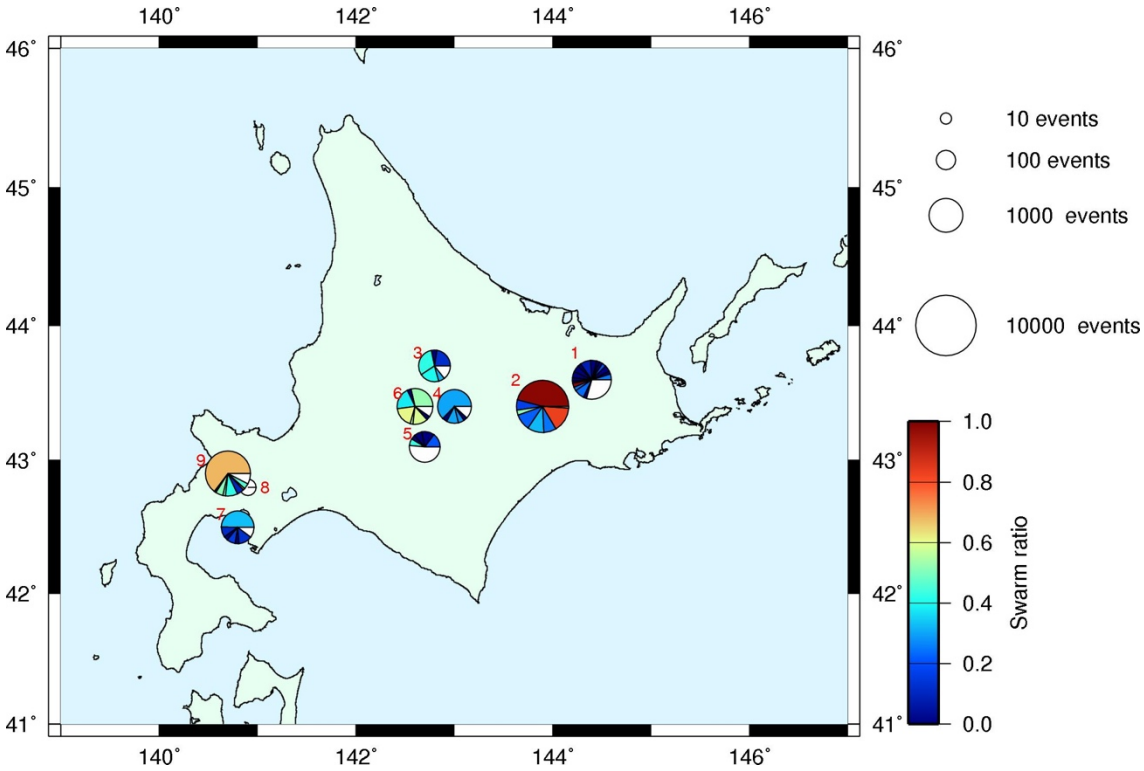

Figure 3.9 Swarm ratio (SR) at each region in the Hokkaido district. Sizes of circles show the number of DLF earthquakes detected by this study. Circles are divided into two-stages classified groups in proportion to the number of DLF earthquakes and colors show the SR values in each group. White parts mean the number of DLF earthquakes in the groups which include less than 30 events.

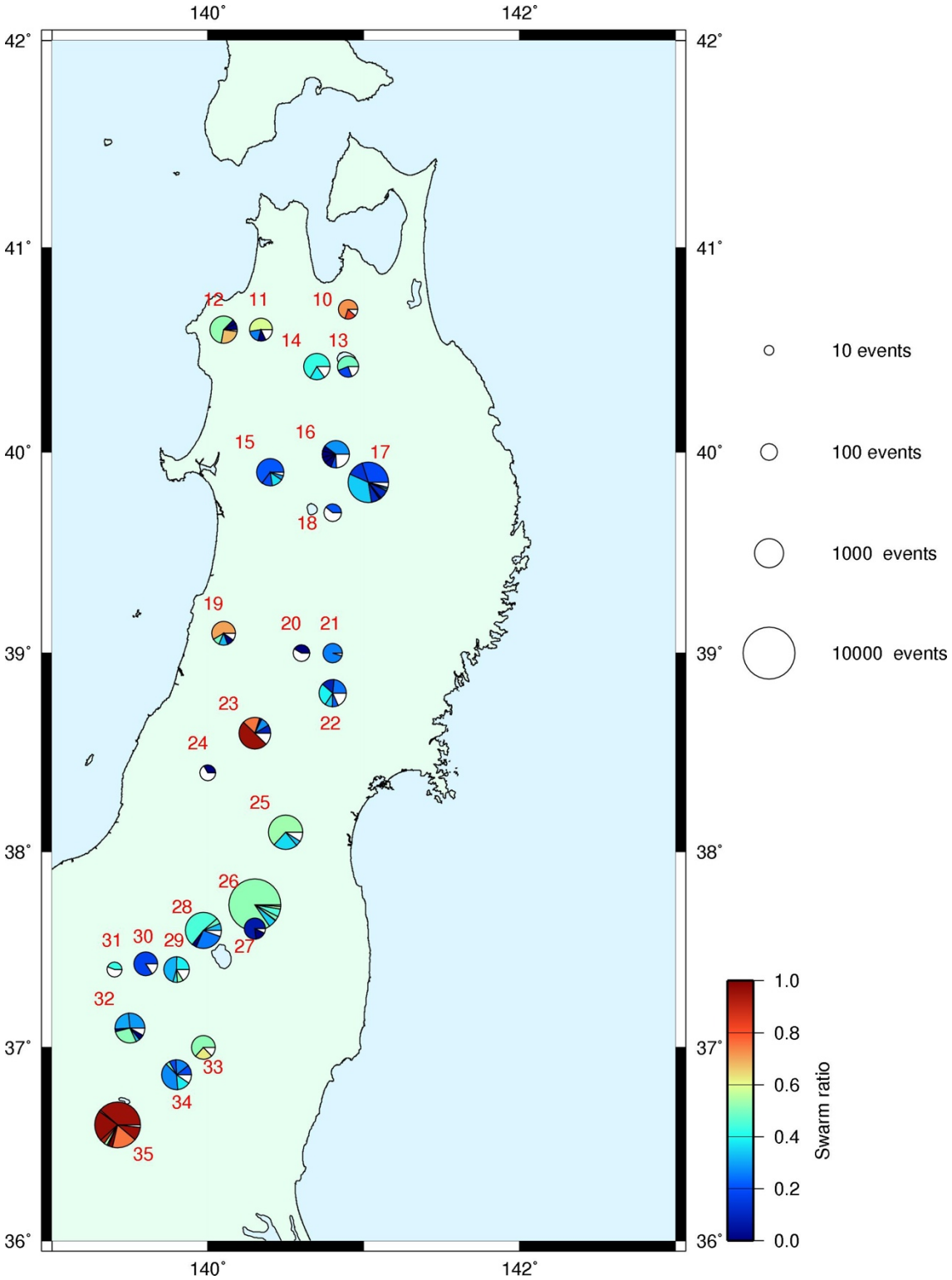

Figure 3.10 Same figure as Figure 3.9 but in the Tohoku district.

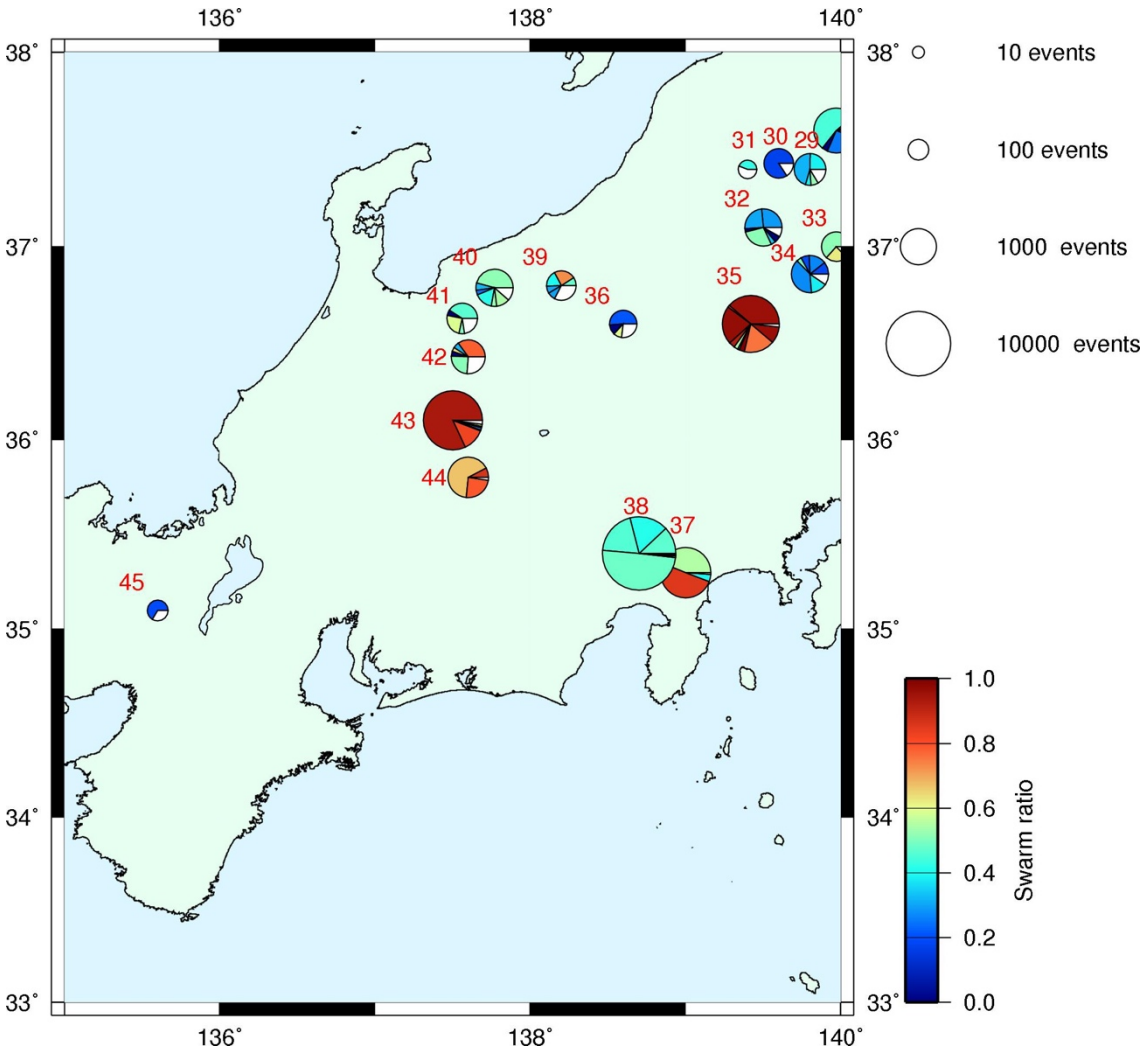

Figure 3.11 Same figure as Figure 3.9 but in the Chubu district.

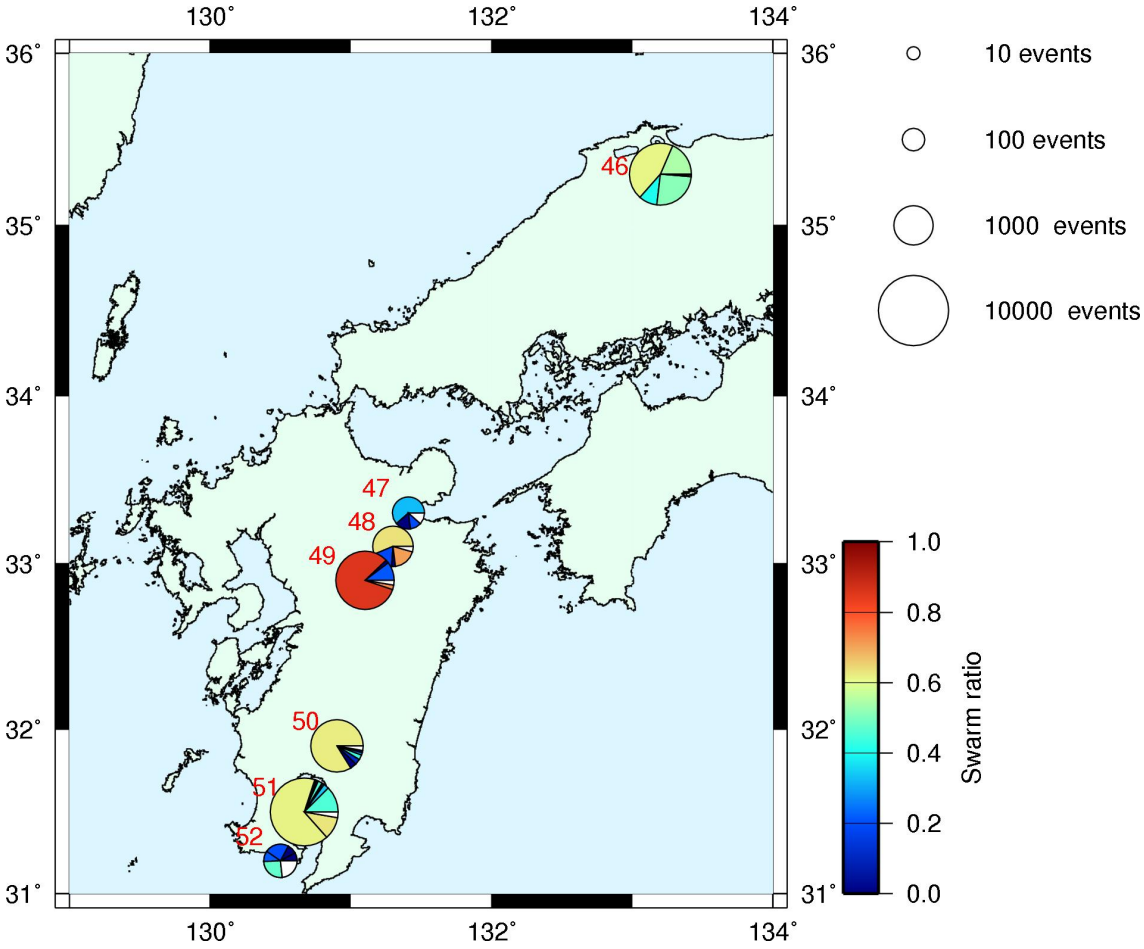

Figure 3.12 Same figure as Figure 3.9 but in the Kyushu district.

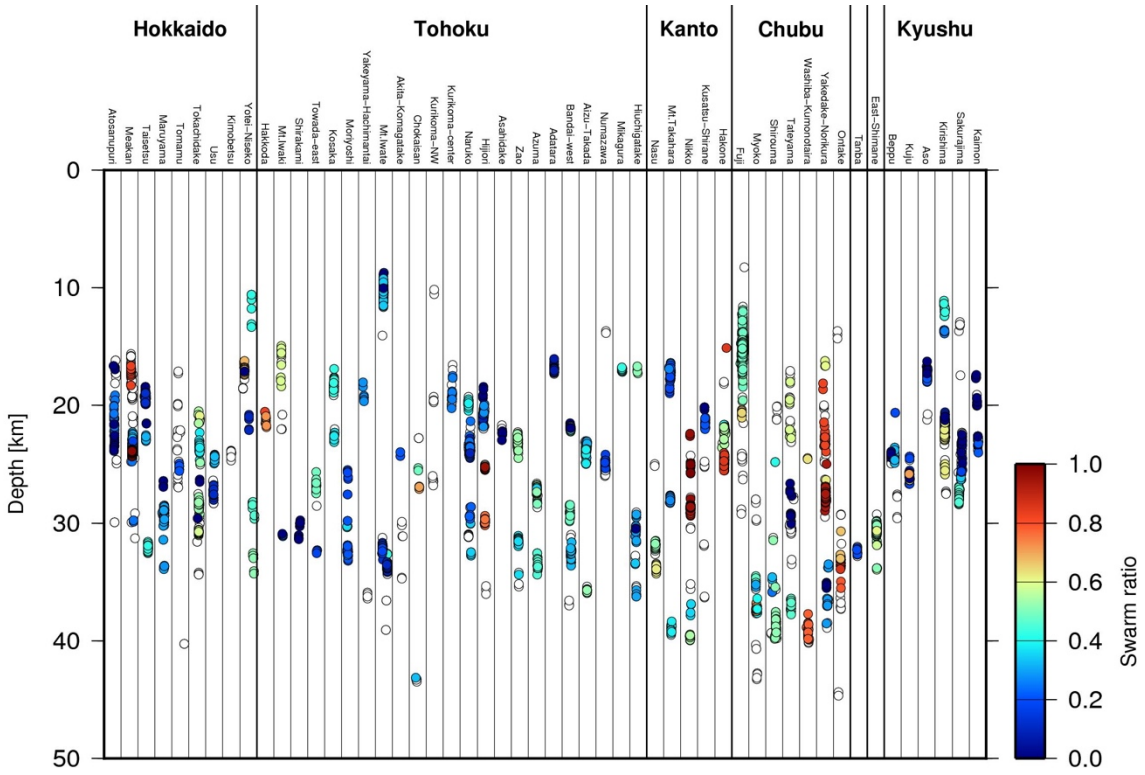

Figure 3.13 Relationship between swarm ratio and depth in each region. Each circle shows the relocated depth of the DLF earthquakes. The color shows the swarm ratio of the groups in which the DLF earthquakes are included.

3.3. Occurrence intervals of DLF earthquakes

Quasi-periodic DLF earthquakes occurred in Klyuchevskoy volcano group in Kamchatka, Russia (Frank et al., 2018). In the former section, episodic occurrences and constant occurrences of DLF earthquakes were found. Therefore, I tried to investigate the characteristics of intervals of DLF earthquakes all over Japan.

In Hijiori (No.23), episodic activities of DLF earthquakes were seen in the Group 2.1 and Group 3.1. In the groups, some DLF earthquakes occurred with very short intervals which are less than 100 seconds (Figure 3.14). In other words, continuous occurrence of DLF earthquakes, which are like tremor, were observed in the episodes of DLF earthquakes.

Quasi-periodic seismicities of DLF earthquakes were seen in some groups in some regions. In Group 1.1 of Yakedake (No.43), there are only few DLF earthquakes that occurred with short intervals of less than 100 seconds (Figure 3.15). In particular, DLF earthquakes did rarely occur with short intervals of less than 1000 seconds before

2014. This result means that there is the lowest limit interval of DLF earthquakes and the DLF earthquakes quasi-periodically occurred. In Hakone (No.37), very short intervals of DLF earthquakes were observed in Group1.1 and the lower limit of the intervals is seen (Figure 3.16). Across Japan, many DLF earthquakes occurred with intervals less than 100 seconds in some regions such as Yotei-Niseko (No.9), Fuji (No. 38), and east-Shimane (No.46), while quasi-periodic DLF earthquakes were observed in some regions such as Yakedake (No.43) and Sakurajima (No.51) (Figure 3.17).

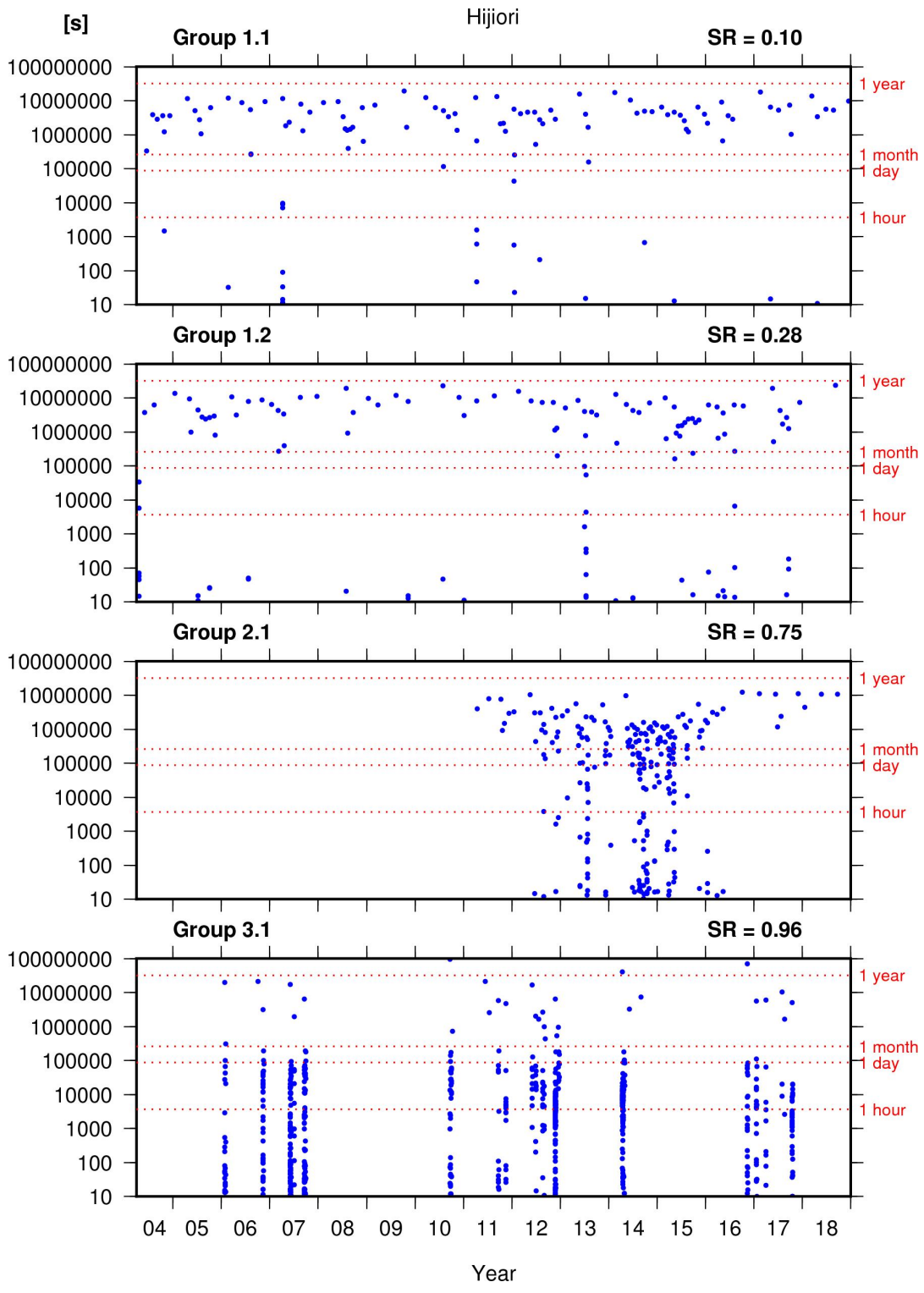

Figure 3.14 Intervals of DLF earthquakes from former earthquakes in the four two-stage groups in Hijiori. Blue dots show the occurrence time of DLF earthquakes and intervals from the former earthquake. Groups that include 100 or more DLF earthquakes are shown.

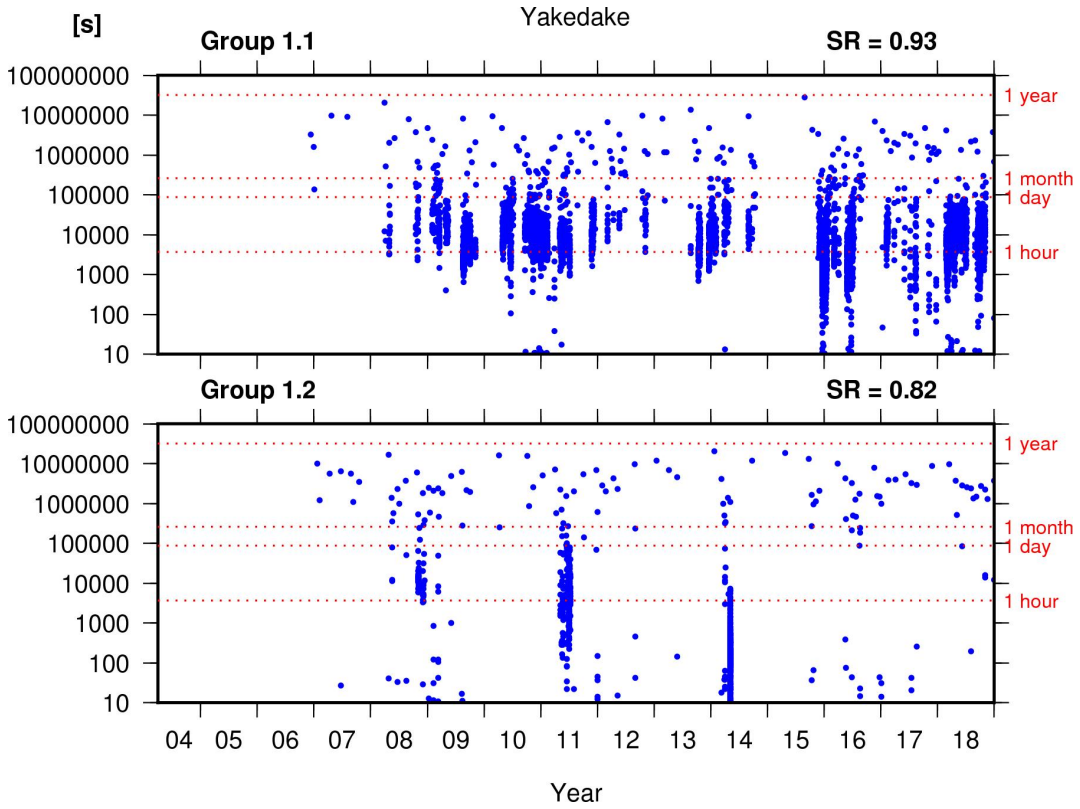

Figure 3.15 Same figure as Figure 3.14 but in Yakedake (No.43).

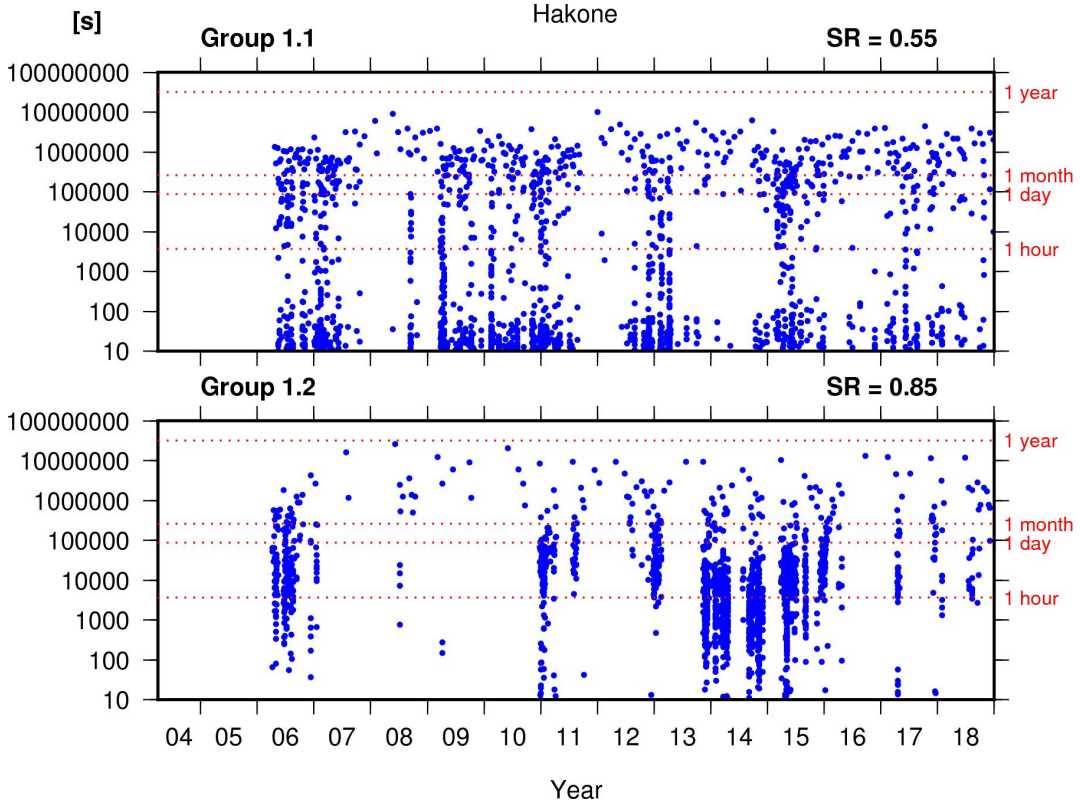

Figure 3.16 Same figure as Figure 3.14 but in Hakone (No.37).

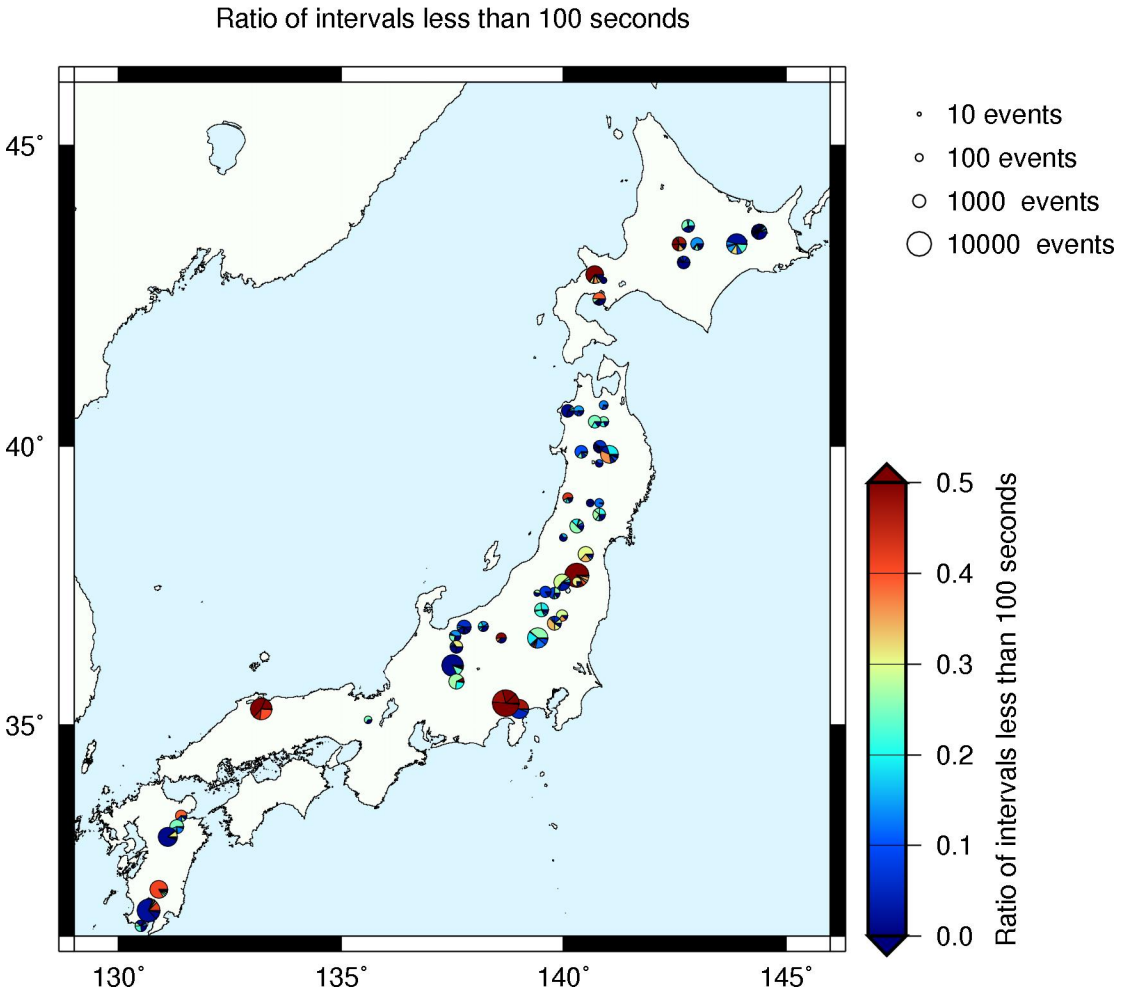

Figure 3.17 The ratio of DLF earthquakes with intervals shorter than 100 seconds of each group all over Japan. The colors of the groups show the ratios of DLF earthquakes with short intervals from the former earthquake less than 100 seconds. Low ratio of the short interval shows the quasi-periodic occurrence.

3.4. Magnitude-frequency distributions of DLF earthquakes

It is well known that magnitude-frequency distributions of regular earthquakes follow the Gutenberg-Richter law (Gutenberg & Richter, 1945). Magnitude-frequency distributions reflect the physical mechanisms of the earthquakes such as the characteristic size of the source. In volcanic regions, volcanic tremor does not follow the Gutenberg-Richter law and follow to exponential distribution (Benoit et al., 2003). In this section, I investigated whether magnitude-frequency distributions of DLF earthquakes follow the Gutenberg-Richter law or not. In addition, I calculated b-values of the Gutenberg-Richter

law in each group using the magnitude-frequency distributions. The data between magnitude 0.5 and 1 with intervals of 0.1 were used for the calculation in the JMA catalog, while data between magnitude 0 and 1 with intervals of 0.1 were used in the new catalog. When the number of DLF earthquakes above the magnitude range is less than 5, then the data were removed from the calculation of the b-value. When there is less than 5 earthquakes over magnitude 0.6 in the JMA catalog and magnitude 0.1 in the new catalog, then the b-value in the group is not defined.

As seen from the magnitude-frequency distributions of each group in Hijiori (No.23), the magnitude-frequency distributions of the groups follow the Gutenberg-Richter law (Figure 3.18). In Hijiori, b-value is the highest in Group 3.1 in which episodic DLF earthquakes occurred. In Yakedake, Group1.1 (No.43) shows very high b-value, 6.67 (Figure 3.19). In those cases, the maximum magnitudes of DLF earthquakes are lower than those of the other groups. The range of magnitudes of DLF earthquakes are narrow because large DLF do not occur and lower limit of DLF earthquakes is controlled by detection. Thus, high b-values and low maximum magnitudes means that small-size DLF earthquakes are concentrated in the groups. In all over Japan, there are some groups with very high b-values over 3.0 (Figure 3.20). The groups with high b-values are located in Nikko (No.35), Yakedake (No.43), Ontake (No.44), Kuju (No.48), and Aso (No.49). The distribution of the high b-value groups is similar to the distribution of high-SR groups.

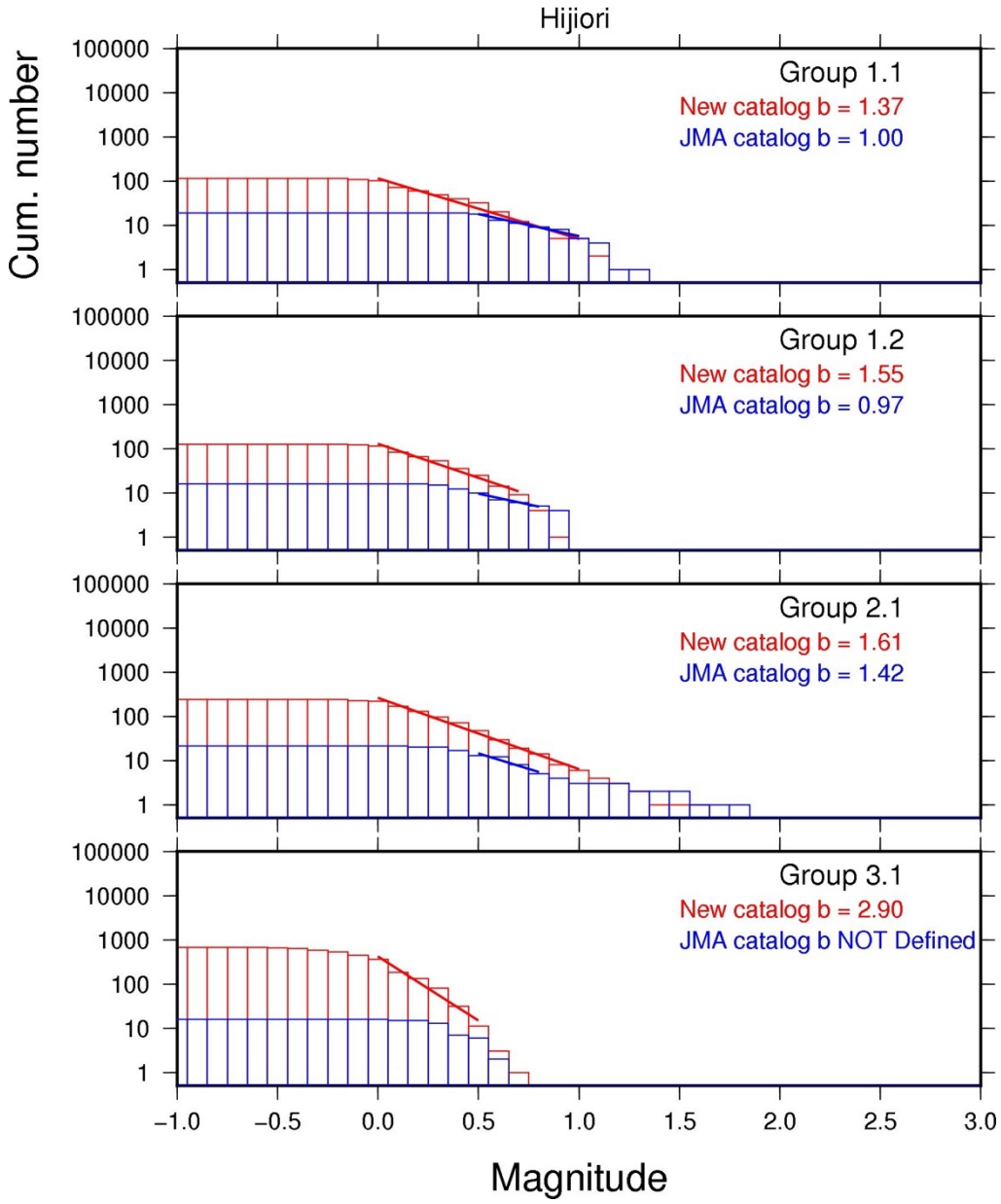

Figure 3.18 Magnitude-frequency distributions of DLF earthquakes of each group in Hijiori. Red boxes show the number of DLF earthquakes larger than the magnitudes in the new catalog obtained in this study. Blue boxes show the number of DLF earthquakes larger than the magnitudes in the JMA catalog. Red and blue lines are the fitting lines to calculate b-values.

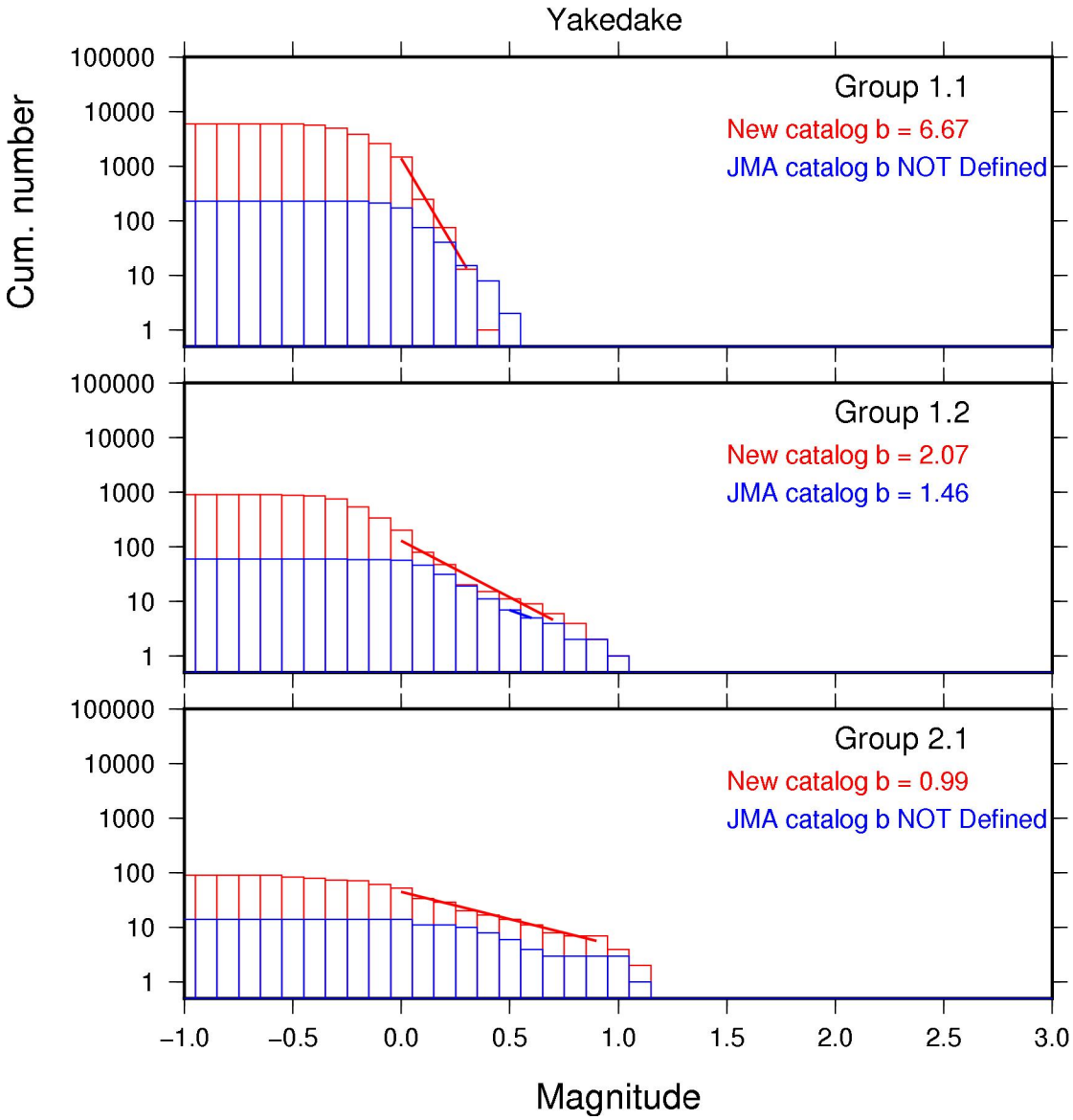

Figure 3.19 Magnitude-frequency distributions of DLF earthquakes of each group in Yakedake.

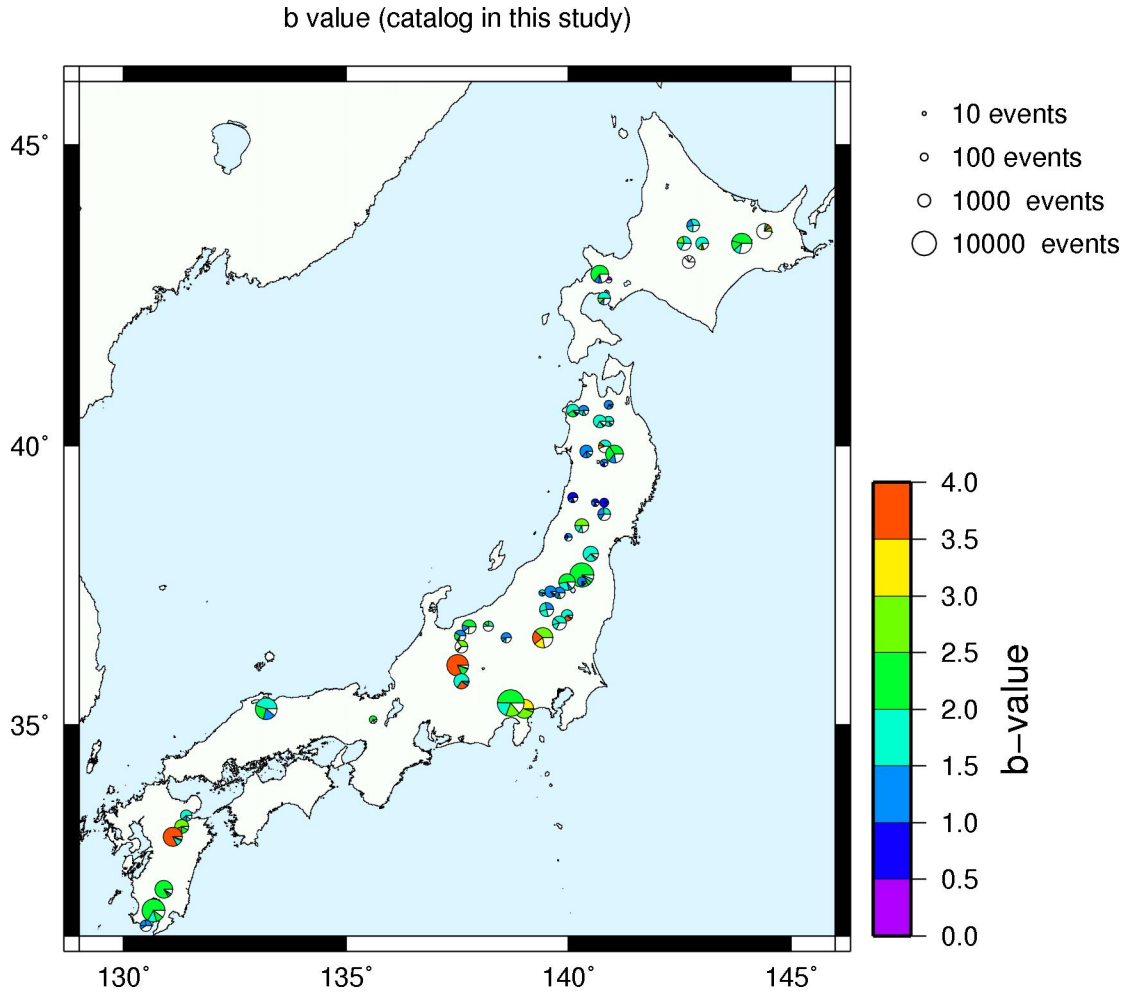

Figure 3.20 Distribution of b-value of each group all over Japan in the new catalog of DLF earthquakes. When the b-value is not defined in the group, the portion of the circle is filled in white.

3.5. Waveform characteristics of DLF earthquakes

In the former section, I showed the results of the spatio-temporal distributions and magnitude-frequency distribution of DLF earthquakes. DLF earthquakes were also known to have variety in the waveforms (e.g. Kosuga et al., 2017). In this section, I focused on the waveform characteristics of DLF earthquakes and calculated the amplitude ratios of S wave to P wave and amplitude ratio of different frequency bands.

Most newly detected DLF earthquakes do not have enough SN ratios for the analysis of waveforms. Then, I used the waveforms of DLF earthquakes in the JMA catalog. I used two indices characterizing observed seismograms of DLF earthquakes in order to compare the characteristics of the waveforms.

The first index is the amplitude ratio of S wave to P wave (PS ratio). This index is defined as the ratio of the average amplitudes of P wave to S waves in one representative station of each region (Yellow triangle in Figure 2.6 and Appendix). Average amplitudes of P and S waves are calculated for five seconds time-windows from arrival times of both waves. When the difference time between the arrival times of P and S waves is less than five seconds, then the time-window of the P wave is limited before the arrival of S wave.

It is difficult to estimate the dominant frequencies of DLF earthquakes from waveforms without any bandpass filter because SN ratios of DLF earthquakes are generally low. Thus, the second index is the spectral amplitude ratio for different frequency bands. First, the Fourier spectrum was calculated by the following equation.

$$S(i,t) = \sqrt{a^2 + b^2}$$

$$a = \int_{\tau=0s}^{\tau=5s} \left(v(t+\tau) \sin\left(2\pi f(i)(t+\tau)\right) \right) d\tau$$

$$b = \int_{\tau=0s}^{\tau=5s} \left(v(t+\tau) \cos\left(2\pi f(i)(t+\tau)\right) \right) d\tau$$

Here, i shows the label of frequency and t shows the occurrence time of the DLF earthquake. $f(i)$ is defined as

$$f(i) = 5 * 10^{(i-25)*0.04} \quad (1 \le i \le 50, i \in \mathbb{Z}).$$

Therefore, the frequency band from 0.5 to 50 Hz divided into 50 bands with logarithm intervals. Using data of spectrum, the spectrum ratio is defined as the ratio of the average amplitudes between 1–2 to 2–4 Hz bands in the 5 seconds time-windows after the arrival of S wave. The ratios were calculated by the ratio of average values in each band using horizontal components of the one representative station.

As a result, the characteristics of waveforms are different in each group in some regions. In Hijiori (No.23), DLF earthquakes of Group 3 have low PS ratios and DLF earthquakes of Group 2 have high PS ratios, respectively (Figure 3.21). In Kirishima (No.50), PS ratios of Group 1 are lower than those of Group 2 and the spectrum ratios of Group 1 are higher than those of Group 2 (Figure 3.22). As these examples, waveform characteristics are corresponding to the classification in some regions (see Appendix).

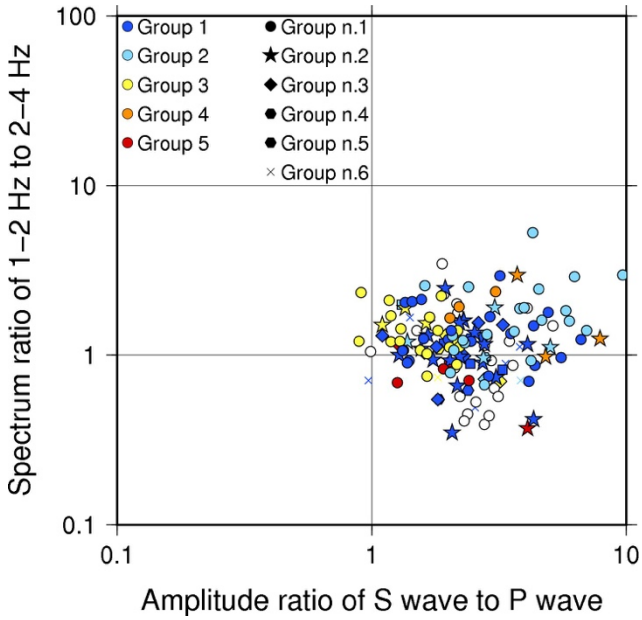

Figure 3.21 Amplitude ratio of S wave to P wave and spectrum ratio of 1–2 Hz to 2–4 Hz of each DLF earthquakes in the JMA catalog in Hijiori. Colors and symbols correspond to the two-stage groups, respectively.

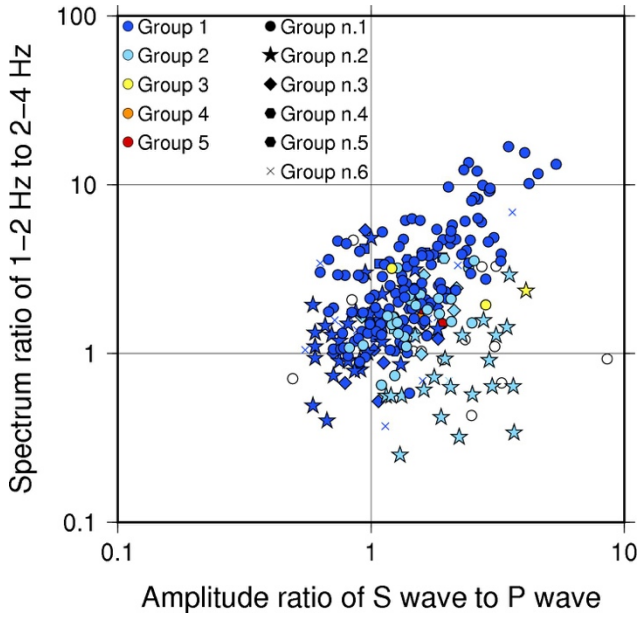

Figure 3.22 Same figure of Figure 3.21 but in Kirishima.

3.6. Discussion

In previous sections of this chapter, I demonstrated distribution, temporal activity pattern, magnitude-frequency distribution and waveform characteristics of DLF earthquakes of each group in each region. I found that DLF earthquakes are classified into some groups and there are groups in which DLF earthquakes episodically and constantly occur. In this section, I discuss the relationships between such parameters and the characteristics of DLF earthquakes. Eight parameters of each group are shown in Table 3.2.

Table 3.2 Eight parameters of DLF earthquakes of each group in each region. In this table, the groups including 30 or more DLF earthquakes in the new catalog are shown.

Region	Group[1]	DLFs in the JMA catalog[2]	DLFs in the new catalog[3]	Depth [km][4]	Swarm ratio (SR)	Average CC[5]	b-value	Spectrum ratio (1-2Hz)/(2-4 Hz)[6]	PS ratio[6]
Atosanupuri	1.1	21	80	21.1	0.25	4.1	1.14	0.76	1.23
Atosanupuri	1.2	12	41	21.9	0.00	4.8	0.90	0.74	1.33
Atosanupuri	1.3	6	90	18.2	0.00	4.6	1.31	1.17	1.22
Atosanupuri	1.5	4	53	22.5	0.21	4.9	1.89	0.54	1.67
Atosanupuri	2.1	12	48	23.1	0.00	5.1	0.77	0.51	1.55
Atosanupuri	2.2	3	38	23.1	0.00	5.4	1.18	0.33	1.80
Atosanupuri	19	1	87	--	0.00	--	2.33	0.58	1.15
Atosanupuri	28	1	144	--	0.08	--	2.67	1.95	1.15
Atosanupuri	30	1	45	--	0.00	--	2.34	0.91	0.94
Atosanupuri	35	1	95	--	0.00	--	2.32	0.43	2.47
Atosanupuri	64	1	86	--	0.00	--	2.20	0.45	1.01
Atosanupuri	68	1	47	--	0.00	--	2.41	0.57	1.05
Atosanupuri	74	1	30	--	0.00	--	1.33	0.31	1.63
Atosanupuri	75	1	58	--	0.98	--	2.95	0.74	1.48
Atosanupuri	80	1	52	--	0.25	--	1.93	0.50	1.08
Atosanupuri	83	1	140	--	0.24	--	4.12	1.98	0.98
Atosanupuri	84	1	45	--	0.00	--	2.34	0.77	0.90
Meakan	1.1	262	2530	23.9	0.98	7.7	2.39	3.28	1.64
Meakan	1.2	75	354	23.3	0.17	5.1	1.49	1.12	2.82
Meakan	1.3	78	169	23.6	0.51	4.6	1.57	1.17	2.10
Meakan	1.4	131	558	23.2	0.22	4.0	1.62	1.37	1.71
Meakan	1.5	170	564	23.1	0.32	3.5	1.71	1.99	1.74
Meakan	1.6	292	425	23.4	0.25	2.9	2.00	1.44	1.89

Meakan	2.1	67	851	17.0	0.83	6.4	2.02	2.19	1.90
Taisetsu	1.1	47	171	19.3	0.12	4.3	1.47	1.15	2.03
Taisetsu	1.2	10	43	19.7	0.00	4.3	1.10	1.23	2.02
Taisetsu	2.1	43	235	31.9	0.42	5.4	1.86	0.85	1.76
Taisetsu	2.3	5	152	32.3	0.40	5.2	1.78	0.54	1.98
Taisetsu	3.1	10	47	22.8	0.00	7.1	1.31	1.13	1.66
Maruyama	1.1	73	587	29.1	0.30	4.7	1.83	0.89	1.37
Maruyama	1.3	5	44	29.0	0.00	6.4	1.59	1.23	1.44
Maruyama	2.1	12	106	33.8	0.30	7.7	2.73	0.83	1.29
Maruyama	2.2	3	53	33.6	0.28	9.1	3.98	1.14	1.32
Maruyama	3.1	4	34	26.6	0.00	8.2	3.42	1.66	1.54
Tomamu	1.1	6	101	25.2	0.21	6.5	--	1.64	1.80
Tomamu	17	2	92	--	0.00	--	--	2.41	1.52
Tomamu	18	2	58	--	0.00	--	--	1.59	2.60
Tomamu	31	1	32	--	0.00	--	--	1.11	1.68
Tomamu	33	1	49	--	0.00	--	--	1.49	1.01
Tokachidake	1.1	107	354	28.4	0.53	4.4	1.61	0.73	1.73
Tokachidake	1.3	12	44	28.4	0.00	4.3	1.29	0.65	1.76
Tokachidake	2.1	65	247	23.6	0.38	5.6	2.55	0.37	2.26
Tokachidake	2.2	32	230	21.2	0.61	7.1	1.93	0.47	1.81
Tokachidake	2.3	9	31	21.1	0.00	5.9	1.01	0.43	2.08
Tokachidake	3.1	45	167	30.7	0.59	6.4	1.76	0.53	2.18
Tokachidake	3.6	2	45	--	0.00	8.9	1.26	1.84	2.42
Usu	1.1	30	413	24.5	0.33	7.4	1.93	1.88	2.61
Usu	1.2	33	85	27.4	0.12	4.0	1.21	1.42	2.04
Usu	1.7	3	34	--	0.00	5.7	1.65	1.21	1.68
Usu	1.12	1	70	--	0.16	--	5.44	2.16	0.90
Usu	2.1	2	32	--	0.00	6.0	1.08	10.55	1.73
Usu	14	1	112	--	0.12	--	2.68	3.55	0.92
Yotei_Niseko	1.1	41	1990	16.9	0.68	6.7	2.25	2.64	1.69
Yotei_Niseko	1.4	6	43	17.2	0.00	6.7	0.96	0.76	2.54
Yotei_Niseko	2.1	36	163	33.2	0.52	4.7	1.04	1.96	1.89
Yotei_Niseko	2.2	17	59	28.6	0.46	4.9	0.95	2.31	2.04
Yotei_Niseko	3.1	27	268	11.7	0.42	4.4	1.44	2.84	2.25
Yotei_Niseko	4.1	8	155	21.4	0.10	8.7	1.34	2.52	2.81
Yotei_Niseko	27	1	42	--	0.00	--	3.11	1.15	1.09
Yotei_Niseko	29	1	124	--	0.45	--	0.79	3.67	0.60
Hakkoda	1.1	17	146	21.3	0.72	5.2	1.40	1.33	2.63
Hakkoda	1.2	5	39	21.0	0.00	5.1	1.15	1.20	2.10

Mt.Iwaki	1.1	17	189	16.3	0.59	5.3	1.32	1.17	1.66
Mt.Iwaki	3.1	4	66	31.0	0.26	8.5	1.83	3.12	3.72
Mt.Iwaki	3.2	1	40	30.9	0.00	--	1.85	2.20	2.75
Shirakami	1.1	8	58	30.3	0.00	7.0	0.91	2.37	1.73
Shirakami	1.2	3	42	31.2	0.00	6.8	1.03	1.13	1.59
Shirakami	1.3	2	468	--	0.52	5.8	1.79	1.34	1.49
Shirakami	7	1	202	--	0.67	--	2.03	1.69	1.25
Towada_east	1.1	22	149	26.7	0.49	6.5	1.92	1.43	3.11
Towada_east	2.1	3	66	32.4	0.18	8.4	1.91	0.94	2.58
Kosaka	1.1	27	461	18.3	0.43	7.1	1.78	2.21	1.34
Kosaka	2.1	20	126	22.7	0.38	6.1	1.80	1.28	1.67
Moriyoshi	1.1	56	501	32.2	0.21	4.5	1.02	2.64	2.56
Moriyoshi	1.2	16	99	26.3	0.19	5.3	1.36	2.83	2.70
Moriyoshi	1.3	10	101	31.1	0.37	4.8	1.49	3.06	1.73
Moriyoshi	1.7	2	41	29.8	0.00	3.9	1.40	3.53	1.16
Yakeyama_Hachimantai	1.1	28	297	19.1	0.28	4.8	1.97	3.09	1.73
Yakeyama_Hachimantai	1.3	4	47	--	0.00	5.1	2.05	2.83	2.13
Yakeyama_Hachimantai	6	1	57	--	0.00	--	3.11	2.37	1.87
Yakeyama_Hachimantai	17	1	52	--	0.00	--	2.38	2.84	1.18
Yakeyama_Hachimantai	25	1	64	--	0.00	--	3.62	4.58	0.61
Yakeyama_Hachimantai	27	1	48	--	0.00	--	1.88	5.45	1.03
Mt.Iwate	1.1	164	1065	32.1	0.19	4.1	2.03	1.26	1.81
Mt.Iwate	1.2	22	474	32.2	0.14	4.3	1.44	1.95	1.80
Mt.Iwate	2.1	117	1216	10.3	0.34	4.5	2.28	1.05	1.57
Mt.Iwate	2.2	13	238	9.7	0.11	4.3	1.04	1.96	1.63
Mt.Iwate	2.9	3	59	9.4	0.00	4.3	0.85	1.55	1.79
Mt.Iwate	3.1	54	251	33.7	0.11	4.9	1.70	1.44	1.90
Mt.Iwate	3.2	23	48	33.6	0.00	4.2	1.79	1.21	1.43
Mt.Iwate	51	1	58	32.3	0.26	--	1.83	0.68	0.98
Akita-Komagatake	1.1	10	47	24.1	0.00	7.5	1.19	1.69	2.13
Chokaisan	1.1	6	239	27.0	0.70	8.8	0.93	1.43	2.22
Chokaisan	1.2	2	41	25.4	0.00	11.3	0.85	1.17	2.39
Chokaisan	2.2	2	49	43.1	0.00	9.0	1.10	4.99	1.78
Chokaisan	4	1	39	--	0.00	--	0.71	0.24	4.19
Kurikoma_NW	3.1	2	42	--	0.00	8.8	0.65	6.96	2.02
Kurikoma_center	1.1	41	183	19.0	0.26	5.5	0.87	2.38	2.30
Naruko	1.1	77	176	23.7	0.24	4.1	1.04	2.20	1.57
Naruko	1.2	34	112	23.7	0.09	4.3	1.35	2.13	1.69
Naruko	2.1	39	203	19.9	0.39	4.9	1.96	1.28	1.37

Naruko	3.1	16	66	32.0	0.35	5.2	1.01	2.38	1.38
Naruko	4.1	11	54	29.4	0.22	6.0	0.92	2.03	1.23
Hijiori	1.1	21	115	21.0	0.10	3.9	1.37	1.30	2.50
Hijiori	1.2	17	125	20.5	0.28	4.2	1.55	0.99	2.28
Hijiori	1.3	7	31	18.9	0.00	5.2	1.16	1.10	1.97
Hijiori	2.1	21	240	29.8	0.75	5.6	1.61	1.63	3.59
Hijiori	3.1	17	674	25.3	0.96	10.0	2.90	1.34	1.51
Asahidake	2.1	5	31	22.6	0.00	5.7	1.14	1.28	3.90
Zao	1.1	81	1201	23.2	0.53	4.2	1.79	2.22	1.51
Zao	2.1	28	437	31.6	0.36	8.0	1.59	1.10	1.90
Zao	2.5	1	94	--	0.34	--	1.69	2.29	1.36
Azuma	1.1	252	8385	27.2	0.52	10.3	2.14	3.11	2.64
Azuma	1.2	26	491	27.2	0.35	9.7	2.15	1.62	1.88
Azuma	1.6	4	30	27.3	0.00	8.8	2.04	3.37	1.78
Azuma	1.18	5	263	28.3	0.50	10.6	2.45	1.41	2.90
Azuma	2.1	35	483	33.6	0.45	5.7	1.97	2.97	2.05
Azuma	2.4	2	165	--	0.55	5.2	5.44	3.19	1.12
Adatara	1.1	29	200	16.9	0.07	4.8	1.17	3.23	1.39
Adatara	1.2	8	42	17.1	0.00	4.8	0.58	4.90	2.03
Bandai_west	1.1	33	141	32.5	0.33	4.2	1.22	1.73	2.30
Bandai_west	1.2	31	112	29.1	0.48	4.8	1.46	1.20	2.30
Bandai_west	2.1	25	1181	22.0	0.45	6.3	2.31	2.00	2.46
Bandai_west	2.2	11	93	21.9	0.00	6.6	1.00	1.46	2.62
Bandai_west	2.4	1	576	--	0.25	--	1.56	6.05	1.37
Aizu_Takada	1.1	33	150	23.8	0.39	4.7	1.12	1.41	2.65
Aizu_Takada	1.2	16	276	23.4	0.32	5.4	1.22	2.90	3.74
Aizu_Takada	1.3	9	34	24.3	0.00	5.3	0.66	1.40	2.39
Aizu_Takada	2.1	12	46	35.7	0.00	8.1	2.36	0.79	2.38
Numazawa	1.1	16	378	24.9	0.17	6.4	1.37	3.07	2.39
Mikagura	1.1	9	33	17.0	0.00	7.3	1.70	1.10	1.97
Hiuchigatake	1.1	27	288	30.6	0.29	4.7	1.54	3.98	2.04
Hiuchigatake	1.2	17	266	33.5	0.30	4.7	1.60	3.55	1.88
Hiuchigatake	1.3	4	32	30.5	0.00	4.4	1.50	1.81	1.96
Hiuchigatake	2.1	8	304	17.0	0.51	7.4	1.43	3.68	1.78
Hiuchigatake	3	2	44	33.4	0.00	--	1.90	2.24	1.70
Hiuchigatake	7	1	63	--	0.00	--	1.57	5.45	2.70
Nasu	1.1	37	274	31.9	0.51	6.4	1.77	1.70	2.27
Nasu	2.1	13	103	33.8	0.62	6.3	4.54	0.64	1.68
Mt.Takahara	1.1	44	122	17.6	0.19	4.5	2.14	1.01	1.79

Mt.Takahara	1.2	24	173	17.1	0.27	4.1	1.51	1.43	2.44
Mt.Takahara	1.3	14	83	18.1	0.19	4.5	1.66	1.28	2.20
Mt.Takahara	1.4	15	49	17.3	0.00	4.3	0.97	0.99	2.35
Mt.Takahara	2.1	64	446	28.0	0.27	6.2	1.98	1.20	3.52
Mt.Takahara	3.1	21	162	38.9	0.38	6.4	1.62	2.37	3.43
Nikko	1.1	54	2250	28.7	0.96	7.1	2.52	0.70	2.80
Nikko	1.2	6	69	28.8	0.83	6.4	1.66	0.65	3.58
Nikko	1.4	4	1268	28.4	0.97	6.3	7.45	0.69	2.20
Nikko	1.5	3	196	29.1	0.92	8.5	2.25	0.14	4.08
Nikko	2.1	23	132	39.7	0.55	6.1	1.36	0.93	4.19
Nikko	2.2	7	56	37.3	0.36	6.5	--	0.53	2.12
Nikko	3.1	14	178	25.3	1.00	8.1	7.23	0.49	1.28
Nikko	6	2	1015	22.5	0.75	--	3.22	2.26	2.97
Nikko	7	2	549	22.5	0.96	--	3.96	1.52	1.90
Kusatsu_Shirane	1.1	11	167	21.6	0.21	6.3	1.20	3.49	1.07
Kusatsu_Shirane	1.2	4	39	20.2	0.00	9.4	1.02	1.94	1.05
Kusatsu_Shirane	4.2	2	32	--	0.00	5.7	1.53	3.39	1.29
Hakone	1.1	127	1601	22.1	0.55	5.0	2.66	2.19	1.43
Hakone	1.2	77	1838	24.5	0.85	4.9	3.45	1.65	1.72
Hakone	1.3	10	169	23.0	0.40	4.5	2.65	3.09	1.74
Fuji	1.1	47	1941	15.3	0.47	10.4	1.91	0.73	2.91
Fuji	1.2	122	2754	15.0	0.41	7.8	2.59	0.89	3.35
Fuji	1.3	225	3173	14.9	0.46	5.0	1.99	0.95	2.88
Fuji	1.4	651	8025	15.0	0.48	3.1	2.20	1.02	2.63
Fuji	1.5	31	110	15.6	0.50	2.9	2.95	0.54	2.47
Fuji	1.6	15	30	15.0	0.00	3.5	0.44	0.63	1.95
Fuji	1.7	20	44	15.3	0.00	3.0	1.69	1.48	2.55
Fuji	2.1	6	45	20.6	0.00	12.1	2.26	0.31	2.60
Myoko	1.1	13	38	34.9	0.00	4.7	1.51	1.08	1.36
Myoko	1.2	14	99	37.2	0.73	5.1	1.73	1.00	1.46
Myoko	3.1	7	75	37.2	0.40	7.0	2.47	1.44	2.24
Myoko	4.1	4	33	35.3	0.00	7.2	1.16	0.81	1.81
Myoko	7	2	37	--	0.00	--	1.14	2.12	1.27
Shirouma	1.1	64	505	38.6	0.52	4.3	2.00	1.00	2.10
Shirouma	2.1	8	71	34.7	0.32	5.4	1.27	1.58	0.98
Shirouma	3.1	3	45	35.9	0.00	6.8	1.33	1.28	2.50
Shirouma	4	2	175	24.8	0.42	--	1.39	5.15	1.22
Shirouma	40	1	52	--	0.52	--	--	1.22	1.20
Shirouma	45	1	129	--	0.54	--	--	1.31	1.30

Tateyama	1.1	37	209	37.0	0.46	4.7	1.41	2.27	1.75
Tateyama	1.2	24	30	28.4	0.00	4.4	0.91	1.76	1.67
Tateyama	2.1	14	127	21.5	0.59	5.9	2.33	3.25	1.96
Tateyama	41	1	30	--	0.00	--	1.04	2.09	1.79
Washiba_Kumonotaira	1.1	45	270	39.1	0.78	4.9	2.50	3.06	1.71
Washiba_Kumonotaira	1.2	8	44	39.0	0.00	4.5	2.08	2.98	1.42
Washiba_Kumonotaira	2.2	9	30	24.5	0.00	4.4	2.09	2.11	1.71
Washiba_Kumonotaira	4	2	36	--	0.00	--	1.46	2.93	1.81
Washiba_Kumonotaira	30	1	188	--	0.51	--	--	3.28	2.08
Yakedake	1.1	234	5945	27.5	0.93	6.6	6.67	2.15	0.94
Yakedake	1.2	59	888	22.9	0.82	6.7	2.07	4.14	1.98
Yakedake	1.8	3	37	26.9	0.00	5.5	--	1.76	1.03
Yakedake	2.1	14	90	35.9	0.29	6.3	0.99	2.43	1.45
Yakedake	3.1	9	57	35.3	0.00	9.1	--	2.87	1.40
Yakedake	4.1	4	83	16.4	0.60	9.2	1.61	4.22	2.58
Ontake	1.1	20	115	33.4	0.86	8.9	1.11	2.52	2.10
Ontake	1.2	15	987	32.8	0.67	7.2	1.86	1.48	2.68
Ontake	1.4	2	363	35.3	0.79	6.5	9.03	1.28	1.87
Tanba	1.1	13	71	32.5	0.20	5.9	2.42	1.09	2.30
East-Shimane	1.1	96	1140	30.3	0.54	10.1	1.36	0.73	1.72
East-Shimane	1.2	235	2770	30.5	0.61	8.2	1.85	1.48	1.96
East-Shimane	1.3	171	593	30.2	0.40	6.2	1.48	0.77	1.64
East-Shimane	1.4	504	1574	30.5	0.51	3.9	2.01	1.29	1.49
East-Shimane	1.6	12	52	32.1	0.58	3.4	3.81	1.24	1.24
Beppu	1.1	21	276	24.4	0.33	6.9	1.56	1.06	1.64
Beppu	2.1	11	70	24.2	0.00	6.7	1.03	1.53	3.36
Beppu	4	2	51	20.6	0.20	--	1.82	0.62	1.00
Kuju	1.1	18	651	26.2	0.63	9.0	2.50	0.59	0.87
Kuju	1.2	8	203	25.3	0.19	7.1	2.38	1.39	1.69
Kuju	1.3	5	36	25.9	0.00	6.6	1.73	0.88	1.32
Kuju	2	2	215	25.8	0.71	--	3.92	0.75	1.80
Aso	1.1	55	470	17.7	0.21	4.4	1.79	1.39	1.38
Aso	1.2	25	83	17.1	0.00	4.6	1.50	0.86	1.73
Aso	3	2	3774	--	0.85	--	3.78	2.03	1.47
Aso	4	1	114	--	0.73	--	2.06	2.00	0.96
Kirishima	1.1	128	2486	22.4	0.62	4.2	2.01	2.90	1.52
Kirishima	1.2	30	117	21.3	0.00	4.6	2.08	1.29	0.90
Kirishima	1.4	7	103	20.7	0.11	4.7	1.96	1.87	1.30
Kirishima	2.1	24	89	11.7	0.43	4.2	2.33	1.64	1.48

Kirishima	2.2	21	46	13.2	0.00	4.3	1.33	0.73	2.18
Kirishima	21	1	38	--	0.00	--	2.02	4.67	0.85
Sakurajima	1.1	151	1085	27.8	0.45	5.0	1.93	0.96	2.22
Sakurajima	2.1	11	218	26.1	0.34	8.4	1.52	2.43	1.85
Sakurajima	2.2	7	68	25.6	0.18	7.7	1.11	1.39	1.86
Sakurajima	3.1	13	36	23.6	0.00	5.6	0.91	1.43	1.54
Sakurajima	4.1	12	174	27.1	0.45	9.4	1.97	1.50	2.05
Sakurajima	5.1	6	40	23.6	0.00	8.7	2.15	0.62	1.57
Sakurajima	7.1	5	37	22.9	0.00	7.6	1.17	3.85	1.75
Sakurajima	9.1	4	30	25.0	0.00	8.1	2.05	1.66	1.45
Sakurajima	10.1	2	44	--	0.00	7.1	1.88	2.58	1.28
Sakurajima	47	1	5775	--	0.61	--	2.37	2.64	1.21
Sakurajima	54	1	926	--	0.63	--	2.20	5.19	2.95
Kaimon	1.1	18	40	22.9	0.00	5.2	0.79	0.87	2.29
Kaimon	1.2	19	45	19.0	0.00	4.2	0.60	2.10	1.64
Kaimon	1.3	3	115	--	0.20	4.1	1.22	3.34	1.16
Kaimon	2.1	15	51	23.2	0.22	6.6	1.00	1.30	2.17
Kaimon	2.2	6	129	22.9	0.47	7.2	1.25	2.02	2.15

1) Group names of the two-stage classification.

2) Number of the DLF earthquakes in the JMA catalog between April 2004 and December 2015.

3) Number of the earthquakes in the new catalog between April 2004 and December 2018.

4) The depth column shows the average of the relocated location of DLF earthquakes in the group. There are no relocated DLF earthquakes, there is no data in the column of depth.

5) Average correlation coefficient values of each pair of DLF earthquakes in the group.

6) Spectrum ratios of 1–2 Hz to 2–4 Hz and PS ratios show the geometric mean values of those of all DLF earthquakes in the group.

3.6.1. Relationship between properties of activities and waveforms

Distributions of the groups with high swarm ratios (SR) and those with high b-values are similar (Figure 3.9–Figure 3.12, Figure 3.20). In addition, Group 3 of Hijiori with high SR shows high correlation coefficients (CCs) between pairs of two DLF earthquakes (Figure 3.3). Therefore, I investigated the relationships between each pair of the three parameters.

SR and b-value in the group have a positive correlation (Figure 3.23). In other

words, many small DLF earthquakes episodically occur and large DLF earthquakes rarely occur in the group with high SR. Therefore, this may mean that episodic DLF earthquakes mostly consist of DLF earthquakes with small magnitudes. The sources of such groups may mostly be small.

SR and average CC have also positive correlation (Figure 3.24). The average CC in the group of DLF earthquakes are calculated by following equation

$$\overline{\mathrm{CC}_2\_\mathrm{group}}\left(G_{i,j}\right)=\frac{1}{n^2}\sum_{p\subset G_{i,j}}\sum_{q\subset G_{i,j}}\mathrm{CC}_2\left(p,q\right)$$

Here, n means the number of DLF earthquakes in the group i,j. The positive correlation means that episodic DLF earthquakes have similar waveforms. Waveforms and magnitudes of constant DLF earthquakes are not similar even in the same groups. The hypocenters or the mechanisms of DLF earthquakes may be a little different in the groups of constant DLF earthquakes. In fact, constant DLF earthquakes of Group 1 in Hijiori (No. 23) have horizontal spread of about 2 km for relocated hypocenters, while groups of episodic DLF earthquakes have just dot-like relocated hypocenters (Figure 3.1).

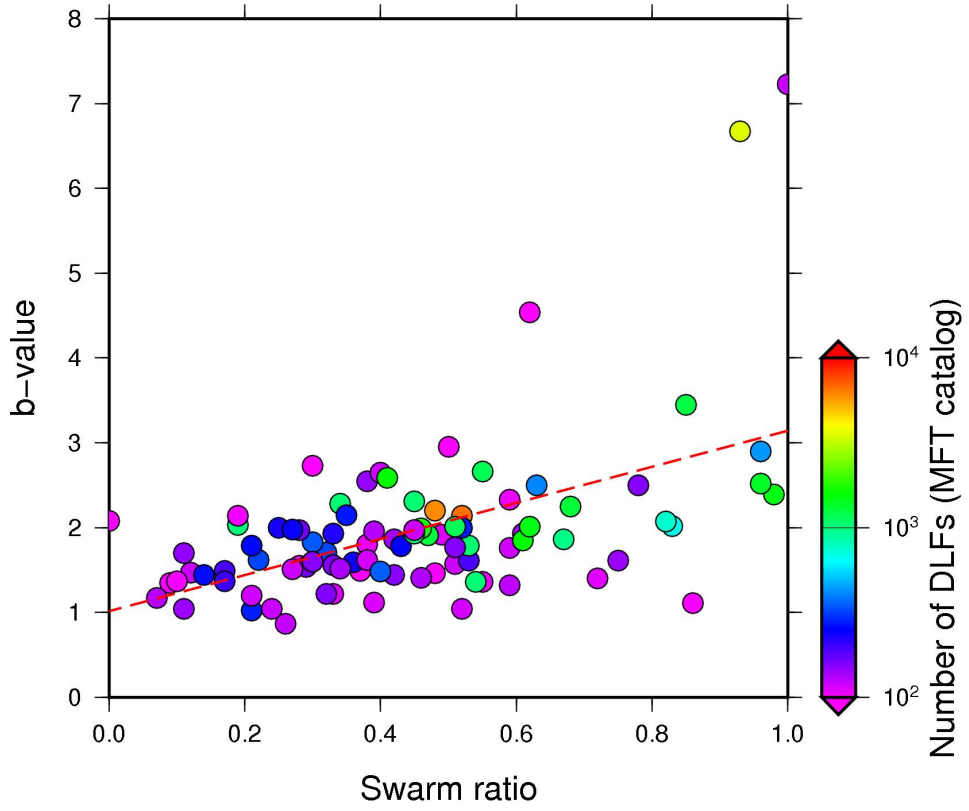

Figure 3.23 The relationship between swarm ratio (SR) and b-value. Groups that have 10 or more DLF earthquakes in the JMA catalog and 100 or more DLF earthquakes detected

by matched filter technique (MFT) are plotted. The color shows the number of DLF earthquakes detected by MFT in the groups. The red broken line is the regression line. The trend of the regression line is 2.124±0.187.

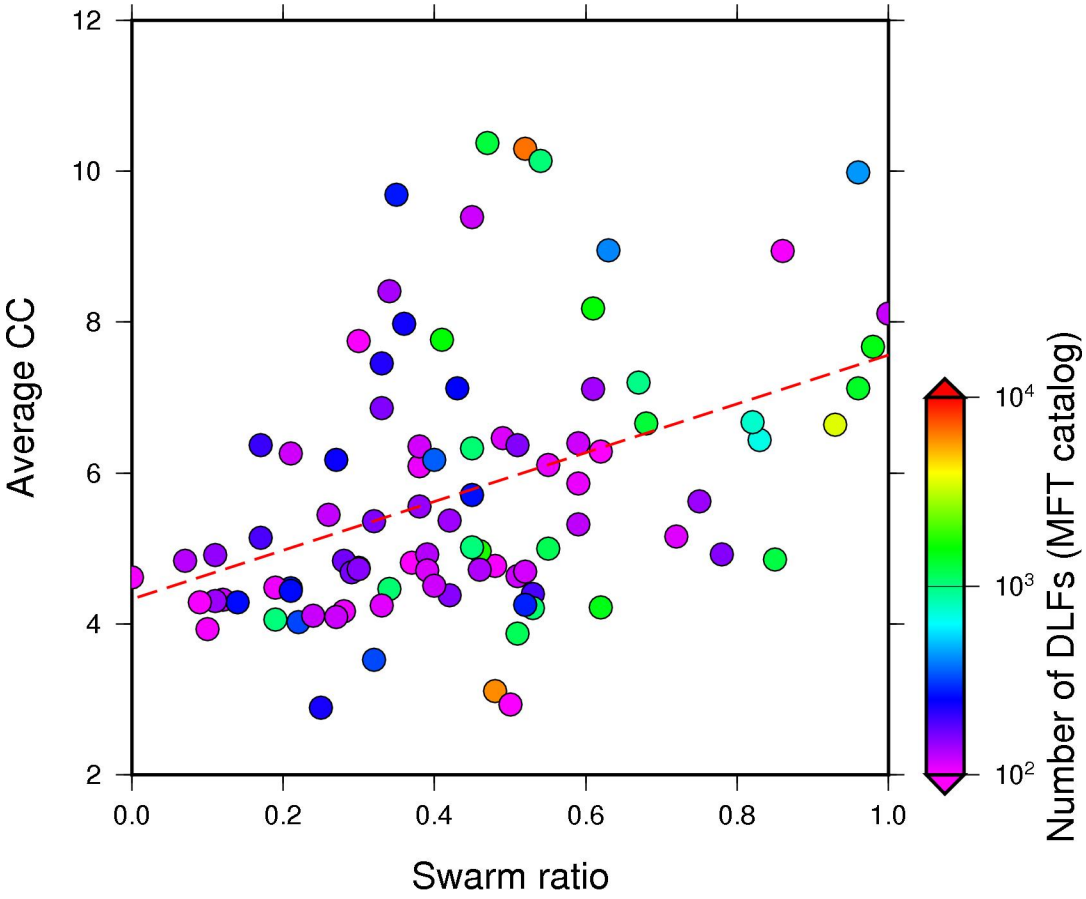

Figure 3.24 The relationship between swarm ratio (SR) and average correlation coefficient (CC). The red broken line is the regression line. The trend of the regression line is 3.236±0.369.

3.6.2. DLF earthquakes affected by the 2011 Tohoku earthquake

In Hijiori, DLF earthquakes in Groups 2.1 and 4.1 were activated between 2011 and 2015 (Figure 3.8). The period of activation is just after the 2011 Tohoku earthquake (Mw 9.0). DLF earthquakes in Hijiori may be induced by the large earthquake. Activation and switch of focal mechanisms of DLF earthquakes just after the 2011 Tohoku earthquake were reported in Zao (Kosuga et al., 2017; Oikawa et al., 2019). The result of Hijiori is similar to the activities of DLF earthquakes in Zao (Appendix 10.1.25).

Although no clear activations of DLF earthquakes were observed directly corresponding to the 2011 Tohoku earthquake in other regions, activations occurred a few

years after the 2011 Tohoku earthquake in some regions of the Tohoku district. Activations of DLF earthquakes were observed in 2013–2014 in some regions in the northern part of the Tohoku district. DLF earthquakes activated in the middle of 2013 in Hakkoda (No.10; Figure 3.25) and the middle of 2014 in Mt.Iwaki (No.11; Figure 3.26). In the southern part of the Tohoku district, activations of DLF earthquakes were observed in 2014–2015. DLF earthquakes were activated at the end of 2014 in Azuma (No.26; Figure 3.27), in 2014–2015 in Bandai-west (No.28; Figure 3.28), and in 2015 in Hiuchigatake (No.32; Figure 3.29).

These activations occurred in some volcanoes at similar periods; therefore, tectonic activity may be related to the activations of DLF earthquakes. Although there are no observations of influences of the 2011 Tohoku earthquake with such long time-lags in regular earthquakes and crustal deformations (Geospatial Information Authority of Japan, 2019; Yoshida et al., 2019), the time-lags of 2–4 years between the 2011 Tohoku earthquake and activations of DLF earthquakes may be explained by the following hypothesis. In Hijiori and Zao, which are in the middle of the Tohoku district and near the hypocenter of the 2011 Tohoku earthquake, DLF earthquakes might be induced by static stress change of the strong motion of the 2011 Tohoku earthquake. In Hakkoda, Mt. Iwaki, Azuma, Bandai-west, and Hiuchigatake, which are in the northern or southern parts of Tohoku district, DLF earthquakes might be induced by fluids movement which gradually occurred. The fluid movement might occur from deeper places because the time-lags are long. However, there is no way to verify the hypothesis.

There are regions in which no activations of DLF earthquakes were observed even in the Tohoku district. For example, in Mt. Iwate (No.17), many DLF earthquakes have been observed. However, there was no clear activation of DLF earthquakes after the 2011 Tohoku earthquake. In such regions, the fluids movement might not occur.

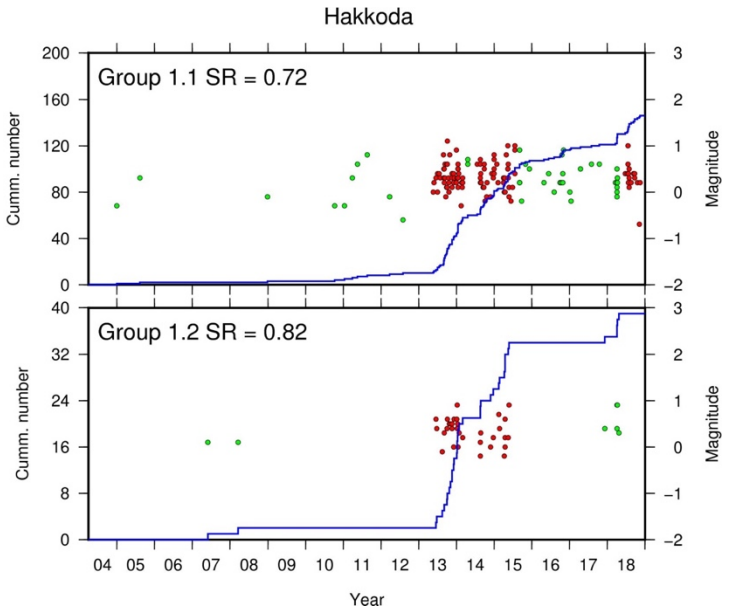

Figure 3.25 Cumulative number of DLF earthquakes from April 2004 and magnitude-time distributions in each group in Hakkoda. Symbols are the same as Figure 3.8. The groups in which have more than 30 DLF earthquakes are shown.

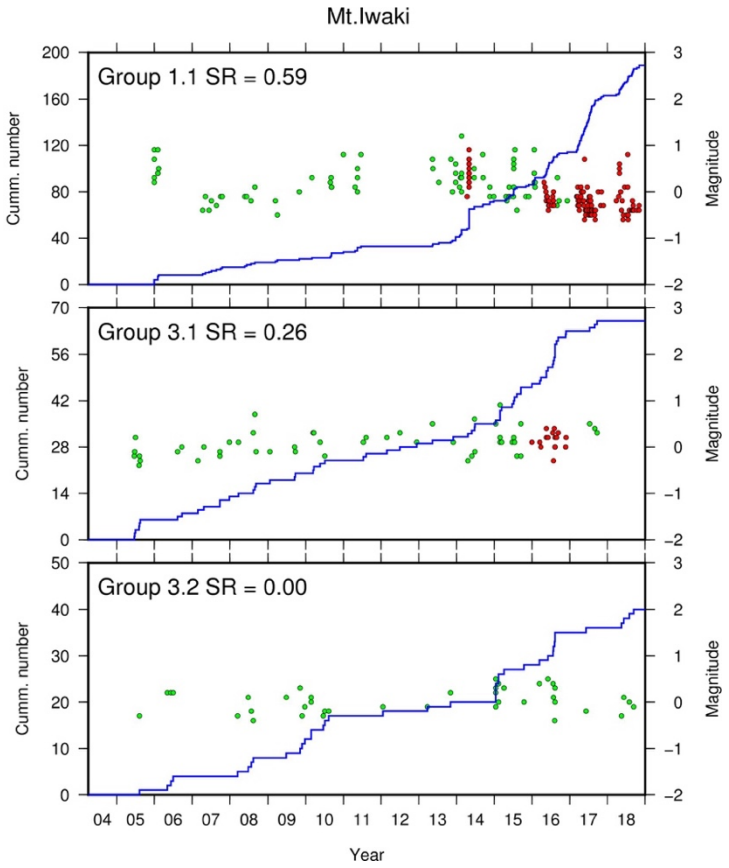

Figure 3.26 Same figure as Figure 3.25 but in Mt. Iwaki. The groups in which have more than 30 DLF earthquakes are shown.

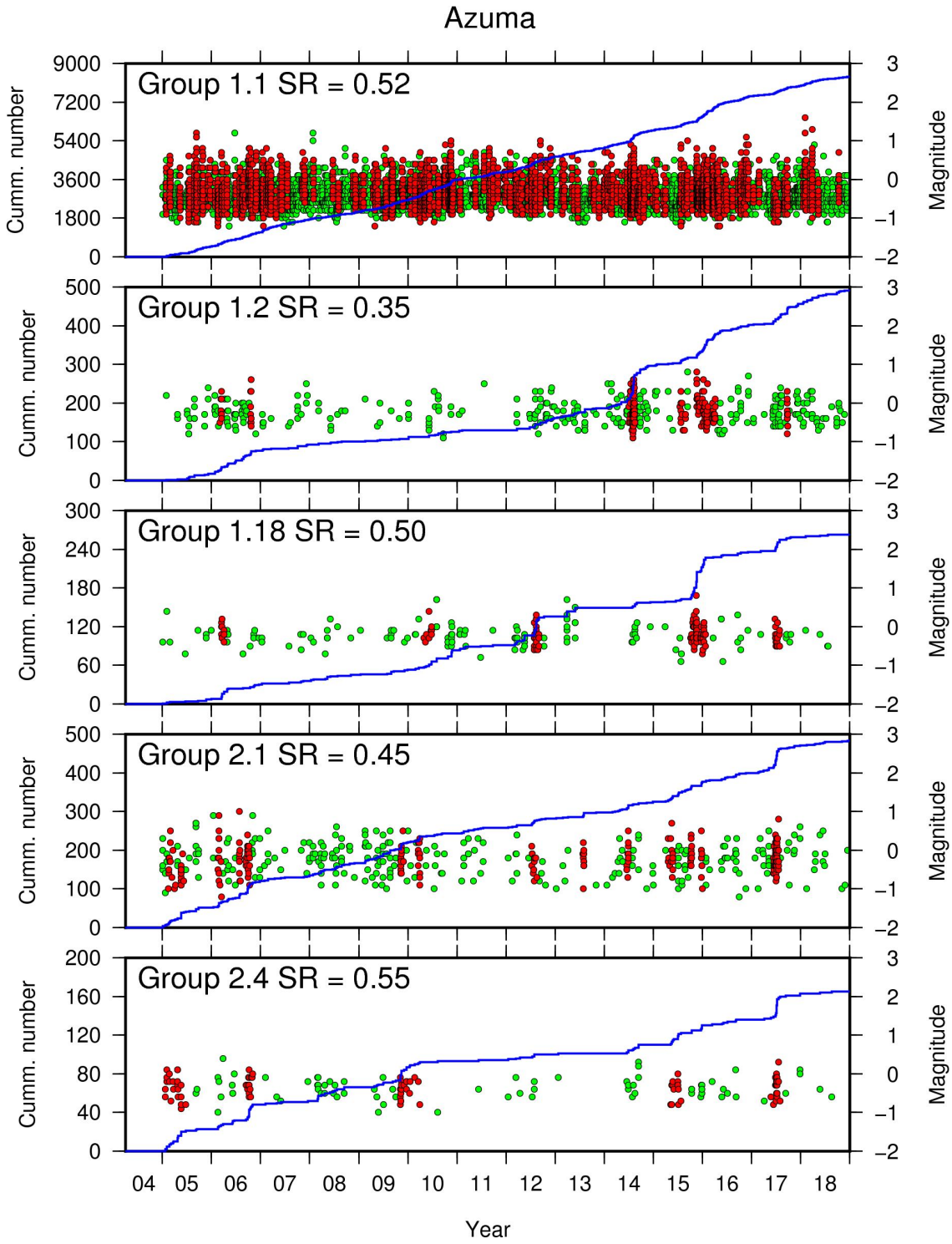

Figure 3.27 Same figure as Figure 3.25 but in Azuma. The groups in which have more than 100 DLF earthquakes are shown.

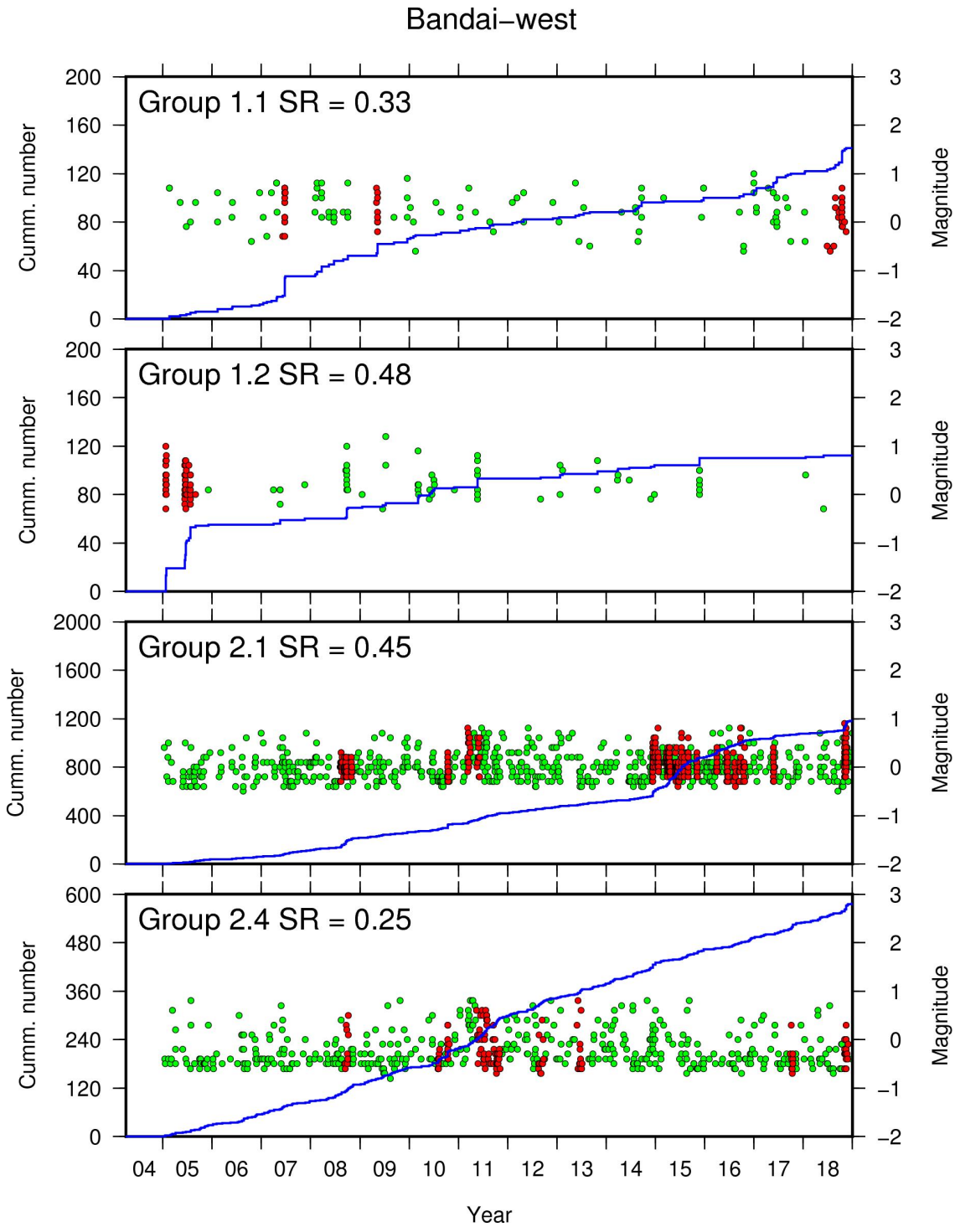

Figure 3.28 Same figure as Figure 3.25 but in Bandai-west. The groups in which have more than 100 DLF earthquakes are shown.

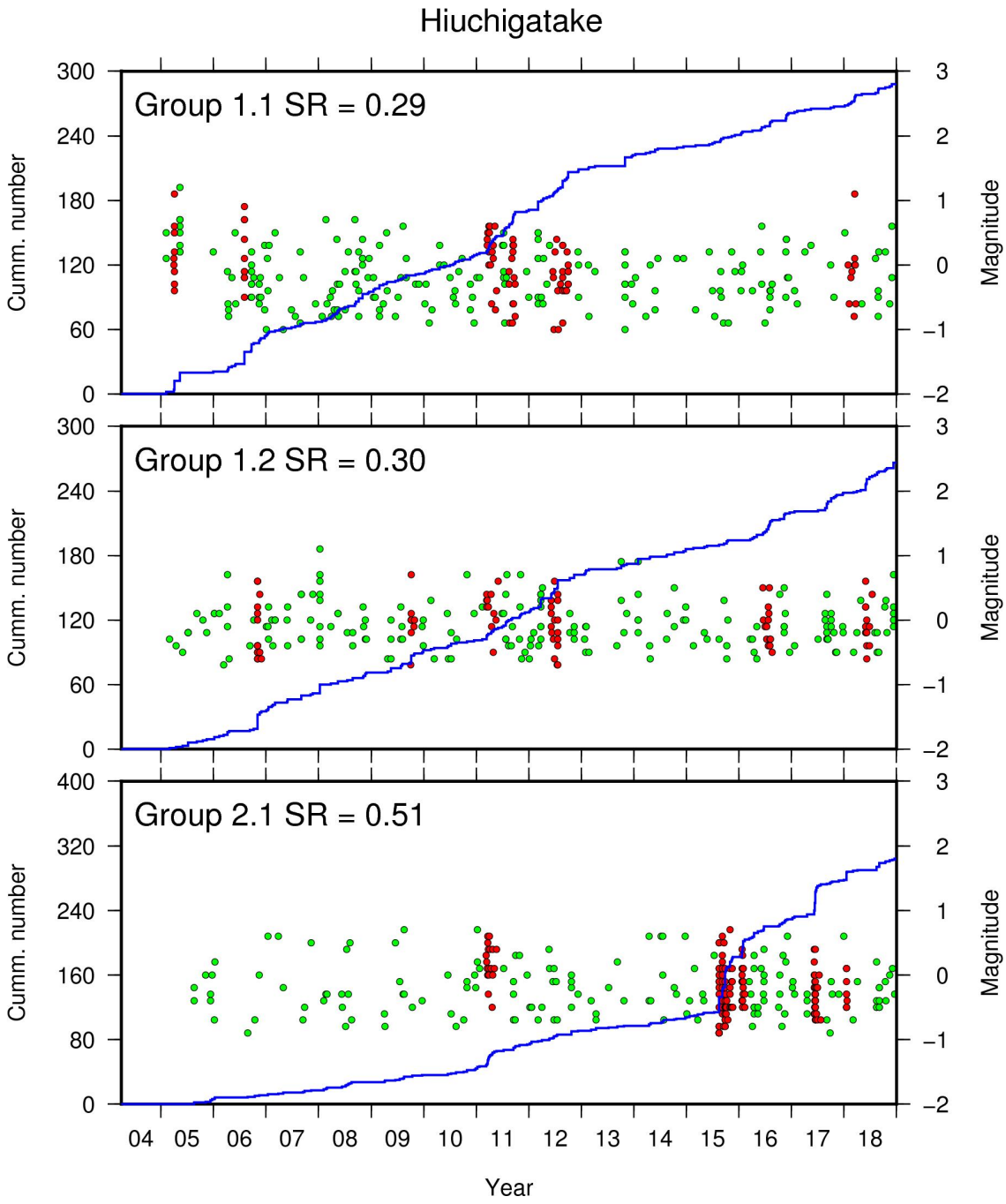

Figure 3.29 Same figure as Figure 3.25 but in Hiuchigatake. The groups in which have more than 100 DLF earthquakes are shown.

3.7. Summary of this chapter

This chapter showed the characteristic activities of DLF earthquakes. Discrete distributions of DLF earthquakes in vertical direction were revealed. DLF earthquakes were classified into some groups in each region based on correlation coefficients. I found

that there are groups in which DLF earthquakes constantly occur and episodically occur. There are the groups in which DLF earthquakes quasi-periodically occur and groups in which DLF earthquakes sometimes occur with very short intervals like tremor. Magnitude-frequency distributions of DLF earthquakes follow the Gutenberg-Richter law and b-values in the groups of episodic DLF earthquakes were high. Waveform characteristics were different for each group even in the same region. Swarm ratios correlate with b-value and average correlation coefficients. Therefore, the same source may repeatedly cause DLF earthquakes in the groups of episodic DLF earthquakes, while many sources cause DLF earthquakes in the groups of constant DLF earthquakes. In the Tohoku district, activations of DLF earthquakes were observed just after the 2011 Tohoku earthquake in Hijiori and Zao. On the other hand, activations of DLF earthquakes were observed 2–4 years after the 2011 Tohoku earthquake in five regions of the northern and southern part of the Tohoku district.

4. Relationship between DLF earthquakes and volcanic activity in Kirishima volcanoes

I found activations of DLF earthquakes associated with the eruptions in Kirishima, Meakan, Sakurajima, Ontake, and Hakone volcanoes. The result in Kirishima is most significant. Therefore, I focused on Kirishima in this chapter. This chapter is modified from a published paper of Kurihara et al. (2019). This work is mainly analyzed and wrote by myself and other authors helped the discussion and revised the draft. The data were little changed from the published paper because the method of estimation of the magnitudes was changed.

4.1. DLF earthquakes and eruptions of Kirishima

Kirishima volcanoes are volcano group located in the southern part of Kyushu island includes three active volcanoes—Shinmoe-dake, Io-yama, and Ohachi (Figure 4.1). Shinmoe-dake has been one of the most active volcanoes in Japan over the past few decades. It recently erupted in 2008–2011 and 2017–2018. Phreatic eruptions as precursory activity occurred in 2008–2010 (Suzuki et al., 2013), subplinian eruptions occurred in 26–27 January 2011, after which vulcanian eruptions occurred until April 2011, and phreatomagmatic eruptions occurred from June to September 2011 (Nakada et al., 2013). Shinmoe-dake also erupted in October 2017 and March–April 2018. Io-yama, located northwest of Shinmoe-dake erupted in April 2018 as well (Japan Meteorological Agency, 2018). In Kirishima volcanoes, DLF earthquakes occurred at depths of approximately 10–15 km and 20–27 km, according to the JMA catalog. In the vicinity of these DLF earthquakes, low-velocity anomalies at depths of 5–15 and 25–35 km have been imaged by tomography and seismic interferometry (Yamamoto & Ida, 1994; Nagaoka et al., 2018; Zhao et al., 2018). However, DLF earthquakes have been constantly observed from 2004 to 2018 in the JMA catalog. DLF seismicity associated with eruptions has not been documented in Kirishima volcanoes up to now.

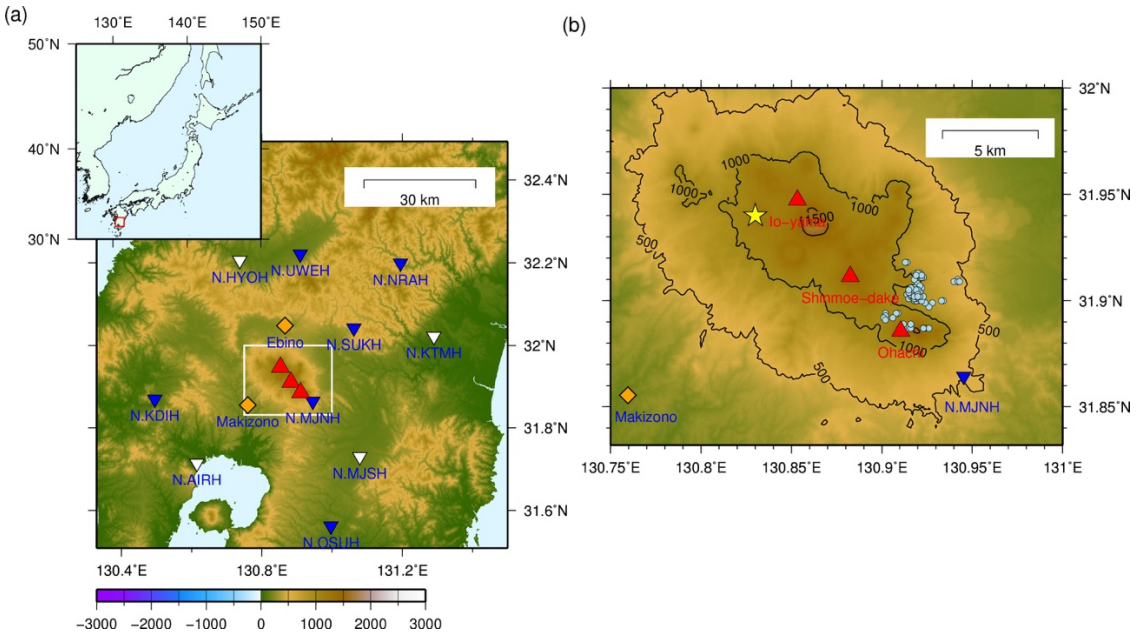

Figure 4.1. (a) Locations of Kirishima volcanoes and observation stations used in this study. Red triangles show the locations of Io-yama, Shinmoe-dake, and Ohachi volcanoes in Kirishima volcanoes. Inverted triangles indicate the locations of Hi-net stations used for relocation and detection (blue) and used only for relocation (white). N.KTMH and N.AIRH stations are also used for detection when one or two blue stations are missing observations. Orange diamonds show the locations of global navigation satellite system (GNSS) stations in the GNSS earth observation network system (GEONET) (Sagiya, 2004) operated by Geospatial Information Authority of Japan. (b) Enlarged view in the white rectangle in (a) with the same symbols. Besides, light blue circles show the hypocentral locations of DLF earthquakes obtained by the relocation. A yellow star represents the location of the estimated pressure source of the 2011 Shinmoe-dake eruptions at a depth of approximately 8 km (Nakao et al., 2013).

4.2. Spatio-temporal distribution of DLF earthquakes in Kirishima

4.2.1. Distribution of the hypocenters of DLF earthquakes

Figure 4.2a shows the distribution of DLF earthquakes in Kirishima in the JMA catalog. One characteristic of DLF earthquakes in Kirishima is that there is a seismic gap at a depth of 15–20 km even in the JMA catalog.

Using the newly constructed DLF earthquake catalog, relocated hypocenters are also separated at depths of 10–15 km and 20–27 km. Unlike the original catalog of

the JMA, the hypocenters are concentrated in some small spots (Figure 4.2) like other regions discussed in Chapter 3. Beneath the Ohachi volcano, the hypocenters are concentrated at depths of approximately 12 and 14 km. Most of the DLF earthquakes which occurred deeper than 20 km were concentrated in the largest spot at a depth of 22 km, while some earthquakes are in small spots at depths of 25–27 km. The DLF earthquakes deeper than 20 km are in the north of Ohachi (Figure 4.2). I found the difference of DLF seismicity by the depths even if the distance between the earthquakes is smaller than a few kilometers, as discussed in the next subsection.

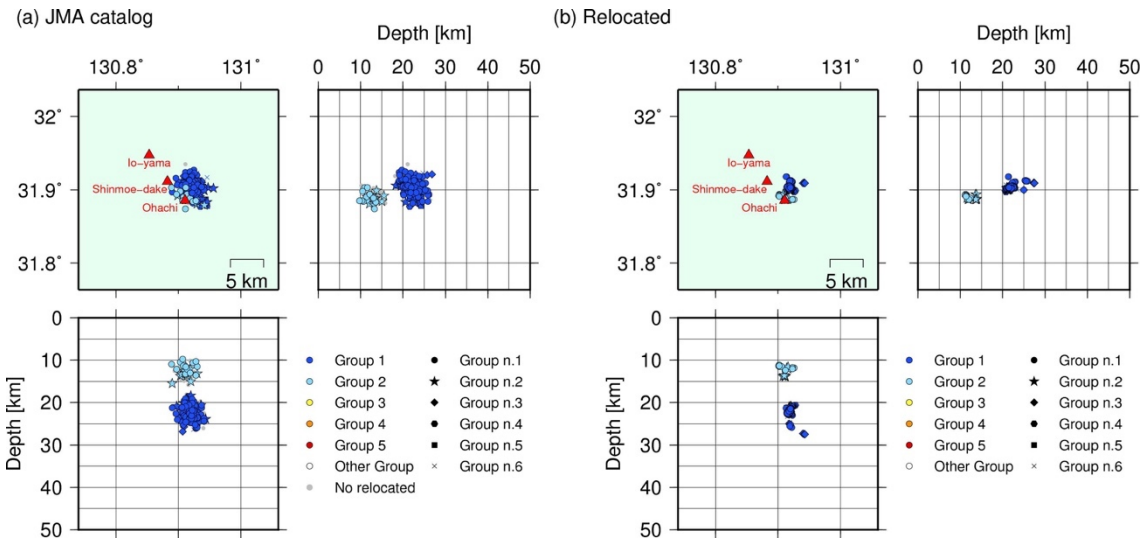

Figure 4.2 Distribution of hypocenters of DLF earthquakes in the JMA catalog and relocated in this study. Same figure as Figure 3.1 but in Kirishima.

4.2.2. Temporal distributions of DLF earthquakes

From April 2004 to December 2018, 2,964 DLF earthquakes were detected by this study. In Kirishima, the number of detected DLF earthquakes in the new catalog constructed in Chapter 3 is approximately 10 times larger than that in the JMA catalog. Cumulative numbers of DLF earthquakes in the JMA catalog and the newly constructed catalog are shown in Figure 4.3. DLF earthquakes in the JMA catalog constantly occurred but those in the new catalog significantly increased between 2010 and 2011.

Around the 2011 subplinian eruptions, a long-term increase of DLF earthquakes for about two years and swarms of DLF earthquakes in a few days were observed. The two-year increasing seismicity from December 2009 to September 2011 was commonly observed for DLF earthquakes with all ranges of magnitude (Figure 4.4).

Swarms of DLF earthquakes were observed in August 2010, December 2010, and February 2011(Figure 4.5). Although swarms of DLF earthquakes mainly consist of small events, the swarms were also observed with all ranges of magnitude (Figure 4.6). There is no significant activation of DLF earthquakes directly corresponding to the subplinian eruptions on 26–27 January 2011. After the swarm of DLF earthquakes in February 2011, the long-term increase in DLF earthquakes had gradually finished by the end of 2011.

These results are also seen in the results of detection test using 10-seconds time-window instead of 5 seconds time-window in matched filter technique (Chapter 10.3).

The DLF earthquakes are generally separated into two depths shallower and deeper than the depth of 17 km. Most DLF earthquakes detected by this study are located in the depths deeper than 17 km (Figure 4.3e) while a number of those in the depths shallower than 17 km is smaller than 200 without significant activations near the 2011 eruptions (Figure 4.3d).

The seismicity of DLF earthquakes from December 2009 was correlated with crustal deformation. Figure 4.3a and Figure 4.5a show the distance change of the radial component of horizontal displacement of Ebino relative to Makizono (see Figure 4.1), calculated from GNSS data (F3 solutions) provided by the Geospatial Information Authority of Japan. Horizontal displacement is supposed to show the volume change in the magma reservoir located near Io-yama (yellow star in Figure 4.1) at a depth of 8 km (Nakao et al., 2013). The trend of horizontal displacement was also changed at the end of 2009, when DLF earthquakes increased, and the extension trend corresponded to the 2011 eruptions of Shinmoe-dake. The change in the trend lasted until the end of 2011, except for the shortening by the eruptions in January 2011.

After the sequence of DLF earthquakes associated with the 2011 eruptions, another small activation of DLF earthquakes was observed after the middle of 2017 (Figure 4.3). This increase is also correlated with the eruptions of Shinmoe-dake and Io-yama that occurred in 2017–2018. This increase was observed in the JMA catalog as well. The horizontal displacement was also extended in this period.

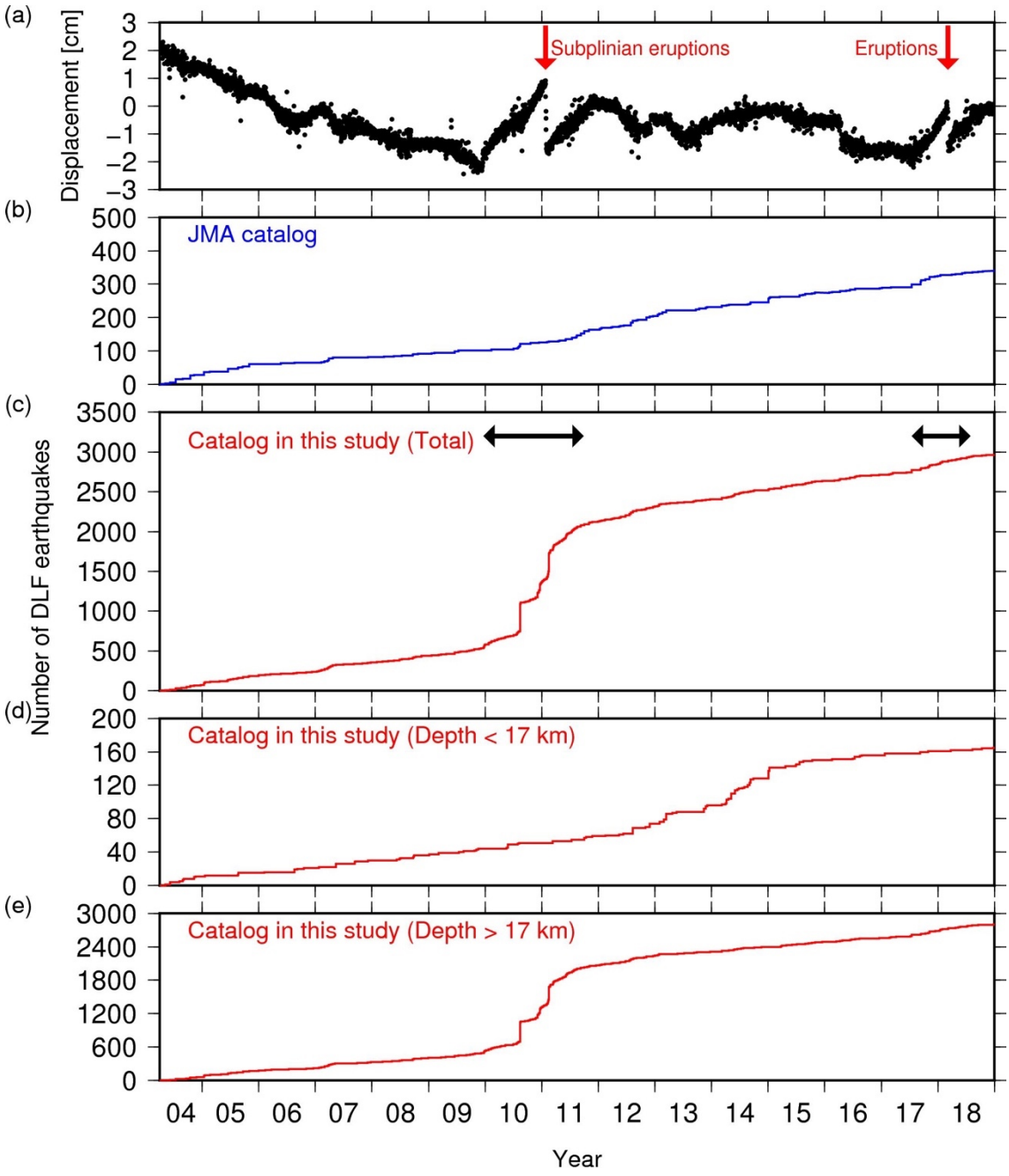

Figure 4.3 (a) The amount of the horizontal displacement of Ebino relative to Makizono (see Figure 4.1) calculated from GNSS data. I use F3 solutions provided by the Geospatial Information Authority of Japan. (b) A cumulative number of DLF earthquakes in the JMA catalog from April 2004. (c) A cumulative number of DLF earthquakes in the catalog of this study. Black arrows show the period of increase of DLF earthquakes. (d) A cumulative number of DLF earthquakes located shallower than 17 km in the catalog of this study. (e) A cumulative number of DLF earthquakes located deeper than 17 km in the catalog of this study.

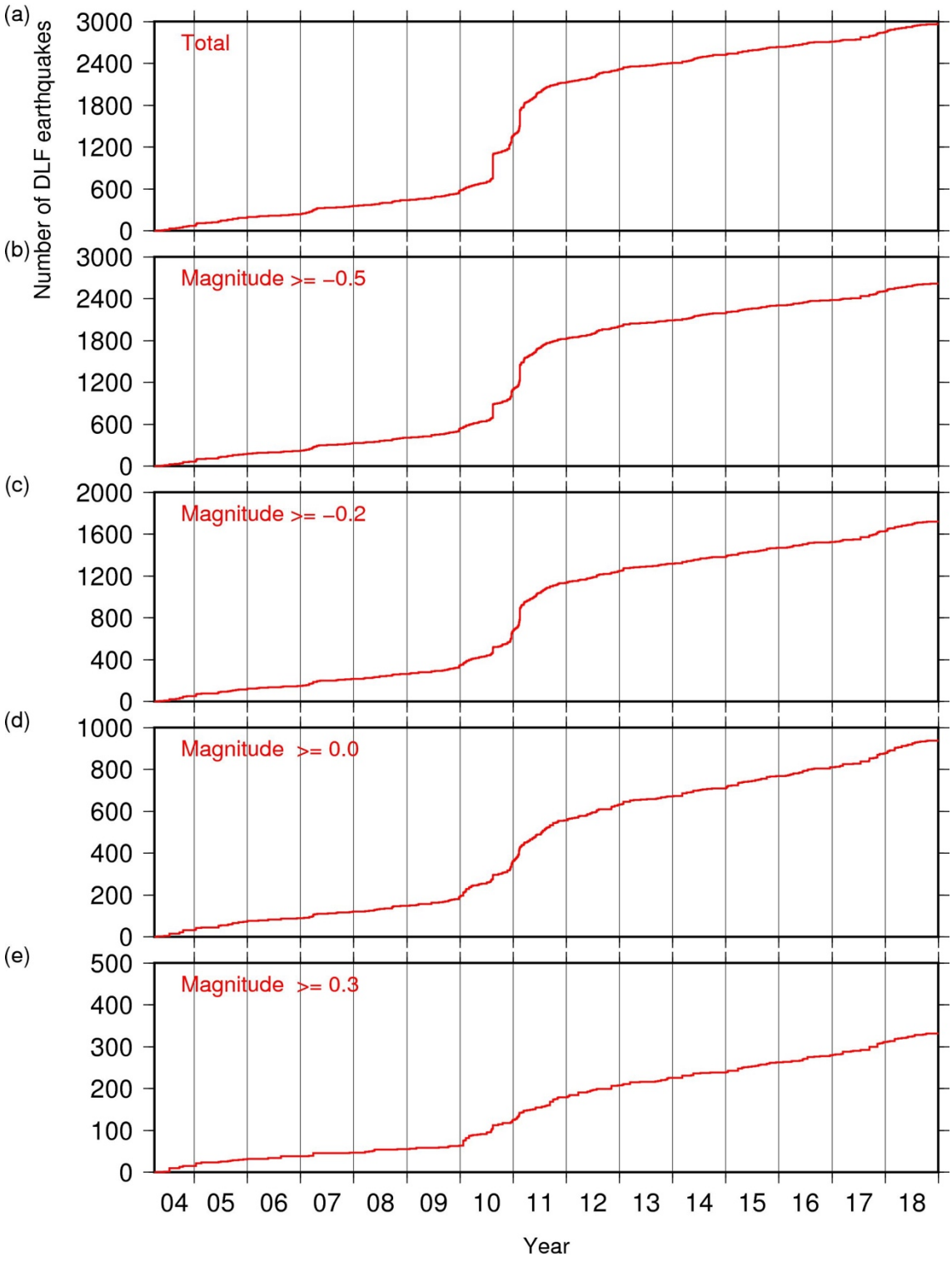

Figure 4.4 A cumulative number of DLF earthquakes in Kirishima with magnitude filters. (a) Total number of events, (b)–(e) number of DLF earthquakes whose magnitudes larger than (b) -0.5, (c) -0.2, (d) 0.0 (e) 0.3.

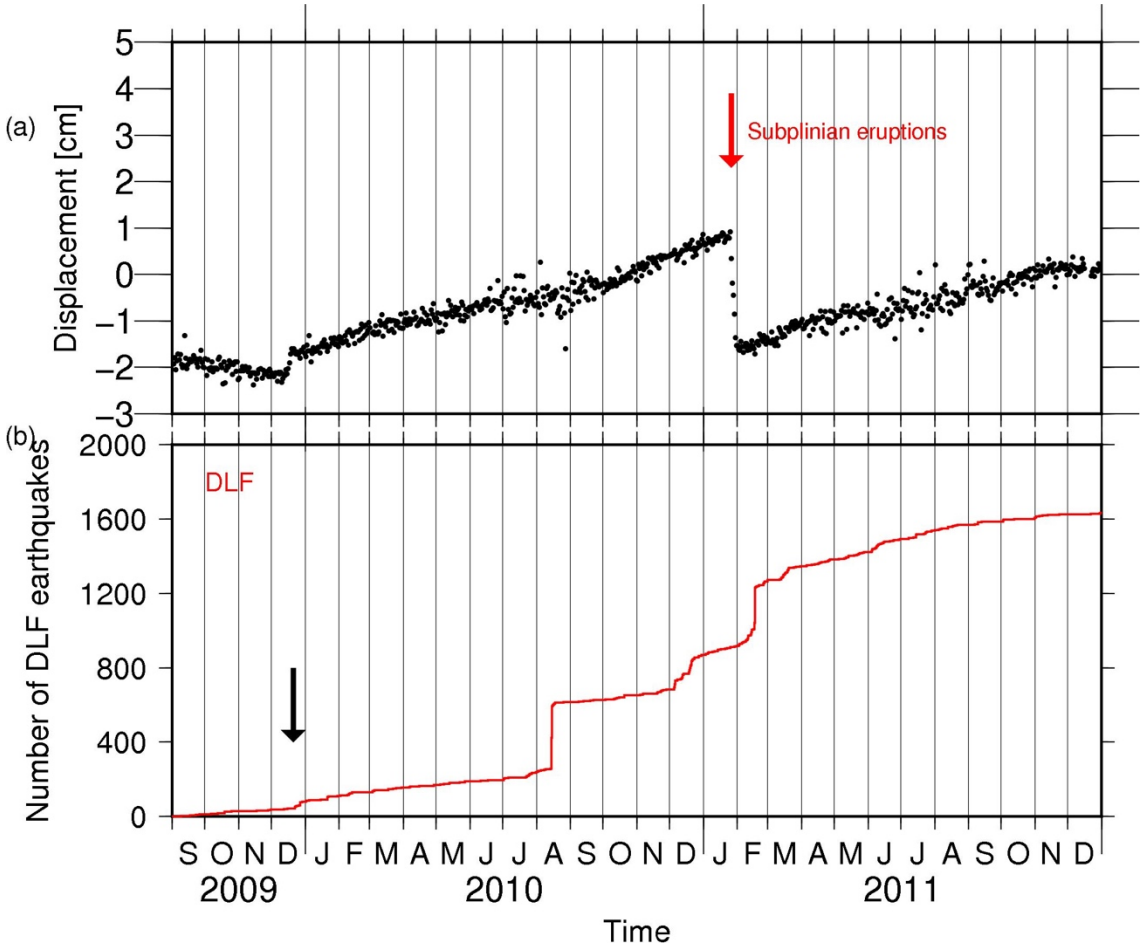

Figure 4.5 The enlarged portions of Figure 4.3a and Figure 4.3c from September 2009 to December 2011. Arrow shows the initiation of increasing of DLF earthquakes in December 2009.

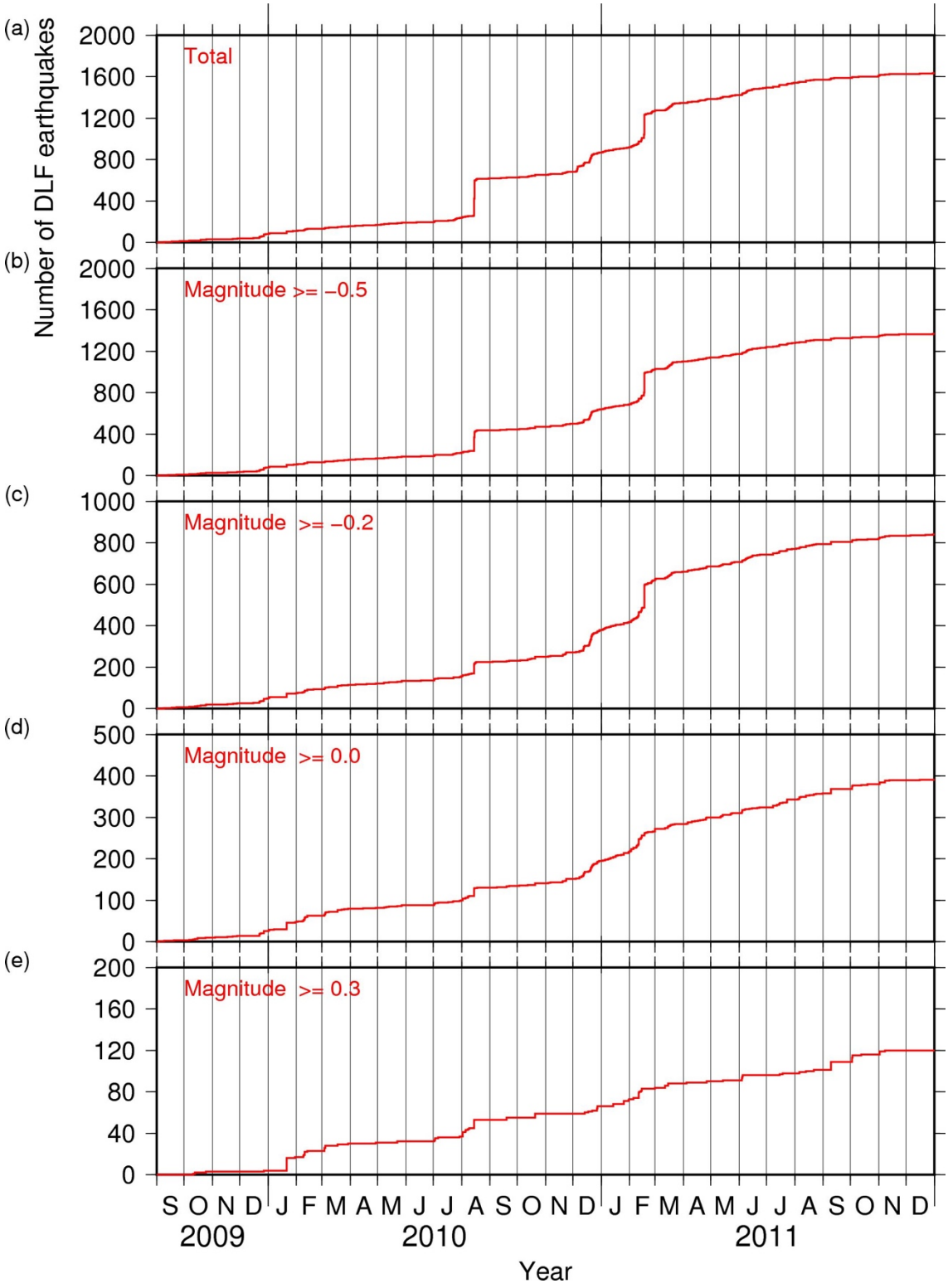

Figure 4.6 The enlarged portions of Figure 4.4 from September 2009 to December 2011

4.3. Classification of DLF earthquakes

To investigate the activations of DLF earthquakes, classifications of the DLF earthquakes were used. The results of the two-stage classifications developed in Section 2.3 based on correlations of waveforms are seen to be not good for discussion about the activities of DLF earthquakes in Kirishima. Many DLF earthquakes were classified into Group 1.1 (Figure 4.7). Therefore, I developed another method to classify the DLF earthquakes in Kirishima. On the cumulative number of DLF earthquakes detected by each template, clear differences in cumulative patterns are seen (Figure 4.8). For example, a cumulative number of DLF earthquakes detected by a DLF earthquake shows a constant increase from 2004 to 2018, while a cumulative number of DLF earthquakes detected by another DLF earthquake show sudden increase around the time of the subplinian eruptions on January 2011. Thus, I tried to classify DLF earthquakes based on the period in which the detected earthquakes are concentrated.

To classify template DLF earthquakes, I determine the concentration ratio (CR) of each template earthquake as follows:

$$\mathrm{CR}_i\left(T_{\mathrm{Start}}, T_{\mathrm{end}}\right) = \frac{N_i\left(T_{\mathrm{start}} < t < T_{\mathrm{end}}\right)}{N_i^{\mathrm{Total}}} \quad \cdot\cdot\cdot (4.1)$$

Where N_i^{Total} refers to the total number of detected earthquakes by the i th template in all periods of analysis, which is from April 2004 to December 2018. T_{Start} and T_{end} show the start times and end times of the periods defined for each analyzed period (Table 4.1). Three periods were used corresponding to the periods of eruptions: December 2009–June 2010 for Type A1, July 2010–September 2011 for Type A2, and September 2017–December 2018 for Type B1. Type A means the association with the 2011 eruptions. $N_i\left(T_{\mathrm{start}} < t < T_{\mathrm{end}}\right)$ is the number of detected earthquakes in the period. Then, if CR is over the threshold of each type (see Table 4.1), the template earthquake is classified into the type. I determined the types of template earthquakes from the top to the bottom in Table 4.1. When CRs were not over than thresholds of any type, the template events were classified into Type B2. When a template fits two or more types, the template was classified into topmost type along Table 4.1. Template earthquakes which detected less than eight DLF earthquakes were not classified. Finally, all detected earthquakes were

classified according to the types of the template earthquakes that detected them. In other words, the DLF earthquakes concentrated between December 2009 and June 2010 were classified into Type A1; those between July 2010 and September 2011 into Type A2; those which were activated in the period of the 2018 eruptions into Type B1; and those occurring constantly from 2004 to 2018 into Type B2 (Figure 4.9).

As a result of the above classification, the number of Type A2 earthquakes is the largest of all types in my classification (Table 4.1). Additionally, the numbers of Types A1 and B1 are smaller than those of Types A2 and B2. The DLF earthquakes of Type A1 are located around and within the largest spot at a depth of 22 km and Type A2 earthquakes are deeper than the other types (Figure 4.10). Some DLF earthquakes of Type A2 and Type B1 or B2 were in the vicinity. However, the temporal activity patterns were clearly different. Type A2 earthquakes are separated into three detailed types by their spatial distributions (A2.1–A2.3); therefore, I discuss the differences in DLF seismicity in each group in section 4.4. Types A1 and A2.3 earthquakes are located farther northern than any other type. Types B1 and B2 compose the largest spot together and are not separated from each other. In addition, some of DLF earthquakes at a depth of 12 km are classified into Type B2. As the results of jackknife test, the distribution is also seen in each sample using any nine stations (Chapter 10.2.2). The tendency that type A2 have deep hypocenters is consistent with each sample of jackknife test.

Waveforms of DLF earthquakes have large variations. However, the differences in the waveforms between the types are clear. In particular, Type A2 earthquakes have the lowest dominant frequency at approximately 1 Hz, and they show no or small onsets of P waves (Figure 4.11). Detections of type A2 earthquakes were difficult due to the waveform characteristics; therefore, it is possible that most type A2 earthquakes were not detected by JMA. The other types (Types A1, B1, and B2) have higher dominant frequencies at approximately 3 Hz and show clear P wave onsets. Furthermore, the earthquakes of Type A1 have a lower dominant frequency than those of Types B1 and B2. Most of the earthquakes of Type A2 have lower dominant frequencies and larger ratios of the amplitudes of S waves to P waves, that is, the typical P wave of Type A2 is weaker than those of the others (Figure 4.12).

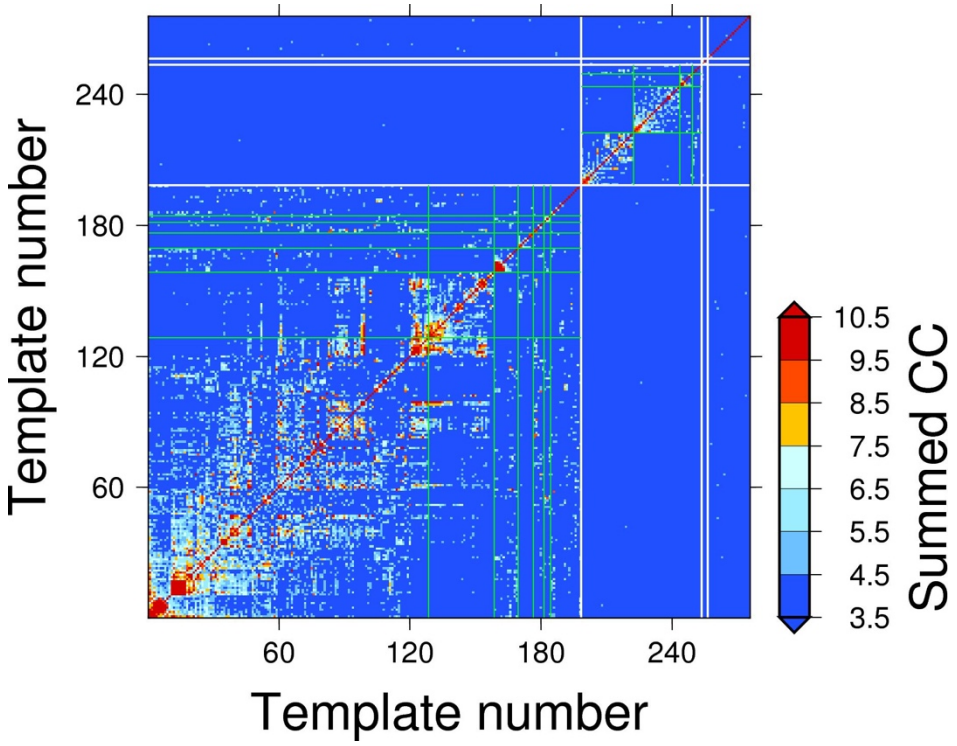

Figure 4.7 Summed correlation coefficients between all pairs of DLF earthquakes in Kirishima. White and green lines show the boundaries of the first-stage and the second-stage classifications, respectively.

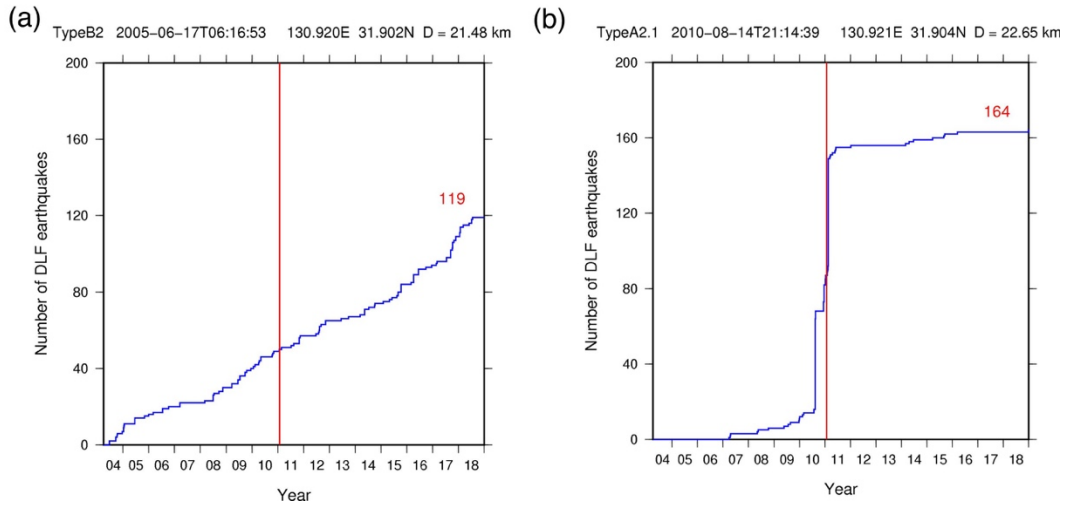

Figure 4.8 Cumulative number of DLF earthquakes detected by templates, (a) a DLF earthquake occurred in 2005 and (b) a DLF earthquake occurred in 2010. Origin time and relocated locations are written above the figures. Red lines show the time of the subplinian eruptions of Shinmoe-dake.

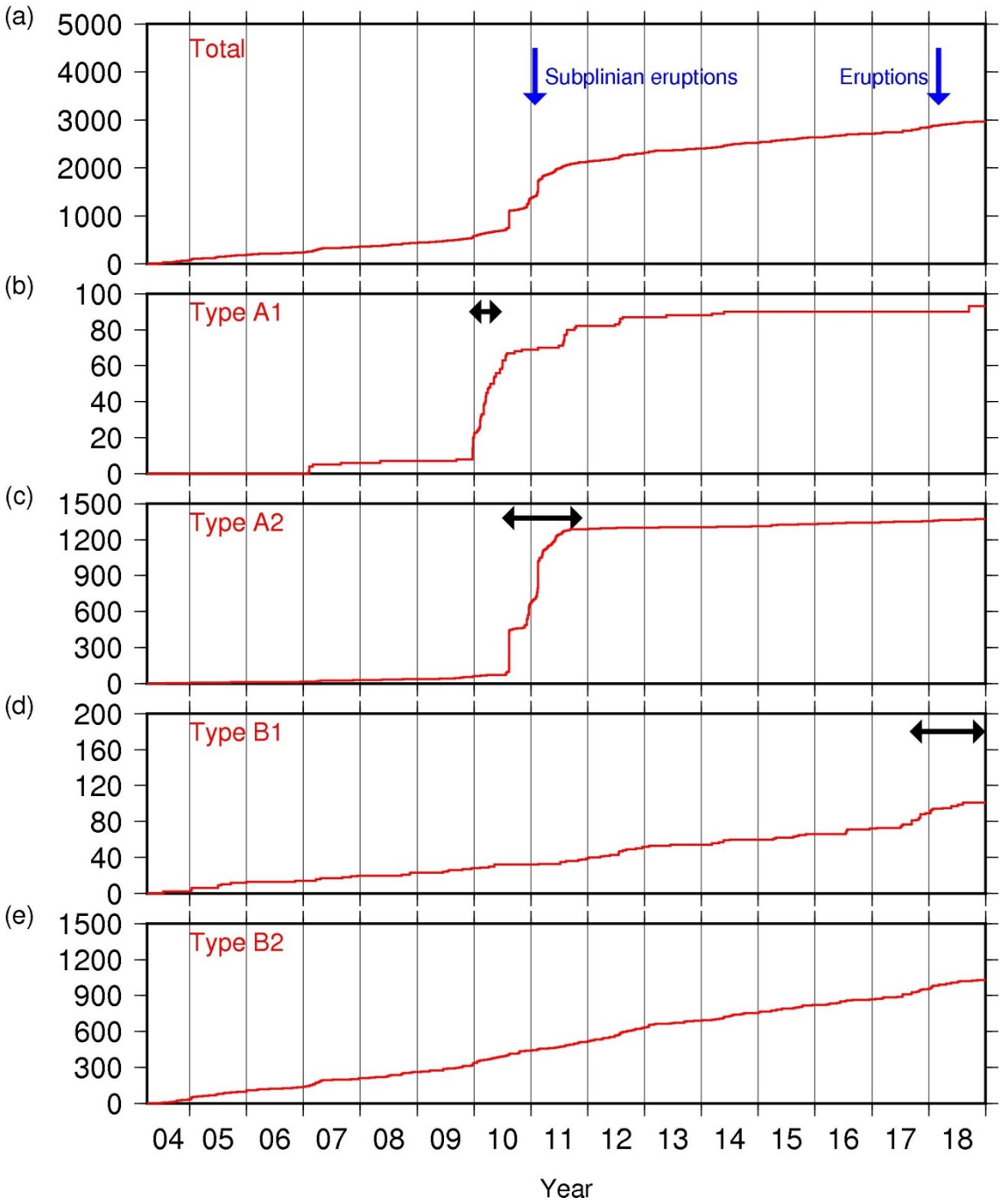

Figure 4.9 A cumulative number of DLF earthquakes. (a) Same figure as Figure 4.3c. (b–e) Total cumulative number of DLF earthquakes classified into each type. Black arrows show the periods in which each type of earthquakes are concentrated.

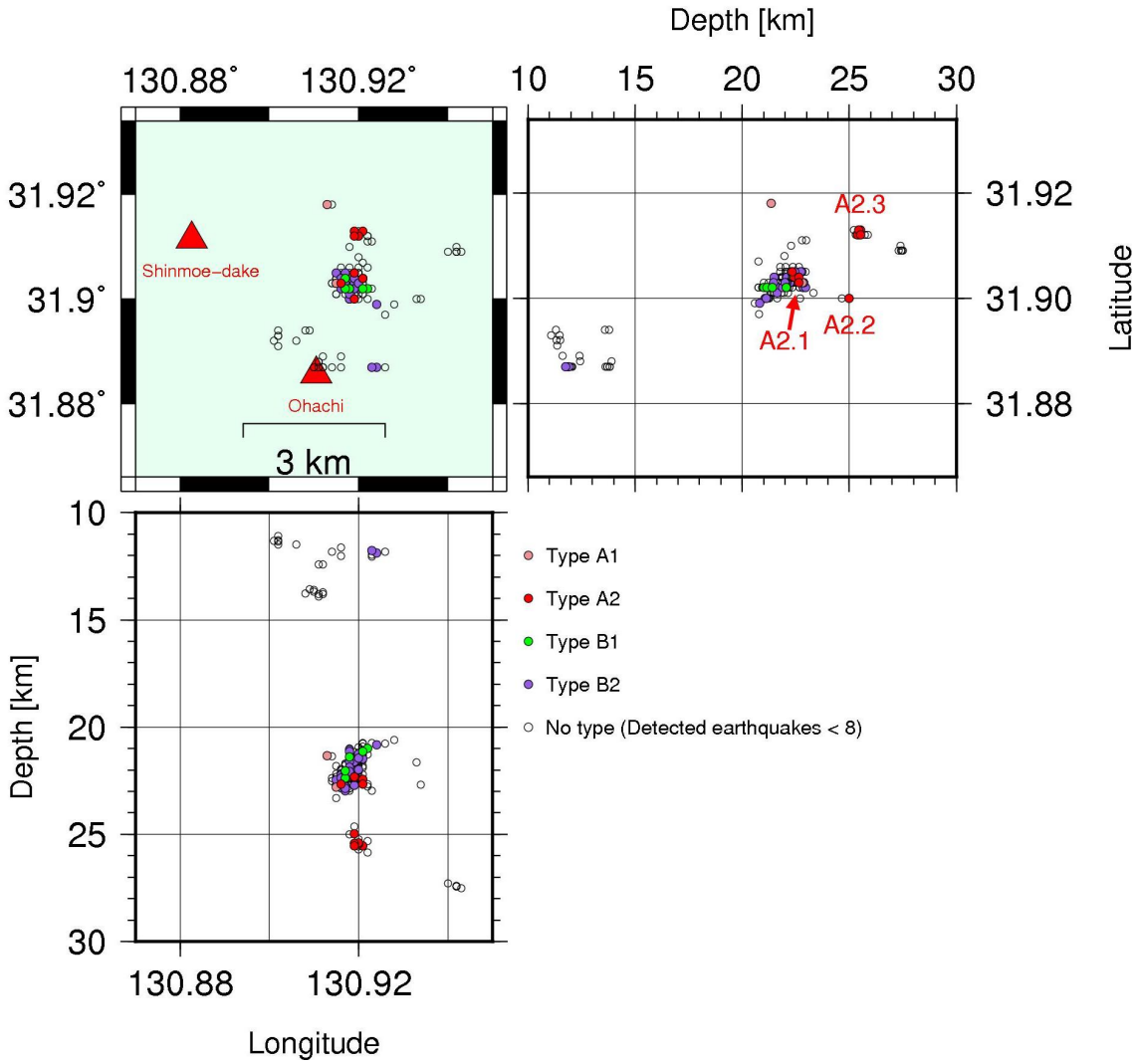

Figure 4.10 Three-dimensional distribution of DLF earthquakes. The circles indicate the relocated hypocenters of DLF earthquakes, and the colors of the circles show the types of earthquakes (Table 4.1). Red triangles represent the summits of Shinmoe-dake and Ohachi volcanoes. White circles are the relocated but unclassified hypocenters of DLF earthquakes, for which fewer than eight earthquakes were detected. A2.1–A2.3 show the locations of Type A2 earthquakes discussed in section 4.4.

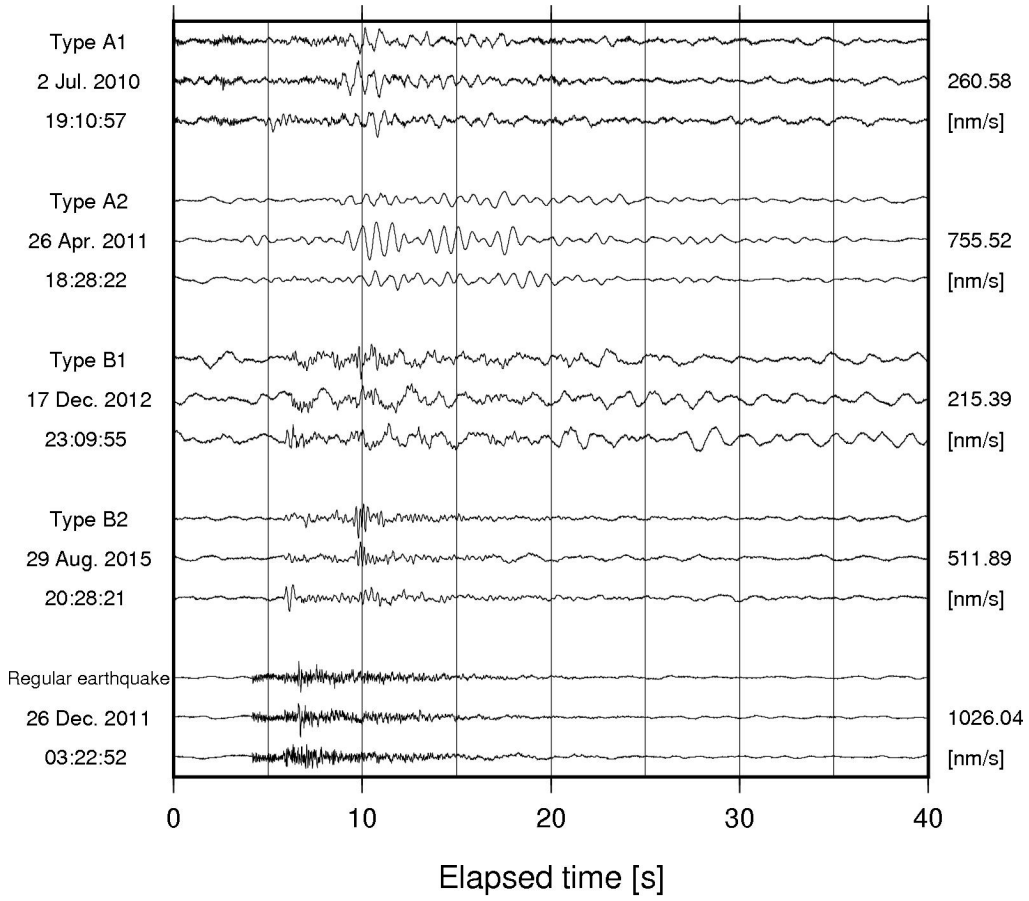

Figure 4.11 Three components of typical velocity waveforms of each type of DLF earthquake and a regular earthquake observed at the N.SUKH station (see Figure 4.1). The three waveforms correspond to the east-west, north-south, and up-down components from the top. The type of DLF earthquake and occurrence time (Japan standard time) are written to the left of the waveforms. All waveforms are normalized by the maximum amplitudes of each earthquake written in right. A bandpass filter is not applied to this waveform.

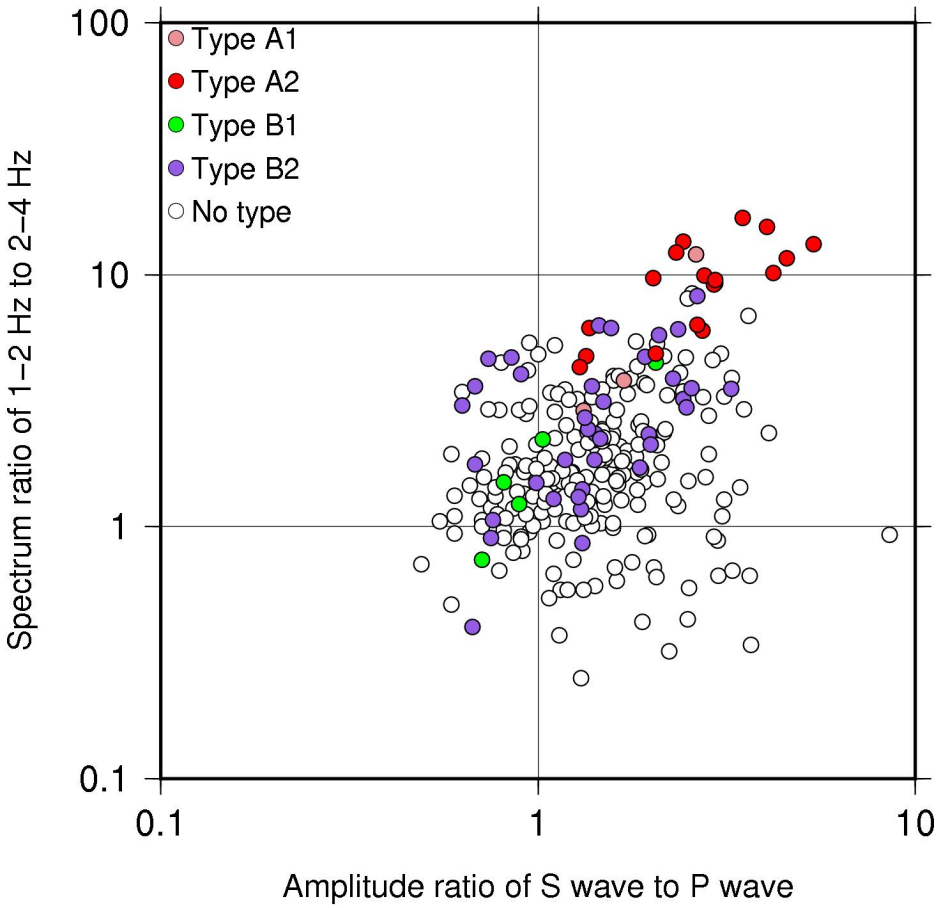

Figure 4.12 Distribution of the amplitude ratios of S wave to P wave and the ratio of the average spectrum of 1–2 Hz to 2–4 Hz at N.SUKH station. The circles show the DLF earthquakes, and the colors indicate the types of the earthquakes listed in Table 4.1.

Table 4.1. Definition and number of each type of DLF earthquakes.

Type of DLF earthquakes	Periods	Thresholds of CR	Number of template earthquakes (Relocated earthquakes)	Number of detected earthquakes
A1	December 2009–June 2010	0.4	4 (2)	93
A2	July 2010–September 2011	0.4	17 (9)	1372
B1	September 2017–December 2018	0.2	5 (5)	101
B2	All template earthquakes except above		37(33)	1028
No type	Detected earthquakes less than 8 or not used for MFT		212 (152)	370

4.4. DLF seismicity in the activation period including the 2011 eruptions

In section 4.3, the DLF earthquakes were classified according to time variabilities of the detected earthquakes, and Type A2 earthquakes were further separated into three types (A2.1–A2.3) by their spatial distributions. Thus, we attempt to find differences in DLF seismicity of the groups.

Type A2 earthquakes are located at depths of 23 km and 25 km (A2.1–A2.3 in Figure 4.10). Types A2.1, A2.2, and A2.3 consist of three, one, and five template DLF earthquakes. The characteristics of temporal DLF activity depend on the groups (Figure 4.13). In other words, Types A2.1, A2.2, and A2.3 had their activation periods. As explained above, Types A2.1–A2.3 were first separated based on their spatial distributions but they also differ by the characteristics of time variabilities.

Type A2.1 increased from August 2010 (Figure 4.13). Type A2.2 also increased from August 2010 and gradually from December 2010. On the other hand, Type A2.3 earthquakes were observed from December 2010 and activated after the subplinian eruptions.

The transitions of the DLF types are consistent with the changes in eruption styles (Figure 4.14). The first stage of the eruption was the phreatic stage from 2008 to July 2010 (e.g. Nakada et al., 2013; Suzuki et al., 2013). In this stage, Type A1 earthquakes mainly occurred. In August 2010, a swarm of Type A2.1 was observed without eruptions. Although Types A2.2 and A2.3 also appear, those numbers were not large. In December 2010, DLF swarms occurred again and included many earthquakes of Type A2.3 at this time. On January 26-27, 2011, the subplinian eruptions occurred and were followed by lava accumulation events (Nakada et al., 2013), but the number of DLF earthquakes is small. In this period, the ratio of Type A2.2 is larger than those in the other periods. Following the subplinian eruptions, vulcanian eruptions and a swarm of DLF earthquakes occurred in February 2011. After the swarm, Type A2.3 increased and lasted until about September 2011. From June 2011, phreatomagmatic eruptions occurred and Type A1 increased again. After the eruptions, Types A1 and A2 were not observed.

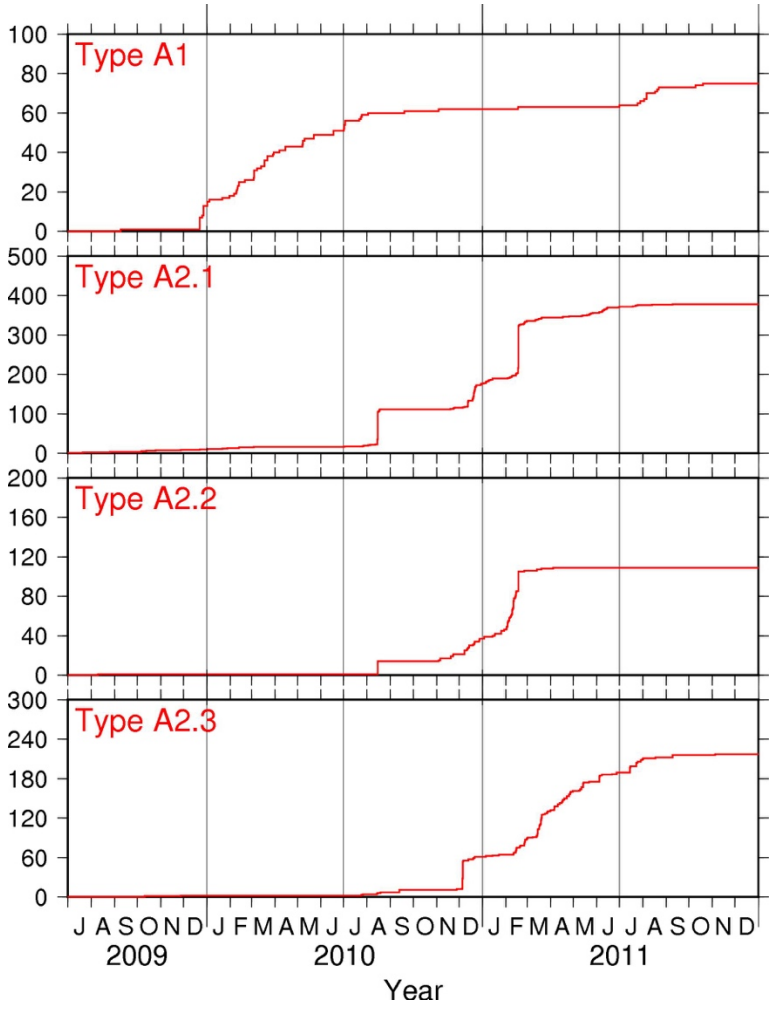

Figure 4.13 Cumulative number of DLF earthquakes of Type A1, A2.1, A2.2, and A2.3 from July 2009 to December 2011.

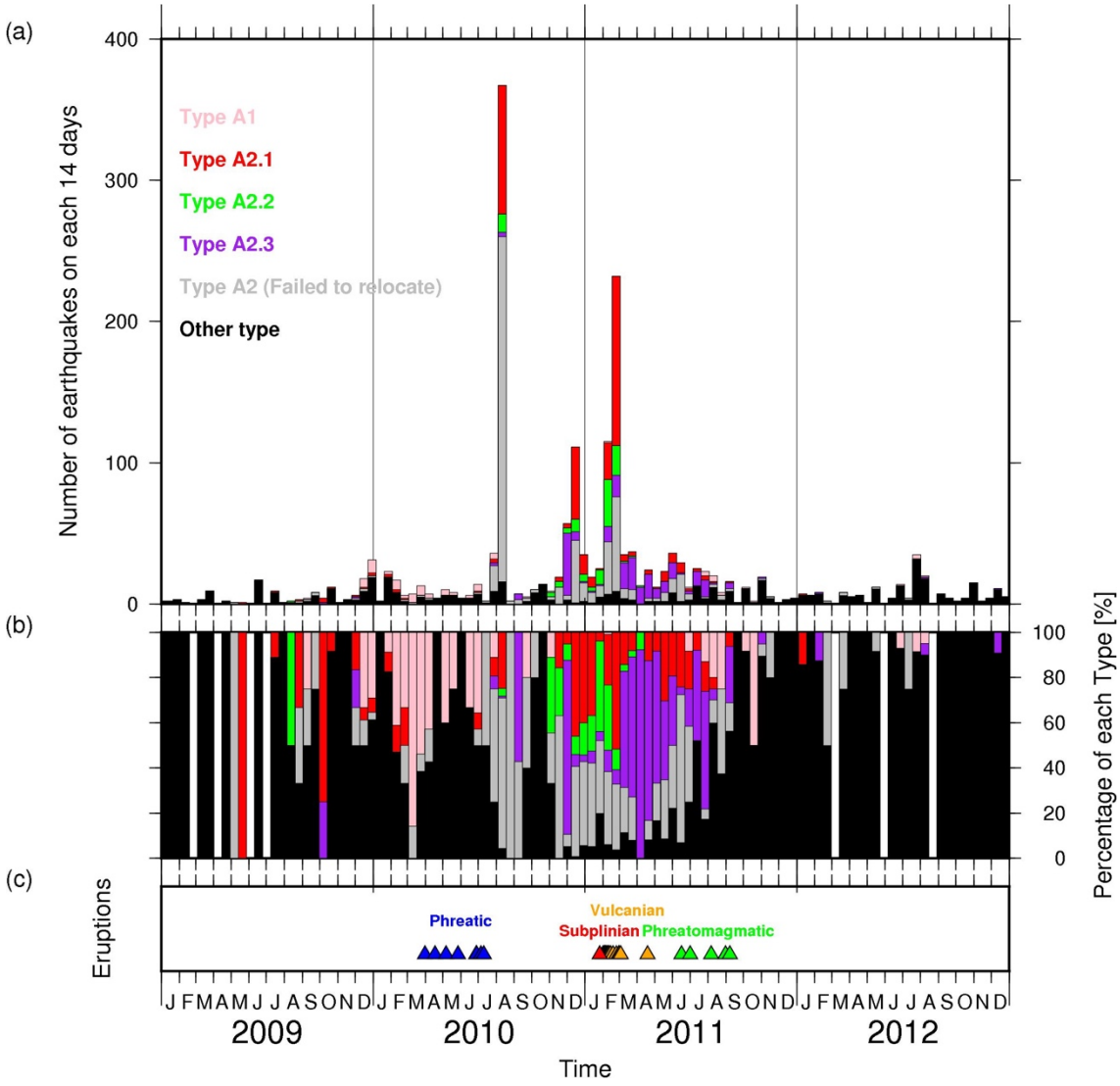

Figure 4.14 Number of DLF earthquakes in a 14-days time-window. Bars show the number of earthquakes, and their colors indicate the types of the earthquakes. (b) Percentages of each type of DLF earthquakes. White lines show the absence of earthquakes in a 14-days time-window. (c) The transition of the eruptions of Shinmoe-dake volcano. The times of the eruptions were reported in Nakada et al. (2013). Eruption stages of less than a few days were excluded.

4.5. Discussion of DLF earthquakes in Kirishima volcanoes

4.5.1. Deep volcanic structure and hypocenters of DLF earthquakes

As explained in section 4.2, the relocated hypocenters of DLF earthquakes are separated in the depths of 10–15 km and depths of 20–27 km. The result shows that the

scattering of the hypocenters is smaller than in the original catalog of the JMA. It should be noted that DLF earthquakes are distributed not continuously, but separately, in a vertical direction. In addition, hypocenters of DLF earthquakes can be separated into some types based on classification analysis by their seismicity and relocated hypocenters. Vertical discontinuous distributions of DLF earthquakes were also observed at Laacher See volcano in Germany and Iwate volcano in Japan (Nakamichi et al., 2003; Hensch et al., 2019). Although these previous studies showed 5–20 km scale separation in the vertical discontinuous distribution, the results in Kirishima indicated a separation of a few hundred meters such as the cluster of type B1 and B2, and the cluster of type A2.

Hypocenters of DLF earthquakes also correspond to large-scale heterogeneities. Yamamoto & Ida (1994) and Nagaoka et al. (2018) showed a low-velocity anomaly of P-wave and S-wave beneath Kirishima volcanoes using seismic tomography and interferometry, respectively. The low-velocity anomaly is located beneath a depth of 5–15 km. Another low-velocity anomaly is located between 20 km and 35 km (Zhao et al., 2018). These two low-velocity anomalies roughly correspond to the depths of DLF earthquakes. Furthermore, the observations are consistent with the idea that DLF earthquakes occur in or around low-velocity zones and high-attenuation zones in many volcanoes (Hasegawa et al., 2005; Nakajima, 2017; Shiina et al., 2018). The results in Kirishima suggest that hypocenters of DLF earthquakes are concentrated at many small sources such as magma reservoirs located in the magma sills and conduits in the low-velocity zone (Figure 4.15). The models of DLF earthquakes are also discussed in Chapter 6.

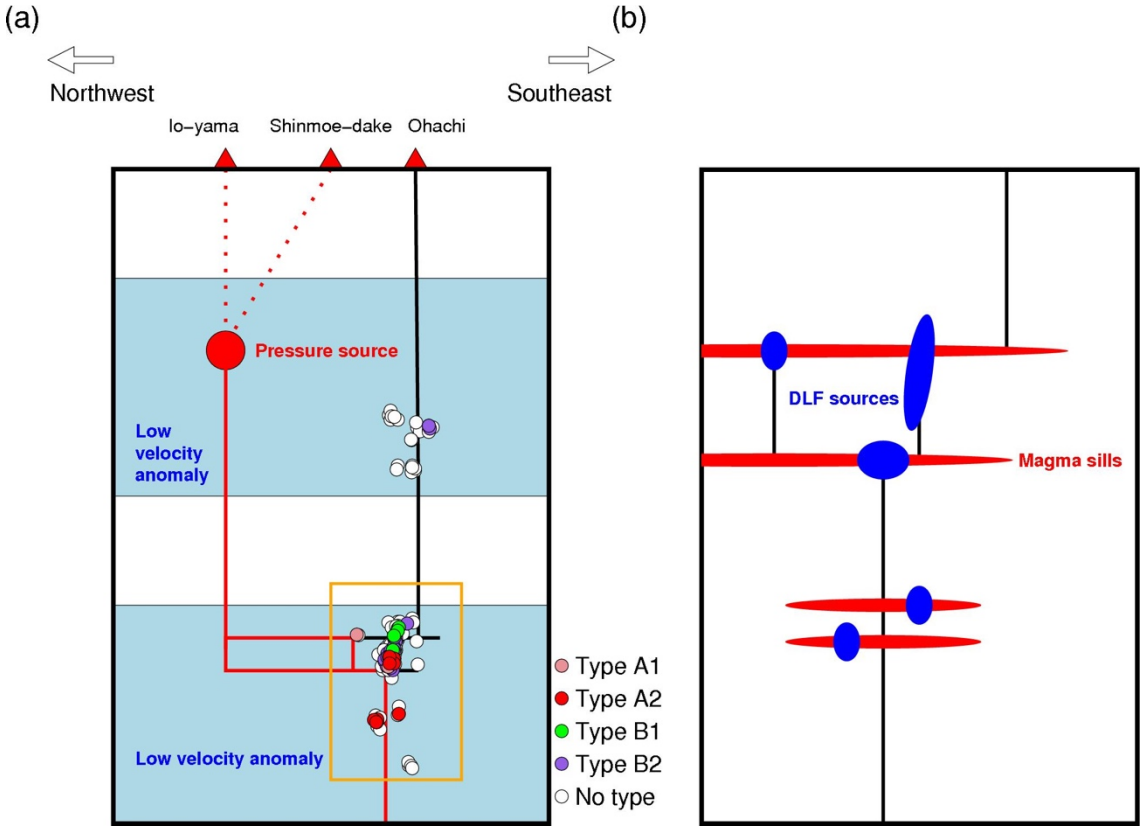

Figure 4.15 Schematic view of a possible underground structure in Kirishima volcanoes along the northwest-southeast line. A large red circle is the magma reservoir (Nakao et al., 2013). Colored small circles are DLF earthquakes, and the colors are the same as in Figures 4.10 and 4.12. Red dotted lines represent the estimated conduits for Shinmoe-dake and Io-yama from the magma reservoir. Black and red solid lines indicate the estimated paths of magma for the volcanoes based on DLF seismicity. Red lines show the estimated active paths at the 2011 eruptions and black lines show the estimated paths which were not active at the 2011 eruptions.

4.5.2. DLF earthquakes correlated with the eruptions

DLF earthquakes shallower than 17 km did not increase around the 2011 and 2018 eruptions unlike those deeper than 17 km (Figure 4.3). Many previous studies proposed the hypothesis that DLF earthquakes are affected by the movement of fluid (Aki & Koyanagi, 1981; Hasegawa et al., 2005; Hensch et al., 2019; Hotovec-Ellis et al., 2018). The results in Kirishima suggest that the fluid movement occurred near the hypocenters of DLF earthquakes at 20–25 km. Alternatively, no increase in DLF earthquakes shallower than 17 km suggests that the fluid might not pass near it. Therefore, one

reasonable interpretation of the shallow hypocenters of DLF earthquakes is that they are located along the conduit, connected not to Shinmoe-dake but to Ohachi volcano, which did not erupt in the periods (Figure 4.15). This is consistent with the idea of Kagiyama (1994) regarding magnetoelectric and petrological observations that Ohachi volcano can have a different magma supply system from the depth of approximately 20 km. The spatial pattern in the DLF seismicity may suggest that the fluid path directly connects to the pressure source at 8 km from the deep source regions of DLF earthquakes.

Type A1 first increased from December 2009 in the period of phreatic eruptions and was followed by the increase in Type A2 earthquakes before the subplinian eruptions (Figure 4.14). In this sequence, Type A1 earthquakes first occurred at a depth of 21.5 km in the period of phreatic eruptions. Next, Types A2.1 earthquakes were activated at about 23 km without eruptions. Finally, Type A2.2 and A2.3 earthquakes were activated at approximately 25 km after the subplinian eruptions (Figure 4.16).

It is considered that fluid movement probably started beneath the magma reservoir before the subplinian eruptions. Reduction in pressure, which possibly occurred at a depth of 10–20 km, might have triggered the ascent of fluid from the lower crust. Magma mixing process, which might trigger the 2011 subplinian eruptions, occurred 0.4 and 3 days before the eruptions in the shallow magma chamber (Tomiya et al., 2013). Magma mixing process might be affected by the injection of magma from the deep part. Although there were no significant activities of DLF earthquakes directly corresponding to the estimated timing of magma mixing 0.4 and 3 days before the eruptions. However, swarms of DLF earthquakes in August and December 2010 suggest the change of injection rates of magma. In addition, the peak of DLF seismicity appeared after the large crustal deformation triggered by the subplinian eruptions on 26–27 January 2011 (Figure 4.5). These observation results can be explained by the repressurization of the magma reservoir (e.g. Segall, 2016). These complex time-variable activities in many depths were also observed at Laacher See volcano (Hensch et al., 2019). The result in Kirishima volcanoes, that DLF seismicity is different even if the hypocenters are close to each other, provides an idea that many fluid paths are forming a network and they sometimes switch. In the network of paths, there are some sources of DLF earthquakes such as small magma reservoirs corresponding to magma intrusions. DLF earthquakes are perhaps observed only when the fluid passes near sources such as small magma reservoirs.

While Types A1 and A2 were activated associated with the 2011 eruptions,

Type B1 earthquakes were associated with the 2018 eruptions (Figure 4.9). This result suggests that the fluid path of the 2018 eruptions may have differed from that of the 2011 eruptions (Figure 4.16).

There is another hypothesis of activation of DLF earthquakes that pressure from shallow pressure source may trigger the DLF earthquakes. However, this hypothesis has little probability because DLF earthquakes were activated in deep limited source. If shallow pressure source triggered the DLF earthquakes, shallow DLF earthquakes at depths of 15 km would be activated. In addition, this hypothesis is difficult to explain the transition of hypocenters of activated DLF earthquakes.

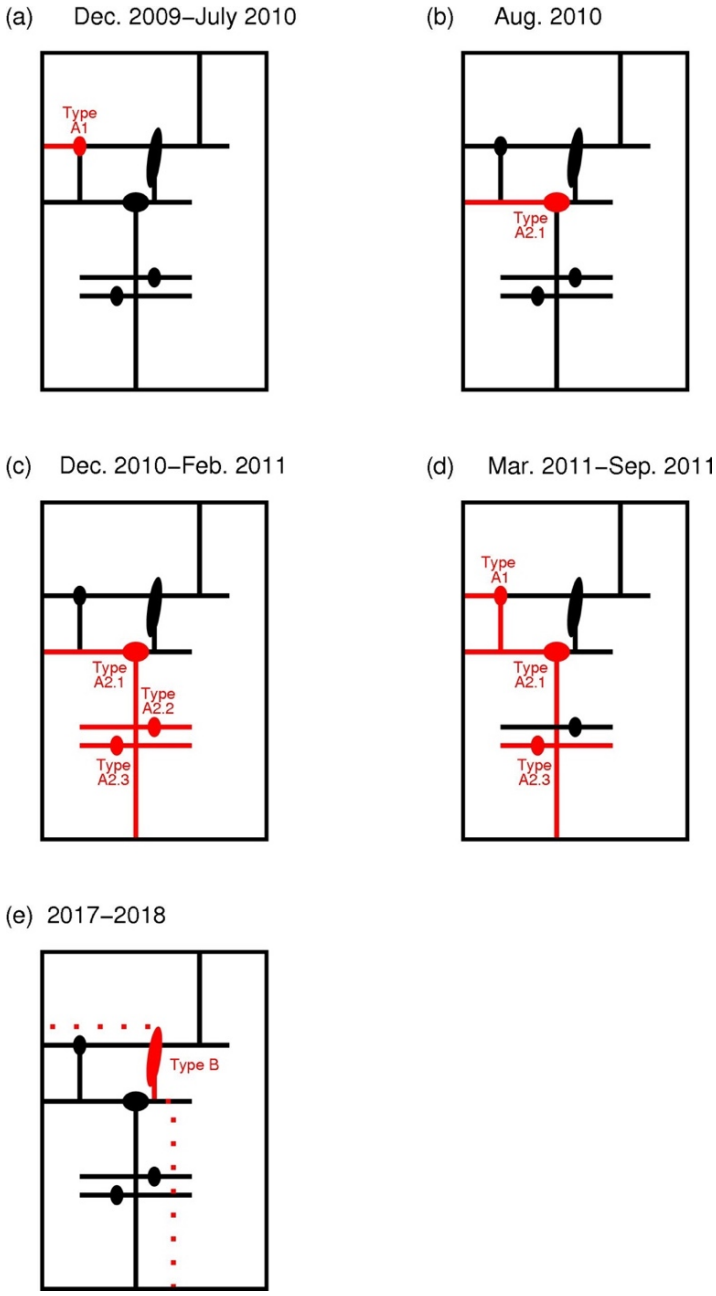

Figure 4.16 Distribution of DLF earthquakes and estimated fluid flow paths on each term. The area of figures is shown as the orange rectangle in Figure 4.15. Red and black lines show the active and non-active paths of fluid, respectively. Ellipses show the hypocenters of DLF earthquakes such as magma reservoirs. (a–d) are in terms of the 2011 eruptions, December 2009 – July 2010, August 2010, December 2010 – February 2011, and March 2011 – September 2011, respectively, and (e) for the 2018 eruptions.

4.6. Conclusions of this chapter

We analyzed DLF earthquakes that occurred at depths of 10–30 km in Kirishima volcanoes and found the following features:

1. Relocated hypocenters of DLF earthquakes show the discrete distributions.
2. DLF earthquakes were activated at depths of 20–27 km associated with the 2011 and 2018 eruptions.
3. DLF earthquakes had been activated with the 2011 eruptions for approximately two years since December 2009, associated with crustal deformation.
4. Waveforms of the DLF earthquakes associated with the 2011 eruptions had lower dominant frequencies and weaker P waves.
5. DLF earthquakes whose hypocenters are deeper than those of the other DLF earthquakes were associated with the 2011 eruptions and activated clusters were switched with transitions of eruption styles.
6. The waveforms and hypocenters of DLF earthquakes associated with the 2 018 eruptions are almost the same as those of the earthquakes which constantly occurred from 2004 to 2018.

The concentrated locations suggest that DLF earthquakes can occur only in particular locations, such as small magma reservoirs near magma sills. The activations of DLF earthquakes may reflect the fluid flow in the lower crust. In addition, different locations of DLF earthquakes for the 2011 and 2018 eruptions suggest that the fluid paths are different. These results show the possibility that eruption processes are directly related to fluid flow in the lower crust.

5. Relationship between activities of DLF earthquakes and volcanic activity –Other volcanoes–

In Kirishima, DLF earthquakes associated with eruptions are revealed in the previous chapter. Next, I investigated activities of DLF earthquakes associated with volcanic activities in four volcanoes, Meakan (No.2), Sakurajima (No.51), Ontake (No.44), and Hakone (No.37).

5.1. Meakan

5.1.1. Spatio-temporal distributions of DLF earthquakes

Meakan volcano is a volcano located in Hokkaido, north Japan. Large eruptions were not recorded in the observation by JMA started from the 1950s. However, small eruptions were observed in 2006 and 2008 (Japan Meteorological Agency, 2009).

In Meakan, many DLF earthquakes have been observed, although the level of surface volcanic activity is not high. 5508 DLF earthquakes were observed by this study and the DLF earthquakes occurred just beneath the edifice of the Meakan volcano (Figure 5.1). However, the activities of DLF earthquakes in Meakan have not been understood.

DLF earthquakes are distributed beneath the edifice of Meakan volcano at depths of 10–30 km (Figure 5.2). The distribution of depths of DLF earthquakes in the JMA catalog seems to be like Gaussian distribution (Figure 5.3). After relocation, DLF earthquakes are mainly separated into two spots at depths of 16–18 km and 22–24 km and the almost of all DLF earthquakes are concentrated at the deeper spot. In addition, some DLF earthquakes classified as Groups 3, 4, and 5 occur north of the largest spot and the depths are about 18–20 km.

DLF earthquakes in Meakan were classified into some groups by the two-stages classification (Figure 5.4). As the case of Hijiori, constant and episodic occurrences of DLF earthquakes were observed in Meakan (Figure 5.5). In Group 1.1, DLF earthquakes episodically occurred in 2008, 2013, 2015–2016, 2017. In Groups 1.2–1.6, DLF earthquakes constantly occurred. In Group 2.1, DLF earthquakes episodically occurred but the periods of the activations are not the same as those of Group 1.1.

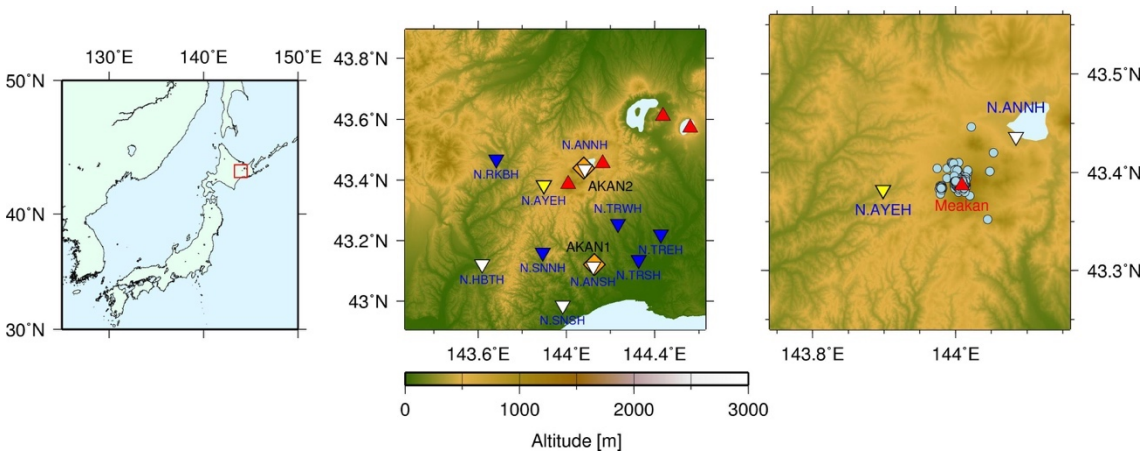

Figure 5.1 Distributions of observation stations and DLF earthquakes. Same figure as Figure 2.6 but in Meakan. Three different scales of maps are illustrated in each panel. Inverted triangles in middle and right panels indicate the locations of Hi-net stations used for relocation, estimation of magnitude and detection (yellow), relocation and detection (blue) and used only for relocation (white). Stations plotted as white inverted triangles are also used for detection when one or two stations plotted as yellow or blue triangles are missing observations. Orange diamonds show the locations of GNSS stations in GEONET. Light blue circles in the right panels show the epicenters of DLF earthquakes obtained by the relocation in this study.

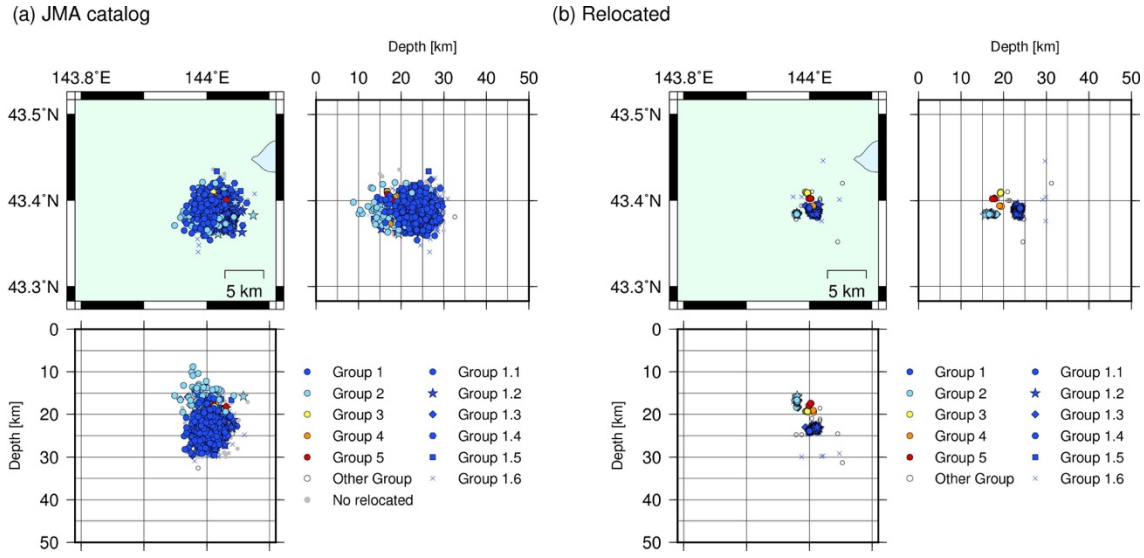

Figure 5.2 Three-dimensional hypocenter distribution of DLF earthquakes in Meakan in the JMA catalog and in the new catalog after the relocation.

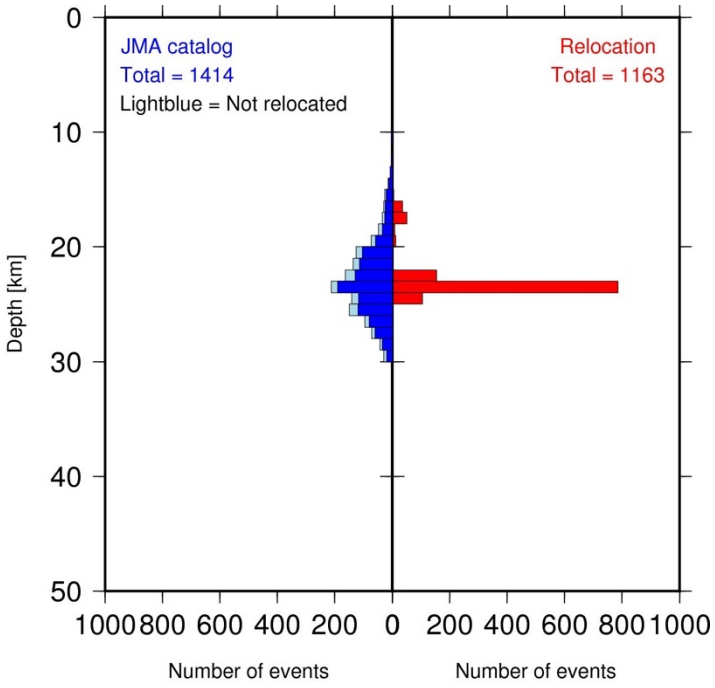

Figure 5.3 Depth distributions of DLF earthquakes in the JMA catalog and those after the relocation in Meakan.

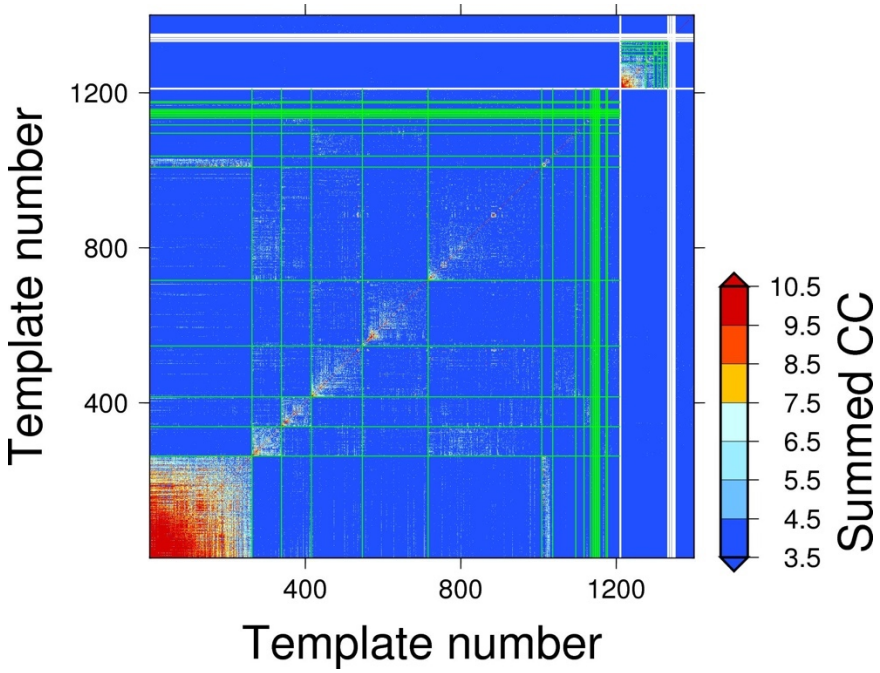

Figure 5.4 Summed correlation coefficients between all pairs of DLF earthquakes in Meakan.

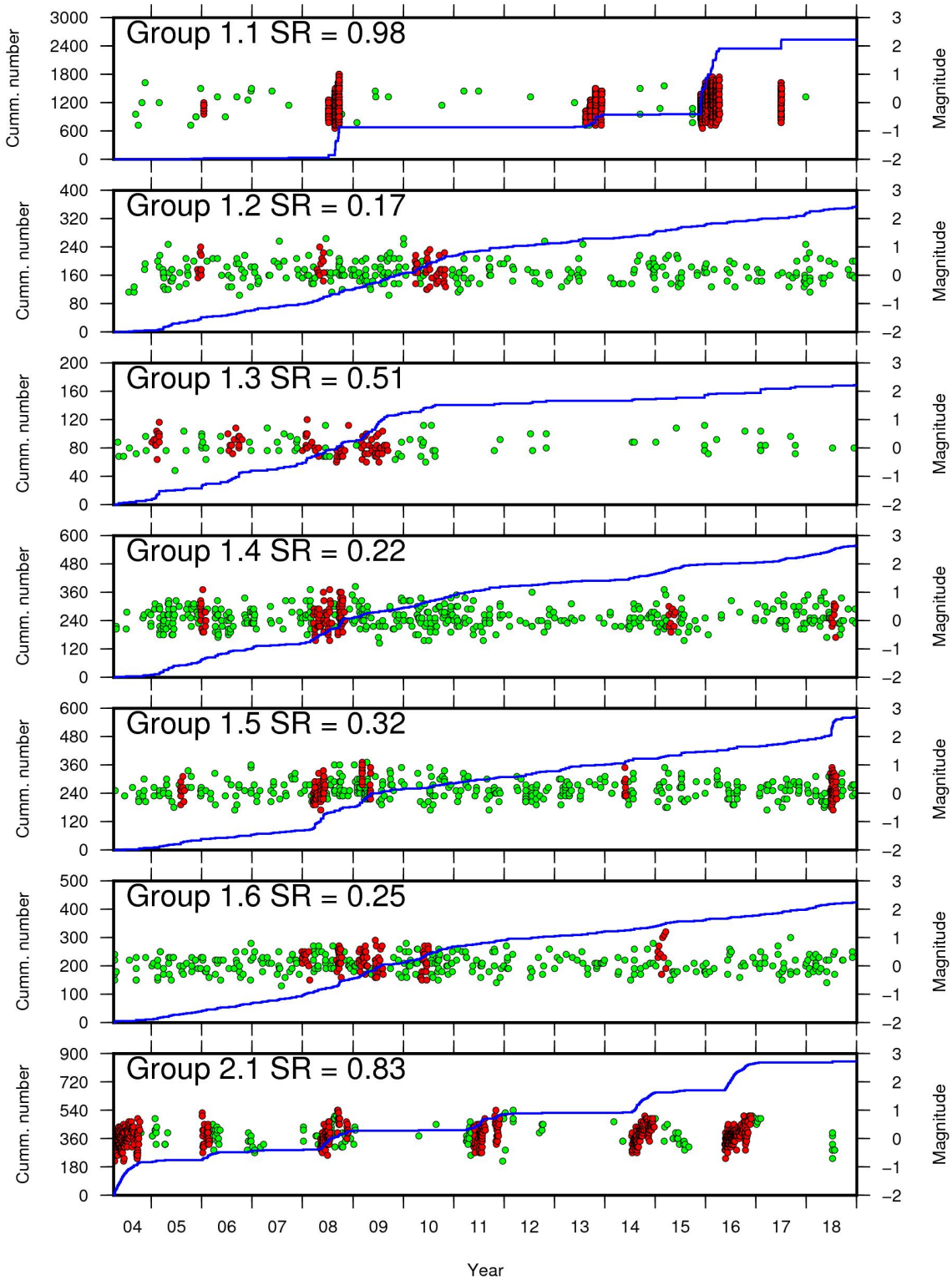

Figure 5.5 A cumulative number of DLF earthquakes and magnitudes of DLF earthquakes of each group in Meakan. Swarm ratios (SR) of the groups were written in each figure.

5.1.2. Episodic DLF earthquakes in Meakan

The swarms of DLF earthquakes of Group 1.1 at a depth of 24 km were observed in 2008, 2013, 2015–2016, and 2017 (Figure 5.6). These swarms of DLF earthquakes were roughly correlated with the crustal deformations. About one year after the swarms, crustal deformations between two GNSS stations, AKAN1 and AKAN2 (see Figure 5.1), were initiated at the episodes of 2008 and 2015–2016. In 2008, a small phreatic eruption also occurred.

According to the enlarged view of DLF seismicity, the three episodes of DLF earthquakes of Group 1.1 consisted of some small swarms with intervals of two weeks to one month (Figure 5.7–Figure 5.9). The small swarms have interesting characteristics about the magnitudes of DLF earthquakes. The upper limits of the magnitudes of DLF earthquakes in the swarms gradually grew in all three periods (Figure 5.7–Figure 5.9). The upper limits of the magnitudes in the first swarms were approximately 0 and those in the last swarms were approximately 1 in the three periods.

Episodic occurrences of DLF earthquakes were also observed in Group 2.1. However, in the enlarged view, temporal activity patterns of the DLF seismicity in Group 2.1 were different from those of Group 1.1. DLF earthquakes in Group 2.1 had continuously occurred in each episode whose duration is approximately one year, while the episodes in Group 1.1 consists of some small swarms. Furthermore, gradual increases of magnitudes of DLF earthquakes were also seen in each episode of DLF earthquakes in Group 2.1. In Group 2.1, not the upper limit of magnitudes but the average magnitudes of DLF earthquakes are seen to increase. The activation periods of Group 2.1 do not correspond to those of Group 1.1.

Groups 1.2–1.6 show the continuous occurrences of DLF earthquakes, although the hypocenters are very close to those of Group 1.1. It is like the case of Kirishima discussed in Chapter 4.

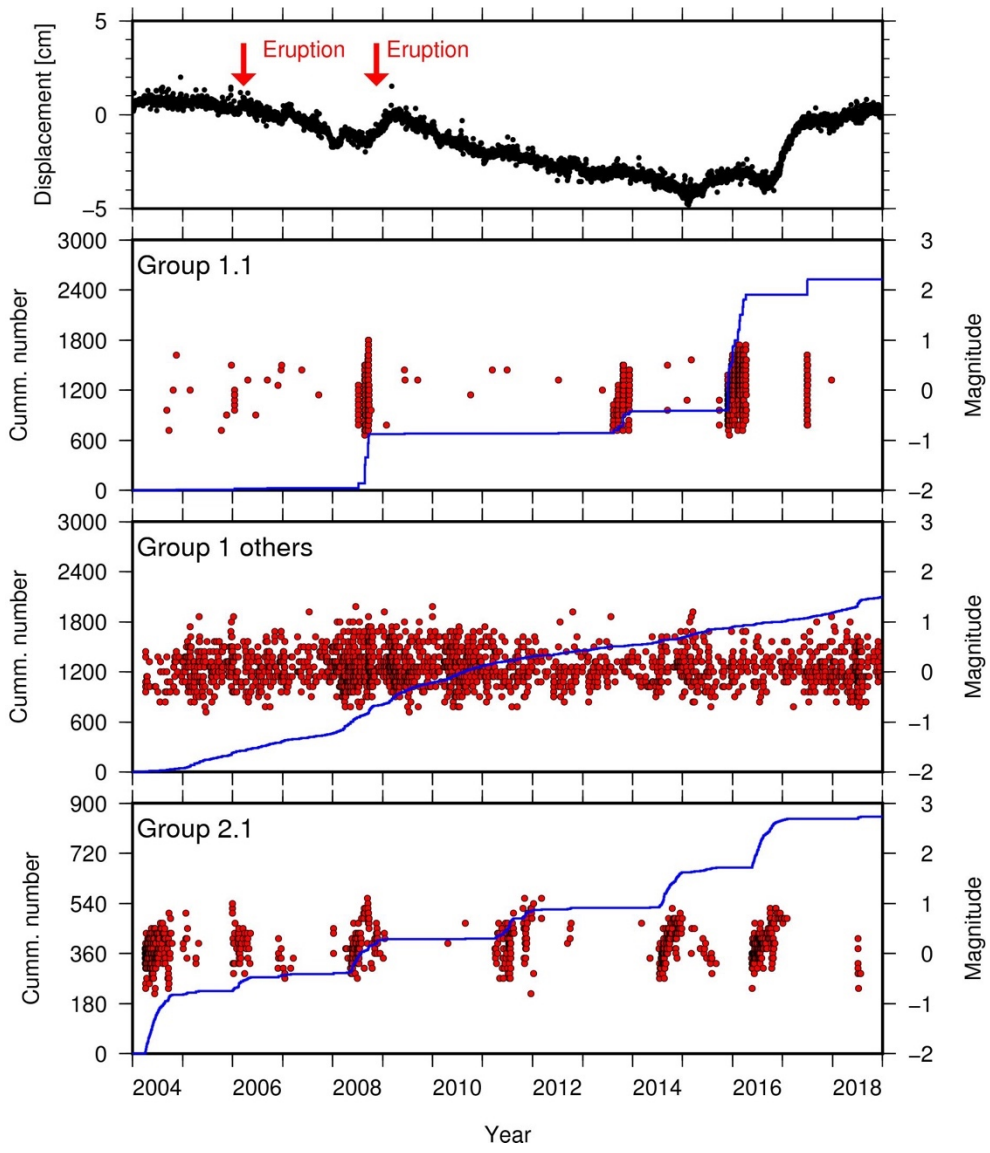

Figure 5.6 Activities of DLF earthquakes in Group 1.1, in Group 1 except Group1.1, and Group 2.1 in Meakan. Top figure shows the horizontal displacement between two GNSS stations AKAN1 and AKAN2 (see Figure 5.1).

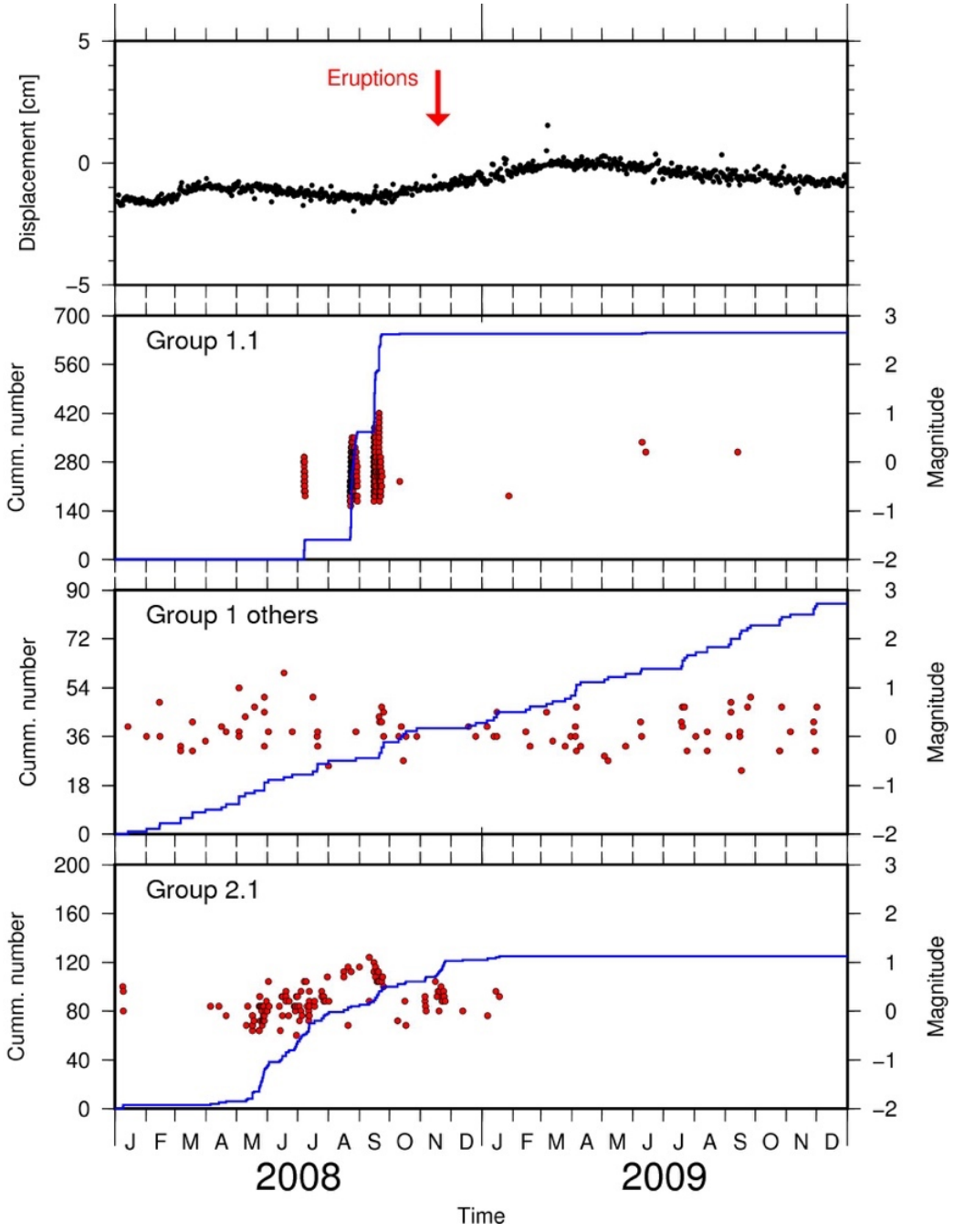

Figure 5.7 Enlarged portions of Figure 5.6 between 2008 and 2009.

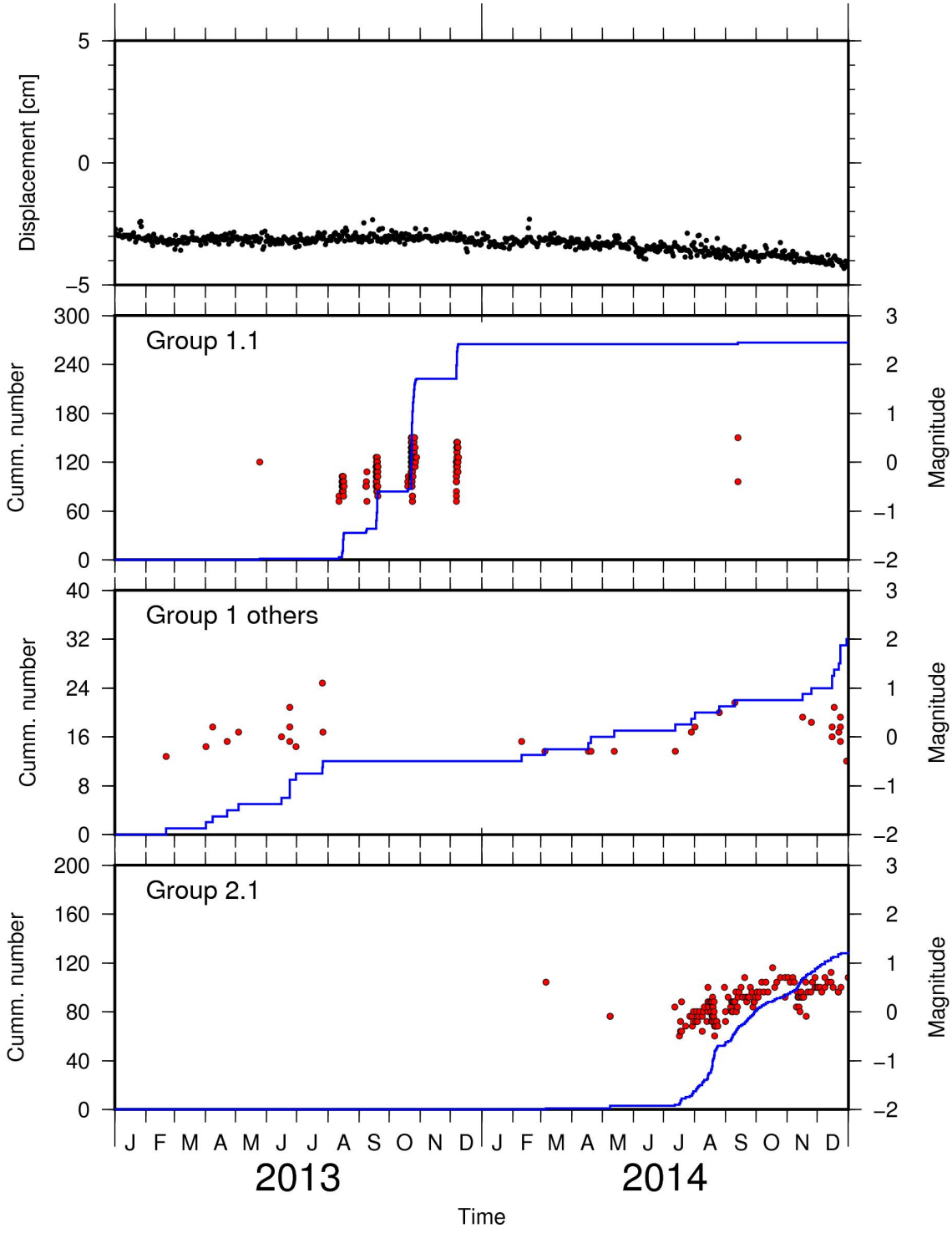

Figure 5.8 Enlarged portions of Figure 5.6 between 2013 and 2014.

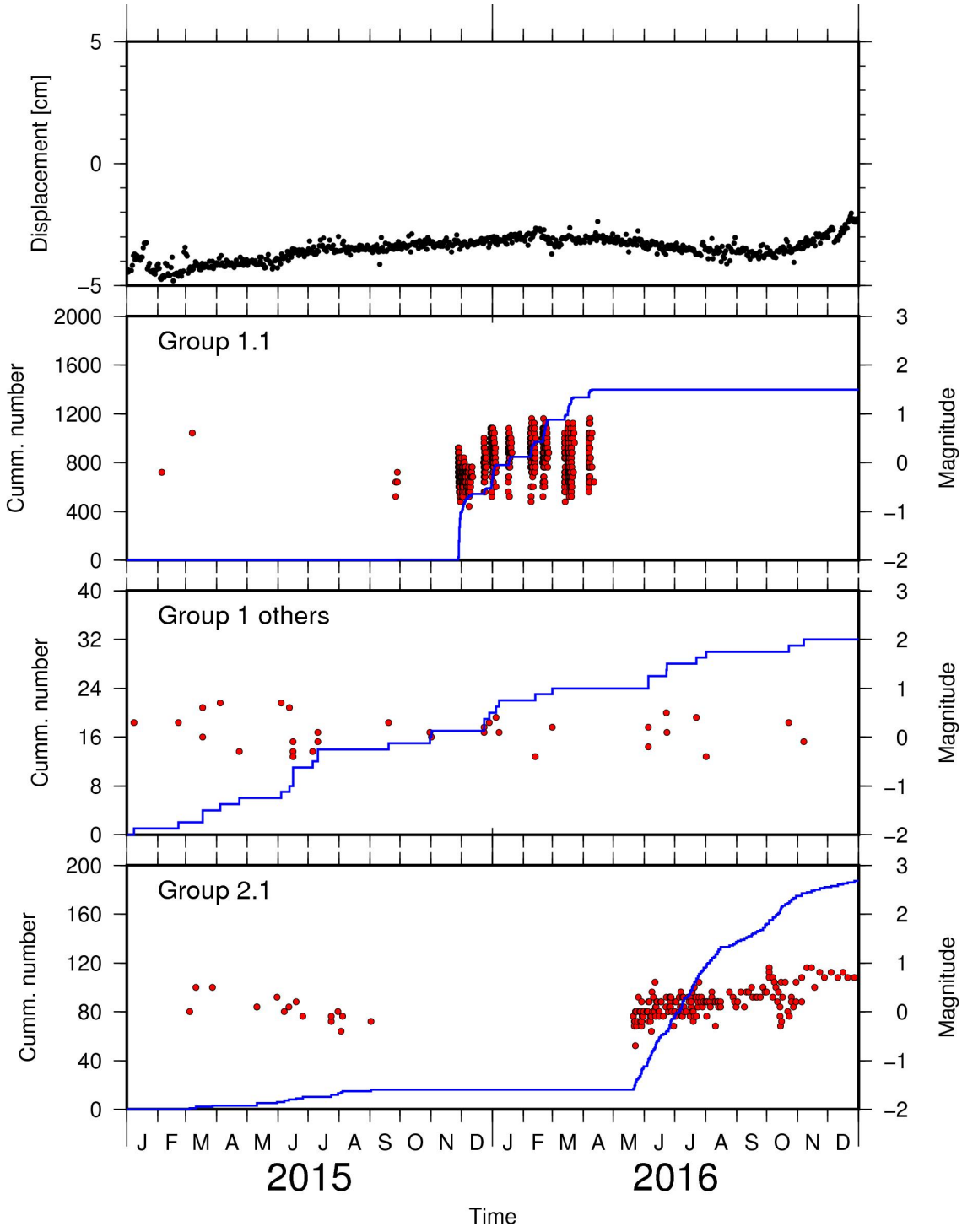

Figure 5.9 Enlarged portions of Figure 5.6 between 2015 and 2016.

5.1.3. Interpretations of DLF earthquakes in Meakan

The activations of DLF earthquakes of Group 1.1 occurred about one year before the crustal deformations and an eruption. This result suggests that DLF earthquakes in Group 1.1 may relate to the volcanic activities of the Meakan volcano. The source of the crustal deformation in 2016 was located northwest of Meakan volcano (Geospatial Information Authority of Japan, 2017), while DLF earthquakes occurred just beneath the edifice of the volcano. The horizontal distance between the edifice and the center of the source of the crustal deformation is about 4 km. The depth of the source was estimated at about 3–4 km (Kobayashi & Yamada, 2019; Shiraki & Murakami, 2019). Therefore, magmas might ascend from just beneath the Meakan volcano at a depth of 24 km to the northwest of the volcano (Figure 5.10). In addition, volcanic tremor had been observed from September 2008, which was before the 2008 eruption (Ogiso & Yomogida, 2012). The tremor occurred at the surface near the summit of the volcano. These observations suggest that magmas might not ascend directly from the source region of DLF earthquakes but ascend via the northwest part of the volcano.

Gradual increases of magnitudes of DLF earthquakes were observed in Meakan. However, there are no other regions in which such a gradual increase of magnitudes was observed. The gradual increases of magnitudes may be explained by source size growth. I propose in Chapter 6 the magma sill model that DLF earthquakes occur in magma sills intruded in the lower crust. Based on the model, when magma intruded from the deeper part to the magma sills, magma sills may gradually enlarge. Therefore, the gradual increases of magnitudes of DLF earthquakes may be explained by the enlargement of DLF source size.

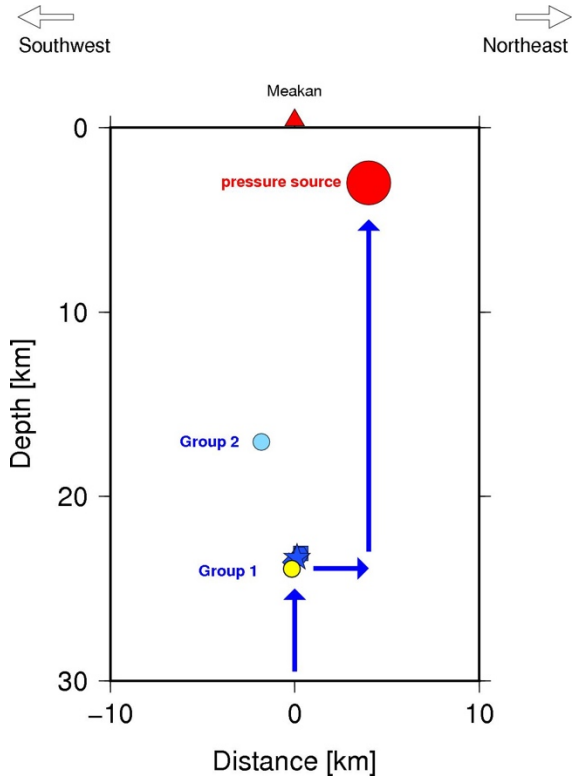

Figure 5.10 Model of the underground structure of the Meakan volcano. The yellow circle shows the average location of DLF earthquakes of Group 1.1. Blue symbols show the average location of DLF earthquakes of Groups 1.2–1.6. Symbols are same as Figure 5.2. A light blue circle shows the average location of DLF earthquakes of Group 2.1. A red circle shows the estimated location of the shallow pressure source. Arrows show the estimated path of ascending fluid.

5.2. Sakurajima

Sakurajima is one of the most active volcanoes in Japan in this decade. It erupted approximately 1000 times a year. DLF earthquakes occurred just beneath the volcano and north of the volcano. In this section, I focus on the DLF earthquakes occurred just beneath the volcano.

In Sakurajima, DLF earthquakes mainly occurred in the five groups, Groups 1.1, 2.1, 4.1, 47, and 54 (Figure 5.11). Activations of the DLF earthquakes were observed in four groups around August 2015, when dike intrusions occurred at a depth of 1 km (Hotta et al., 2016). Especially many DLF earthquakes in Groups 47 and 54 occurred at the time. The large crustal deformation due to the dike intrusion and end of the activations of DLF earthquakes were well correlated (Figure 5.11). In addition, DLF earthquakes in

Groups 47 and 54 were well correlated with the number of vulcanian eruptions at Showa Crater (Japan Meteorological Agency, 2019). Those activities increased from 2009 and decreased after the 2015 dike intrusion.

Many DLF earthquakes in Groups 47 and 54 were observed in this study. However, in the JMA catalog, each group includes only one earthquake, which was used as the template earthquake of the matched filter technique (Section 2.4). In addition, both DLF earthquakes were not relocated by the NCC method (Section 2.2). The absence of DLF earthquakes in the JMA catalog may be caused by their waveform characteristics. Figure 5.12 shows the waveforms of two DLF earthquakes in Groups 47 and 54, respectively. Compared to other DLF earthquakes (Figure 5.13), the waveforms of DLF earthquakes in Groups 47 and 54 have longer durations and lower dominant frequencies as like Type A2 DLF earthquakes in Kirishima (cf. Figure 4.11; Figure 4.12). The hypocenters of DLF earthquakes in Groups 47 and 54 in the JMA catalog are in the source regions of DLF earthquakes. I located a DLF earthquake in Group 47, which is shown in Figure 5.12, by manual picking of the phases. Then, the hypocenters of DLF earthquakes in Groups 47 and 54 may be located beneath the edifice of the volcano and the depth is about 24 km (Figure 5.14). The hypocenters of the DLF earthquakes of Groups 47 and 54 may be close to those of the other DLF earthquakes.

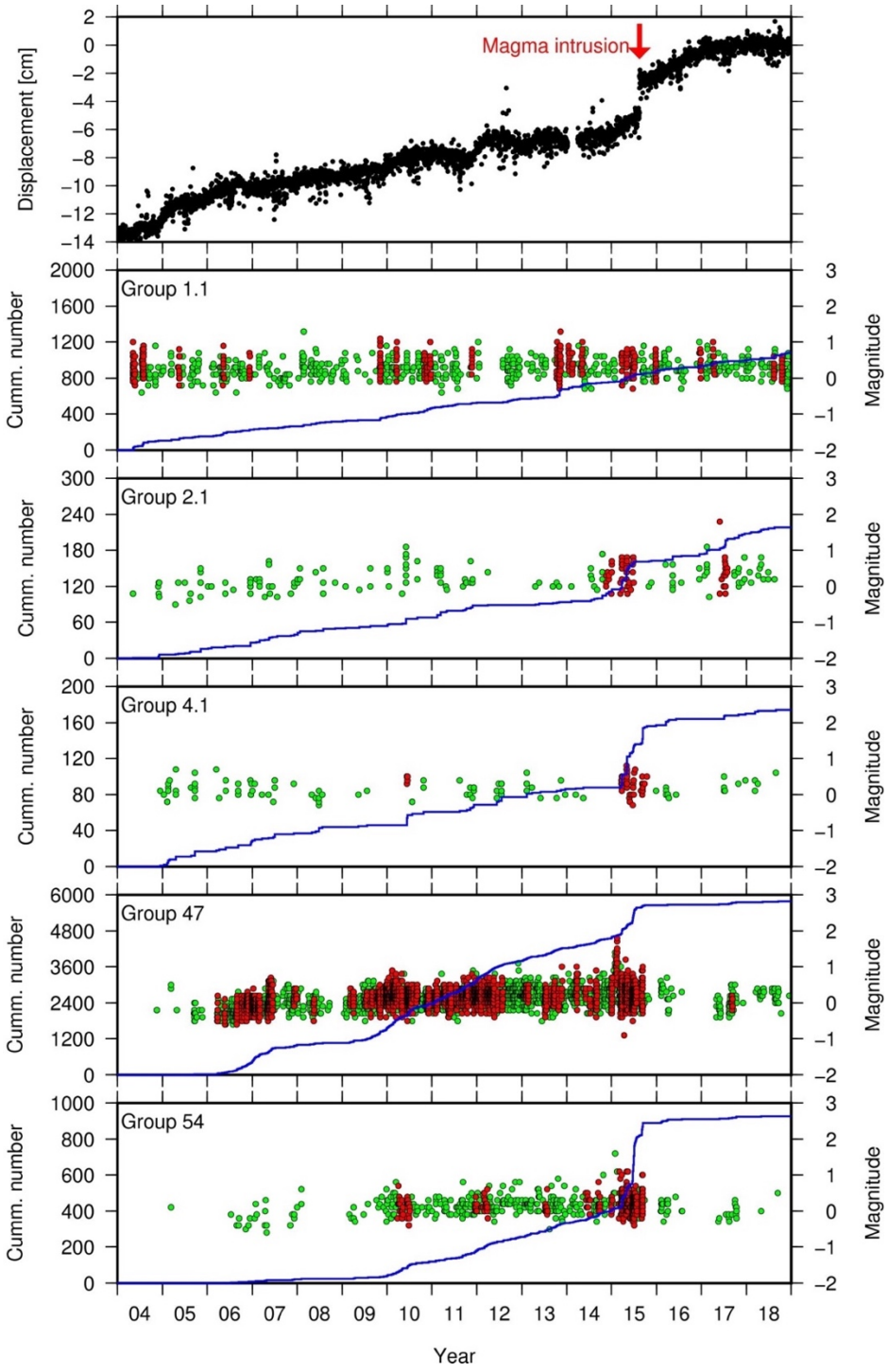

Figure 5.11 Cumulative number of DLF earthquakes from April 2004 and magnitude-time distributions in each group in Sakurajima with horizontal displacement. The groups in which have more than 100 DLF earthquakes are plotted. The top panel shows the amount of the horizontal displacement between two GNSS stations plotted in Figure 5.14.

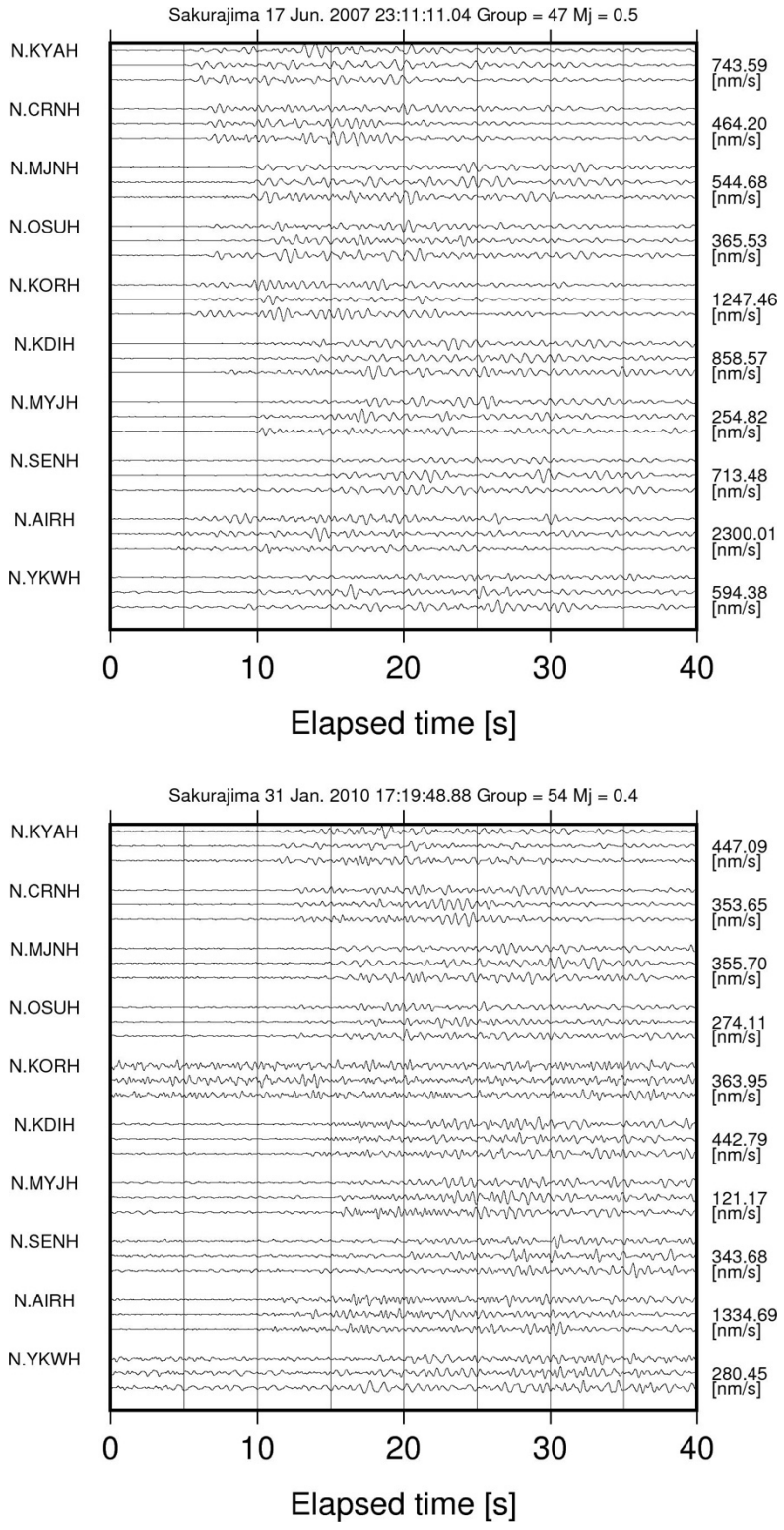

Figure 5.12 Waveforms of two DLF earthquakes of Group 47 and 54 detected in this study. Every three lines show the velocity waveforms of east-west, north-south, and up-down components. The bandpass filter of 1–4 Hz was applied for the waveforms.

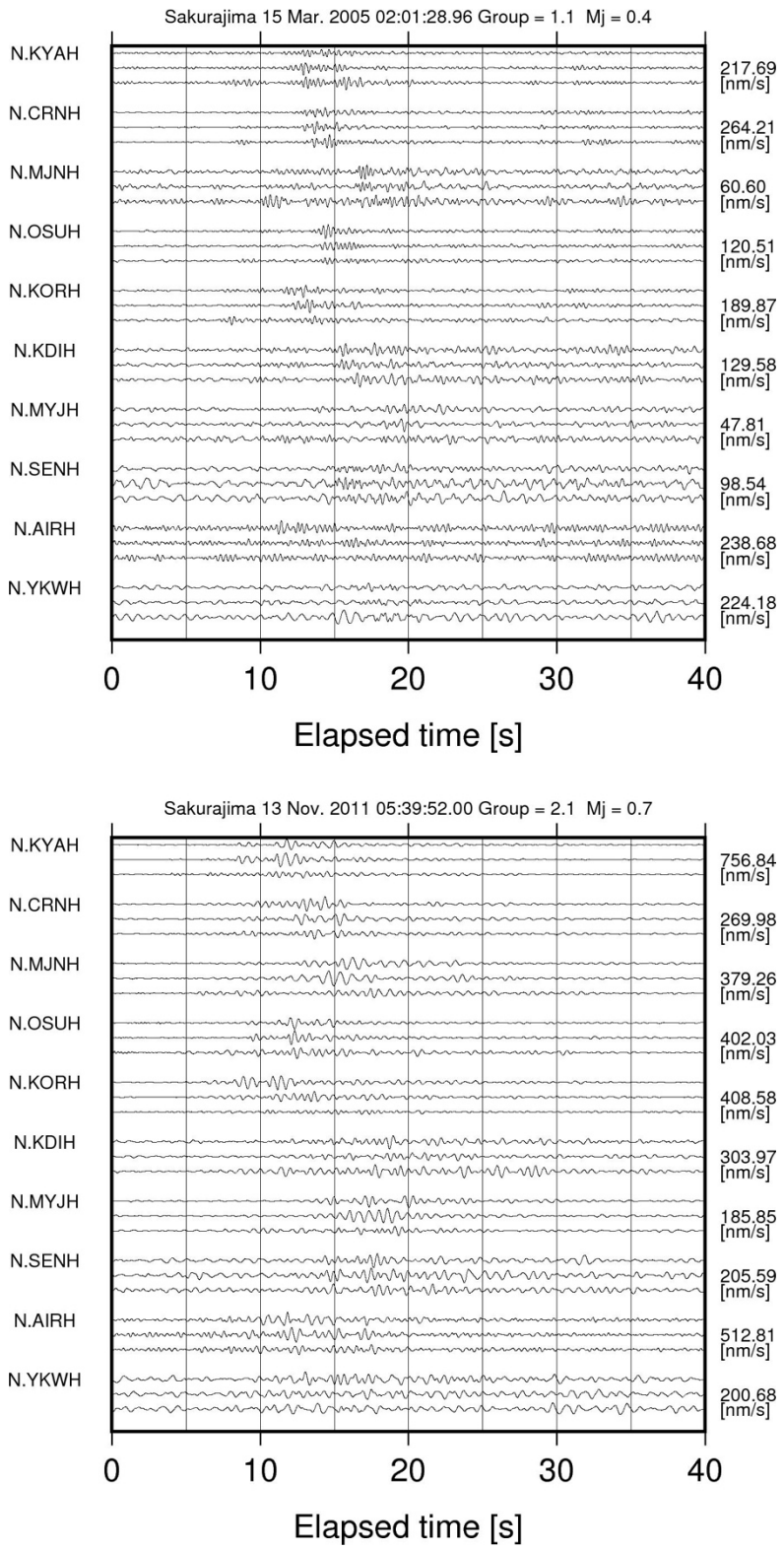

Figure 5.13 Same figure as Figure 5.12 but for two DLF earthquakes in Group 1.1 and 2.1.

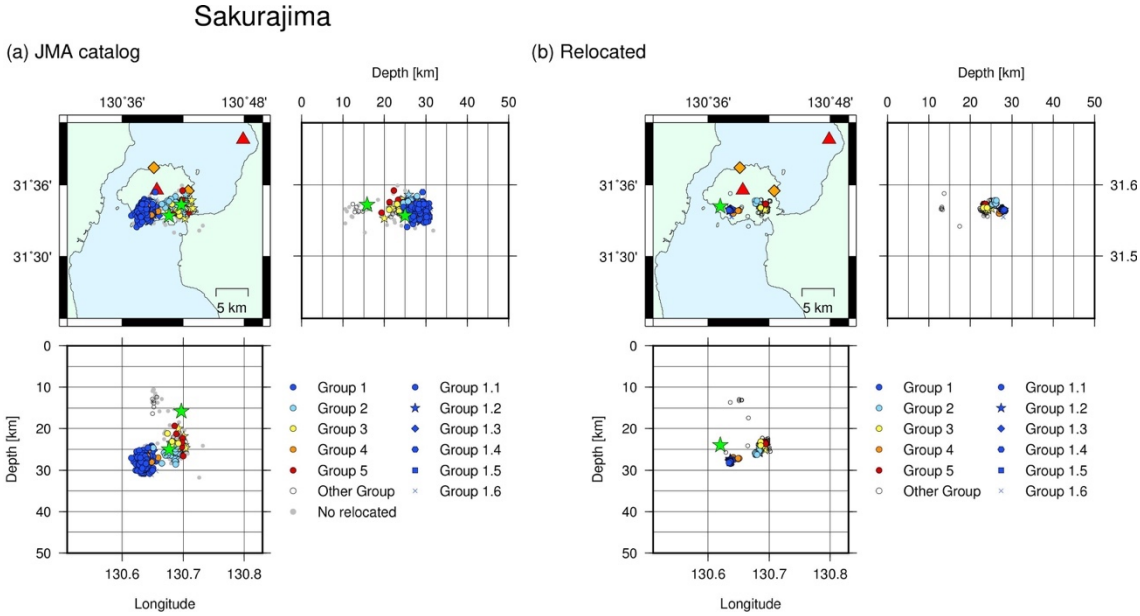

Figure 5.14 Three-dimensional distributions of DLF earthquakes. Green stars show the hypocenters of DLF earthquakes in Group 47 and 54. The locations of template earthquakes in the JMA catalog are plotted in figure (a). The location of a detected DLF earthquake occurred at 23:11:11 (JST), 17, June 2007 is plotted in figure (b). Red triangles show the summits of active volcanoes and orange diamonds show the locations of two GNSS stations.

5.3. Ontake

Eruptions of Ontake volcano were observed in 2007 and 2014 (Japan Meteorological Agency, 2007, 2014). Both eruptions were not large, but 63 peoples were killed by the 2014 phreatic eruption. Therefore, even if it is a small phreatic eruption, the prediction of an eruption is very important not only for volcanology but also for disaster mitigation.

The depths of most DLF earthquakes in Ontake are 30–38 km, which are deeper than those in other regions (Figure 5.15 and Figure 3.7). The hypocenters of DLF earthquakes a have horizontal off-sets pf approximately 15 km from the summit (Figure 5.16).

DLF earthquakes of Group 1.1 episodically occurred on 3 February 2010 (Figure 5.17). 100 DLF earthquakes occurred in only one hour. However, no volcanic activity was associated with the episode of DLF earthquakes. DLF earthquakes of Group 1.2 episodically occurred in 2005, 2006–2007, 2011, and 2014. DLF earthquakes of

Group 1.4 also episodically occurred, but the periods of the activations were different from those of Group 1.2.

At the 2014 eruption, activation of volcanic tectonic (VT) earthquakes at depths less than 1 km was observed (Kato et al., 2015). Activation of DLF earthquakes of Group1.2 at a depth of approximately 33 km was well correlated with the activation of VT earthquakes (Figure 5.18). Both activations began 20 days before the eruption. The time-lag between activations of VT earthquakes and DLF earthquakes might be within a day. However, there is no activation of DLF earthquakes on the day of the eruption, while many VT earthquakes were observed on the day. Activations of DLF earthquakes in Group1.4 at depths of approximately 35 km began 8 days before the eruption.

Although the amounts of crustal deformations were small at the periods of eruptions in 2007 and 2014 (Figure 5.17), small crustal deformations associated with both eruptions were reported (Miyaoka & Takagi, 2016). Crustal deformations were started in December 2006 at the 2007 eruption and early September 2014 at the 2014 eruption. The start times of crustal deformations were corresponding to the activations of DLF earthquakes in Group 1.2.

As a result, it is revealed that phreatic eruptions are affected by volcanic activities in the lower crust such as magma flow. In addition, the simultaneous occurrence of the activations of DLF earthquakes and VT earthquakes suggest that pressure perturbation may instantly propagate from the lower crust to near surface of Ontake volcano.

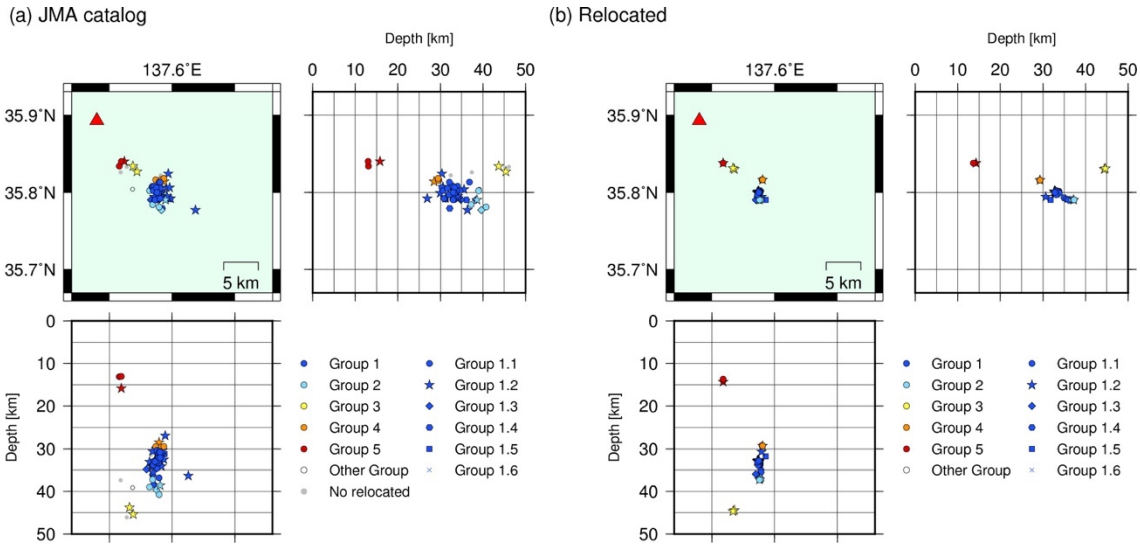

Figure 5.15 Three-dimensional distributions of DLF earthquakes in Ontake.

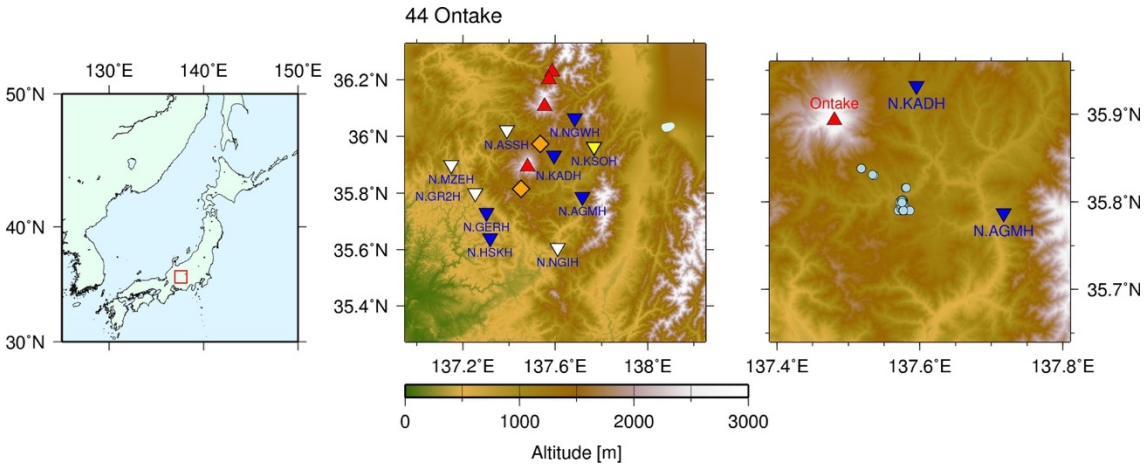

Figure 5.16 Distribution of the stations and DLF earthquakes in Ontake. Same figure as Figure 2.5. Orange diamonds in the middle figure show the GNSS stations.

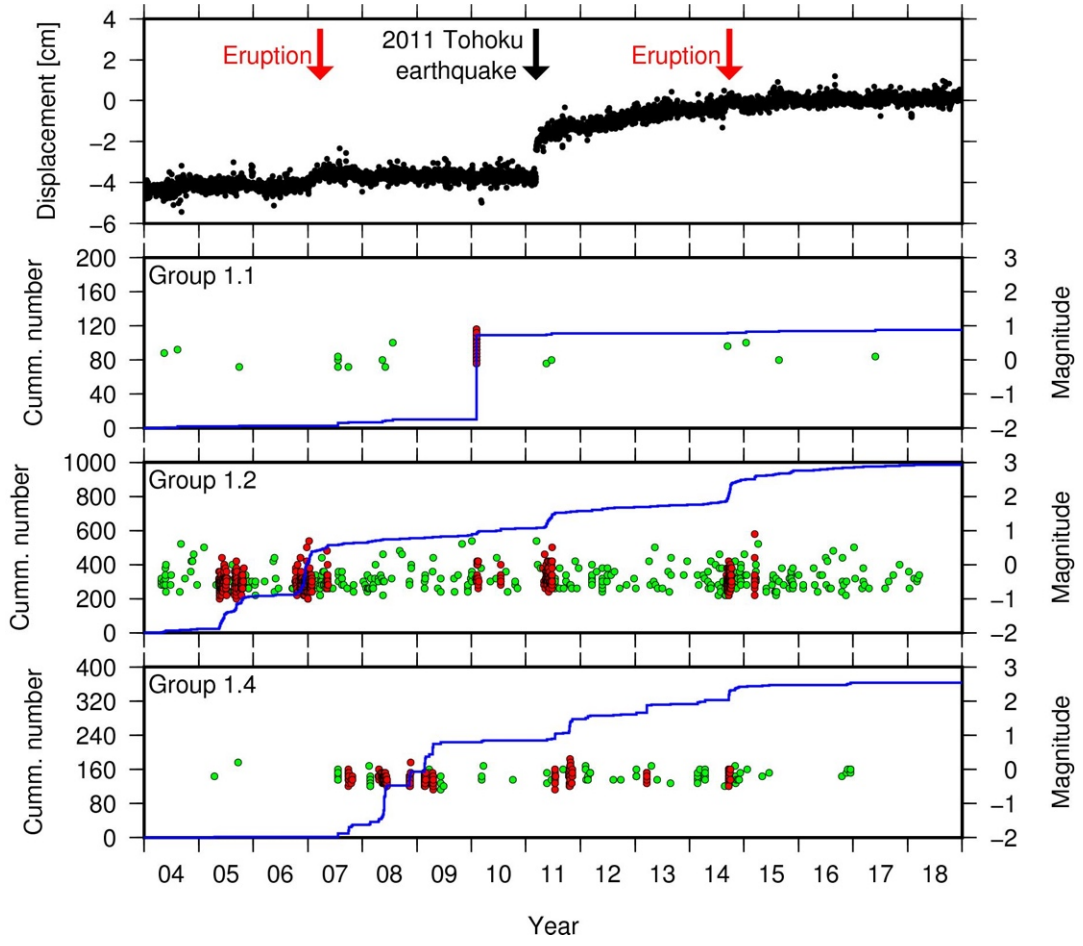

Figure 5.17 Cumulative number of DLF earthquakes from April 2004 and magnitudes of DLF earthquakes in each group in Ontake with horizontal displacement. The groups in which have more than 30 DLF earthquakes are plotted. The top figure shows the amount of horizontal displacement between two GNSS stations (see Figure 5.16).

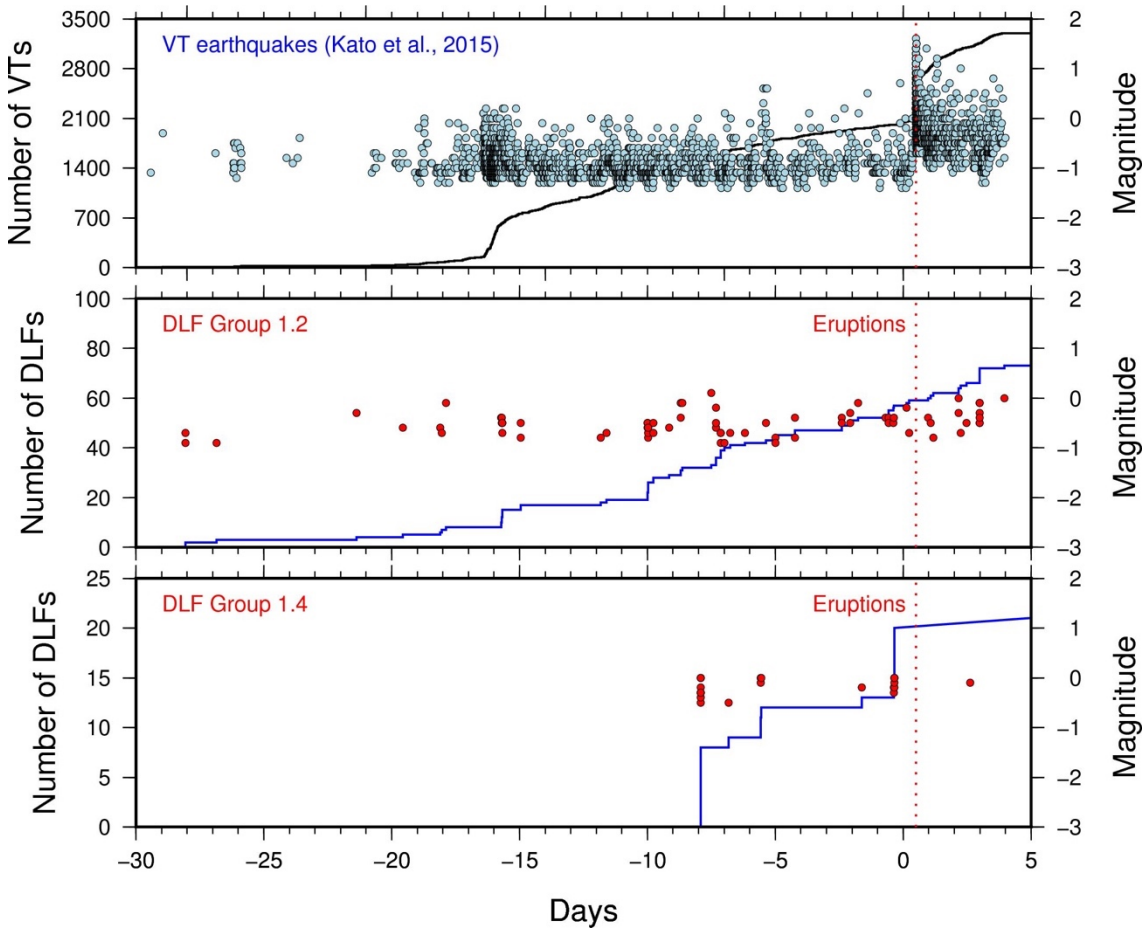

Figure 5.18 Cumulative number and magnitudes of DLF earthquakes in two groups and volcanic tectonic (VT) earthquakes based on the catalog of Kato et al. (2015) around the time of the 2014 phreatic eruption. Solid lines show the cumulative numbers of the earthquakes and colored circles show the magnitudes. Dotted lines show the time of the 2014 phreatic eruption.

5.4. Hakone

In Hakone volcano, small phreatic eruptions occurred on 3 May and 29 June 2015 (Mannen et al., 2018). At the period of eruptions, activation of DLF earthquakes associated with 2015 eruptions was observed (Yukutake et al., 2019). In this study, the two-stage classification of DLF earthquakes reveals more detailed activities of DLF earthquakes associated with the eruption of the Hakone volcano.

In Hakone, most DLF earthquakes occurred at depths of 20–25 km (Figure 5.19). There are mainly three groups of DLF earthquakes, Group 1.1, 1.2, and 1.3. Temporal activity patterns of DLF earthquakes in the three groups are different like other

volcanoes (Figure 5.20). Group 1.2 has large SR and episodes of DLF earthquakes repeatedly occurred with the intervals of a few years. At the period of the 2015 eruptions, all groups of DLF earthquakes were activated.

Figure 5.21 shows the activities of DLF earthquakes around the 2015 eruptions. DLF earthquakes in Group 1.1 gradually increased from March 2015. The activation had finished until the latter phreatic eruption on 29, June 2015. DLF earthquakes in Group 1.2 were suddenly activated in April 2015 and approximately 300 DLF earthquakes occurred around the former eruption on 3 May 2015. There was another activation corresponding to the latter eruption. Although the number of DLF earthquakes in Group 1.3 is very small, activation of the DLF earthquakes was also observed in Group 1.3.

As a result, the activities of DLF earthquakes in the three groups were associated with eruptions. However, the temporal activity patterns of DLF earthquakes are different from each group.

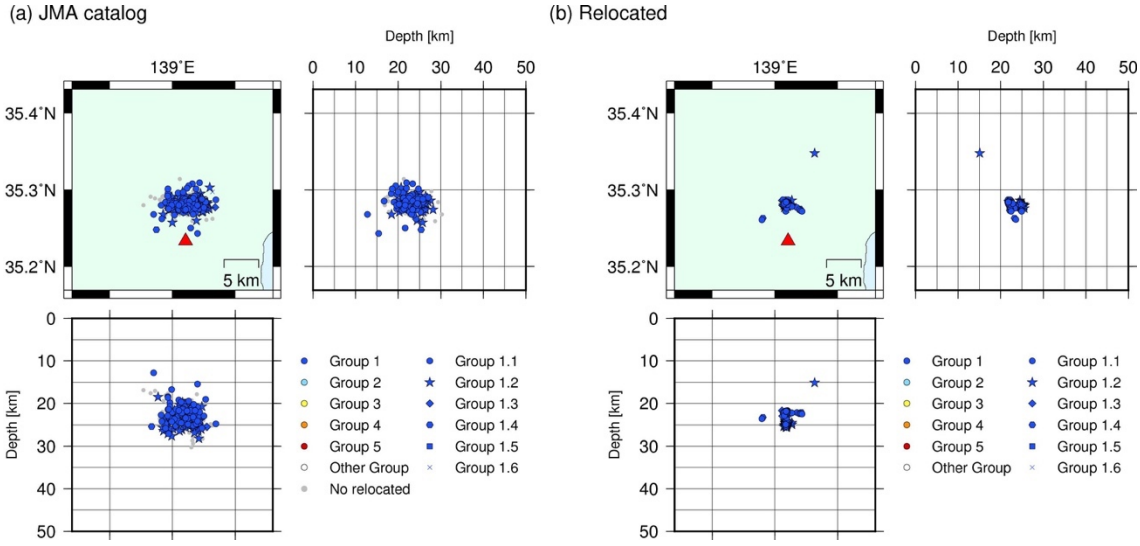

Figure 5.19 Three dimensional distributions of DLF earthquakes in Hakone.

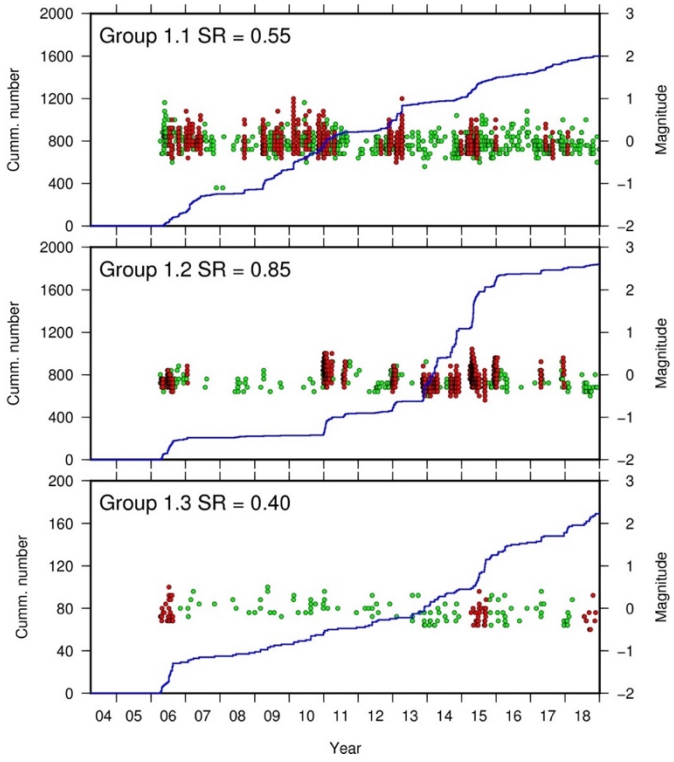

Figure 5.20 Cumulative number of DLF earthquakes from April 2004 and magnitudes of DLF earthquakes of each group.

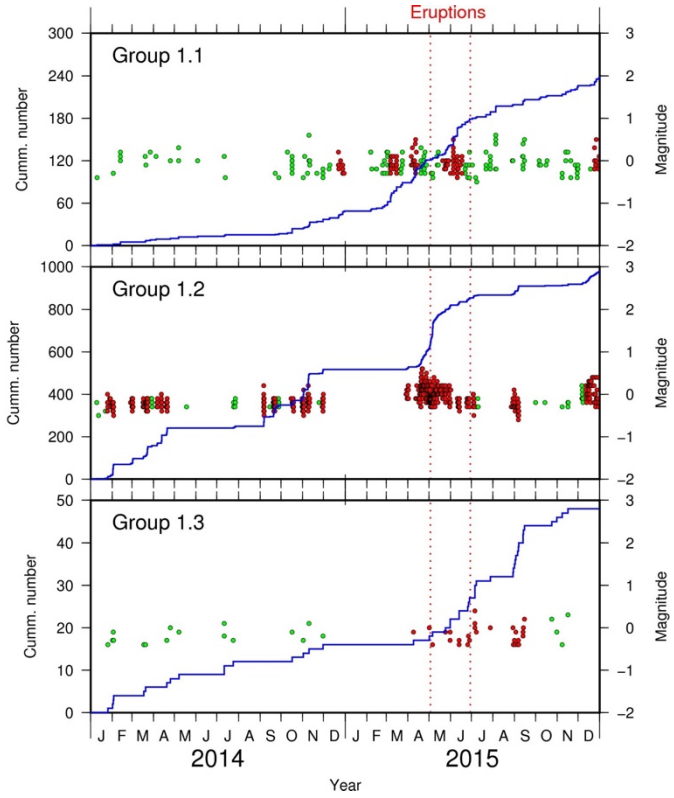

Figure 5.21 Enlarged portions of Figure 5.20 between 2014 and 2015.

5.5. Discussion and conclusions of the relationship between volcanic activity and DLF earthquakes

In Chapters 4 and 5, I showed the activations of DLF earthquakes with various types of eruptions such as phreatic, vulcanian and subplinian eruptions in the five volcanoes. The results suggest that DLF earthquakes may be triggered by volcanic activities such as the movement of magma in the lower crust. These activations of DLF earthquakes were only observed in some groups of DLF earthquakes in all volcanoes. Hypocenters of the DLF earthquakes have horizontal offsets from the edifices of the volcanoes or shallow magma reservoirs in the five volcanoes.

Based on the activity of DLF earthquakes, the five volcanoes were divided into two categories (Figure 5.22). One volcanic category "Kirishima type" includes Kirishima, Meakan, and Sakurajima in which one or a few groups of DLF earthquakes were activated in the periods of eruptions. In the group, DLF earthquakes rarely occur in the other period. In Kirishima and Meakan, groups of DLF earthquakes with deep hypocenters were activated with the eruptions. Those DLF earthquakes associated with eruptions in the three volcanoes have waveforms with dominant frequencies of 1–2 Hz, which is lower than those of DLF earthquakes not associated with volcanic activities (Table 5.1). According to these observations, I interpret that magma ascended to the lower crust and firstly intruded in the deep part of the source regions of DLF earthquakes. There are much intruded magmatic fluids in the depths and the fluids may generate the low-frequency waveforms of DLF earthquakes. On the other hand, another category "Ontake type" include Ontake and Hakone, some groups of DLF earthquakes at different depths in which DLF earthquakes usually occur, were activated with eruptions, although the temporal activity patterns of DLF earthquakes in each group are different. In the cases, magmas might intrude into various depths.

Time-lags between activations of DLF earthquakes and surface volcanic activities are also roughly corresponding to the volcanic category (Table 5.2). It took long time in "Kirishima type" and short time in "Ontake type". In Kirishima and Meakan, it took a few hundred days from activations of DLF earthquakes to eruptions. On the other hand, it took only 20 days from activations of DLF earthquakes to an eruption in Ontake at the 2014 eruption, even the hypocenters of DLF earthquakes were deeper than those of the other volcanoes. In Hakone, Group 1.1 of DLF earthquakes were activated approximately two months before the eruption and Group 1.2 of DLF earthquakes were

activated approximately one month before the eruption. The difference may be due to the capacity of magma reservoirs in the shallow crust. In Ontake, there is only small crustal deformation before the eruption, while large crustal deformations were observed in Meakan and Kirishima. Therefore, the period until the magma reservoirs are filled by magma may be different because of the difference in the size of shallow magma reservoirs and the time-lags between activations of DLF earthquakes and surface volcanic activities.

Above categorization in this study is too simple and there is an exception. For example, in Kirishima, Type B1 of DLF earthquakes were activated at the period of 2018 eruptions. Therefore, the difference of activated type of DLF earthquakes may be different to each eruption, even in the same volcano. The difference may be affected by the movement of magma. However, there is not enough observations to discuss the reasons of the difference.

As a conclusion of this chapter, DLF earthquakes associated with eruptions were observed in five volcanoes. In Kirishima, Meakan and Sakurajima, DLF earthquakes with lower dominant frequency were activated in the period of eruptions. In this case, the time-lags between activation of DLF earthquakes and eruptions were mostly long. On the other hand, in Ontake and Hakone, DLF earthquakes with usual activity were activated in the period of eruptions. In this case, the time-lags between activation of DLF earthquakes and eruptions were mostly short.

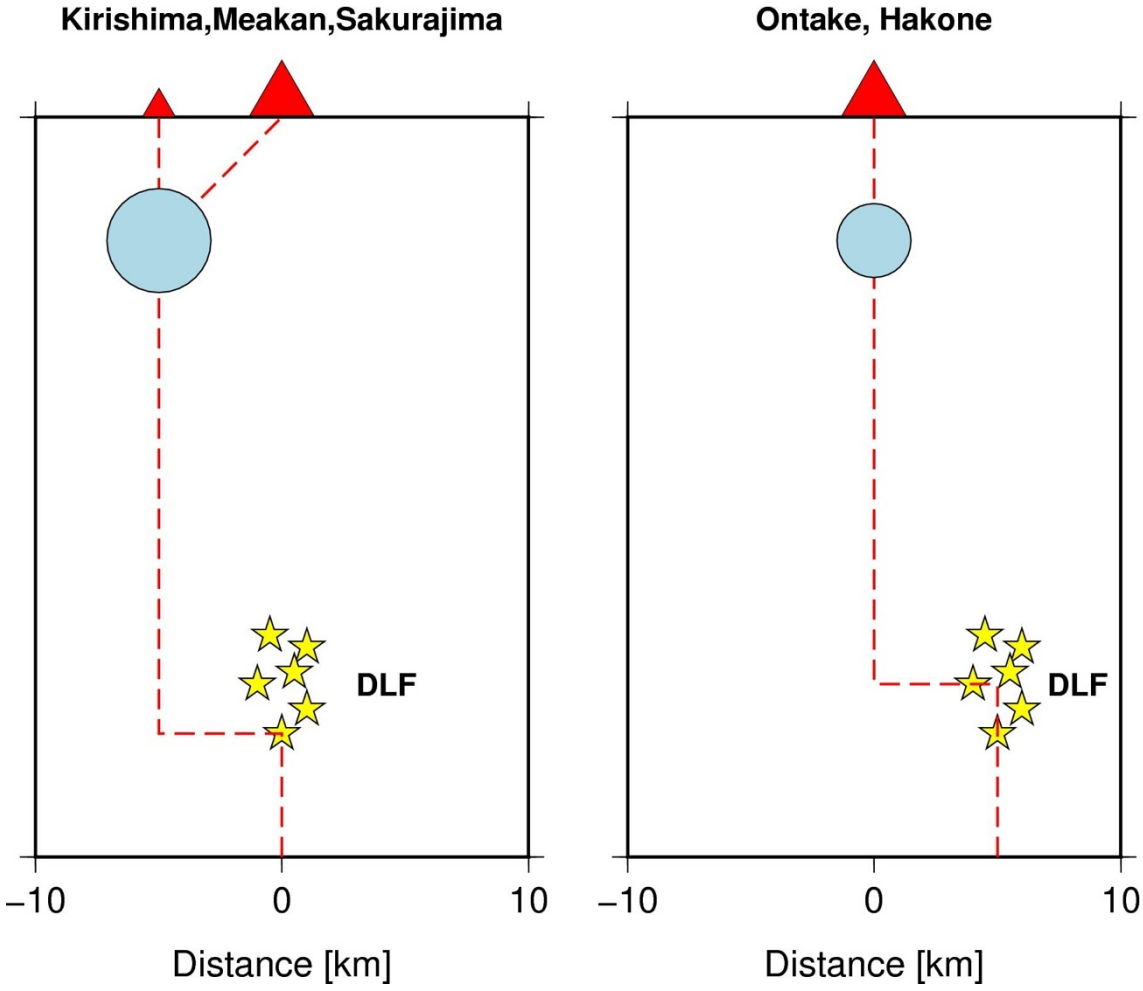

Figure 5.22 Schematic views of hypocenters of DLF earthquakes, shallow magma reservoir and edifice of the volcano. The left figure shows the cases of Kirishima, Meakan, and Sakurajima. The right figure shows the cases of Ontake and Hakone. Red broken lines show the estimated fluid paths from deep part to the surface.

Table 5.1 Properties of DLF earthquakes of each group in the five volcanoes. The properties are parts of Table 3.2. If DLF earthquakes in the group are associated with volcanic activity, “Yes” is in the column of association with volcanic activity.

Region	Group	DLFs in JMA	DLFs in MFT	Depth [km]	(1-2)Hz/(2-4)Hz	PS ratio	Association with volcanic activity
Kirishima	1.1	128	2486	22.4	2.9	1.52	Yes
Kirishima	1.2	30	117	21.3	1.29	0.90	
Kirishima	1.4	7	103	20.7	1.87	1.30	
Kirishima	2.1	24	89	11.7	1.64	1.48	
Kirishima	2.2	21	46	13.2	0.73	2.18	
Meakan	1.1	262	2530	23.9	3.28	1.64	Yes
Meakan	1.2	75	354	23.3	1.12	2.82	
Meakan	1.3	78	169	23.6	1.17	2.10	
Meakan	1.4	131	558	23.2	1.37	1.71	
Meakan	1.5	170	564	23.1	1.99	1.74	
Meakan	1.6	292	425	23.4	1.44	1.89	
Meakan	2.1	67	851	17.0	2.19	1.90	
Sakurajima	1.1	151	1085	27.8	0.96	2.22	
Sakurajima	2.1	11	218	26.1	2.43	1.85	
Sakurajima	4.1	12	174	27.1	1.5	2.05	
Sakurajima	47	1	5775	--	2.64	1.21	Yes
Sakurajima	54	1	926	--	5.19	2.95	Yes
Ontake	1.1	20	115	33.4	2.52	2.10	
Ontake	1.2	15	987	32.8	1.48	2.68	Yes
Ontake	1.4	2	363	35.3	1.28	1.87	Yes
Hakone	1.1	127	1601	22.1	2.19	1.43	Yes
Hakone	1.2	77	1838	24.5	1.65	1.72	Yes
Hakone	1.3	10	169	23.0	3.09	1.74	Yes

Table 5.2 Time-lags between DLF earthquakes and surface volcanic activities. In Sakurajima, dike intrusion event was used instead of eruption because too many eruptions occur. Crustal deformation in Ontake is based on Miyaoka and Takagi (2016). Crustal deformation and eruptions in Hakone are based on Mannen et al. (2018). In Hakone, the days are between activations of DLF earthquakes in Group 1.1 and the first eruption on 3 May 2015.

	Year	DLF activations – Crustal deformation	DLF activations – main eruption/ dike intrusion	Depth of DLF earthquakes which
Kirishima	2011	Approximately 0	400	23–25
	2017	Approximately 0	200	22
Meakan	2008	Approximately 0	100	24
	2013	400	No eruption	24
	2015	200	No eruption	24
Sakurajima	2015	50	50	25
Ontake	2007	0	100	33
	2014	0	20	33
Hakone	2015	20	80	25

6. General discussion

In Chapter 3, discrete distributions of DLF earthquakes and temporal activity patterns of DLF earthquakes were revealed. In Chapters 4 and 5, DLF earthquakes associated with the volcanic activities were shown. In this chapter, I construct a schematic view of the structures around the hypocenters of DLF earthquakes. I also discuss the physical mechanisms of DLF earthquakes and future applications to predict eruptions.

6.1. Schematic view of structure around hypocenters of DLF earthquakes

6.1.1. Sill-magma model and network structure of magma paths

In previous studies, DLF earthquakes were supposed to occur by movement of fluid separated from the melt in low-velocity anomalies with cooling and solidification of melt based on their hypocentral distribution (Hasegawa et al., 2005). The hypocenters were plotted in the edge of the low-velocity anomalous body in the scales of roughly 10 km (Figure 6.1). On the other hand, this study revealed a discrete distribution of DLF earthquakes in the smaller scales of 0–5 km. In many volcanoes, DLF earthquakes are concentrated into some discrete groups and the temporal activity patterns of groups are different even if the groups are close to each other. For example, in Kirishima, the hypocenters of Type A2 DLF earthquakes associated with the 2011 eruptions are located approximately within 1 km from the hypocenters of Types B1 and B2 DLF earthquakes not associated with the 2011 eruptions (Figure 4.10). In Meakan, DLF earthquakes of Group 1.1 show episodic occurrence associated with crustal deformations. However, DLF earthquakes of Groups 1.2–1.6 show constant occurrence (Figure 5.5), although the hypocenters of those DLF earthquakes are very close to each other (Figure 5.2 and Table 5.1). The discrete distribution of DLF earthquakes may suggest that there are heterogeneous structures with a scale of 0–5 km. The scale is too small to be imaged by tomography study; however, some previous studies on seismic wave scattering have revealed strong scattering for the frequency band of 1–2 Hz in volcanic regions (Carcole & Sato, 2010; Takahashi, 2012), whose wavelengths of S wave are 1.5–3.0 km, assuming S-wave velocity of 3.0 km/s. The frequency band indicating strong scattering corresponds to the characteristic scale length from the interval of discrete DLF earthquake spots. This small-scale heterogeneous structure beneath volcanoes derived from this study and previous studies of scattering is well consistent with the sill-magma model proposed in petrological studies (Annen et al., 2006; Cashman et al., 2017; Geshi, 2016). In the sill-

magma model, many magmas intrude at various depths of the lower crust like sills. If DLF earthquakes may occur in or around magma sills, the discrete distribution may be explained (Figure 6.1).

The sill-magma model can also explain the activities of DLF earthquakes associated with volcanic activities. In Section 5.5, I divided five volcanoes into two categories. The difference of the categories may be also explained by the model. In “Kirishima type”, only the deepest parts of DLF earthquakes were activated with eruptions. I interpreted that magmas from deeper source might firstly intrude into the deepest magma sill and directly move to the shallow magma reservoir without intrusion into other magma sills. On the other hand, in the cases of ”Ontake type”, some groups of DLF earthquakes which usually occur were activated, although the temporal activity patterns of DLF earthquakes are different for each depth. The associations with volcanic activities suggest that the magma ascended to some sills including sources of DLF earthquakes. The different temporal activity patterns may be interpreted that there are different magma supply systems in each depth. Therefore, I interpret that there are many paths like complicated network composed of horizontal sills and vertical conduits around the source regions and the selection of paths controls the temporal activity patterns of DLF earthquakes.

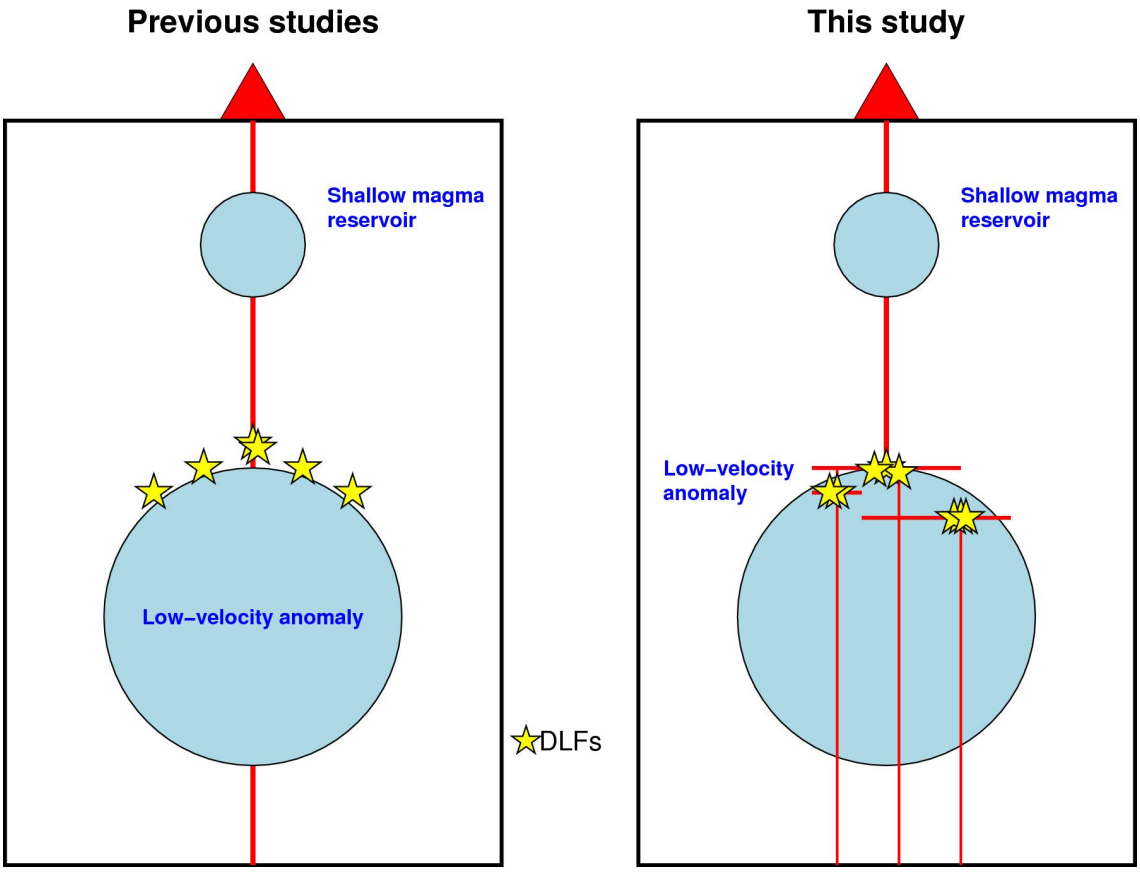

Figure 6.1 Schematic views of the relationship between DLF earthquakes and low-velocity anomaly in the lower crust in the previous study (cf. Figure 11(a) in Hasegawa et al. (2005)) and this study. Red lines show the paths of magma including horizontal sills and vertical conduits. Yellow stars show the hypocenters of DLF earthquakes.

6.1.2. Differences between episodic DLF earthquakes and constant DLF earthquakes

In this study, the DLF earthquakes were classified into some groups based on waveform correlations and there are groups in which DLF earthquakes occurred episodically and constantly. In some regions such as Hijiori, both episodic and constant occurrences of DLF earthquakes were observed by each group. In Chapter 3, the correlation between swarm ratios (SR) and b-values, and between SR and average correlation coefficients of waveforms were found. DLF earthquakes with episodic occurrence indicate high waveform correlations and high b-values. High b-values suggest that many smaller DLF earthquakes occurred in the groups. In other words, groups of the episodic DLF earthquakes have similar hypocenter locations and waveforms, and most

of them are smaller magnitudes. On the other hand, groups of constant DLF earthquakes have different waveforms and hypocenter locations. Magnitudes of constant DLF earthquakes distribute in a wide range compared to the episodic DLF earthquakes.

As the interpretation of the results, the schematic model of sources of DLF earthquakes in which occur episodically or constantly is proposed (Figure 6.2). In source regions of episodic DLF earthquakes, DLF earthquakes may repeatedly occur in one unique source. Episodic occurrences of DLF earthquakes may be explained by filling of small magma reservoir in or around the magma sills. When enough magma filled in the reservoir, then the magma may start to flow and swarms of DLF earthquakes may occur at the small magma reservoir. On the other hand, as for constant DLF earthquakes, DLF earthquakes may occur in many sources. There may be many magma paths forming a complex magma supply system which consists of horizontal sills and vertical conduit. DLF earthquakes may occur based on the physical properties of each source. The size of sources of DLF earthquakes was estimated to be 10–100 m (Aso & Tsai, 2014). Therefore, we cannot distinguish each source, because resolutions of source locations are not enough.

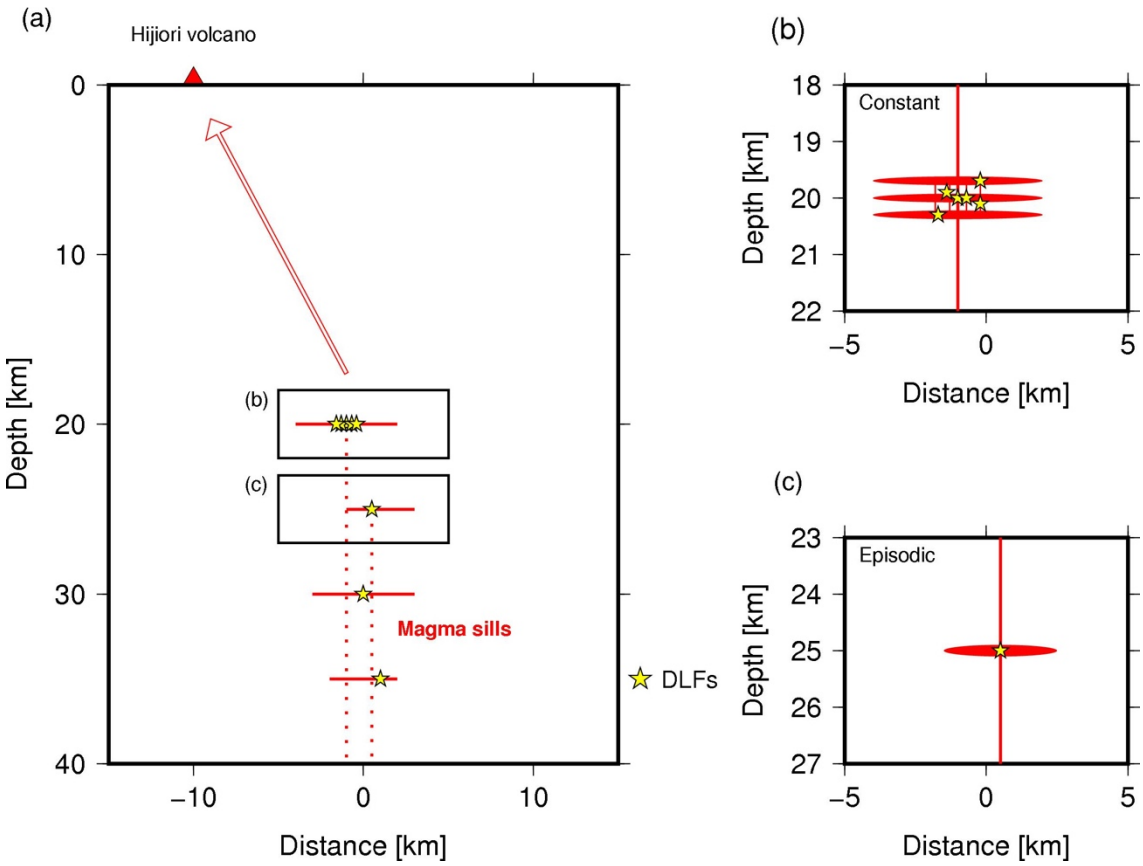

Figure 6.2 Schematic models of DLF earthquakes. Hijiori is selected as an example. (a)

Cross-section view of Hijiori. Red solid lines draw the magma-sills and yellow stars show the sources of DLF earthquakes. (b) Schematic view of source regions in which DLF earthquakes constantly occur. (c) Schematic view of source regions in which DLF earthquakes episodically occur.

6.2. Physical mechanisms of DLF earthquakes

The discrete distributions of DLF earthquakes in depths suggest that DLF earthquakes occur at specific locations, such as small magma reservoirs in or around magma sills, as discussed in previous sections. The episodic occurrence of DLF earthquakes associated with eruptions in some regions suggests that DLF earthquakes may occur when magma or magmatic fluid flow near the sources of DLF earthquakes. In addition, DLF earthquakes associated with eruptions with lower dominant frequencies of approximately 1 Hz in the volcanic category of Kirishima, Meakan, and Sakurajima suggest that magma or magmatic fluid may also affect the waveform characteristics. These results are consistent with the focal mechanisms of DLF earthquakes which include both compensated linear vector dipole (CLVD) and double couple components (Aso & Ide, 2014; Nakamichi et al., 2003; Oikawa et al., 2019).

As interpretations of the results, DLF earthquakes may be triggered by the flow of magma or magmatic fluid. It may be explained to consider a similar model to the cooling magma model in which thermal strain causes brittle failure, and waves are trapped in the resonance (Aso & Tsai, 2014). If the cooling of magma trigger DLF earthquakes, heating of magma by the fluid flow may also trigger the earthquakes and this model can explain the activation of DLF earthquakes associated with eruptions in volcanoes. Although estimation of the physical mechanisms of DLF earthquakes is out of focus of this study, a more comprehensive and accurate analysis of the focal mechanisms of DLF earthquakes will contribute to understanding the mechanisms in the future.

6.3. Possibility to predict eruptions by monitoring DLF earthquakes

It is well known that shallow long-period earthquakes, which occur near the surface, are useful for predicting eruptions (Chouet, 1996). DLF earthquakes are also thought to be useful to predict volcanic eruptions. Deep intrusions of magmas were estimated from petrological studies and DLF earthquakes were observed in some volcanoes (White & McCausland, 2019).

In this study, activations of DLF earthquakes before various types of eruptions in five volcanoes were revealed. Monitoring of DLF earthquakes may also contribute to the improvement of prediction accuracy with observations of shallow volcanic earthquakes. However, there are some problems to predict eruptions based on activities of DLF earthquakes. One factor making it difficult to use DLF earthquakes for prediction is their diversity. DLF earthquakes in Kirishima in Chapter 4 exhibit many different characteristics of locations and waveforms between DLF earthquakes at the period of 2011 eruptions and 2018 eruptions; hence, we cannot predict at this moment how DLF earthquakes will occur before the next eruption. Different activity patterns of DLF earthquakes of each group in a volcano suggest that volcanic structure in the lower crust has a complex magma supply system. Therefore, it is difficult to understand which type of DLF earthquakes is related to volcanic eruptions. In addition, time-lags between activations of DLF earthquakes and eruptions are different to each group of each region, for example, two weeks in Ontake and one year in Kirishima. Many case studies are necessary to understand the relationship between DLF earthquakes and eruptions.

Different methods of detections are also necessary to monitor DLF seismicity. The matched filter technique can only detect the earthquakes that have waveforms and locations similar to those of template earthquakes. When a DLF earthquake occurs and there are no templates similar to such DLF earthquakes, the DLF earthquakes will not be detected by the method. Thus, another method not depending on templates is necessary for the prediction of eruptions using the monitoring of DLF earthquakes.

7. Conclusions

In this study, I conducted three analyses of relocation, classification, and comprehensive detection of DLF earthquakes for the understanding of DLF earthquakes. By combination of these analyses, I newly found discrete distributions of DLF earthquakes, constant and episodic occurrences of DLF earthquakes, and DLF earthquakes associated with volcanic activities.

Discrete distributions of DLF earthquakes are shown in Chapter 3. Hypocenters of DLF earthquakes were concentrated in some small groups in each region. There are groups in which DLF earthquakes occur constantly and episodically. The episodic and constant groups of DLF earthquakes were distributed within a few kilometers in some regions. The temporal activity patterns of DLF earthquakes all over Japan were quantitatively compared based on the index "swarm ratio (SR)". As a result, high SR groups of DLF earthquakes distribute in 12 regions all over Japan. In the high SR regions, the DLF earthquakes have similar small magnitudes and similar waveforms. It suggests that DLF earthquakes may repeatedly occur in the same sources in the episodic groups and DLF earthquakes may occur in different sources within vicinity in the constant groups.

DLF earthquakes associated with eruptions in five volcanoes were shown. Kirishima is the most significant case. The activations of DLF earthquakes associated with 2011 and 2018 eruptions were observed and well correlated with crustal deformations. The activations occurred only in some groups of the DLF earthquakes in Kirishima. There are DLF earthquakes without activations even those occurred in the vicinity of the activated DLF earthquakes. DLF earthquakes activated with 2011 eruptions occurred in deeper sources and had lower dominant frequencies than those of other DLF earthquakes. The result suggests that DLF earthquakes may be triggered by fluid flow. The hypocenters of DLF earthquakes were switched with the transitions of eruptions.

DLF earthquakes associated with volcanic eruptions were also observed in Meakan, Sakurajima, Ontake, and Hakone. DLF earthquakes were activated with various types of eruptions, which include subplinian eruptions, vulcanian eruptions, and phreatic eruptions. There are roughly two categories of activation of DLF earthquakes. "Kirishima type" includes Kirishima, Meakan and Sakurajima, in which waveforms of the DLF earthquakes in the period of eruptions have low dominant frequencies compared to the other DLF earthquakes. In this case, the time-lag between activation of DLF earthquakes

and eruptions were generally long. The other category “Ontake type” includes Ontake and Hakone, in which DLF earthquakes which usually occur were activated with eruptions. In this case, the time-lag between activation of DLF earthquakes and eruptions were generally short.

According to the results of this study, I construct the schematic view of source regions of DLF earthquakes and discuss the possibility of application for prediction of eruptions. The sill-magma model proposed by petrological studies is well consistent with the discrete distribution of DLF earthquakes not only in the scales about 10 km but also scales in 0–5 km. DLF earthquakes may occur in or around magma sills. There may be many paths like network around the source regions and the paths may be forming complex magma supply systems from the lower crust to edifices of the volcanoes.

8. Acknowledgements

First of all, I would like to express my heartfelt appreciation to my supervisor, professor Kazushige Obara for his constant advice, various supports, and discussion for about 6 years of my research. I also express great appreciation to Dr. Takuto Maeda, Dr. Akiko Takeo, Dr. Shunsuke Takemura, Dr. Yusaku Tanaka and Dr. Masayuki Kano for advice and various supports.

I appreciate Dissertation Committee, Dr. Mie Ichihara, Dr. Kiwamu Nishida, Professor Aitaro Kato, Professor Makoto Uyeshima, and Dr. Yoshiyuki Tanaka, for reviewing and providing many advises to improve this dissertation.

I appreciate Dr. Kazuaki Ohta for providing the computer program of the network correlation coefficient method. I appreciate professor Aitaro Kato for providing a catalog of volcanic tectonic earthquakes in Ontake. I am grateful for many constructive discussions to members of seismogenic-zone physical-properties and structure seminar and volcanic research center in Earthquake Research Institute, the University of Tokyo. I appreciate professor Motoo Ukawa and professor Kei Kurita for inviting me to special seminars about DLF earthquakes and volcanology.

I appreciate all professors, researchers, staff, and students in Earthquake Research Institute, the University of Tokyo. I appreciate many researchers all over the world for meaningful discussions.

I used Generic Mapping Tools for drawing figures (Wessel and Smith, 1998) and Hi-net seismic observation data (http://www.hinet.bosai.go.jp) operated by the National Research Institute for Earth Science and Disaster Resilience (National Research Institute for Earth Science and Disaster Resilience, 2019). I used the unified earthquake catalog of the Japan Meteorological Agency (http://www.jma.go.jp). I used GNSS data, F3 solutions provided by the Geospatial Information Authority of Japan (http://www.gsi.go.jp). I used the computer systems of the Earthquake and Volcano Information Center of the Earthquake Research Institute, the University of Tokyo. The research was supported by JSPS KAKENHI Grant Number JP16H06473 in Scientific Research on Innovative Areas “Science of Slow Earthquakes” and Grant Number JP19J12571 in Grant-in-Aid for JSPS Fellows. I was supported by Next Generation Volcano Researcher Development Program by MEXT.

9. References

Akaike, H. (1980). Likelihood and the Bayes procedure. *Trabajos de Estadistica Y de Investigacion Operativa*, *31*(1), 143–166. https://doi.org/10.1007/BF02888350

Aki, K., & Koyanagi, R. (1981). Deep Volcanic Tremor and Magma Ascent Mechanism Under Kilauea , Hawaii. *Journal of Geophysical Research*, *86*(B8), 7095–7109.

Annen, C., Blundy, J. D., & Sparks, R. S. J. (2006). The Genesis of Intermediate and Silicic Magmas in Deep Crustal Hot Zones. *Journal of Petrology*, *47*(3), 505–539. https://doi.org/10.1093/petrology/egi084

Aso, N., & Ide, S. (2014). Focal mechanisms of deep low-frequency earthquakes in Eastern Shimane in Western Japan. *Journal of Geophysical Research: Solid Earth*, *119*(1), 364–377. https://doi.org/10.1002/2013JB010681

Aso, N., & Tsai, V. C. (2014). Cooling magma model for deep volcanic long-period earthquakes. *Journal of Geophysical Research: Solid Earth*, *119*(11), 8442–8456. https://doi.org/10.1002/2014JB011180

Aso, N., Ohta, K., & Ide, S. (2011). Volcanic-like low-frequency earthquakes beneath Osaka Bay in the absence of a volcano. *Geophysical Research Letters*, *38*(8), L08303. https://doi.org/10.1029/2011GL046935

Aso, N., Ohta, K., & Ide, S. (2013). Tectonic, volcanic, and semi-volcanic deep low-frequency earthquakes in western Japan. *Tectonophysics*, *600*, 27–40. https://doi.org/10.1016/j.tecto.2012.12.015

Bachmann, O., & Bergantz, G. (2008). The magma reservoirs that feed supereruptions. *Elements*, *4*(1), 17–21. https://doi.org/10.2113/GSELEMENTS.4.1.17

Benoit, J. P., McNutt, S. R., & Barboza, V. (2003). Duration-amplitude distribution of volcanic tremor. *Journal of Geophysical Research: Solid Earth*, *108*(B3), 1–15. https://doi.org/10.1029/2001jb001520

Brenguier, F., Campillo, M., Takeda, T., Aoki, Y., Shapiro, N. M., Briand, X., et al. (2014). Mapping pressurized volcanic fluids from induced crustal seismic velocity drops. *Science*, *345*(6192), 80–82. https://doi.org/10.1126/science.1254073

Carcole, E., & Sato, H. (2010). Spatial distribution of scattering loss and intrinsic absorption of short-period S waves in the lithosphere of Japan on the basis of the Multiple Lapse Time Window Analysis of Hi-net data. *Geophysical Journal International*, *180*(1), 268–290. https://doi.org/10.1111/j.1365-246X.2009.04394.x

Cashman, K. V., Sparks, R. S. J., & Blundy, J. D. (2017). Vertically extensive and

unstable magmatic systems: A unified view of igneous processes. *Science*, *355*(6331). https://doi.org/10.1126/science.aag3055

Chouet, B. A. (1996). Long-period volcano seismicity: its source and use in eruption forecasting. *Nature*, *380*(6572), 309–316. https://doi.org/10.1038/380309a0

Frank, W. B., Shapiro, N. M., & Gusev, A. A. (2018). Progressive reactivation of the volcanic plumbing system beneath Tolbachik volcano (Kamchatka, Russia) revealed by long-period seismicity. *Earth and Planetary Science Letters*, *493*, 47–56. https://doi.org/10.1016/j.epsl.2018.04.018

Geospatial Information Authority of Japan. (2017). Crustal Deformations around Meakan Volcano. *Report of the Coordinating Committee for Prediction of Volcanic Eruptions*, *127*, 17–28.

Geospatial Information Authority of Japan. (2019). Crustal movements in the Tohoku District. *Report of the Coordinating Committee for Earthquake Prediction*, (102), 80–91.

Geshi, N. (2016). Large-scale Pyroclastic Eruption and Collapse Caldera: Their Preparation and Eruption. *Bulletin of the Volcanological Society of Japan*, *61*(1), 101–118. https://doi.org/10.18940/kazan.61.1_101

Gibbons, S. J., & Ringdal, F. (2006). The detection of low magnitude seismic events using array-based waveform correlation. *Geophysical Journal International*, *165*(1), 149–166. https://doi.org/10.1111/j.1365-246X.2006.02865.x

Gutenberg, B., & Richter, C. (1945). Frequency of Earthquakes in California. *Nature*, *156*(3960), 371–371. https://doi.org/10.1038/156371a0

Han, J., Vidale, J. E., Houston, H., Schmidt, D. A., & Creager, K. C. (2018). Deep Long-Period Earthquakes Beneath Mount St. Helens: Their Relationship to Tidal Stress, Episodic Tremor and Slip, and Regular Earthquakes. *Geophysical Research Letters*, *45*(5), 2241–2247. https://doi.org/10.1002/2018GL077063

Hasegawa, A., & Yamamoto, A. (1994). Deep, low-frequency microearthquakes in or around seismic low-velocity zones beneath active volcanoes in northeastern Japan. *Tectonophysics*. https://doi.org/10.1016/0040-1951(94)90243-7

Hasegawa, A., Nakajima, J., Umino, N., & Miura, S. (2005). Deep structure of the northeastern Japan arc and its implications for crustal deformation and shallow seismic activity. *Tectonophysics*, *403*(1–4), 59–75. https://doi.org/10.1016/j.tecto.2005.03.018

Hensch, M., Dahm, T., Ritter, J., Heimann, S., Schmidt, B., Stange, S., & Lehmann, K. (2019). Deep low-frequency earthquakes reveal ongoing magmatic recharge beneath Laacher See Volcano (Eifel, Germany). *Geophysical Journal International*, *216*(3), 2025–2036. https://doi.org/10.1093/gji/ggy532

Hotovec-Ellis, A. J., Shelly, D. R., Hill, D. P., Pitt, A. M., Dawson, P. B., & Chouet, B. A. (2018). Deep fluid pathways beneath Mammoth Mountain, California, illuminated by migrating earthquake swarms. *Science Advances*, *4*(8), eaat5258. https://doi.org/10.1126/sciadv.aat5258

Hotta, K., Iguchi, M., & Tameguri, T. (2016). Rapid dike intrusion into Sakurajima volcano on August 15, 2015, as detected by multi-parameter ground deformation observations. *Earth, Planets and Space*, *68*(1). https://doi.org/10.1186/s40623-016-0450-0

Japan Meteorological Agency. (2003). *Selection of active volcanoes and rank of volcanic actities by the Coordinating Committee for Prediction of Volcanic Eruprtions*.

Japan Meteorological Agency. (2007). Volcanic activity of Ontakesan (from March 2007 to June 2007). *Report of Coordinating Committee for Prediction of Volcanic Eruption*, *97*, 14–29.

Japan Meteorological Agency. (2009). The Eruption of the Meakandake Volcano on November 2008. *Report of Coordinating Committee for Prediction of Volcanic Eruption*, *102*, 1–15.

Japan Meteorological Agency. (2013). National catalogue of the active volcanoes in Japan (the fourth edition, English version). *Japan Meteorological Agency*. https://doi.org/http://www.data.jma.go.jp/svd/vois/data/tokyo/STOCK/souran_eng/menu.htm

Japan Meteorological Agency. (2014). Volcanic Activity of Ontakesan Volcano (October 2014 – February 15 , 2015). *Report of Coordinating Committee for Prediction of Volcanic Eruption*, *120*, 70–91.

Japan Meteorological Agency. (2018). Volcanic Activity of Kirishimayama Volcano －February 1, 2018 – May 31, 2018－. *Report of Coordinating Committee for Prediction of Volcanic Eruption*, *130*, 213–284.

Japan Meteorological Agency. (2019). Volcanic Activity of Sakurajima Volcano－ October 1, 2018 – February 17, 2019－. *Report of Coordinating Committee for*

Prediction of Volcanic Eruption, *132*, 352–379.

Kagiyama, T. (1994). Kirishima volcanoes -- Multi active volcanic group generated in a slughtly tensile stress field. *Journal of Geography*, *103*(5), 479–487.

Kato, A., Terakawa, T., Yamanaka, Y., Maeda, Y., Horikawa, S., Matsuhiro, K., & Okuda, T. (2015). Preparatory and precursory processes leading up to the 2014 phreatic eruption of Mount Ontake, Japan. *Earth, Planets and Space*, *67*(1). https://doi.org/10.1186/s40623-015-0288-x

Katoh, S., Iio, Y., Katao, H., Sawada, M., Tomisaka, K., Miura, T., & Yoneda, I. (2018). The relationship between S-wave reflectors and deep low-frequency earthquakes in the northern Kinki district, southwestern Japan. *Earth, Planets and Space*, *70*(1), 149. https://doi.org/10.1186/s40623-018-0921-6

Katsumata, A. (2010). Depth of the Moho discontinuity beneath the Japanese islands estimated by traveltime analysis. *Journal of Geophysical Research: Solid Earth*, *115*(4), 1–17. https://doi.org/10.1029/2008JB005864

Katsumata, A., & Kamaya, N. (2003). Low-frequency continuous tremor around the Moho discontinuity away from volcanoes in the southwest Japan. *Geophysical Research Letters*, *30*(1), 20-1-20–4. https://doi.org/10.1029/2002GL015981

Kobayashi, T., & Yamada, S. (2019). Exploring magma pluming system of Meakandake and Oakandake volcanoes, inferred from crustal deformation associated with the 2016–2017 volcanic activity. *Volcanological Society of Japan 2019 Fall Meeting Abstract*, B1-13.

Kosuga, M., Noro, K., & Masukawa, K. (2017). Characteristics of Spatiotemporal Variations of Hypocenters and Diversity of Waveforms of Deep Low- frequency Earthquakes in Northeastern Japan. *Bulletin of the Earthquake Research Institute, University of Tokyo*, *92*, 63–80.

Kurihara, R., Obara, K., Takeo, A., & Maeda, T. (2018). Migration of Deep Low-Frequency Tremor Triggered by Teleseismic Earthquakes in the Southwest Japan Subduction Zone. *Geophysical Research Letters*, *45*(8), 3413–3419. https://doi.org/10.1002/2017GL076779

Kurihara, R., Obara, K., Takeo, A., & Tanaka, Y. (2019). Deep Low-Frequency Earthquakes Associated With the Eruptions of Shinmoe-dake in KirishimaVolcanoes. *Journal of Geophysical Research: Solid Earth*, 2019JB018032. https://doi.org/10.1029/2019JB018032

Mannen, K., Yukutake, Y., Kikugawa, G., Harada, M., Itadera, K., & Takenaka, J. (2018). Chronology of the 2015 eruption of Hakone volcano, Japan: geological background, mechanism of volcanic unrest and disaster mitigation measures during the crisis. *Earth, Planets and Space*, *70*(1), 68. https://doi.org/10.1186/s40623-018-0844-2

Matsubara, M., Sato, H., Ishiyama, T., & Van Horne, A. (2017). Configuration of the Moho discontinuity beneath the Japanese Islands derived from three-dimensional seismic tomography. *Tectonophysics*, *710–711*, 97–107. https://doi.org/10.1016/j.tecto.2016.11.025

Miyaoka, K., & Takagi, A. (2016). Detection of crustal deformation prior to the 2014 Mt. Ontake eruption by the stacking method. *Earth, Planets and Space*, *68*(1). https://doi.org/10.1186/s40623-016-0439-8

Miyazawa, M. (2005). Detection of triggered deep low-frequency events from the 2003 Tokachi-oki earthquake. *Geophysical Research Letters*, *32*(10), L10307. https://doi.org/10.1029/2005GL022539

Nakada, S., Nagai, M., Kaneko, T., Suzuki, Y., & Maeno, F. (2013). The outline of the 2011 eruption at Shinmoe-dake (Kirishima), Japan. *Earth, Planets and Space*, *65*(6), 475–488. https://doi.org/10.5047/eps.2013.03.016

Nakajima, J. (2017). Seismic Velocity and Attenuation Structures around Active Volcanoes Beneath Tohoku: Linking Crustal Structure to Low-frequency Earthquakes and S-wave Reflectors. *Bulletin of the Earthquake Research Institute, University of Tokyo*, *92*, 49–62.

Nakamichi, H., Hamaguchi, H., Tanaka, S., Ueki, S., Nishimura, T., & Hasegawa, A. (2003). Source mechanisms of deep and intermediate-depth low-frequency earthquakes beneath Iwate volcano, northeastern Japan. *Geophysical Journal International*, *154*(3), 811–828. https://doi.org/10.1046/j.1365-246X.2003.01991.x

Nakano, S. (2013). Volcanoes of Japan (Third Edition) 1:2,000,000 map series. *Geological Survey of Japan, AIST*. Retrieved from http://www.aist.go.jp/RIODB/strata/VOL_JP/

Nakao, S., Morita, Y., Yakiwara, H., Oikawa, J., Ueda, H., Takahashi, H., et al. (2013). Volume change of the magma reservoir relating to the 2011 Kirishima Shinmoe-dake eruption—Charging, discharging and recharging process inferred from GPS measurements. *Earth, Planets and Space*, *65*(6), 505–515.

https://doi.org/10.5047/eps.2013.05.017

National Research Institute for Earth Science and Disaster Resilience. (2019). NIED Hi-net. *National Research Institute for Earth Science and Disaster Resilience*. https://doi.org/10.17598/nied.0003

Niu, X., Zhao, D., & Li, J. (2018). Precise relocation of low-frequency earthquakes in Northeast Japan: new insight into arc magma and fluids. *Geophysical Journal International*, *212*(2), 1183–1200. https://doi.org/10.1093/gji/ggx445

Obara, K. (2002). Nonvolcanic Deep Tremor Associated with Subduction in Southwest Japan. *Science*, *296*(5573), 1679–1681. https://doi.org/10.1126/science.1070378

Ogiso, M., & Yomogida, K. (2012). Migration of tremor locations before the 2008 eruption of Meakandake Volcano, Hokkaido, Japan. *Journal of Volcanology and Geothermal Research*, *217–218*, 8–20. https://doi.org/10.1016/j.jvolgeores.2011.12.005

Ohmi, S., & Obara, K. (2002). Deep low-frequency earthquakes beneath the focal region of the Mw 6.7 2000 Western Tottori earthquake. *Geophysical Research Letters*, *29*(16), 1807. https://doi.org/10.1029/2001GL014469

Ohmi, S., Hirose, I., & Mori, J. J. (2004). Deep low-frequency earthquakes near the downward extension of the seismogenic fault of the 2000 Western Tottori earthquake. *Earth, Planets and Space*, *56*(12), 1185–1189. https://doi.org/10.1186/BF03353338

Ohta, K., & Ide, S. (2011). Precise hypocenter distribution of deep low-frequency earthquakes and its relationship to the local geometry of the subducting plate in the Nankai subduction zone, Japan. *Journal of Geophysical Research*, *116*(B1), B01308. https://doi.org/10.1029/2010JB007857

Oikawa, G., Aso, N., & Nakajima, J. (2019). Focal Mechanisms of Deep Low-Frequency Earthquakes Beneath Zao Volcano, Northeast Japan, and Relationship to the 2011 Tohoku Earthquake. *Geophysical Research Letters*, 2019GL082577. https://doi.org/10.1029/2019GL082577

Okada, T., Yoshida, K., Ueki, S., Nakajima, J., Uchida, N., Matsuzawa, T., et al. (2011). Shallow inland earthquakes in NE Japan possibly triggered by the 2011 off the Pacific coast of Tohoku Earthquake. *Earth, Planets and Space*, *63*(7), 749–754. https://doi.org/10.5047/eps.2011.06.027

Okada, Y., Kasahara, K., Hori, S., Obara, K., Sekiguchi, S., Fujiwara, H., & Yamamoto,

A. (2004). Recent progress of seismic observation networks in Japan —Hi-net, F-net, K-NET and KiK-net—. *Earth, Planets and Space*, *56*(8), xv–xxviii. https://doi.org/10.1186/BF03353076

Rubinstein, J. L., La Rocca, M., Vidale, J. E., Creager, K. C., & Wech, A. G. (2008). Tidal Modulation of Nonvolcanic Tremor. *Science*, *319*(5860), 186–189. https://doi.org/10.1126/science.1150558

Sagiya, T. (2004). A decade of GEONET: 1994-2003 - The continuous GPS observation in Japan and its impact on earthquake studies -. *Earth, Planets and Space*, *56*(8), xxix–xli. https://doi.org/10.1186/BF03353077

Segall, P. (2016). Repressurization following eruption from a magma chamber with a viscoelastic aureole. *Journal of Geophysical Research: Solid Earth*, *121*(12), 8501–8522. https://doi.org/10.1002/2016JB013597

Shapiro, N. M., Droznin, D. V, Droznina, S. Y., Senyukov, S. L., Gusev, A. A., & Gordeev, E. I. (2017). Deep and shallow long-period volcanic seismicity linked by fluid-pressure transfer. *Nature Geoscience*, *10*(6), 442–445. https://doi.org/10.1038/ngeo2952

Shelly, D. R., Beroza, G. C., & Ide, S. (2007). Non-volcanic tremor and low-frequency earthquake swarms. *Nature*, *446*(7133), 305–307. https://doi.org/10.1038/nature05666

Shiina, T., Takahashi, H., Okada, T., & Matsuzawa, T. (2018). Implications of Seismic Velocity Structure at the Junction of Kuril-Northeastern Japan Arcs on Active Shallow Seismicity and Deep Low-Frequency Earthquakes. *Journal of Geophysical Research: Solid Earth*, *123*(10), 8732–8747. https://doi.org/10.1029/2018JB015467

Shiraki, T., & Murakami, M. (2019). Inflation observed from 2016 in the northeast of Meakan-dake volcano, eastern Hokkaido, Japan. *Volcanological Society of Japan 2019 Fall Meeting Abstract*, P017.

Suzuki, S. (1992). Low-frequency microearthquakes occurring near the Moho boundary beneath Tokachi-dake volcano, Hokkaido. *Bulletin of the Volcanological Society of Japan*, *37*(1), 9–20. https://doi.org/10.18940/kazan.37.1_9

Suzuki, Y., Nagai, M., Maeno, F., Yasuda, A., Hokanishi, N., Shimano, T., et al. (2013). Precursory activity and evolution of the 2011 eruption of Shinmoe-dake in Kirishima volcano—insights from ash samples. *Earth, Planets and Space*, *65*(6),

591–607. https://doi.org/10.5047/eps.2013.02.004

Takada, Y., & Fukushima, Y. (2013). Volcanic subsidence triggered by the 2011 Tohoku earthquake in Japan. *Nature Geoscience*, *6*(8), 637–641. https://doi.org/10.1038/ngeo1857

Takahashi, H., & Miyamura, J. (2009). Deep Low-Frequency Earthquakes occuring in Japanese Islands. *Geophysical Bulletin of Hokkaido University*, *72*, 177–190.

Takahashi, T. (2012). Three-dimensional attenuation structure of intrinsic absorption and wide-angle scattering of S waves in northeastern Japan. *Geophysical Journal International*, *189*(3), 1667–1680. https://doi.org/10.1111/j.1365-246X.2012.05438.x

Tichelaar, B. W., & Ruff, L. J. (1989). How good are our best models? Jackknifing, bootstrapping, and earthquake depth. *Eos, Transactions American Geophysical Union*, *70*(20), 593. https://doi.org/10.1029/89EO00156

Tomiya, A. (2016). Magma Reservoir: Pre-eruptive Magma Processes and the Conditions That Lead to Volcanic Eruptions. *Bulletin of the Volcanological Society of Japan*, *61*(2), 281–294.

Tomiya, A., Miyagi, I., Saito, G., & Geshi, N. (2013). Short time scales of magma-mixing processes prior to the 2011 eruption of Shinmoedake volcano, Kirishima volcanic group, Japan. *Bulletin of Volcanology*, *75*(10), 750. https://doi.org/10.1007/s00445-013-0750-1

Ueno, H., Hatakeyama, S., Aketagawa, T., Funasaki, J., & Hamada, N. (2002). Improvement of hypocenter determination procedures in the Japan Meteorology Agency. *Quarterly Journal of Seismology*, *65*, 123–131. Retrieved from https://www.jma.go.jp/jma/kishou/books/kenshin/vol65p123.pdf

Ukawa, M. (2007). Low frequency earhquakes at mount Fuji. *Fuji Volcano*, 161–172.

Ukawa, M., & Ohtake, M. (1987). A monochromatic earthquake suggesting deep-seated magmatic activity beneath the Izu-Ooshima Volcano, Japan. *Journal of Geophysical Research*, *92*(B12), 12649. https://doi.org/10.1029/JB092iB12p12649

White, R.A. (1996). Precursory deep long-period earthquakes at Mount Pinatubo: Spatio-temporal link to basaltic trigger. *Fire and Mud: Eruptions and Lahars of Mount Pinatubo, Philippines, Philippines. Univ. of Washington Press, Seattle*, 307–326.

White, Randall A., & McCausland, W. A. (2019). A process-based model of pre-

eruption seismicity patterns and its use for eruption forecasting at dormant stratovolcanoes. *Journal of Volcanology and Geothermal Research*, *382*, 267–297. https://doi.org/10.1016/j.jvolgeores.2019.03.004

Yamamoto, K., & Ida, Y. (1994). Three-Dimensional P-wave Velocity Structure of Kirishima Volcanoes Using Regional Seismic Events. *Bulletin of the Earthquake Research Institute, University of Tokyo*, *69*, 267–289.

Yoshida, K., Hasegawa, A., Yoshida, T., & Matsuzawa, T. (2019). Heterogeneities in Stress and Strength in Tohoku and Its Relationship with Earthquake Sequences Triggered by the 2011 M9 Tohoku-Oki Earthquake. *Pure and Applied Geophysics*, *176*(3), 1335–1355. https://doi.org/10.1007/s00024-018-2073-9

Yu, Z., Zhao, D., Niu, X., & Li, J. (2018). Spatiotemporal distribution of low-frequency earthquakes in Southwest Japan: Evidence for fluid migration and magmatic activity. *Journal of Asian Earth Sciences*, *151*, 148–172. https://doi.org/10.1016/j.jseaes.2017.10.033

Yukutake, Y., Abe, Y., & Doke, R. (2019). Deep Low-Frequency Earthquakes Beneath the Hakone Volcano, Central Japan, and their Relation to Volcanic Activity. *Geophysical Research Letters*, 2019GL084357. https://doi.org/10.1029/2019GL084357

Zhao, D., Yamashita, K., & Toyokuni, G. (2018). Tomography of the 2016 Kumamoto earthquake area and the Beppu-Shimabara graben. *Scientific Reports*, *8*(1), 1–11. https://doi.org/10.1038/s41598-018-33805-0

10. Appendix

10.1. Results in all target regions

In this chapter, seven types of figures are shown by each region. Those figures are same figure as Figure 2.6, Figure 2.11, Figure 3.1, Figure 3.8, Figure 3.14, Figure 3.18, and Figure3.21 but in each region. Symbols are same as those figures. In the figures of magnitude-frequency distribution, intervals from events and cumulative number of DLF earthquakes with magnitudes, groups in which top three number of DLF earthquakes are included are plotted. In the figures of cumulative number of DLF earthquakes with magnitudes, total events in the region are also plotted.

10.1.1. Atosanupuri

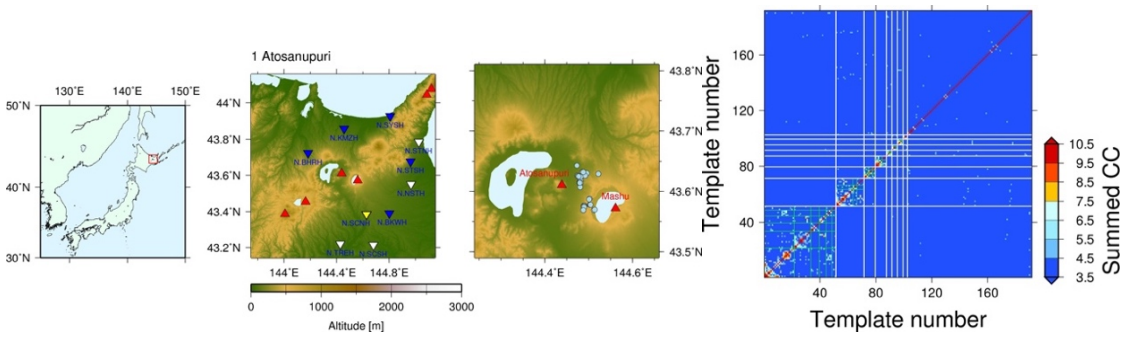

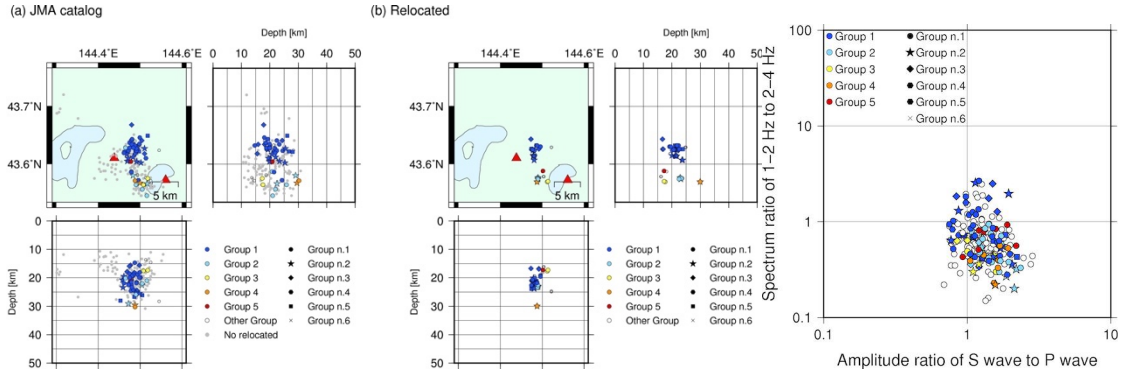

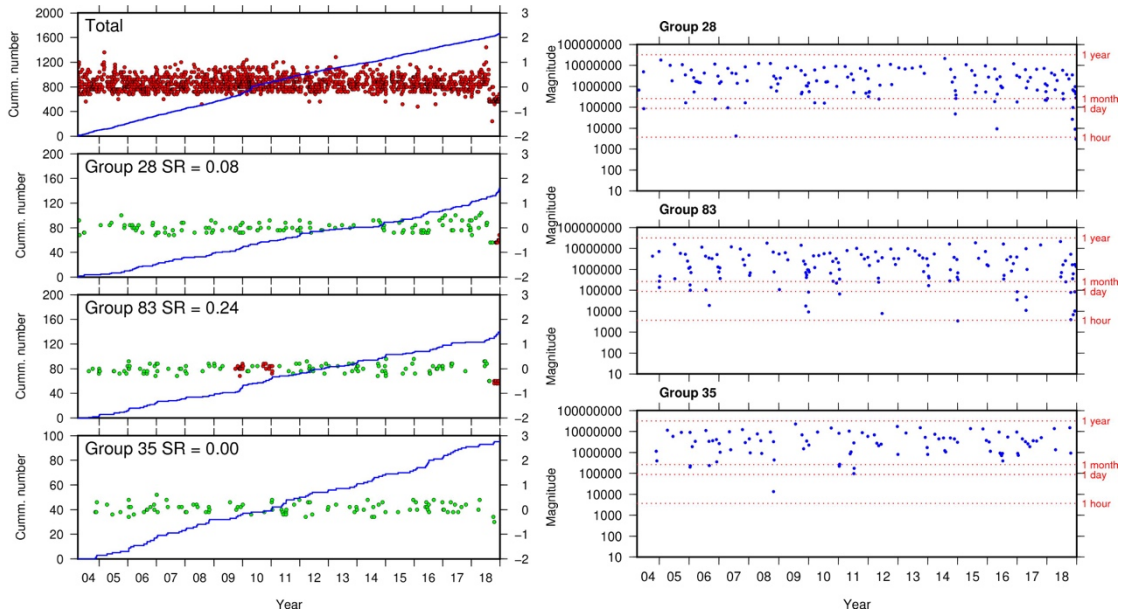

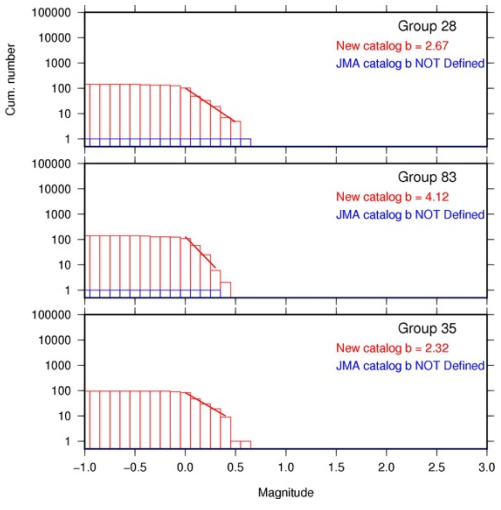

10.1.2. Meakan

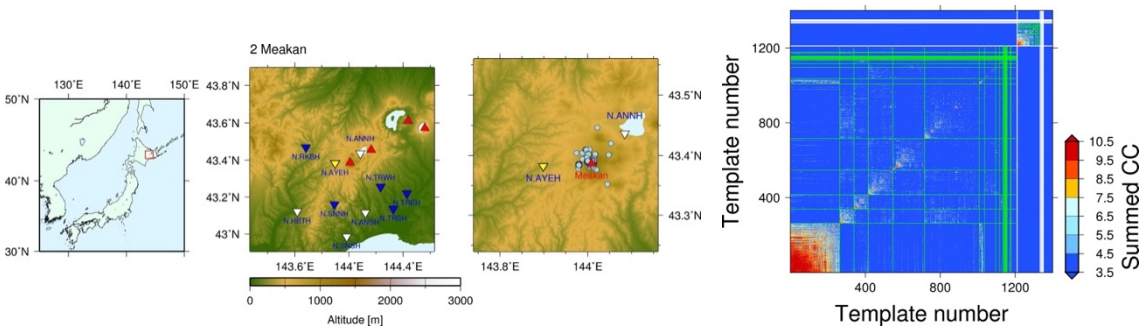
2 Meakan
Altitude [m]
Template number
Summed CC

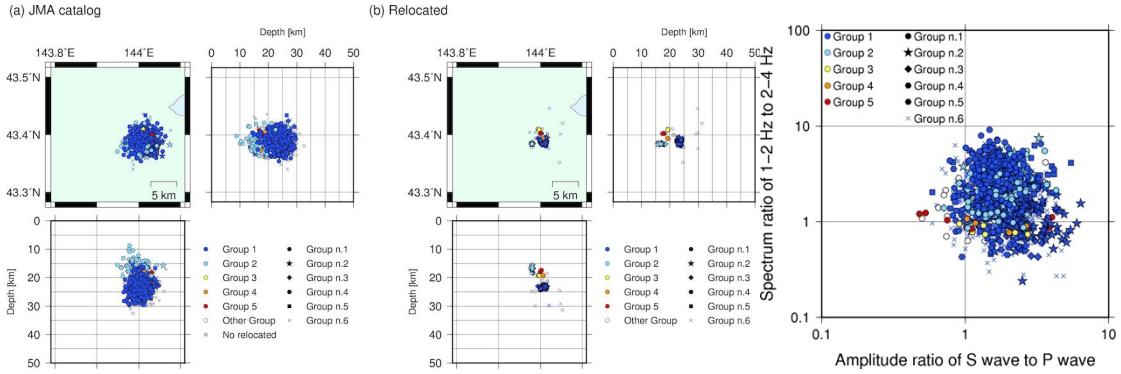
(a) JMA catalog
(b) Relocated
Depth [km]
Group 1
Group 2
Group 3
Group 4
Group 5
Other Group
No relocated
Group n.1
Group n.2
Group n.3
Group n.4
Group n.5
Group n.6
Spectrum ratio of 1–2 Hz to 2–4 Hz
Amplitude ratio of S wave to P wave

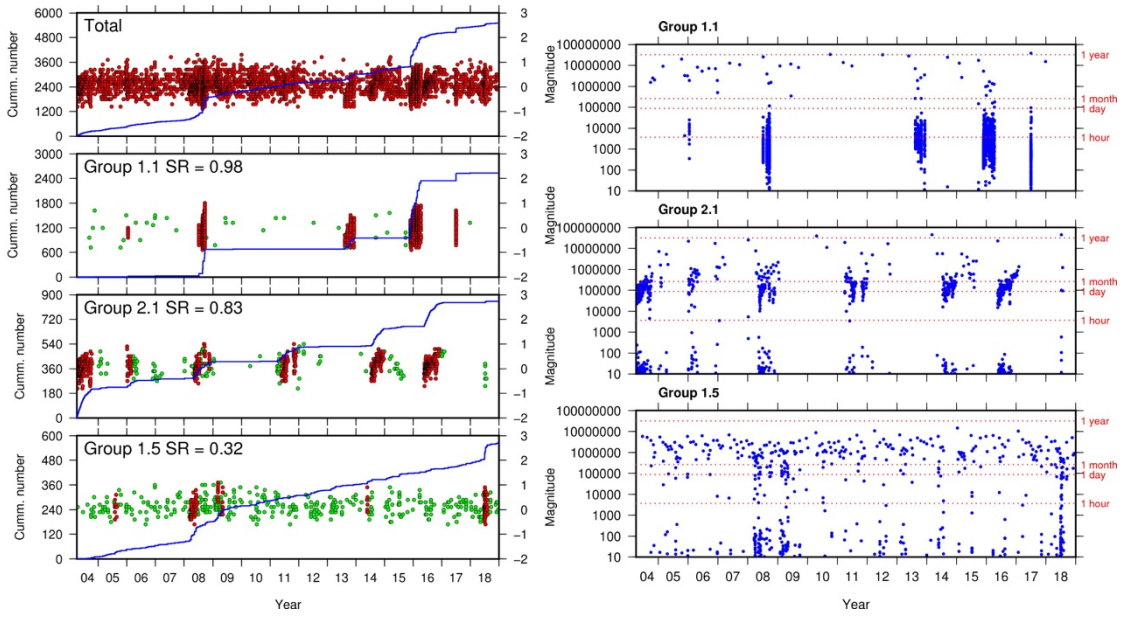
Total
Group 1.1 SR = 0.98
Group 2.1 SR = 0.83
Group 1.5 SR = 0.32
Cumm. number
Year
Group 1.1
Group 2.1
Group 1.5
Magnitude
1 year
1 month
1 day
1 hour

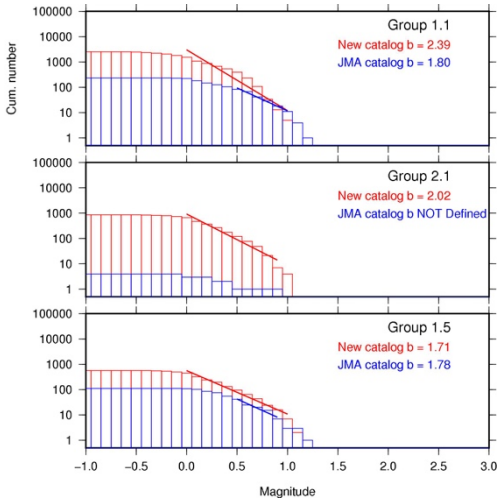
Group 1.1
New catalog b = 2.39
JMA catalog b = 1.80
Group 2.1
New catalog b = 2.02
JMA catalog b NOT Defined
Group 1.5
New catalog b = 1.71
JMA catalog b = 1.78
Cum. number
Magnitude

10.1.3. Taisetsu

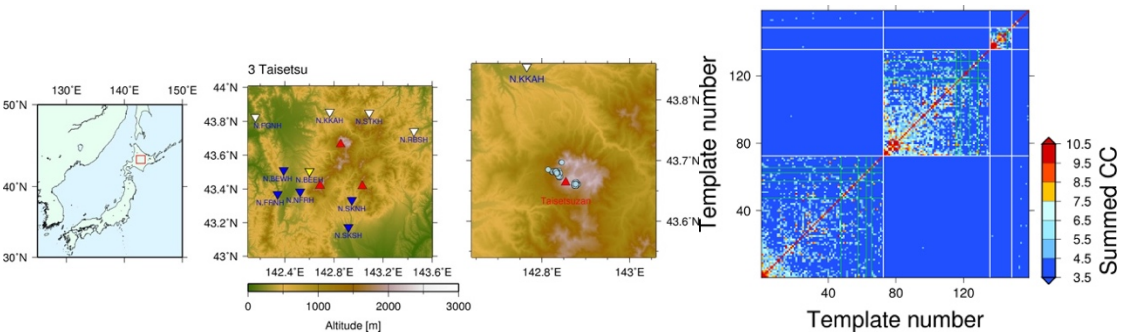

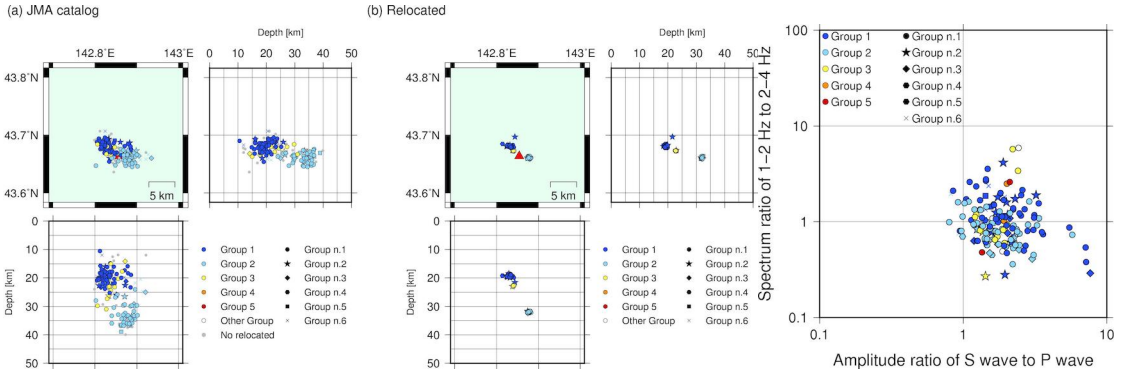

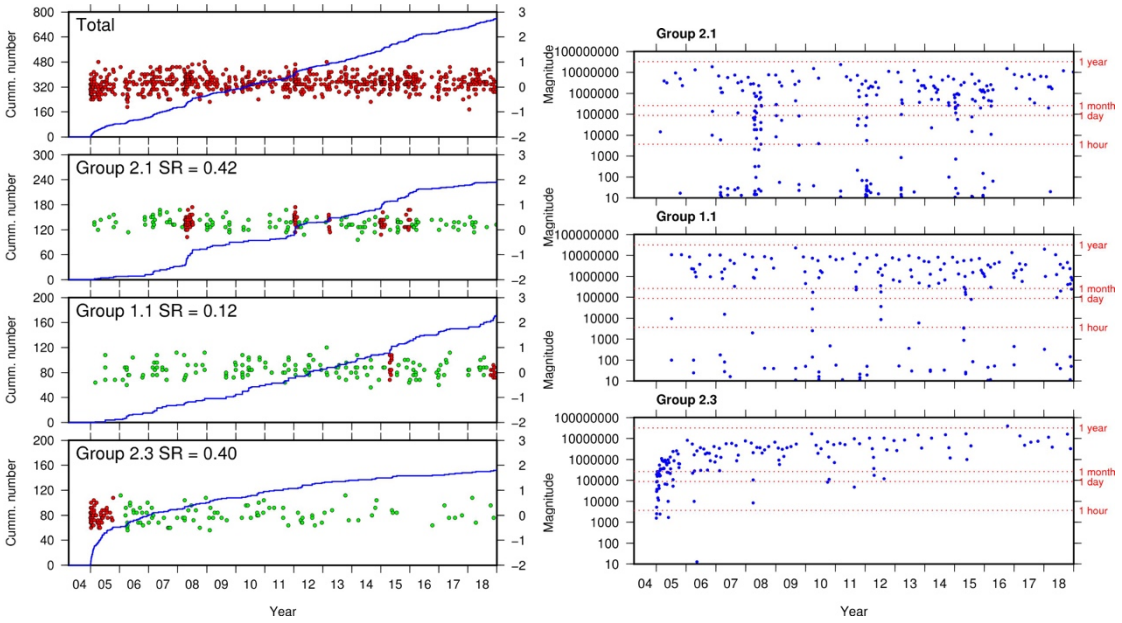

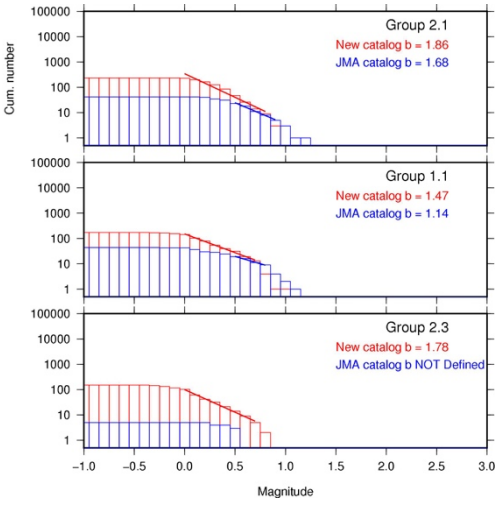

10.1.4. Maruyama

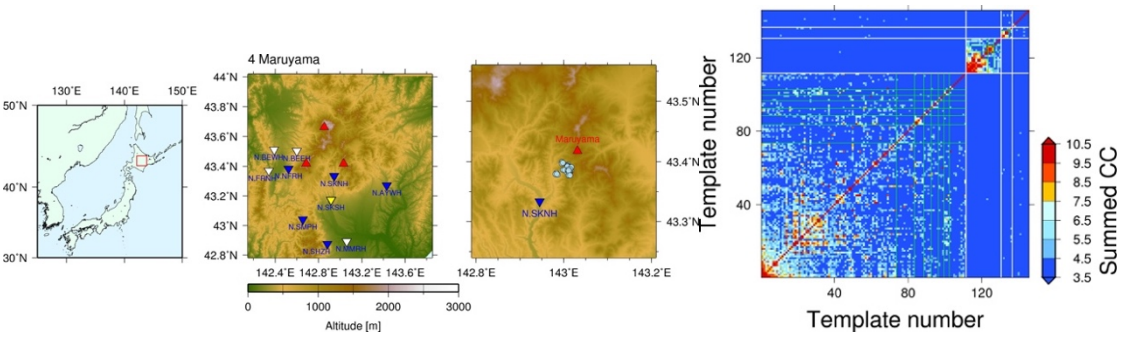

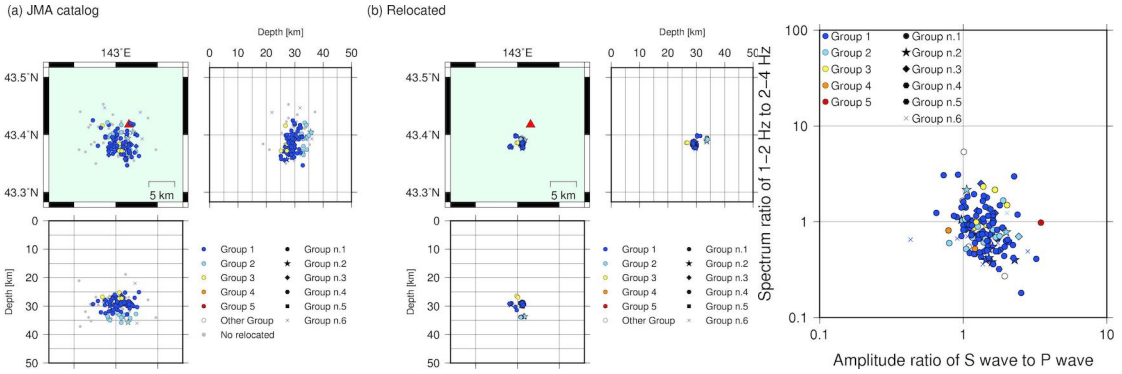

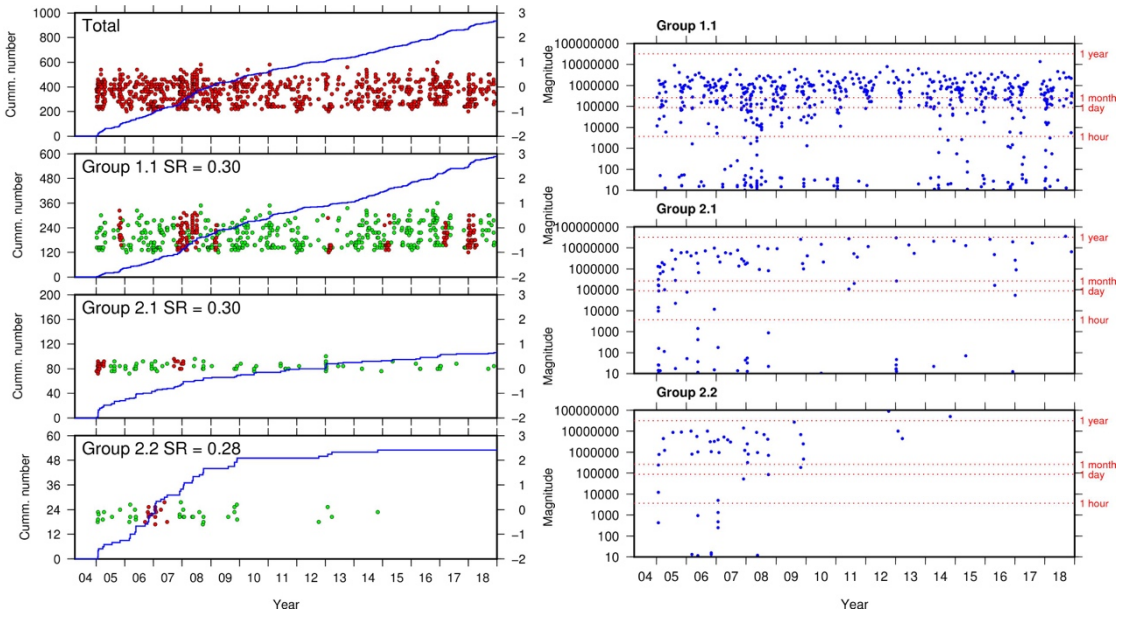

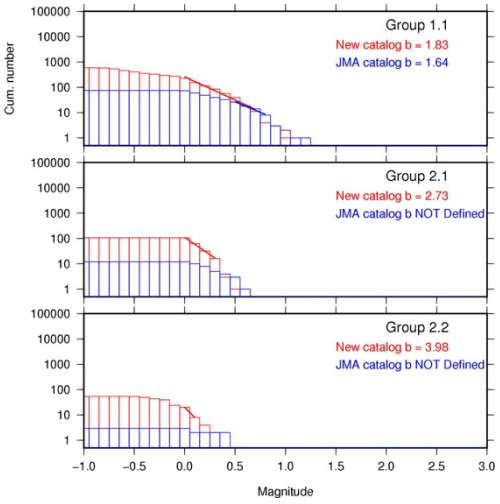

10.1.5. Tomamu

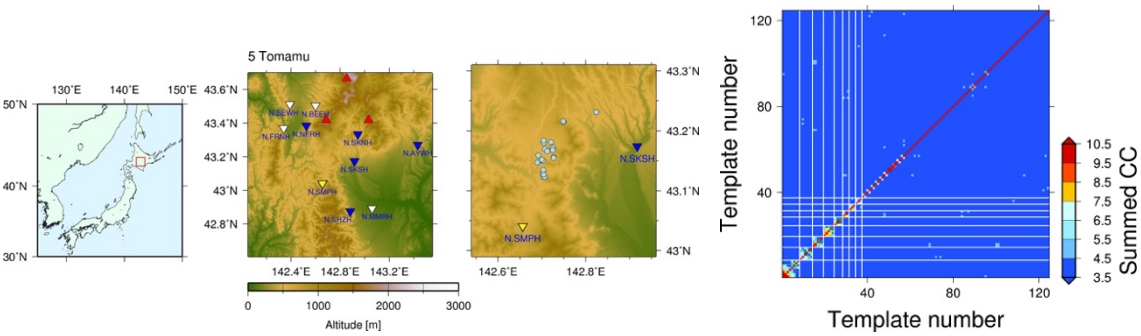
5 Tomamu
Altitude [m]
Template number
Template number
Summed CC

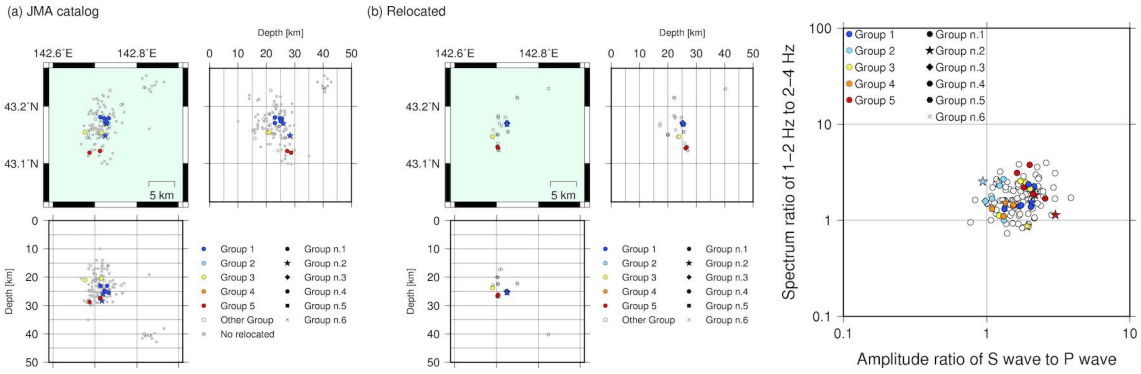
(a) JMA catalog
(b) Relocated
Depth [km]
5 km
Group 1
Group 2
Group 3
Group 4
Group 5
Other Group
No relocated
Group n.1
Group n.2
Group n.3
Group n.4
Group n.5
Group n.6
Spectrum ratio of 1–2 Hz to 2–4 Hz
Amplitude ratio of S wave to P wave

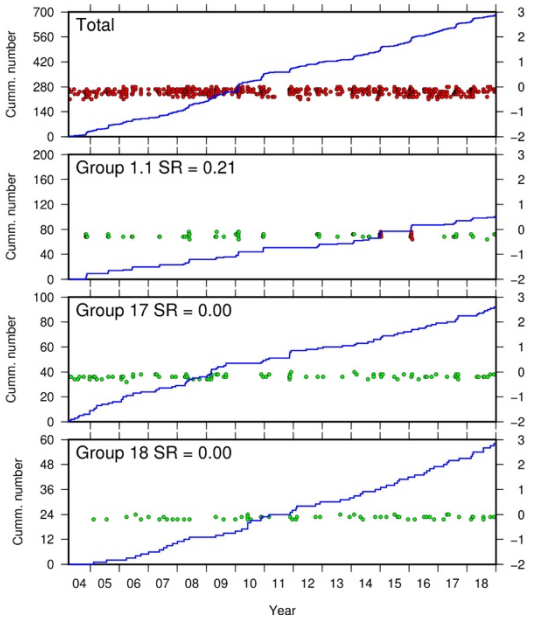
Total
Group 1.1 SR = 0.21
Group 17 SR = 0.00
Group 18 SR = 0.00
Cumm. number
Year

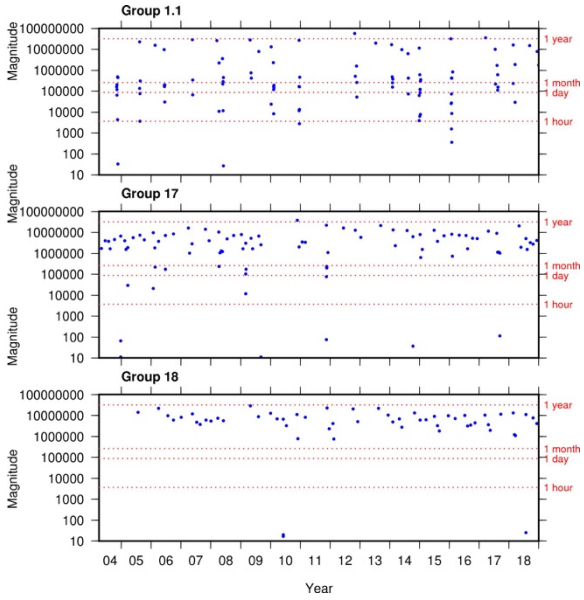
Group 1.1
Group 17
Group 18
Magnitude
1 year
1 month
1 day
1 hour
Year

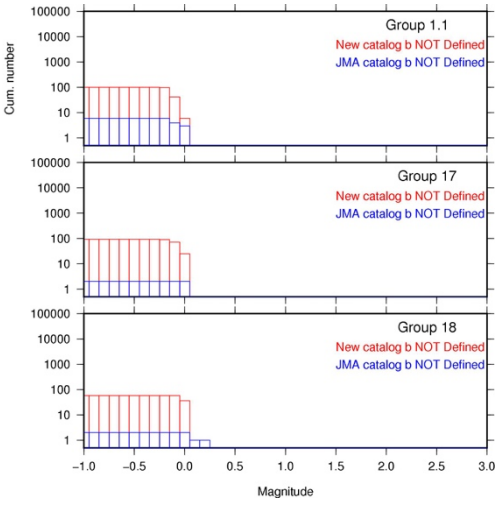
Group 1.1
Group 17
Group 18
New catalog b NOT Defined
JMA catalog b NOT Defined
Cum. number
Magnitude

10.1.6. Tokachidake

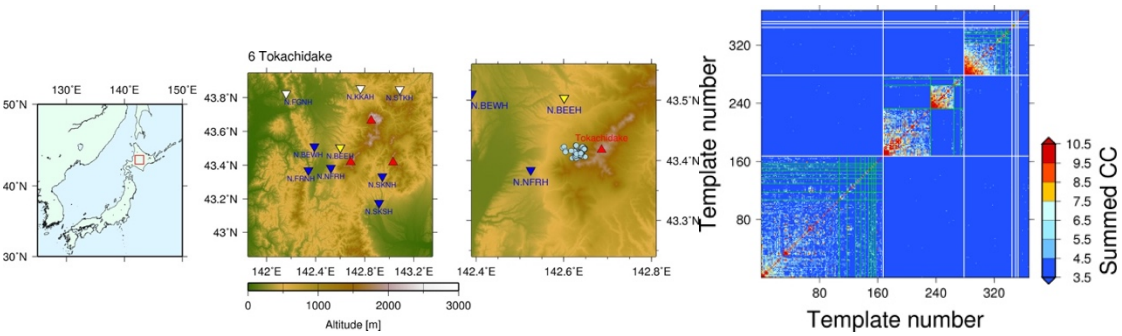

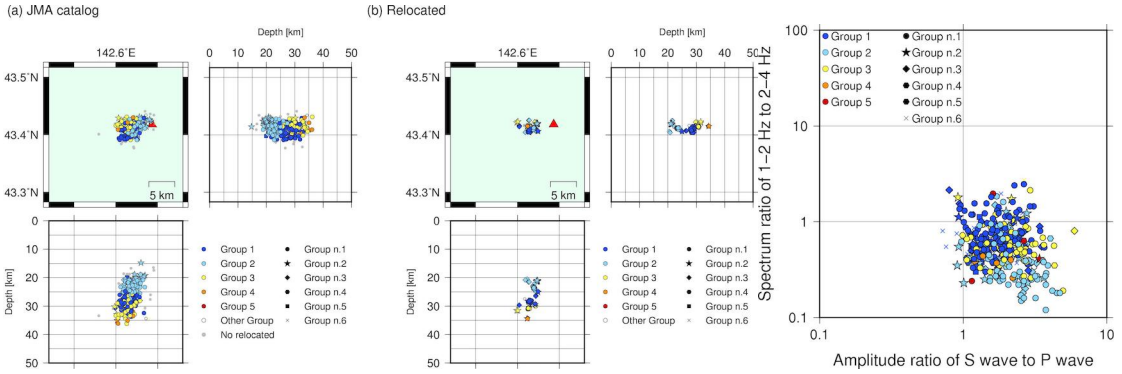

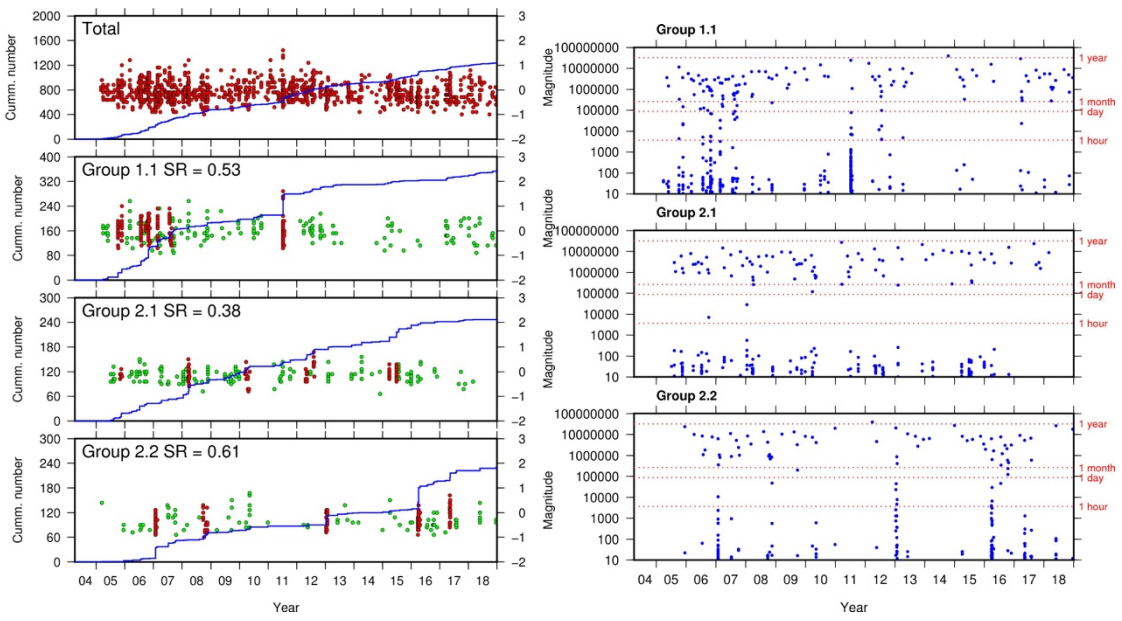

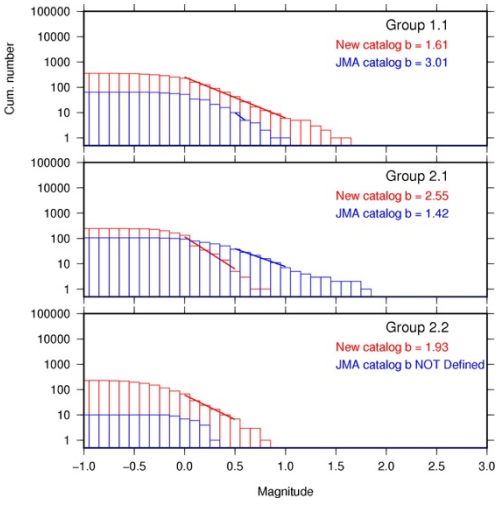

10.1.7. Usu

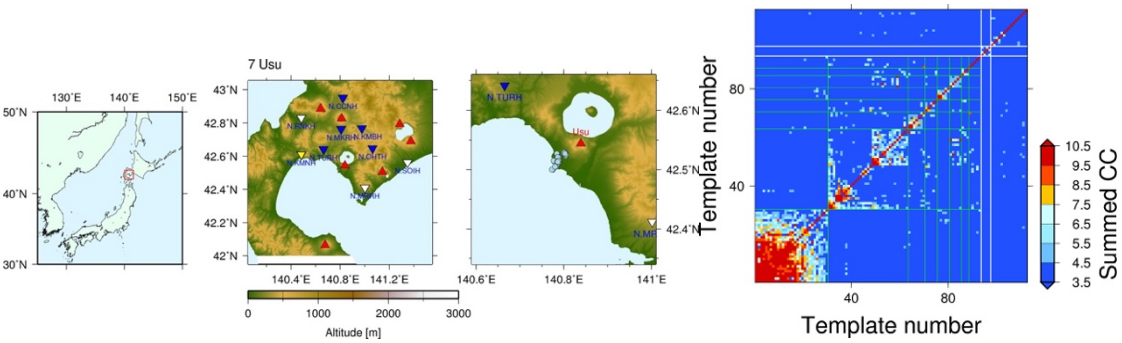
7 Usu
Altitude [m]
Template number
Summed CC

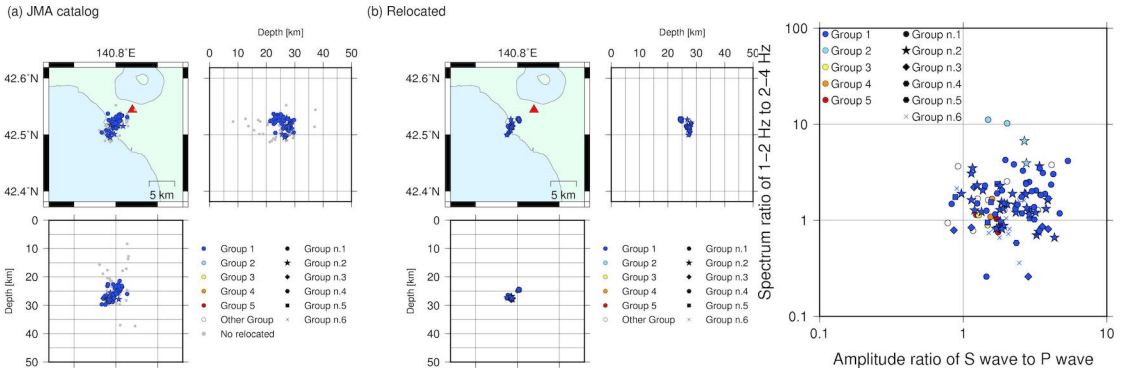
(a) JMA catalog
(b) Relocated
Depth [km]
Group 1
Group 2
Group 3
Group 4
Group 5
Other Group
No relocated
Spectrum ratio of 1–2 Hz to 2–4 Hz
Amplitude ratio of S wave to P wave

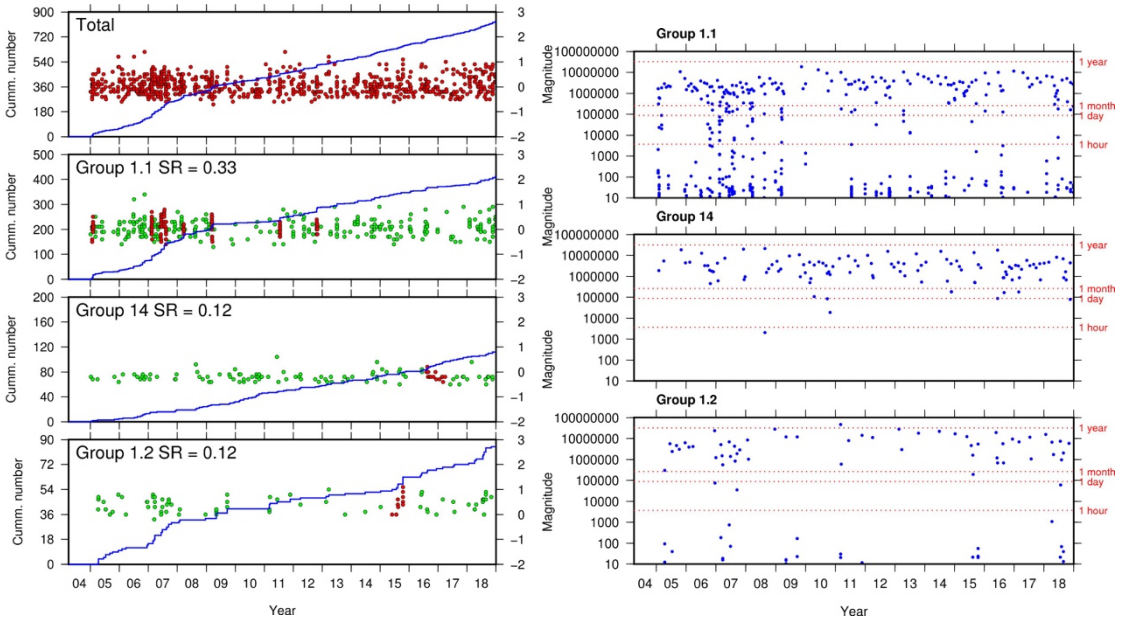
Total
Group 1.1 SR = 0.33
Group 14 SR = 0.12
Group 1.2 SR = 0.12
Cumm. number
Year
Group 1.1
Group 14
Group 1.2
Magnitude
1 year
1 month
1 day
1 hour

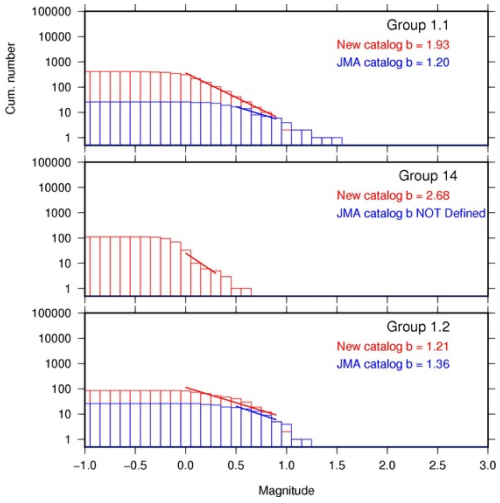
Group 1.1
New catalog b = 1.93
JMA catalog b = 1.20
Group 14
New catalog b = 2.68
JMA catalog b NOT Defined
Group 1.2
New catalog b = 1.21
JMA catalog b = 1.36
Cum. number
Magnitude

10.1.8. Kimobetsu

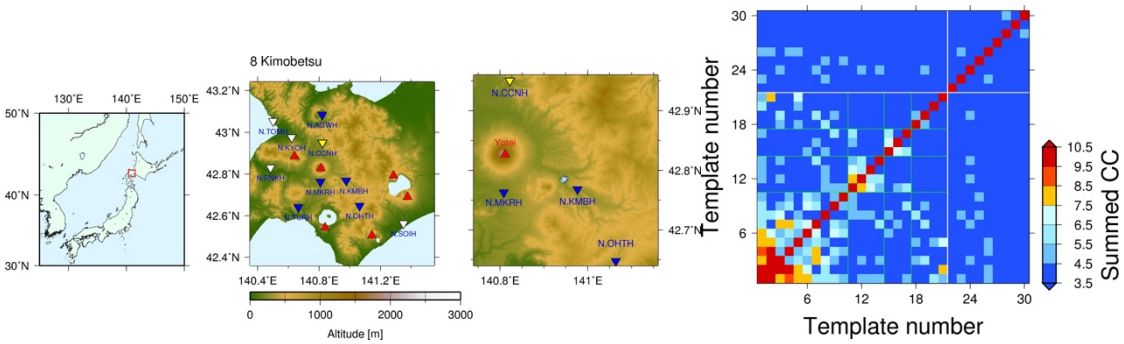

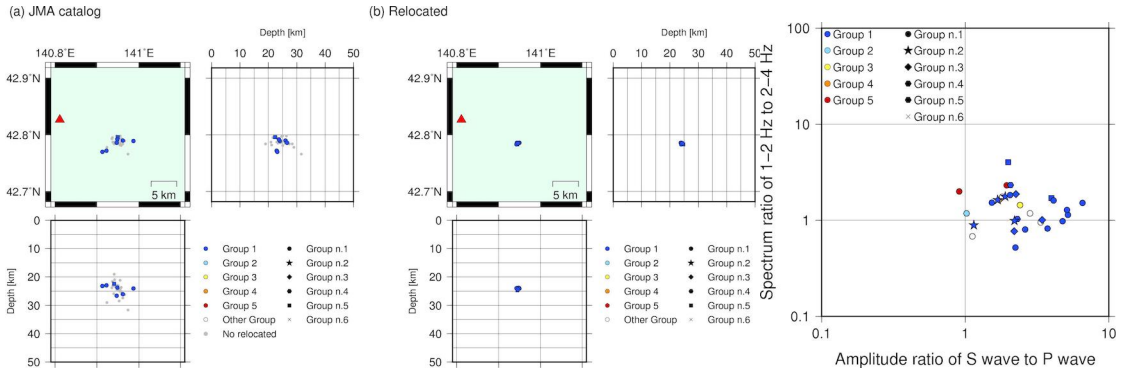

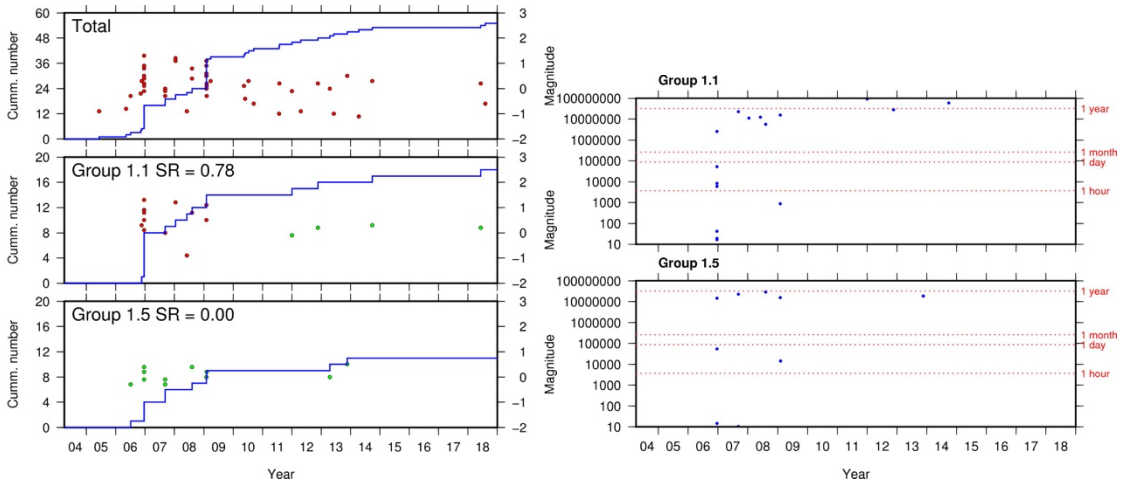

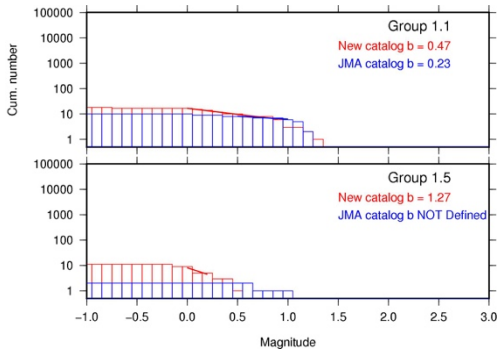

10.1.9. Yotei-Niseko

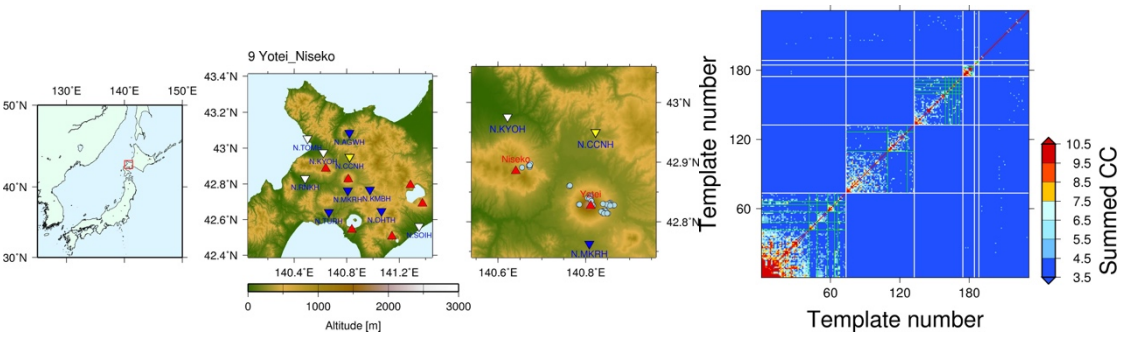

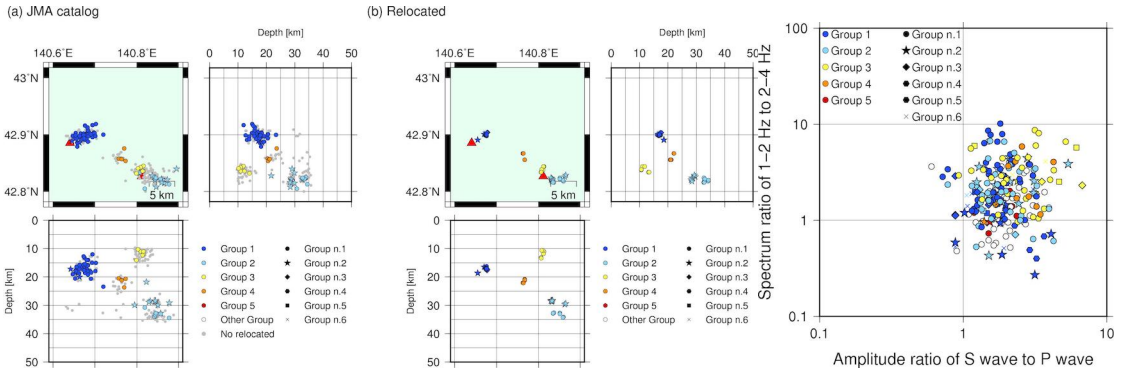

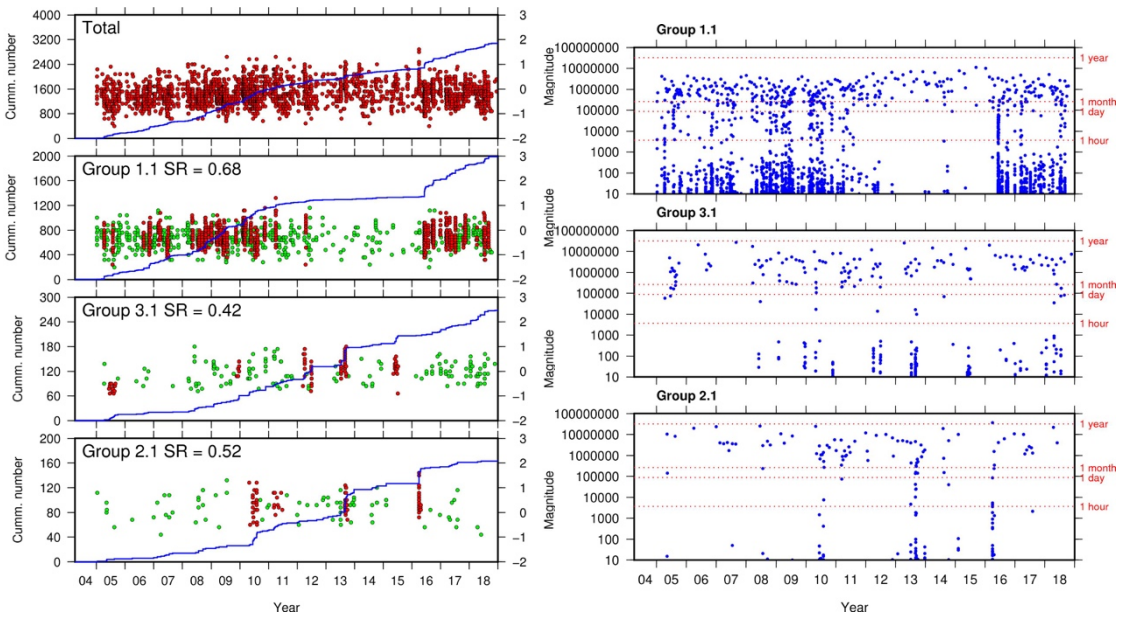

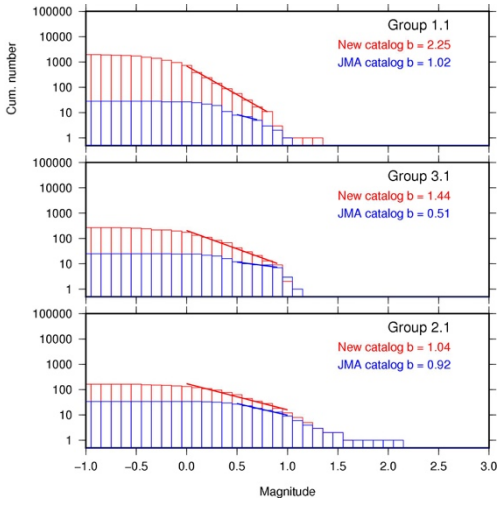

10.1.10. Hakkoda

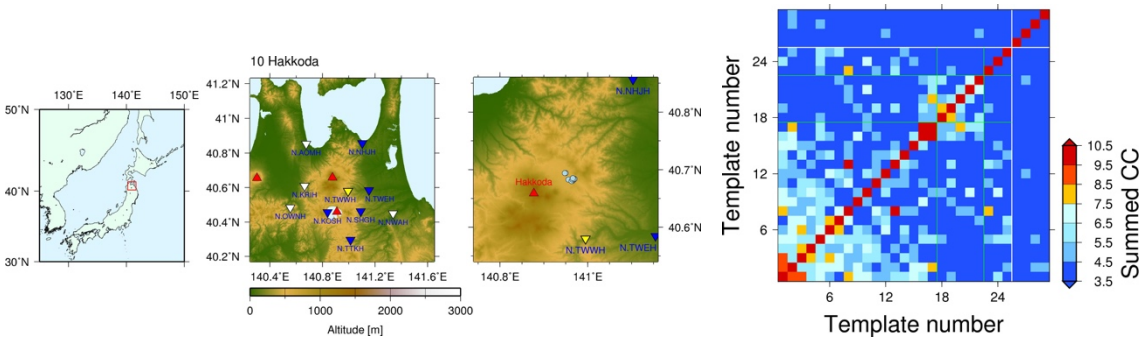

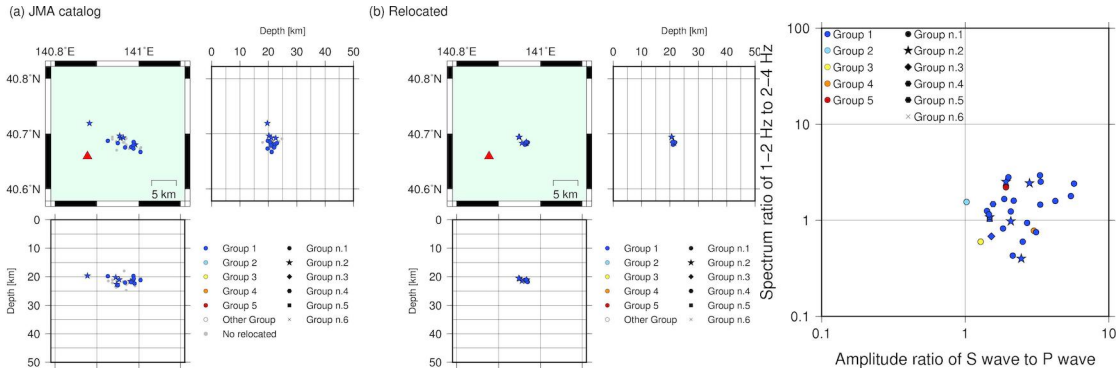

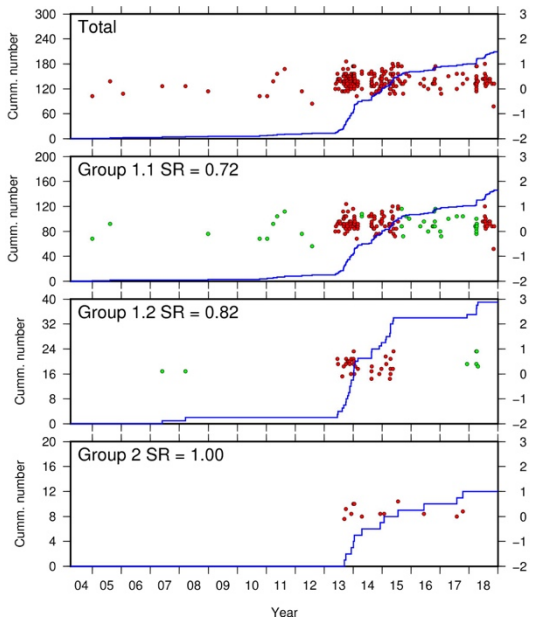

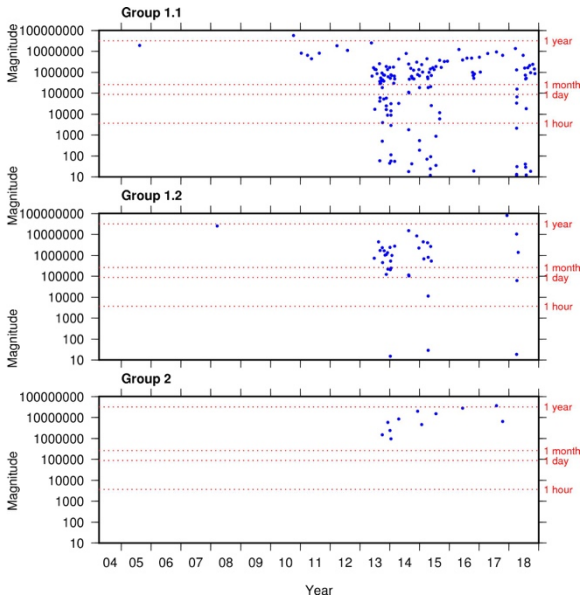

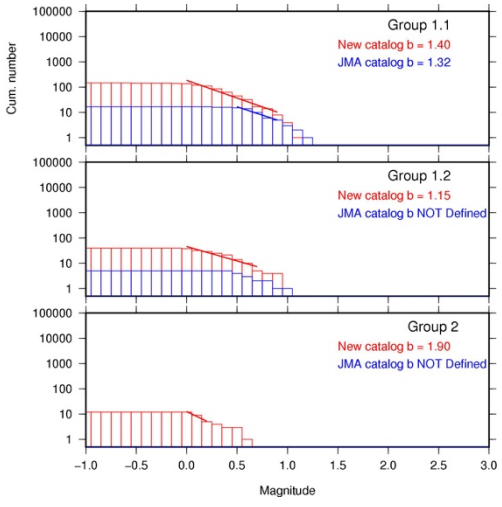

10.1.11. Mt.Iwaki

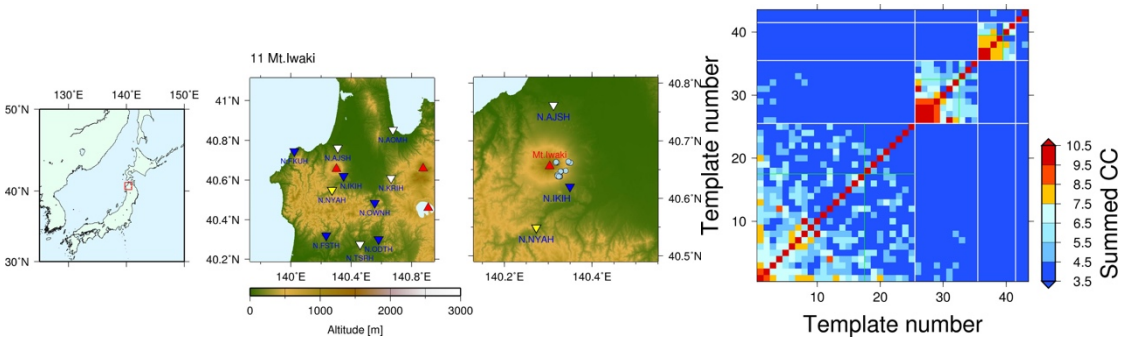

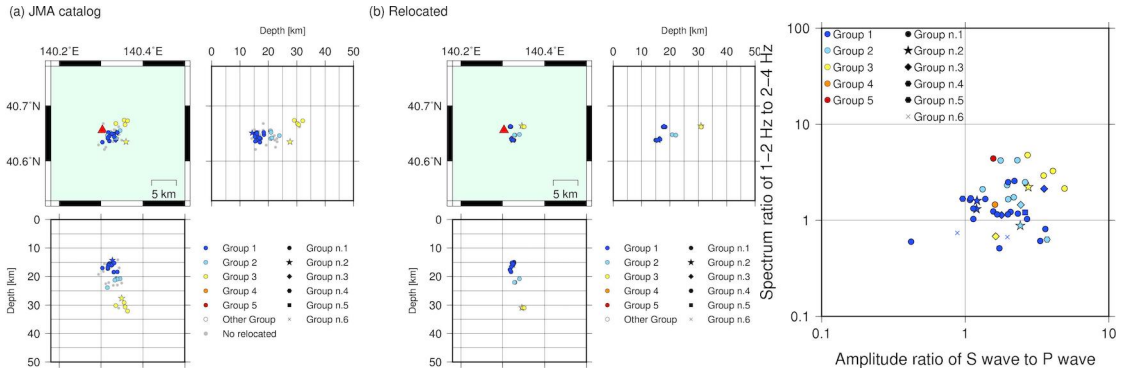

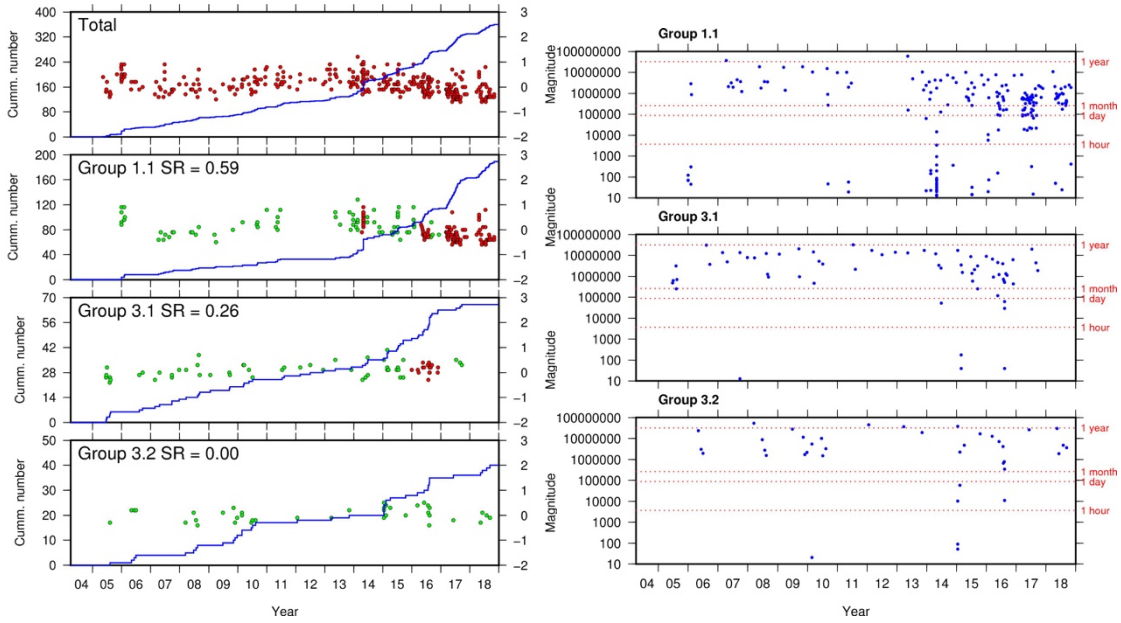

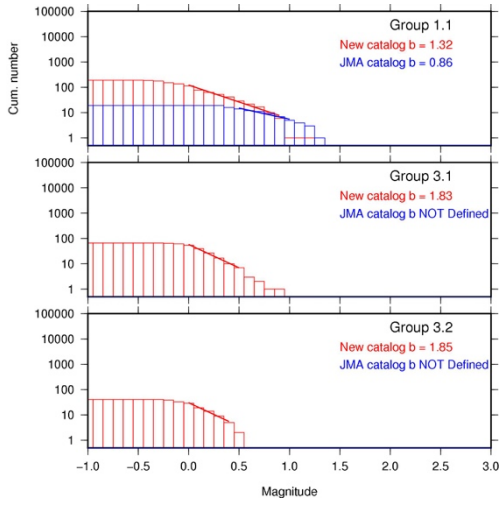

10.1.12. Shirakami

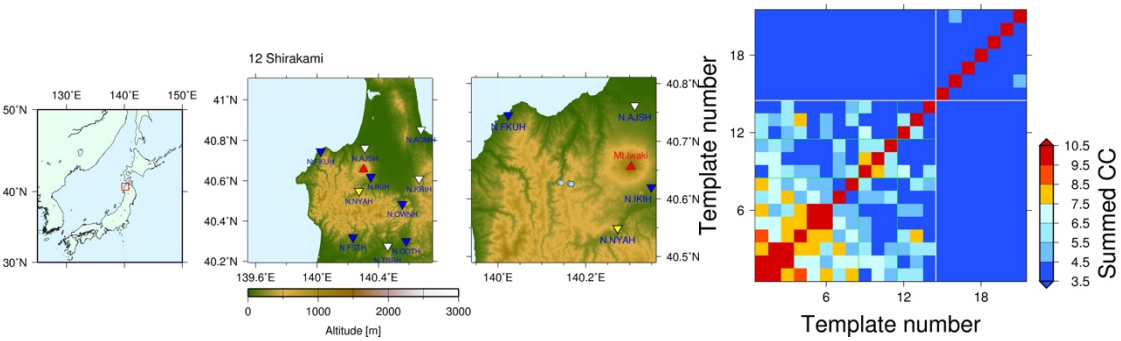

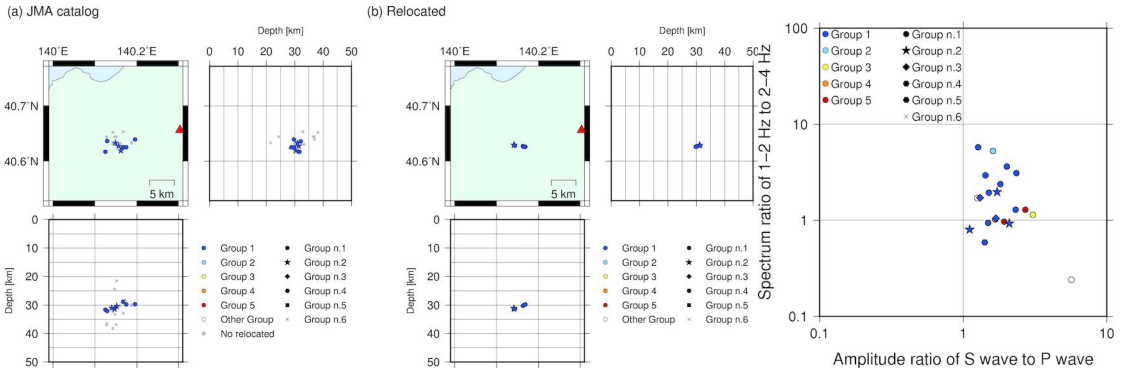

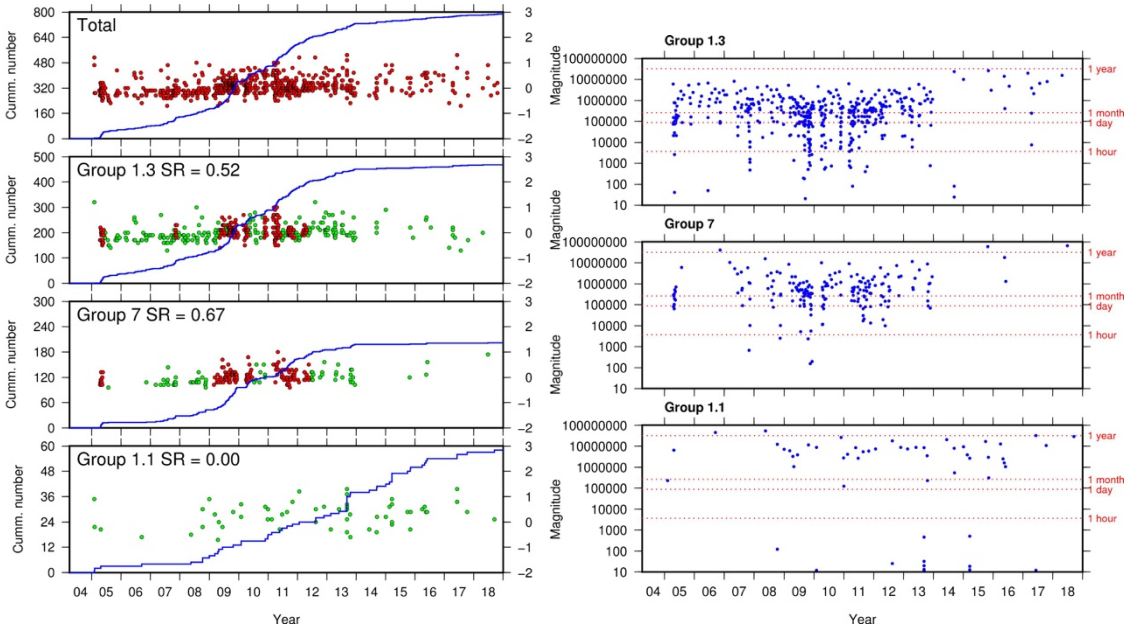

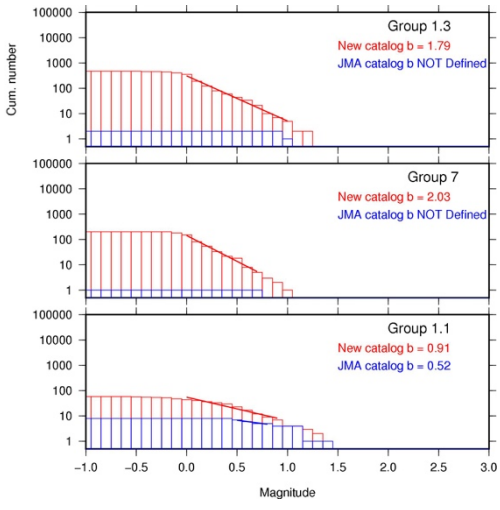

10.1.13. Towada-east

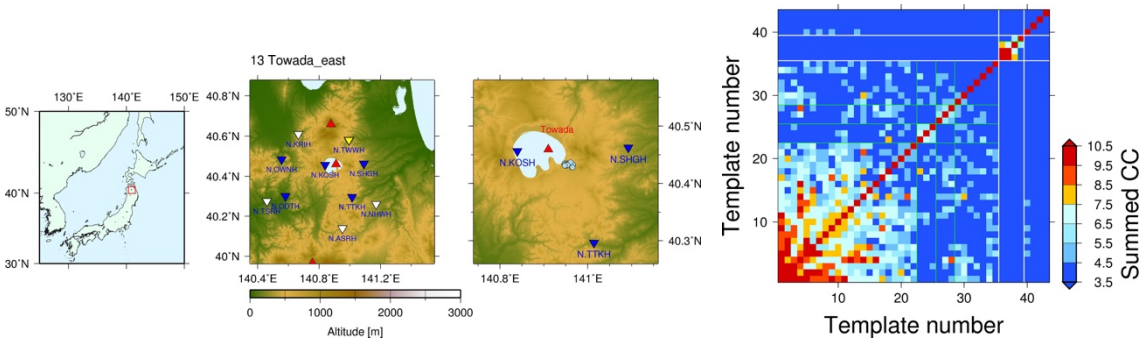

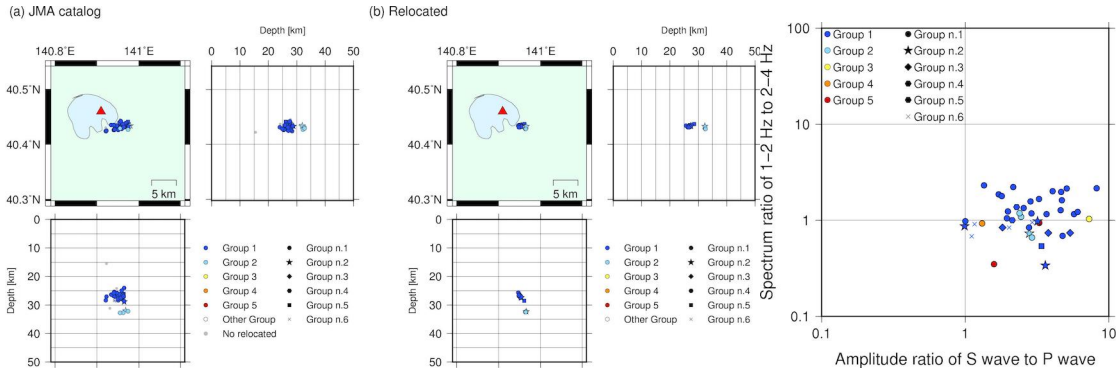

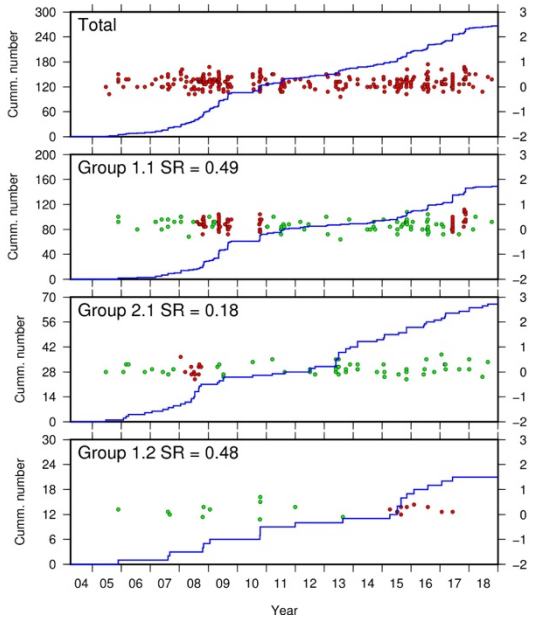

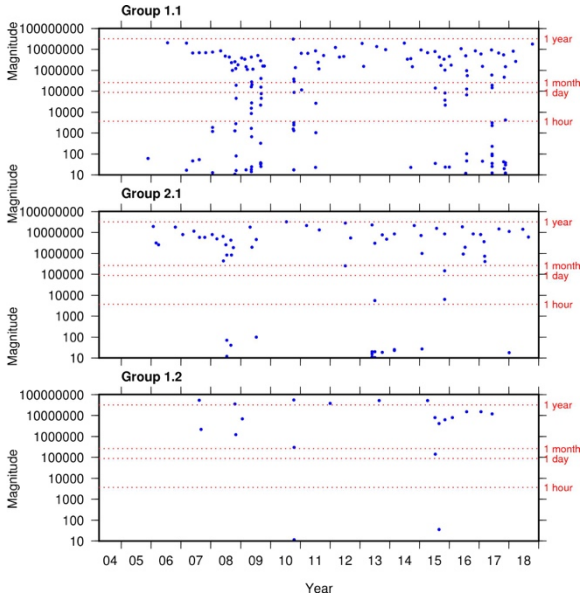

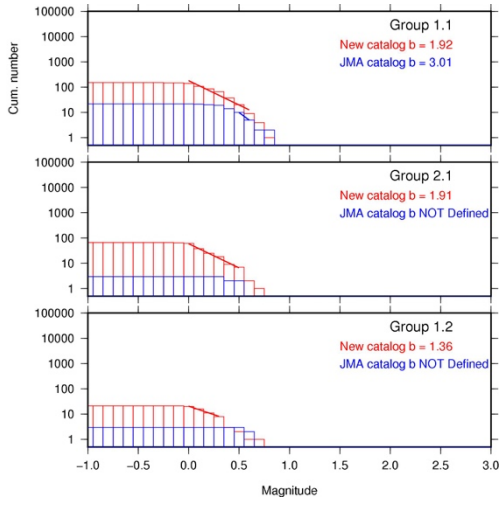

10.1.14. Kosaka

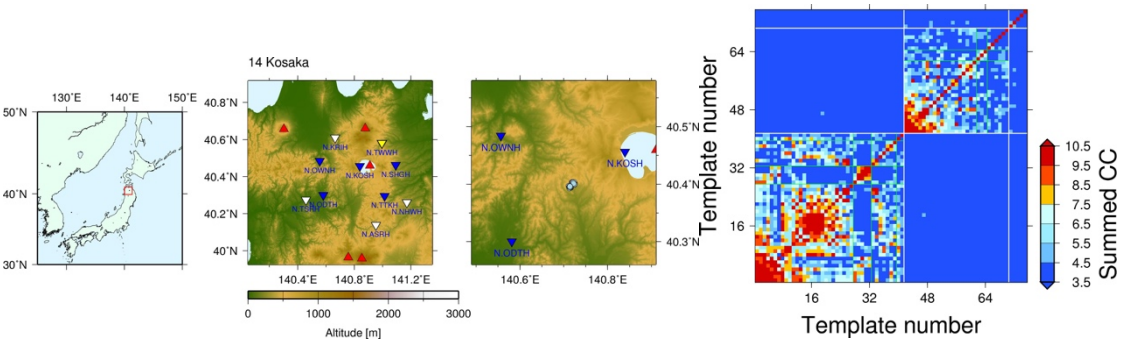

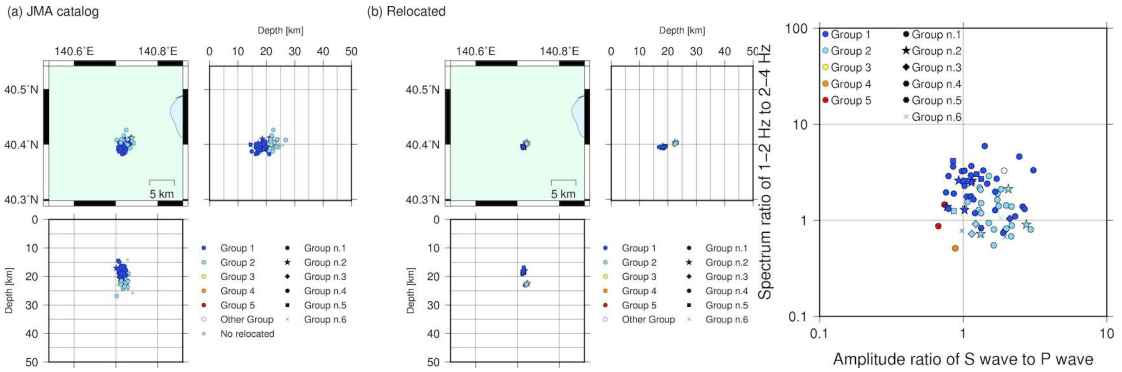

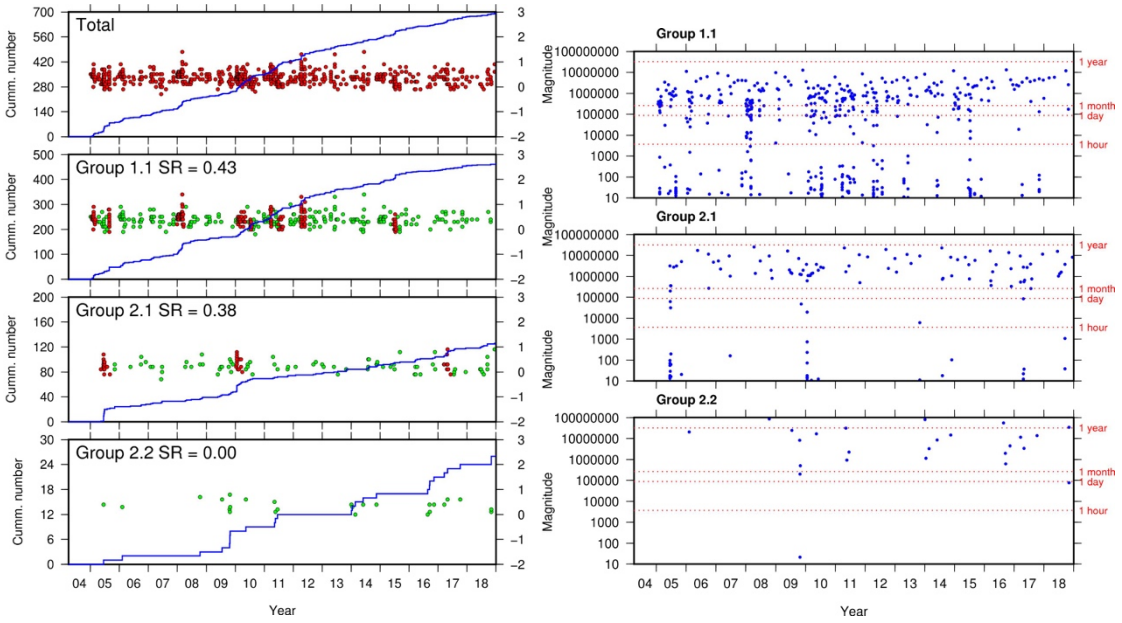

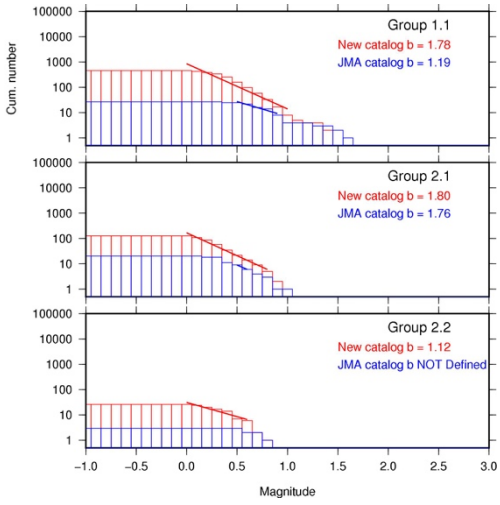

10.1.15. Moriyoshi

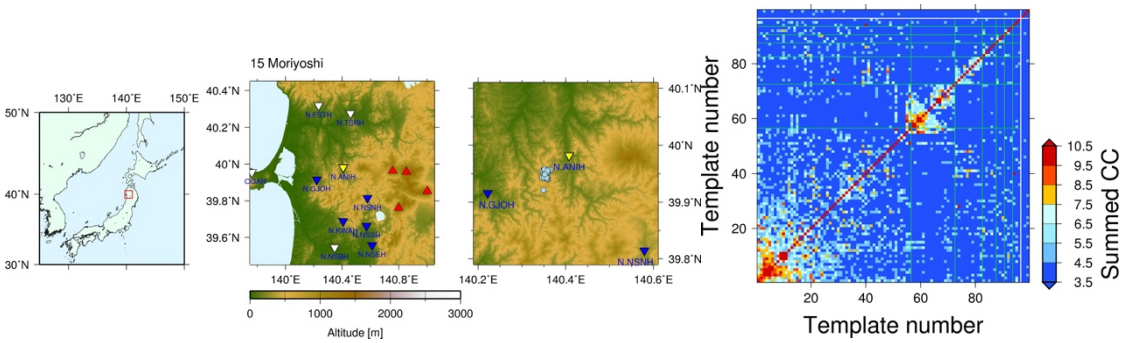

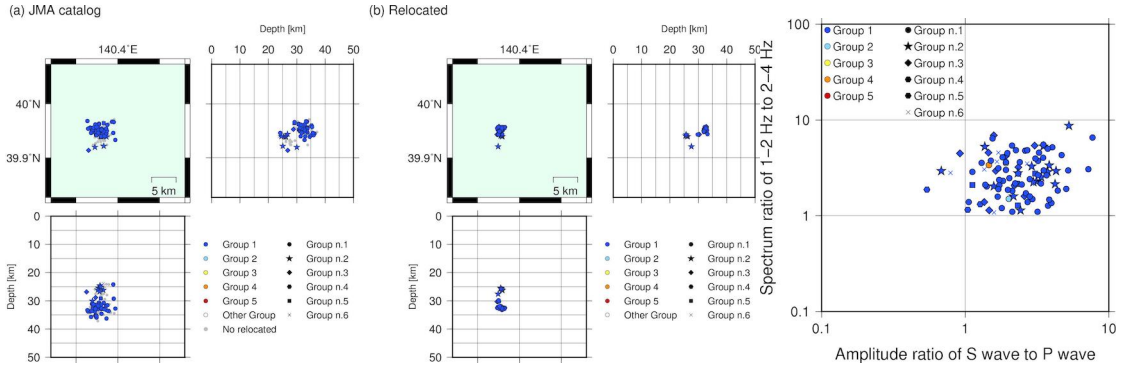

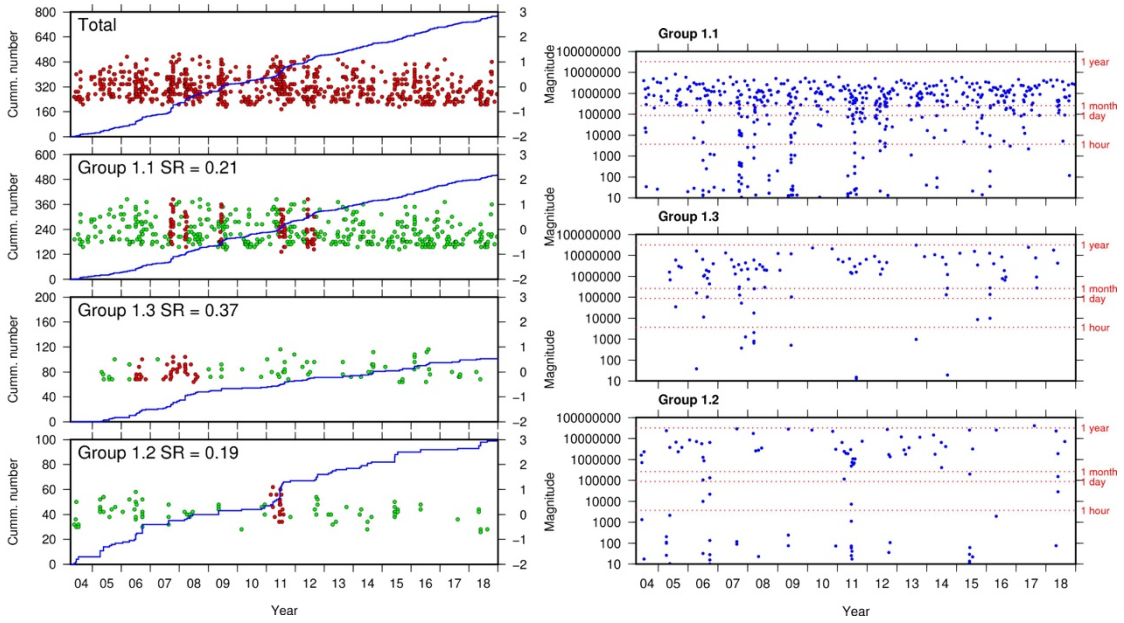

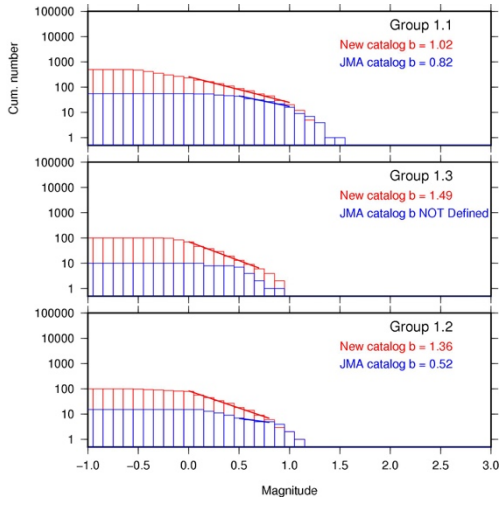

10.1.16. Yakeyama-Hachimantai

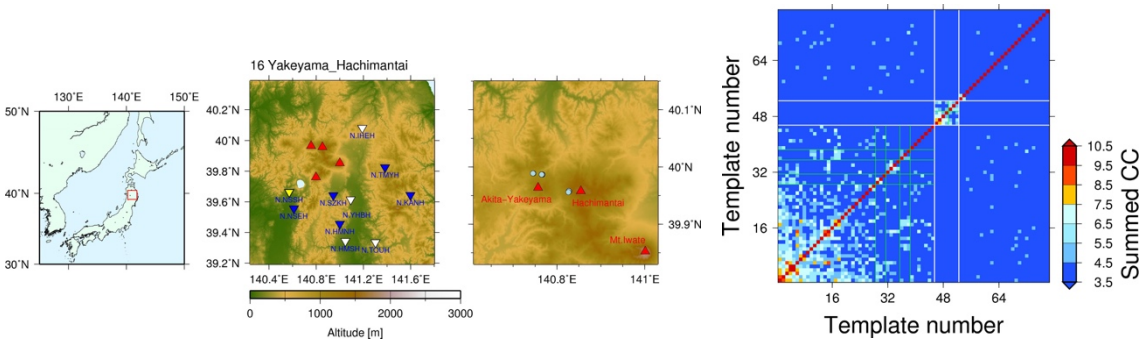

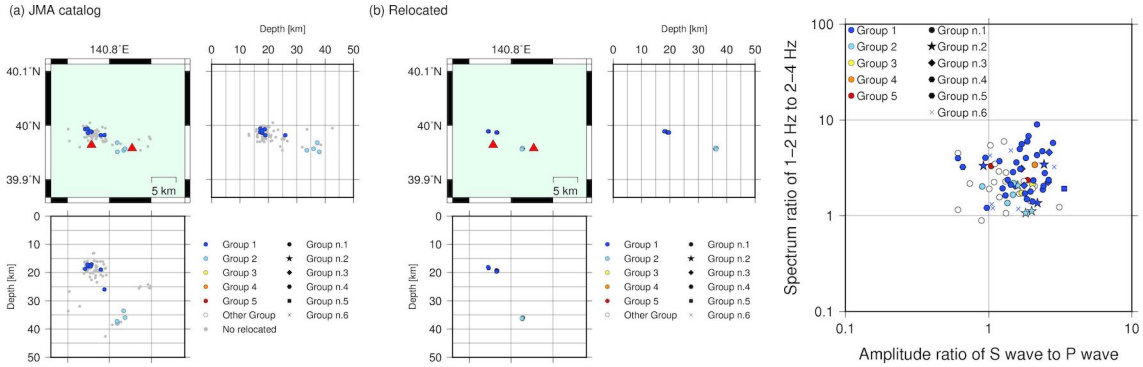

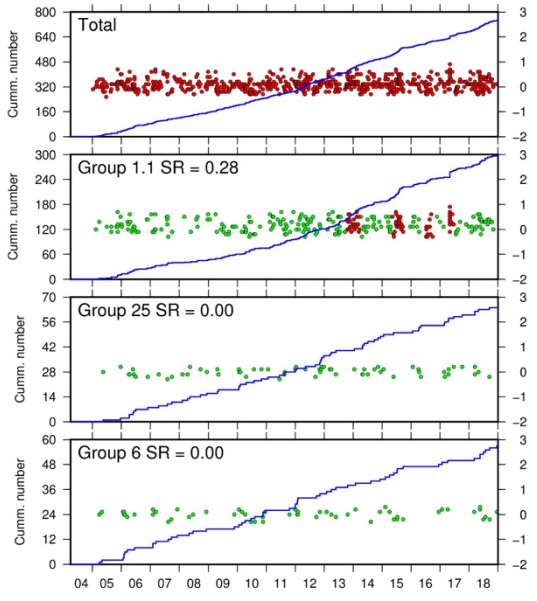

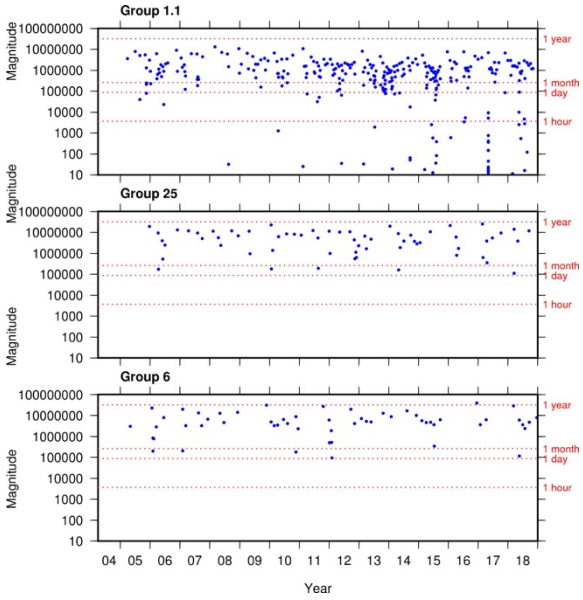

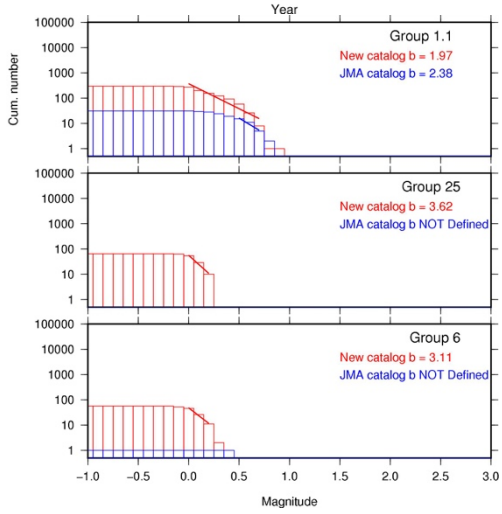

10.1.17. Mt.Iwate

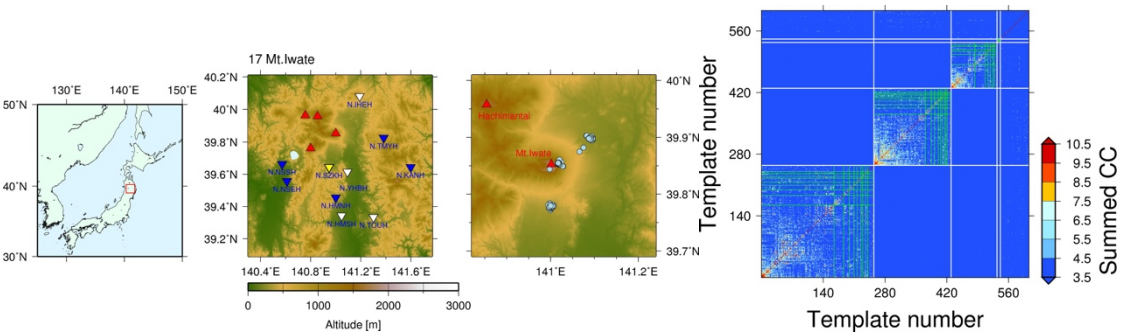

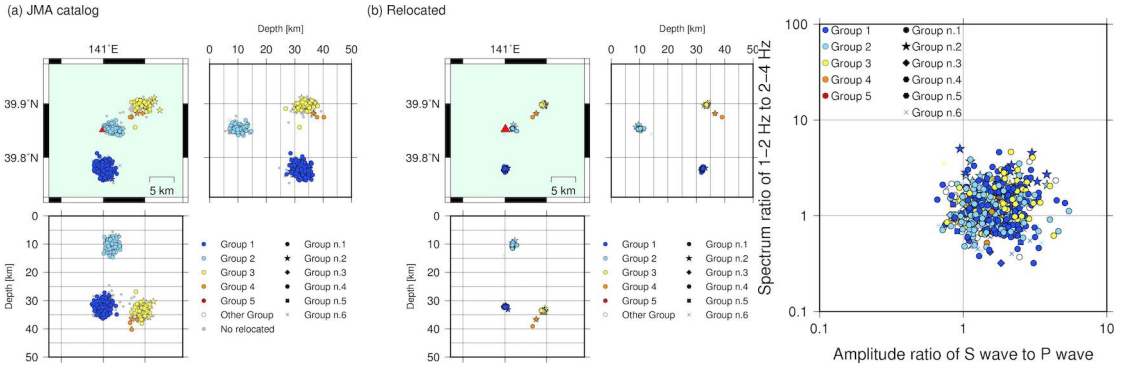

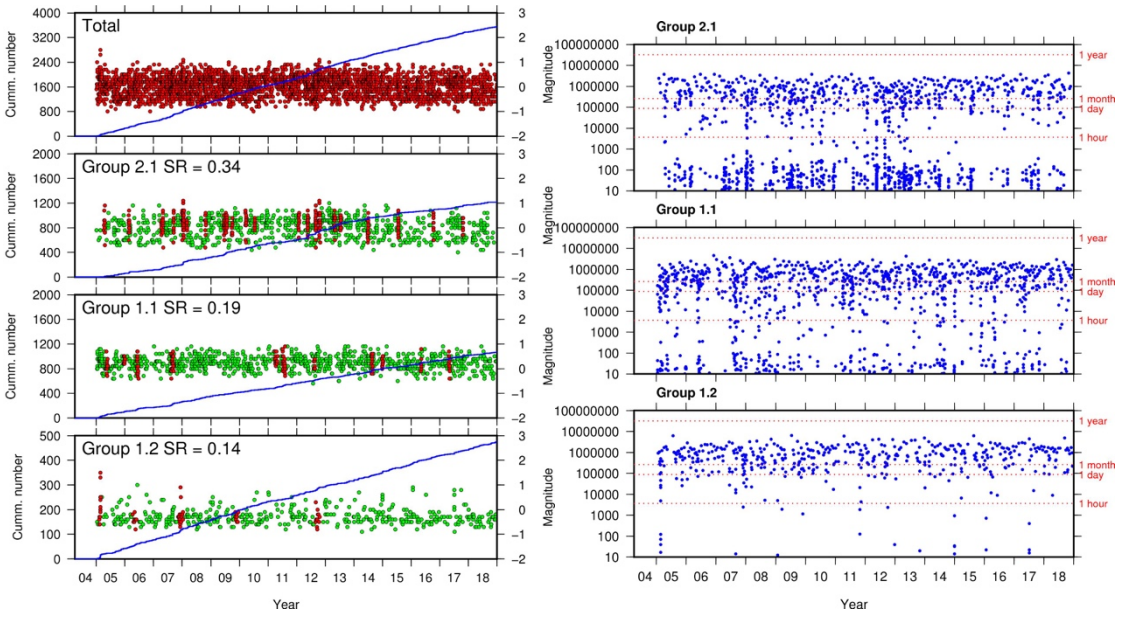

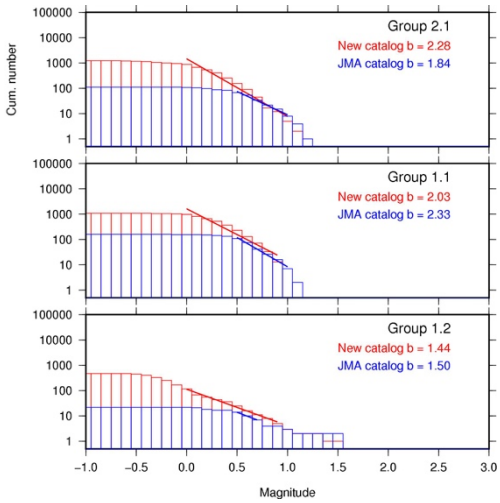

10.1.18. Akita-Komagatake

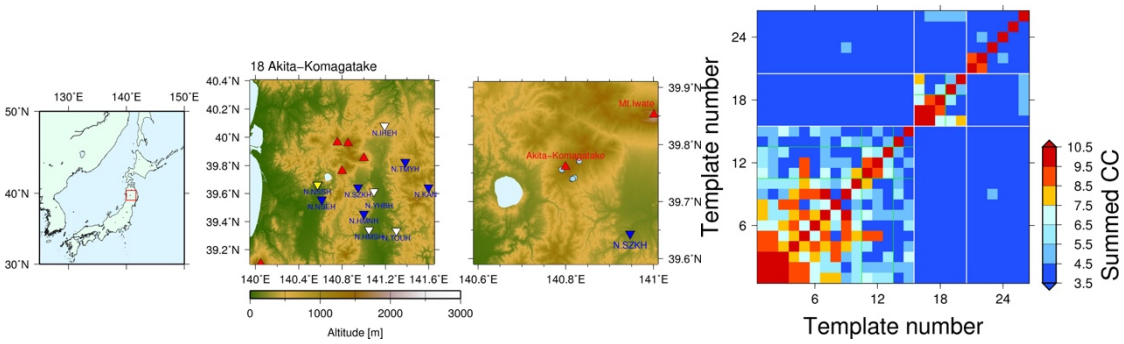

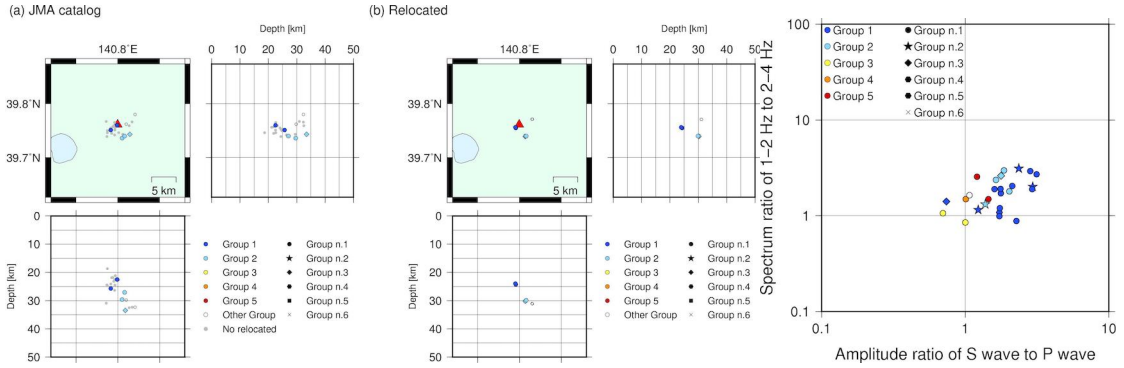

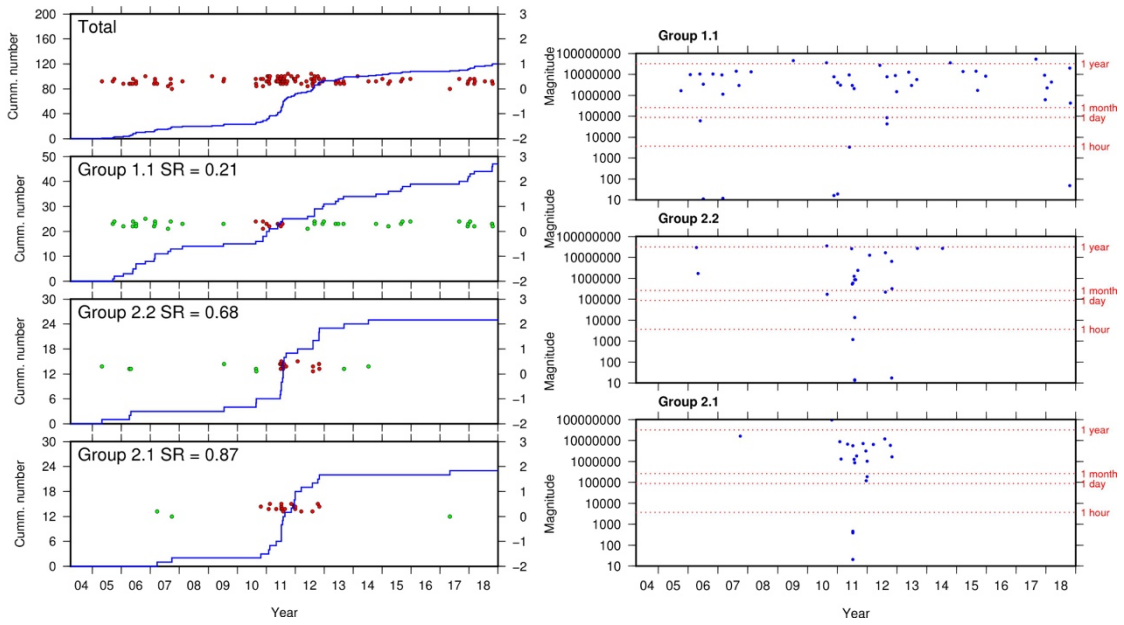

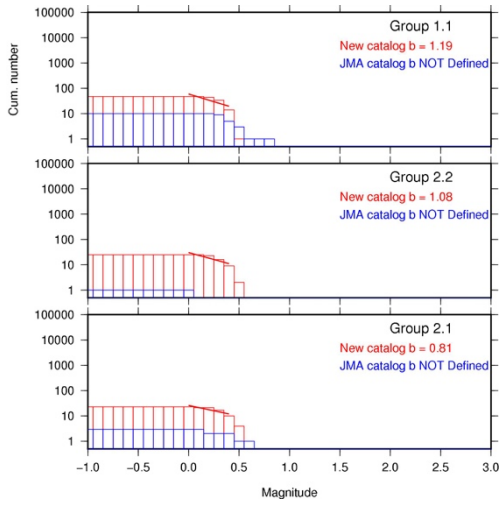

10.1.19. Chokaisan

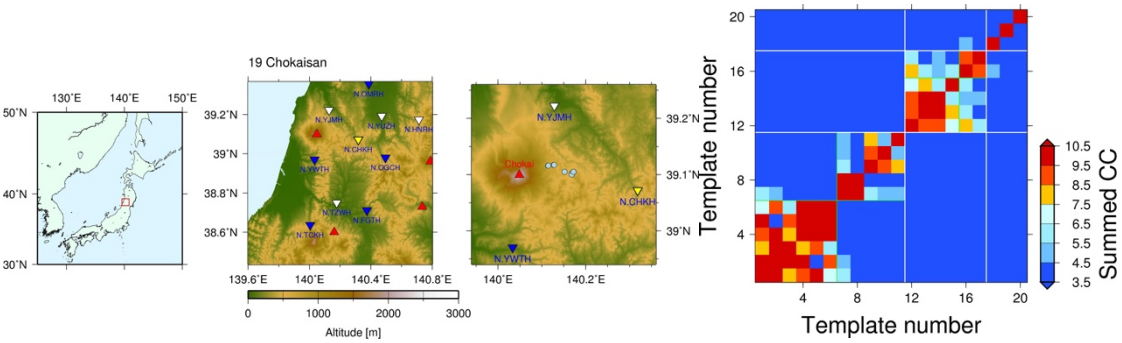

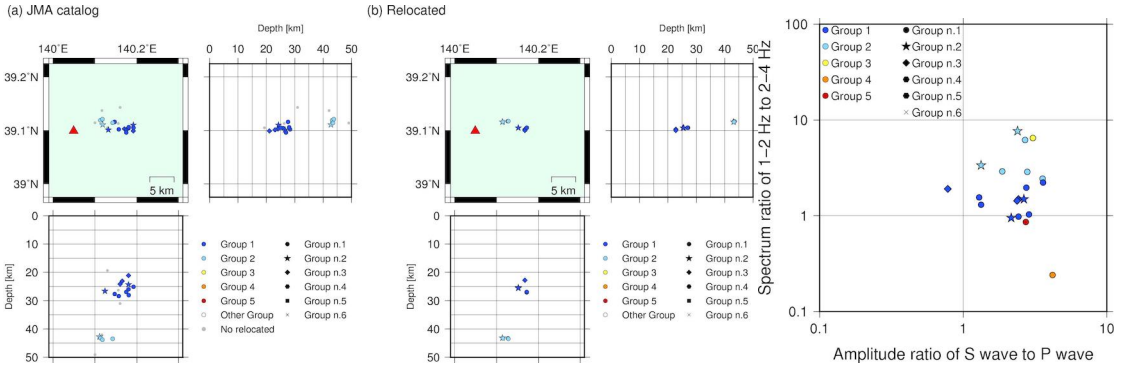

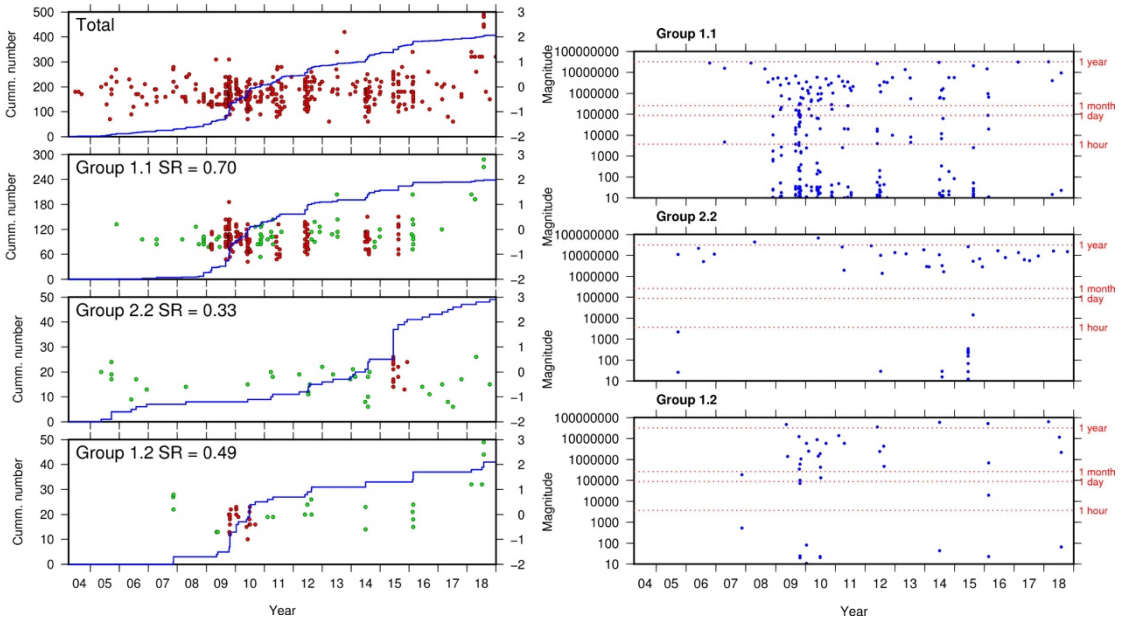

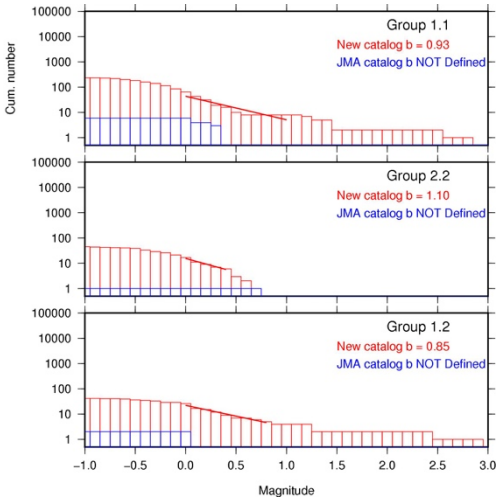

10.1.20. Kurikoma-NW

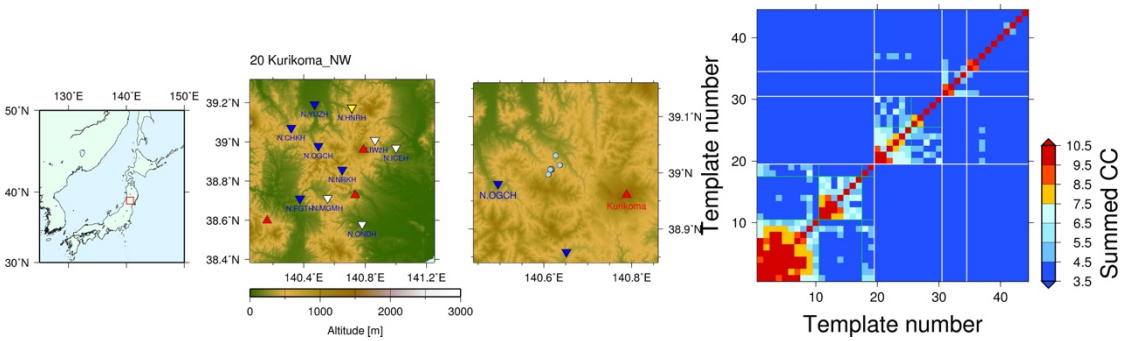

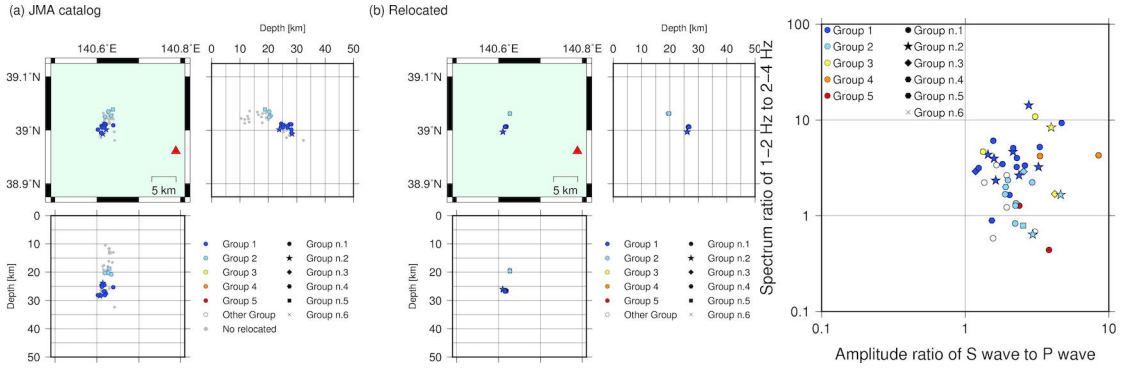

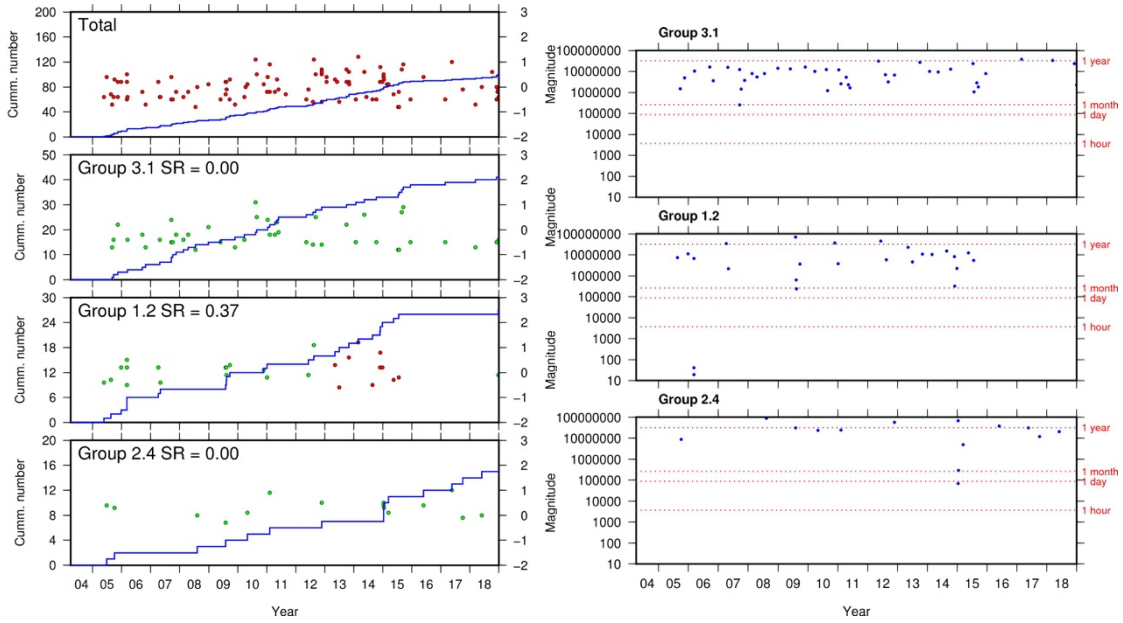

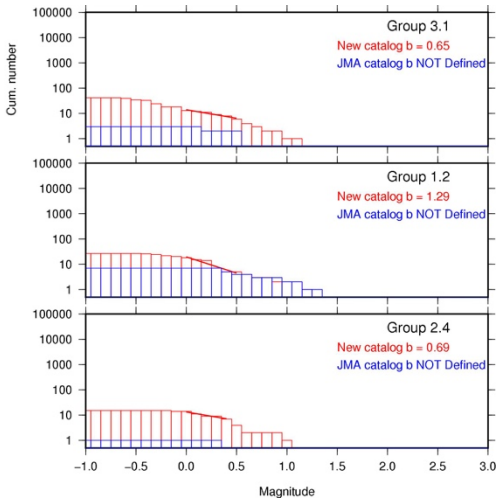

10.1.21. Kurikoma-center

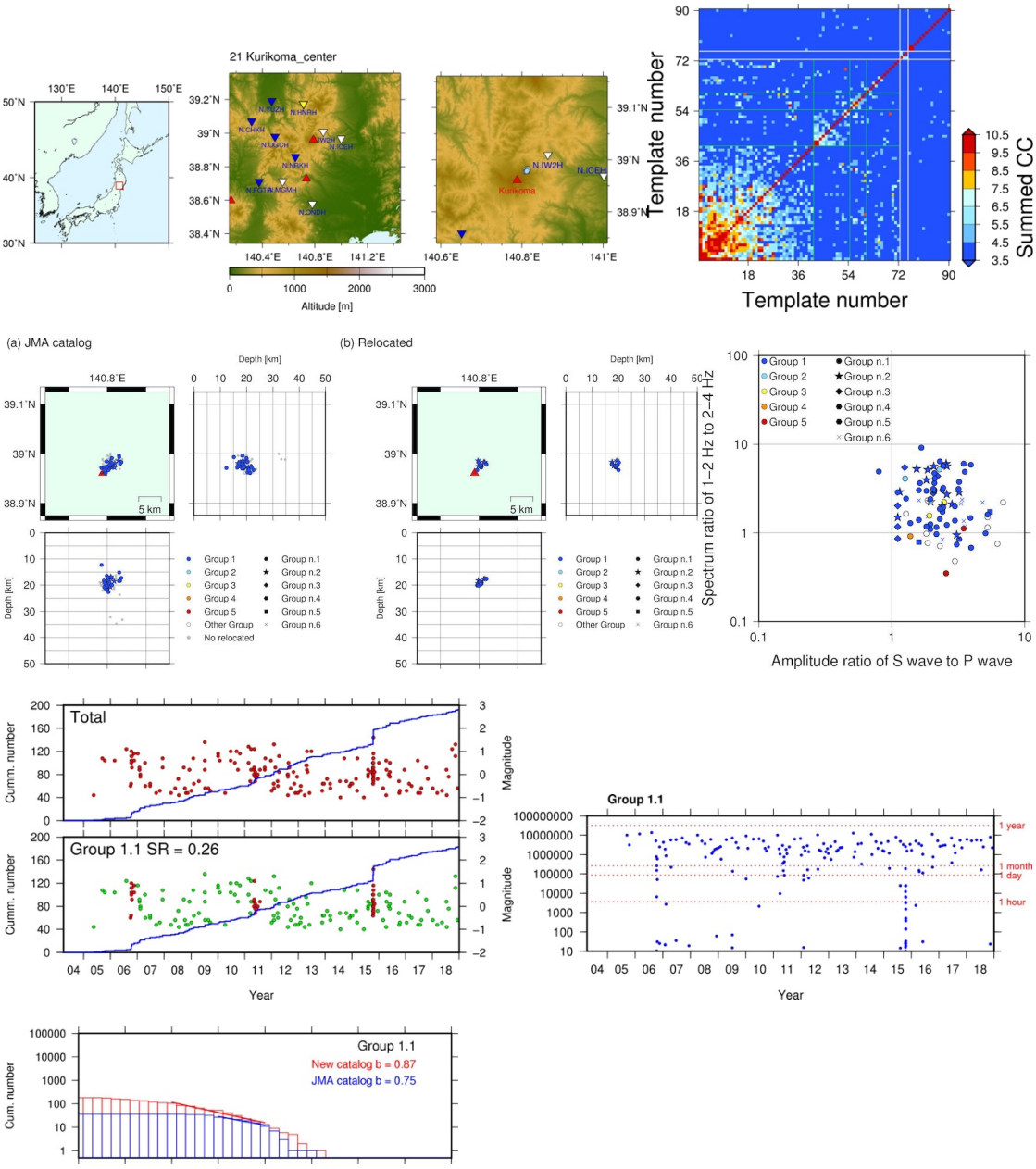

10.1.22. Naruko

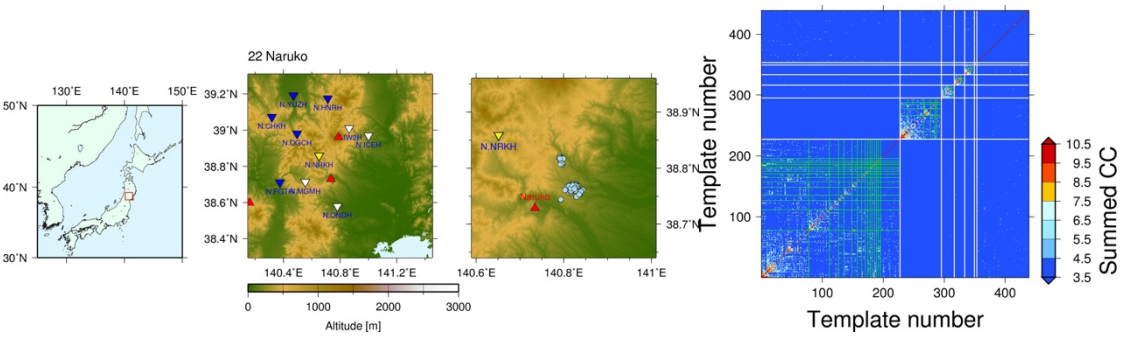

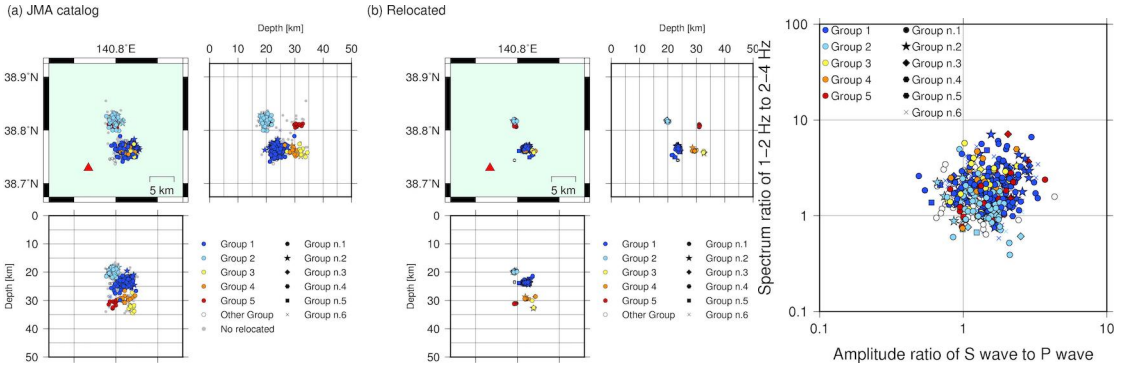

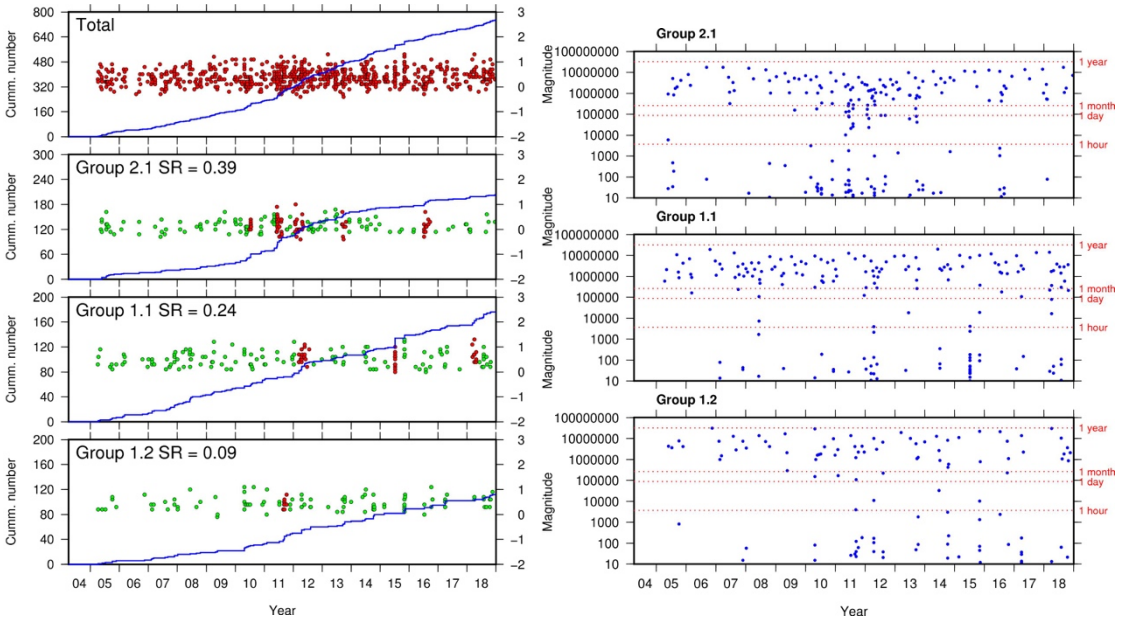

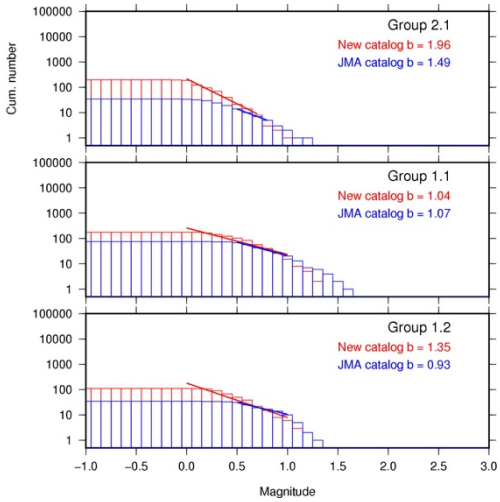

10.1.23. Hijiori

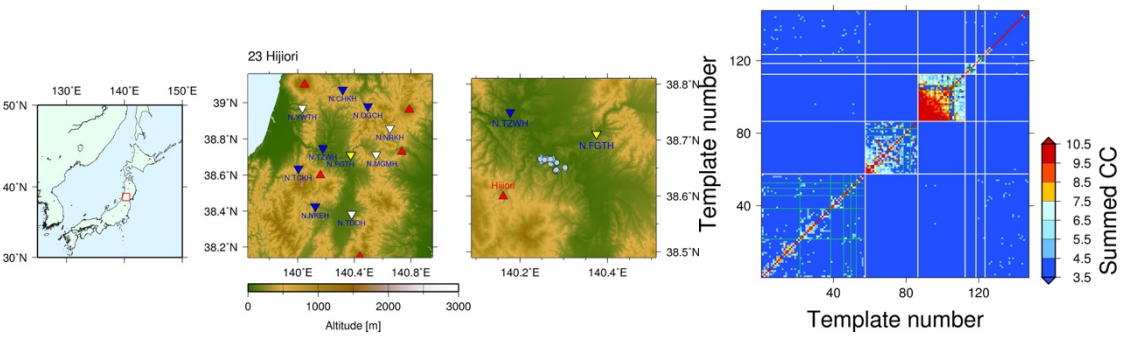

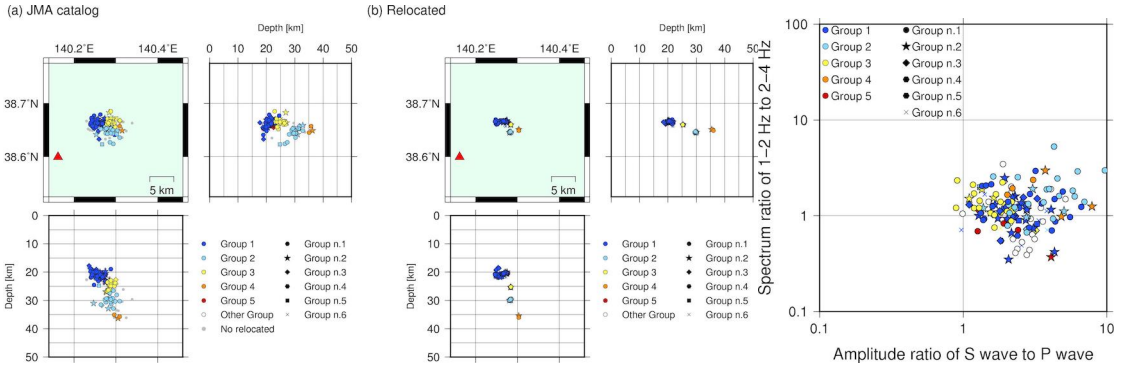

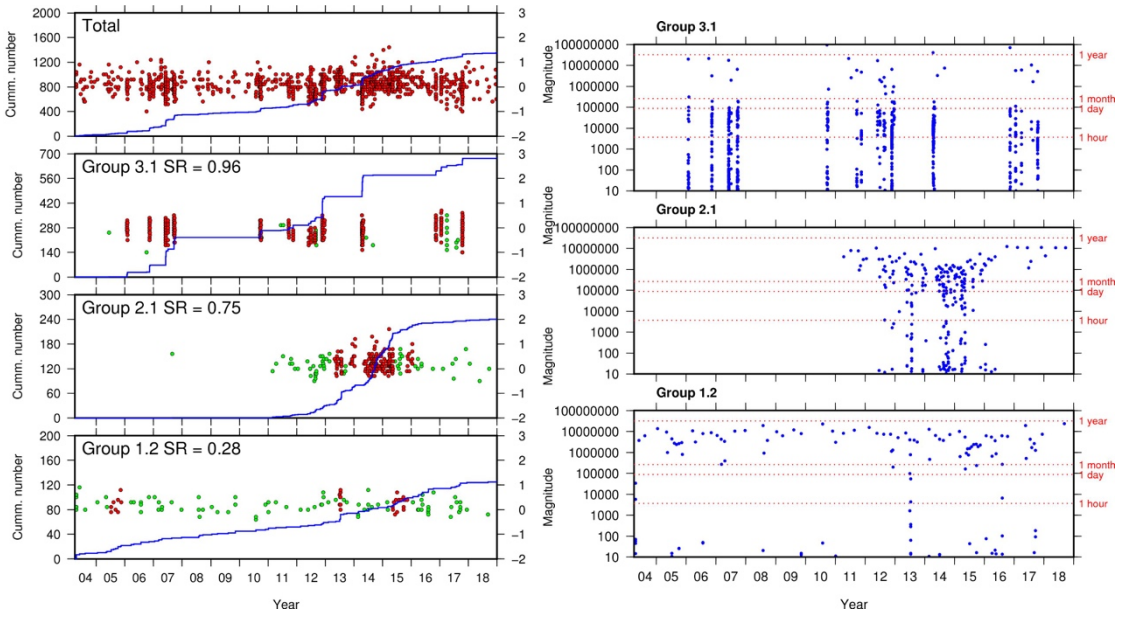

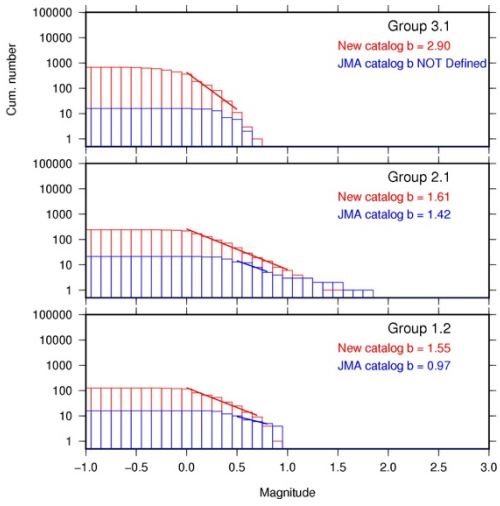

10.1.24. Asahidake

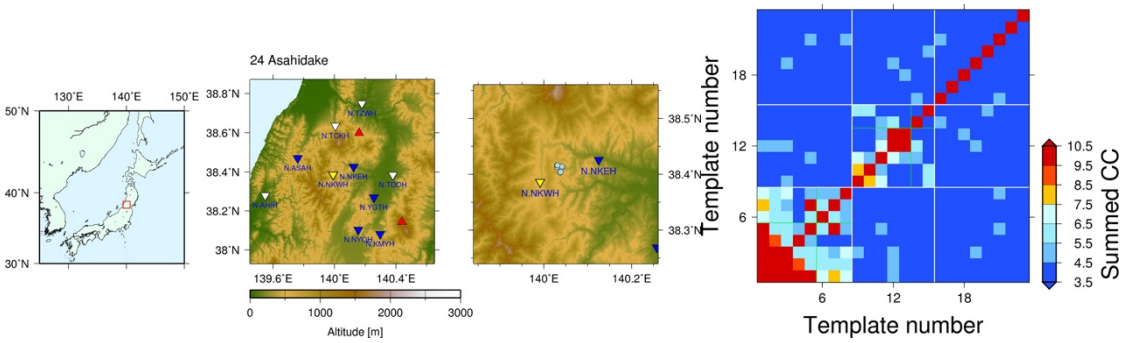

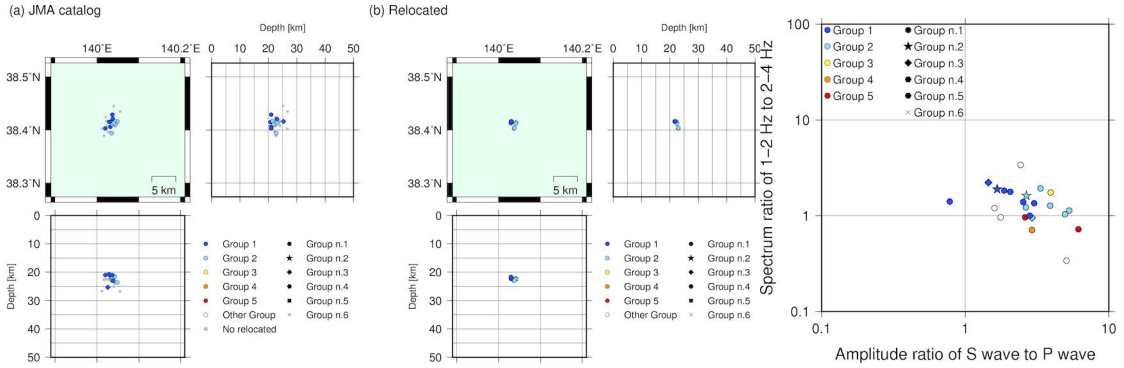

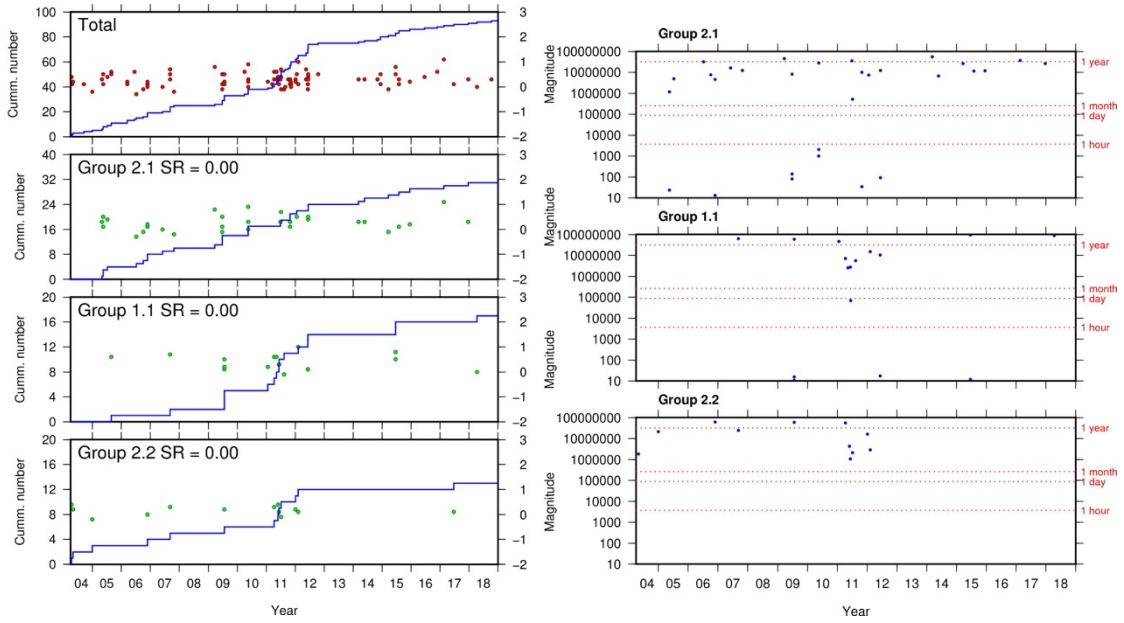

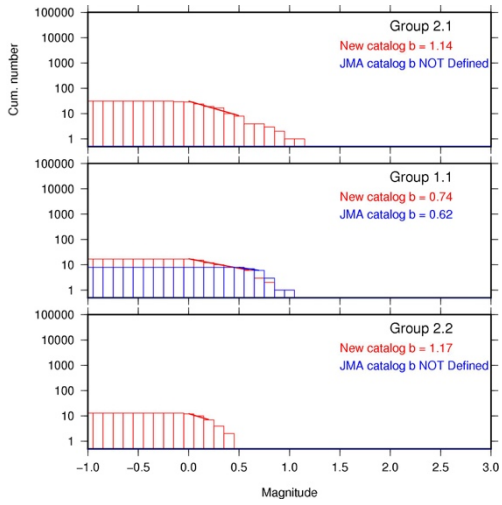

10.1.25. Zao

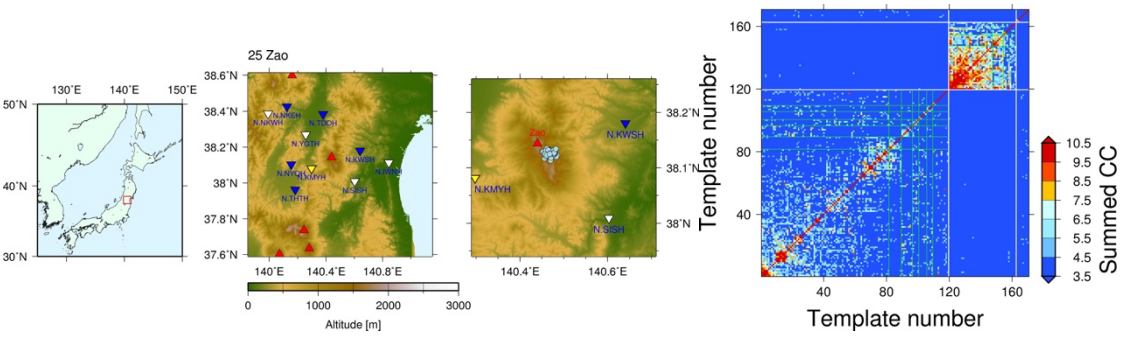
25 Zao
Altitude [m]
Template number
Summed CC

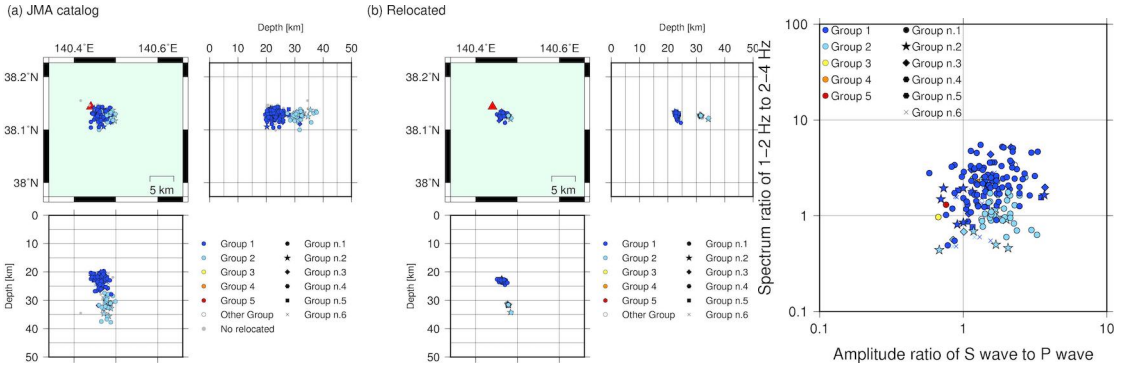
(a) JMA catalog
(b) Relocated
Depth [km]
5 km
Group 1
Group 2
Group 3
Group 4
Group 5
Other Group
No relocated
Spectrum ratio of 1–2 Hz to 2–4 Hz
Amplitude ratio of S wave to P wave

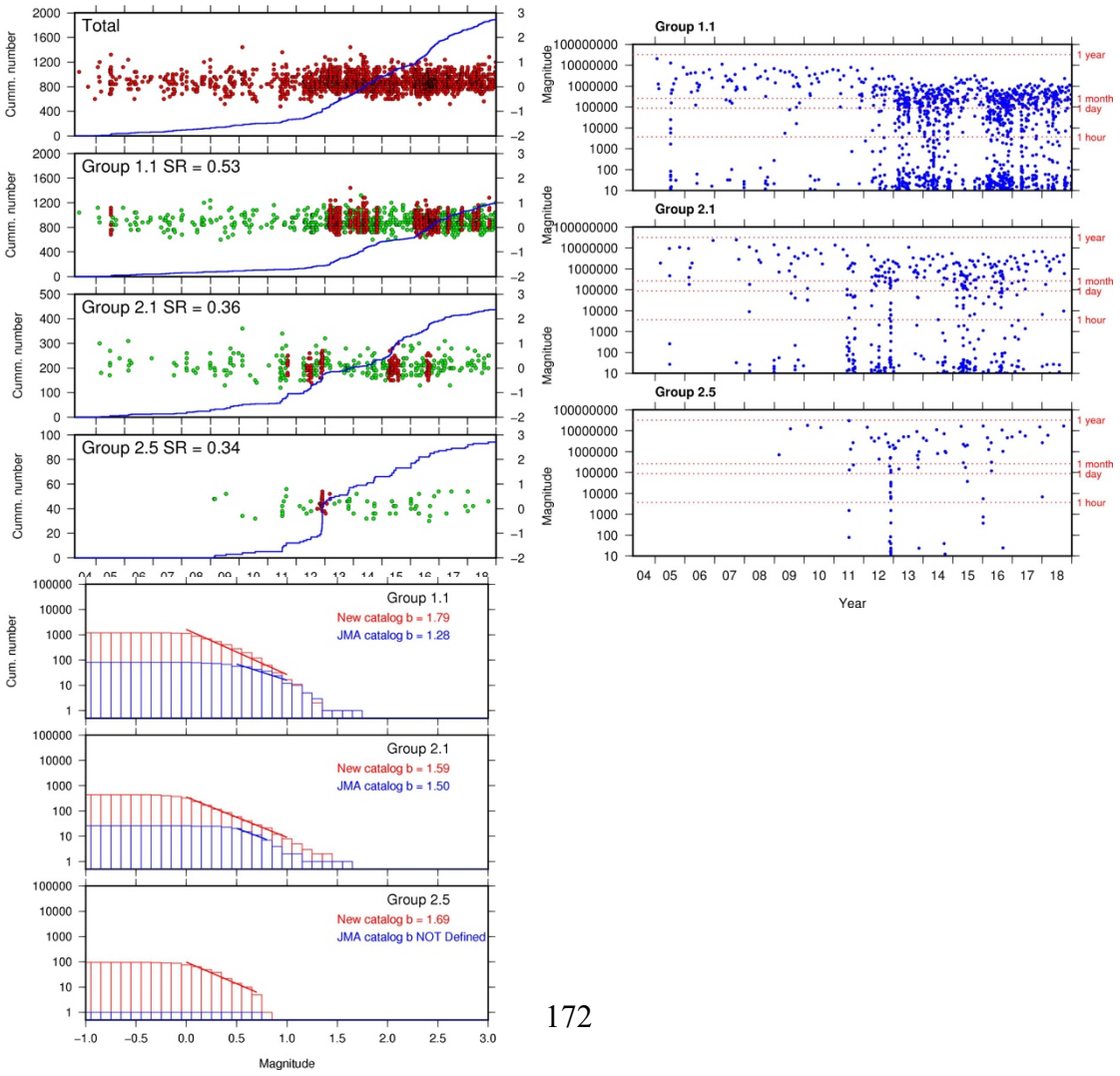
Total
Group 1.1 SR = 0.53
Group 2.1 SR = 0.36
Group 2.5 SR = 0.34
Cumm. number
Group 1.1
Group 2.1
Group 2.5
Magnitude
Year
Cum. number
New catalog b = 1.79
JMA catalog b = 1.28
New catalog b = 1.59
JMA catalog b = 1.50
New catalog b = 1.69
JMA catalog b NOT Defined

10.1.26. Azuma

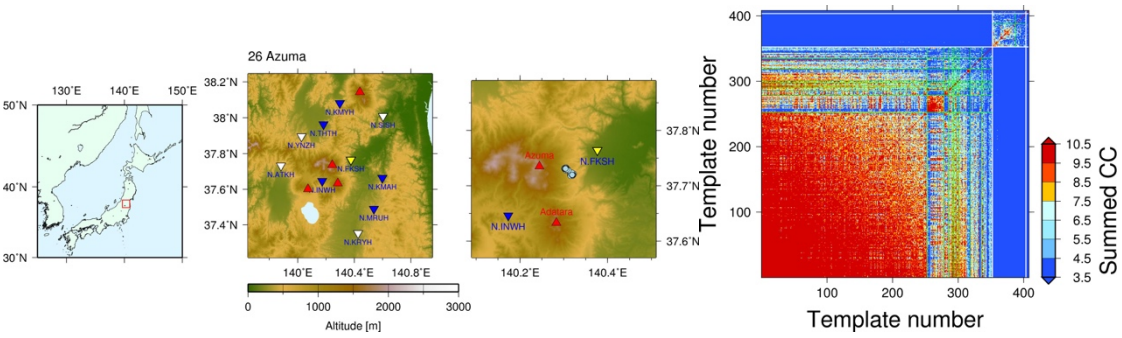
26 Azuma
Altitude [m]
Template number
Summed CC

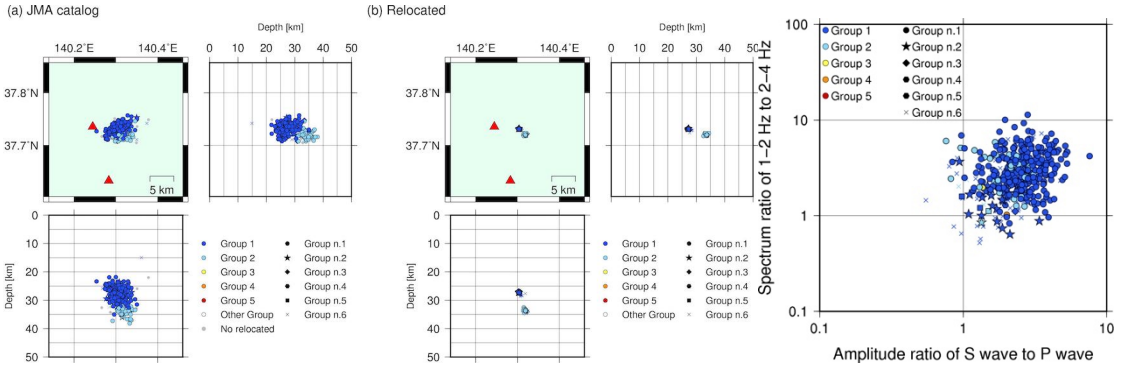
(a) JMA catalog
(b) Relocated
Depth [km]
Group 1
Group 2
Group 3
Group 4
Group 5
Other Group
No relocated
Group n.1
Group n.2
Group n.3
Group n.4
Group n.5
Group n.6
Spectrum ratio of 1–2 Hz to 2–4 Hz
Amplitude ratio of S wave to P wave

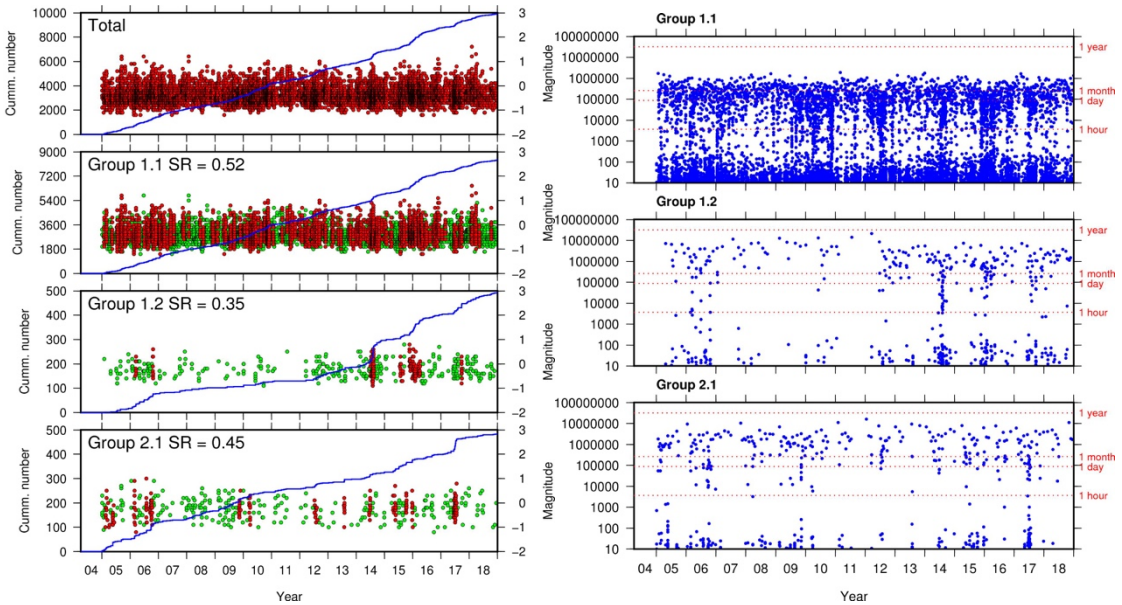
Total
Group 1.1 SR = 0.52
Group 1.2 SR = 0.35
Group 2.1 SR = 0.45
Cumm. number
Year
Group 1.1
Group 1.2
Group 2.1
Magnitude
1 year
1 month
1 day
1 hour

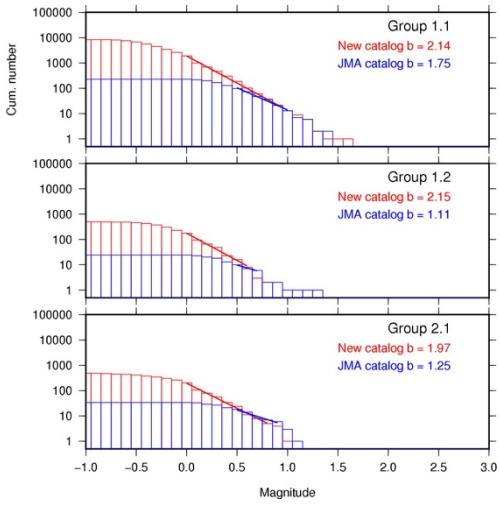
Group 1.1
New catalog b = 2.14
JMA catalog b = 1.75
Group 1.2
New catalog b = 2.15
JMA catalog b = 1.11
Group 2.1
New catalog b = 1.97
JMA catalog b = 1.25
Cum. number
Magnitude

10.1.27. Adatara

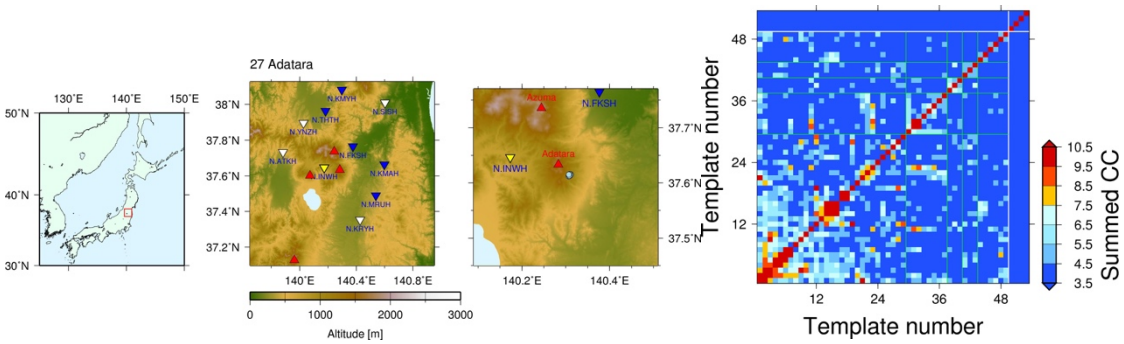

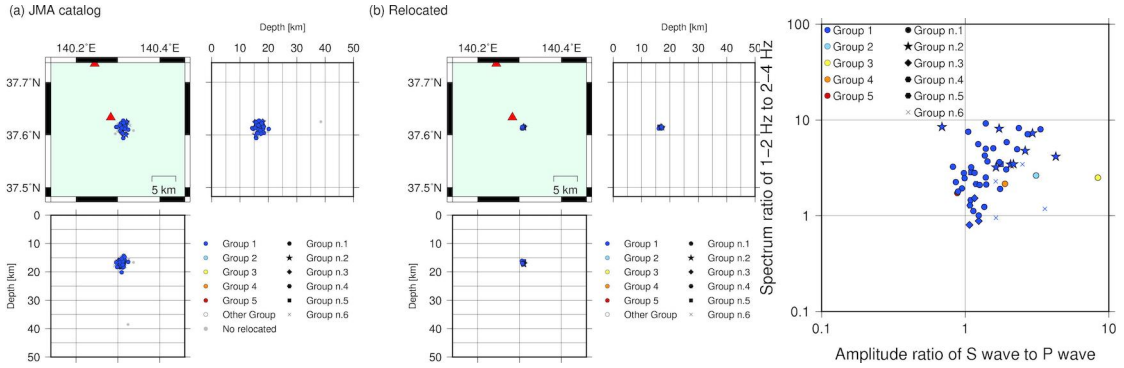

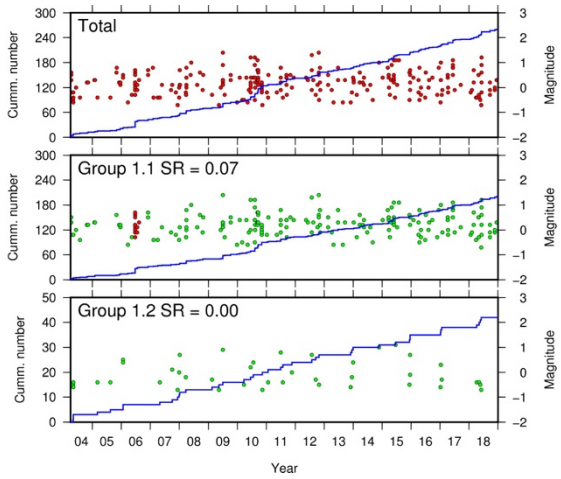

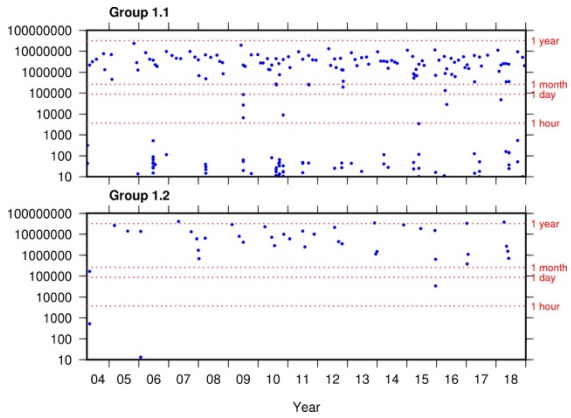

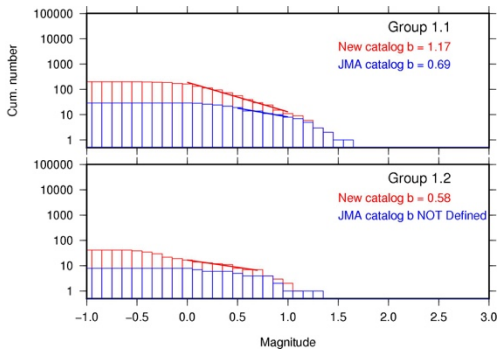

10.1.28. Bandai-west

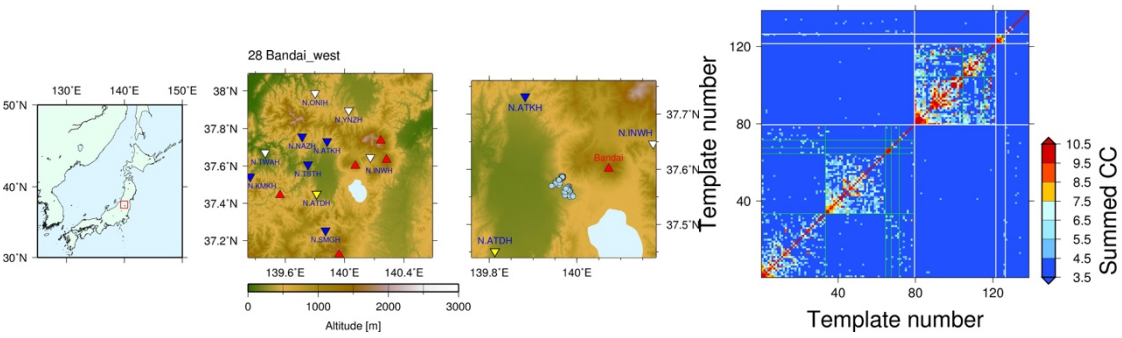

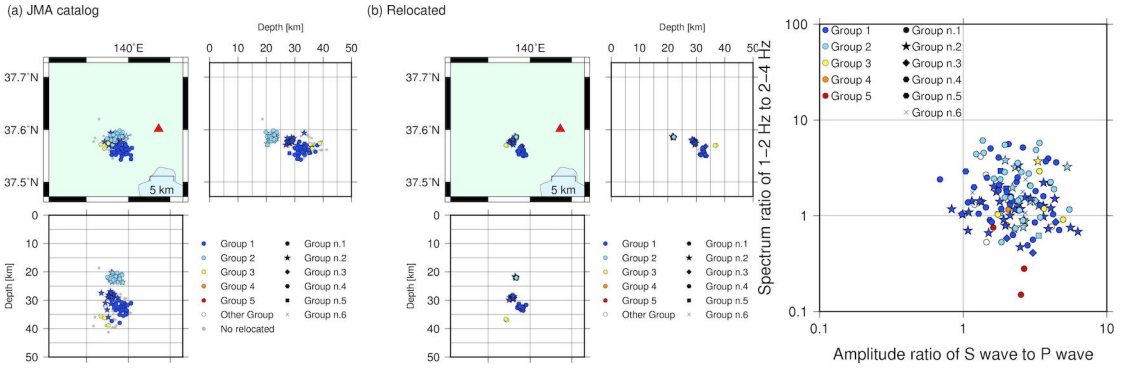

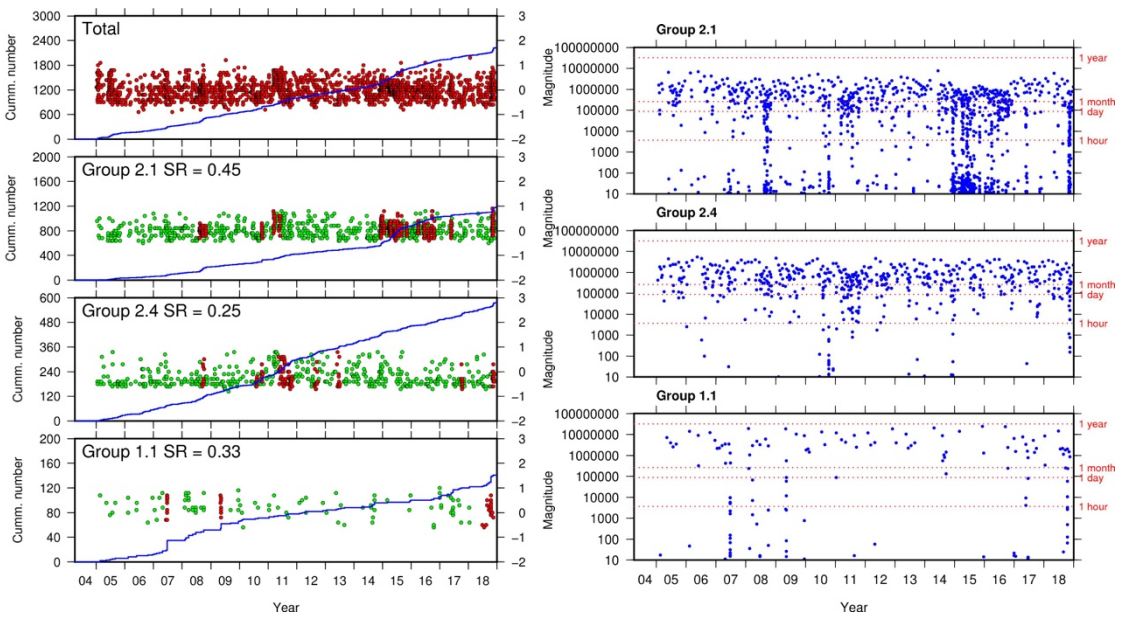

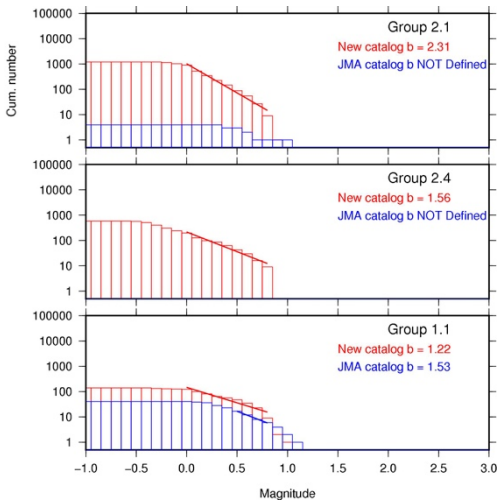

10.1.29. Aizu-Takada

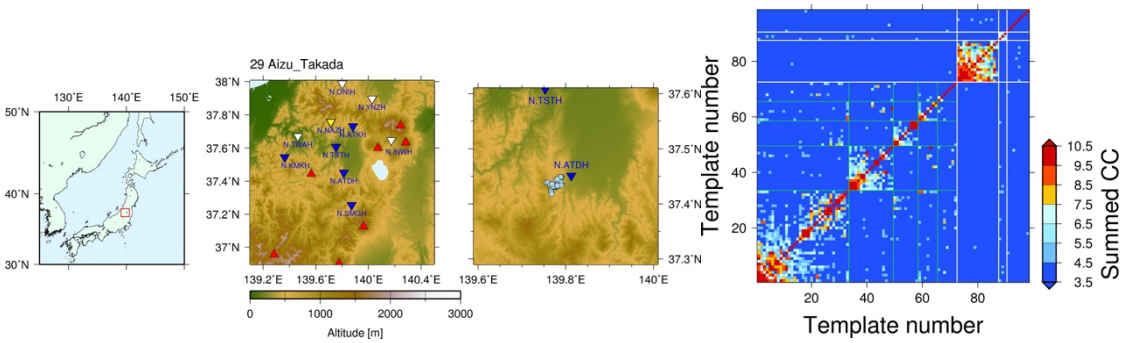

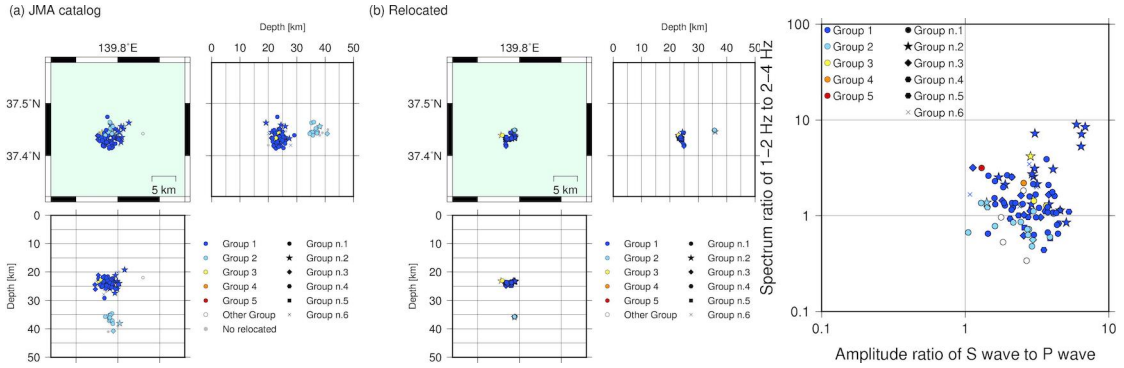

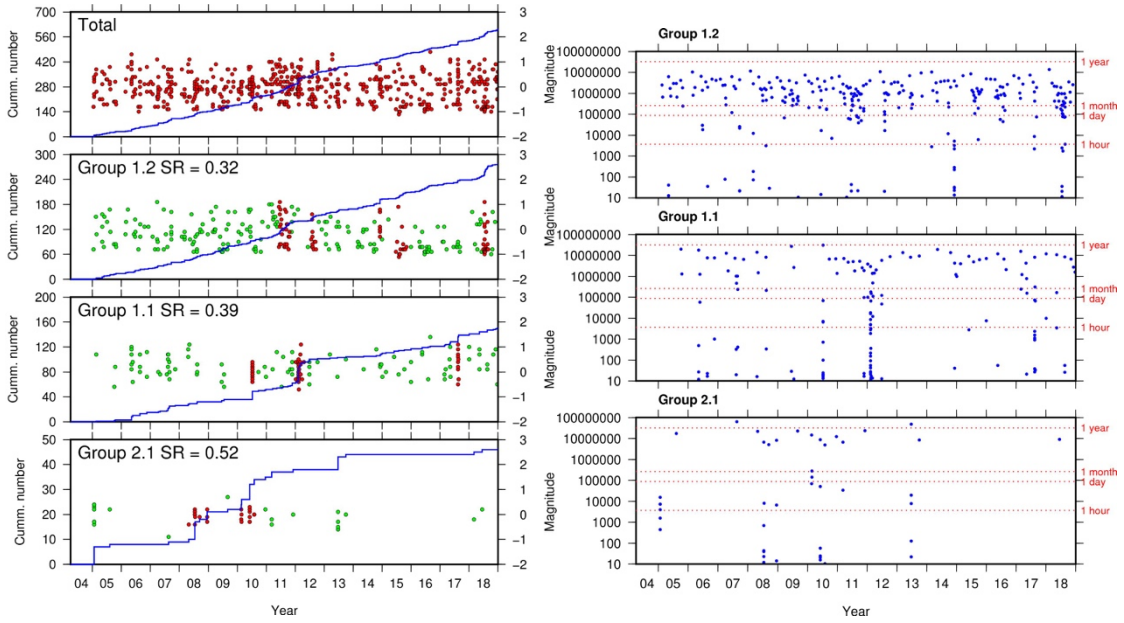

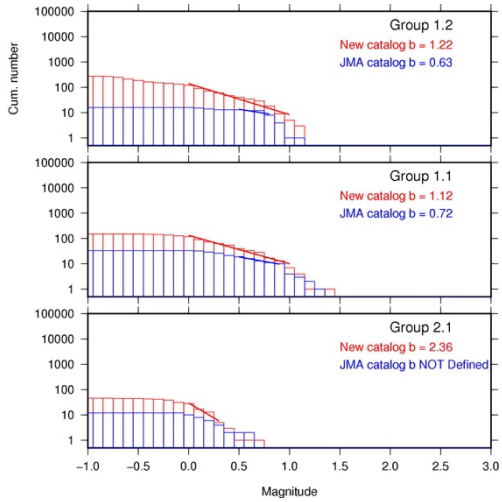

10.1.30. Numazawa

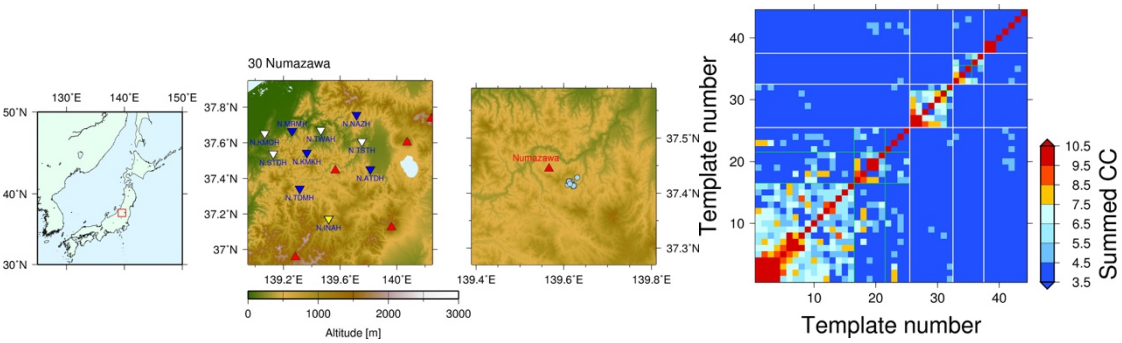

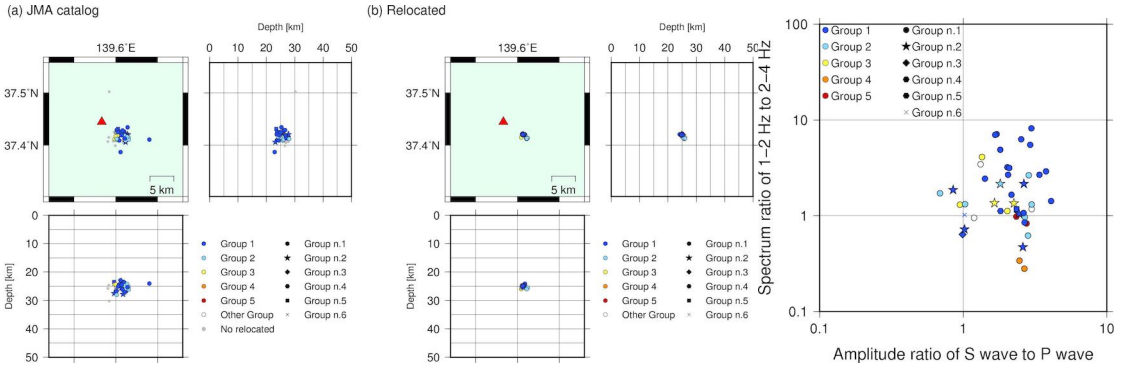

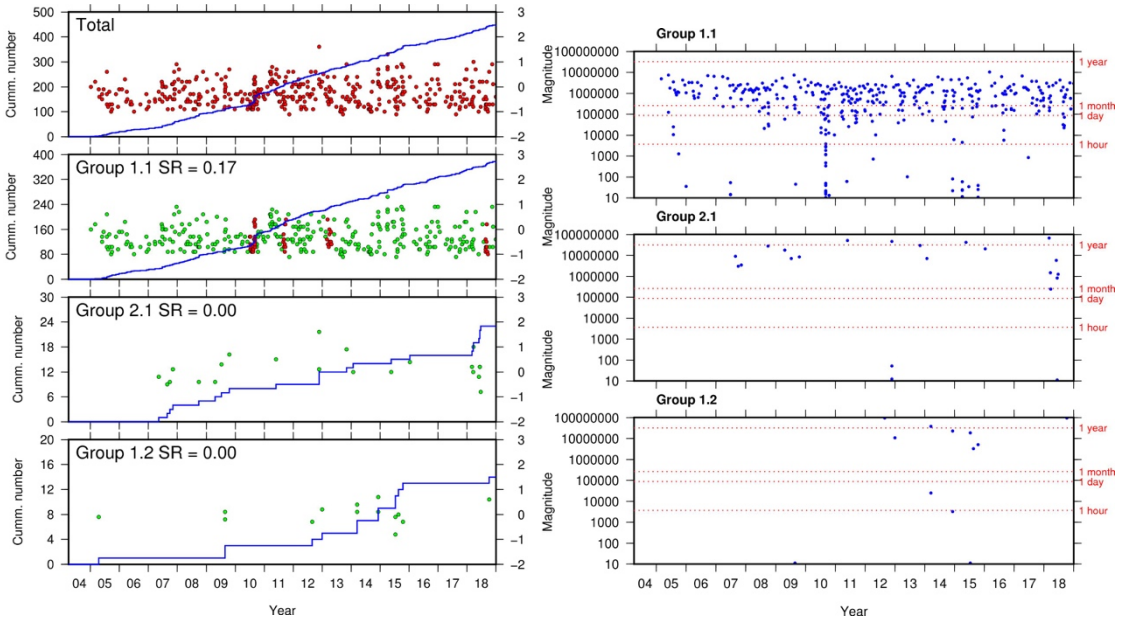

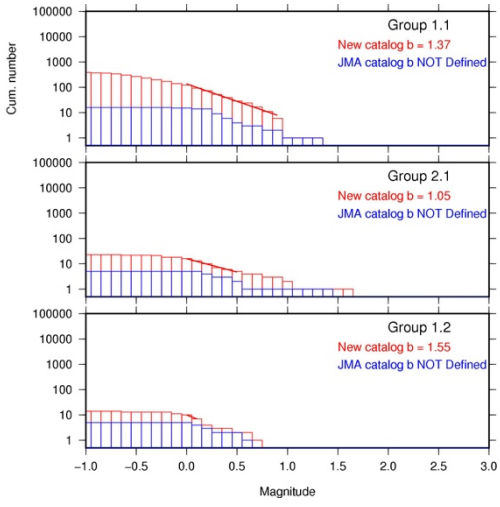

10.1.31. Mikagura

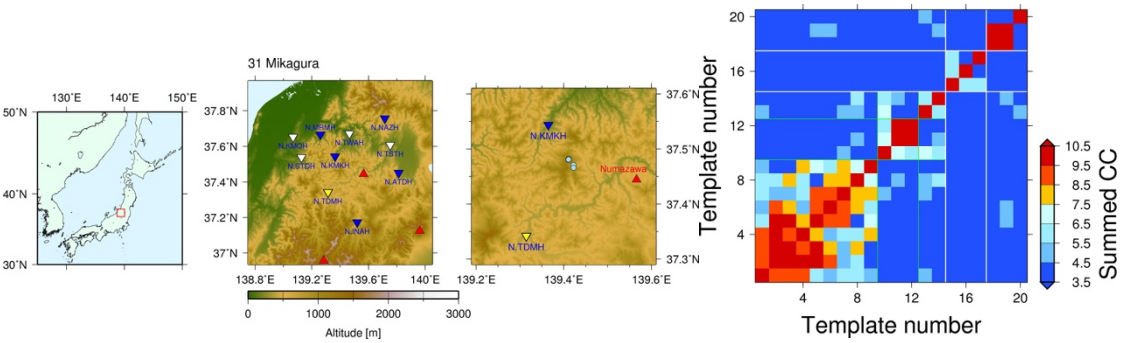

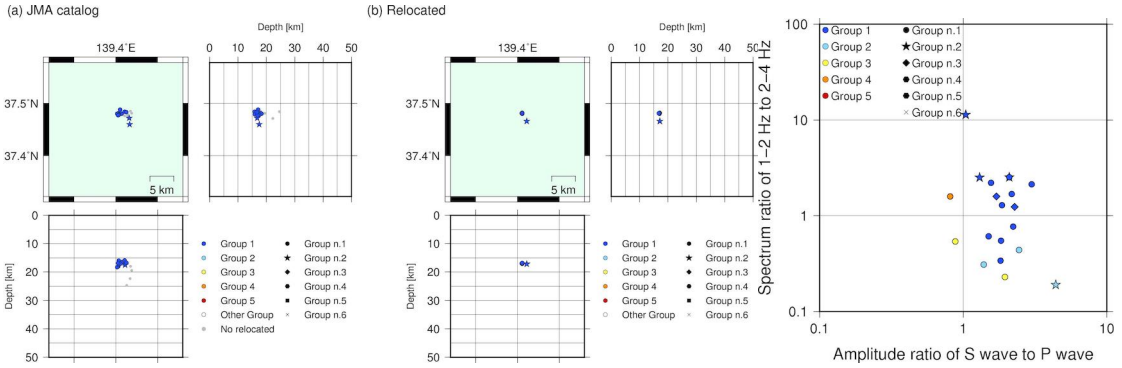

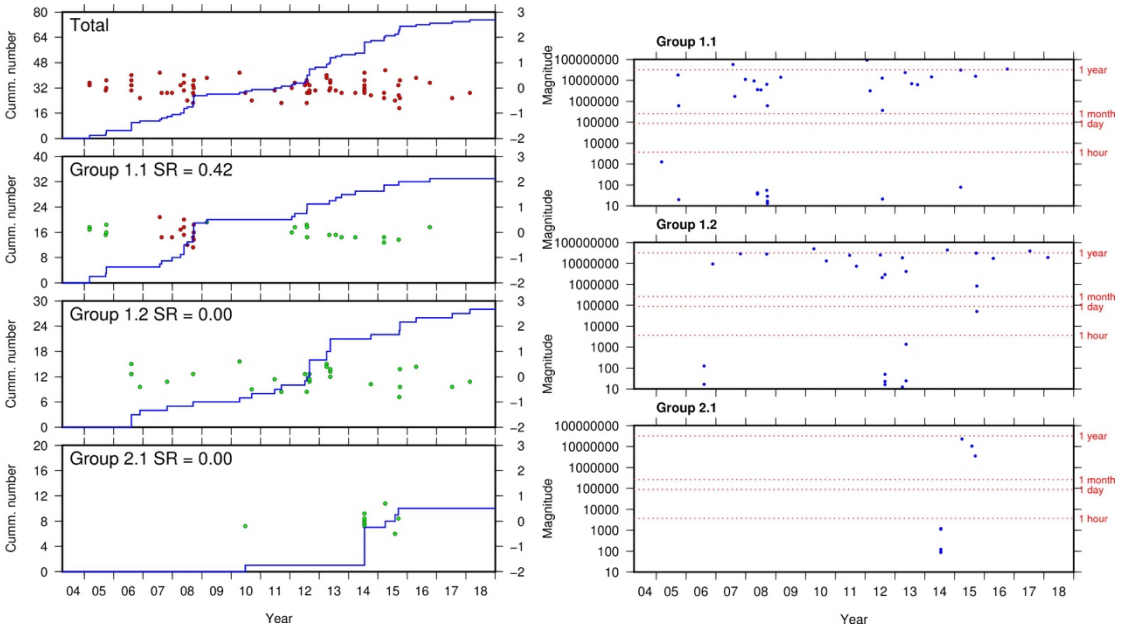

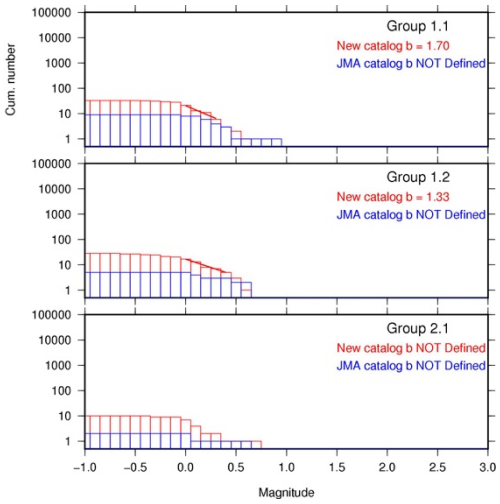

10.1.32. Hiuchigatake

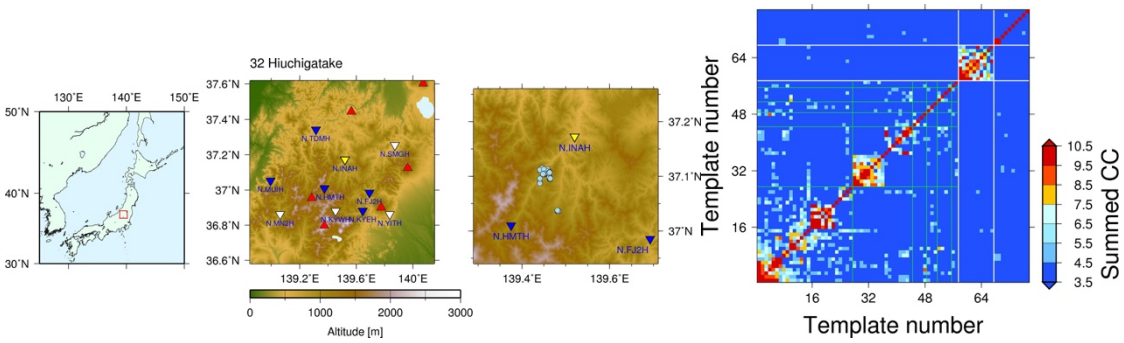

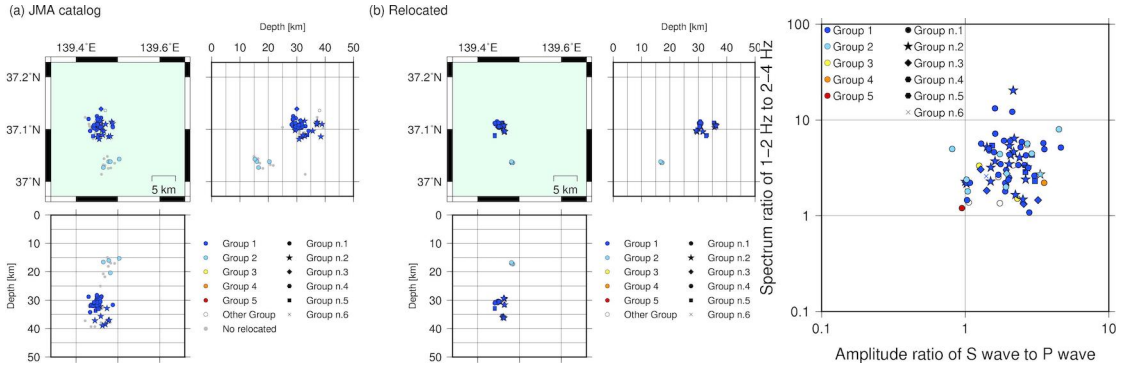

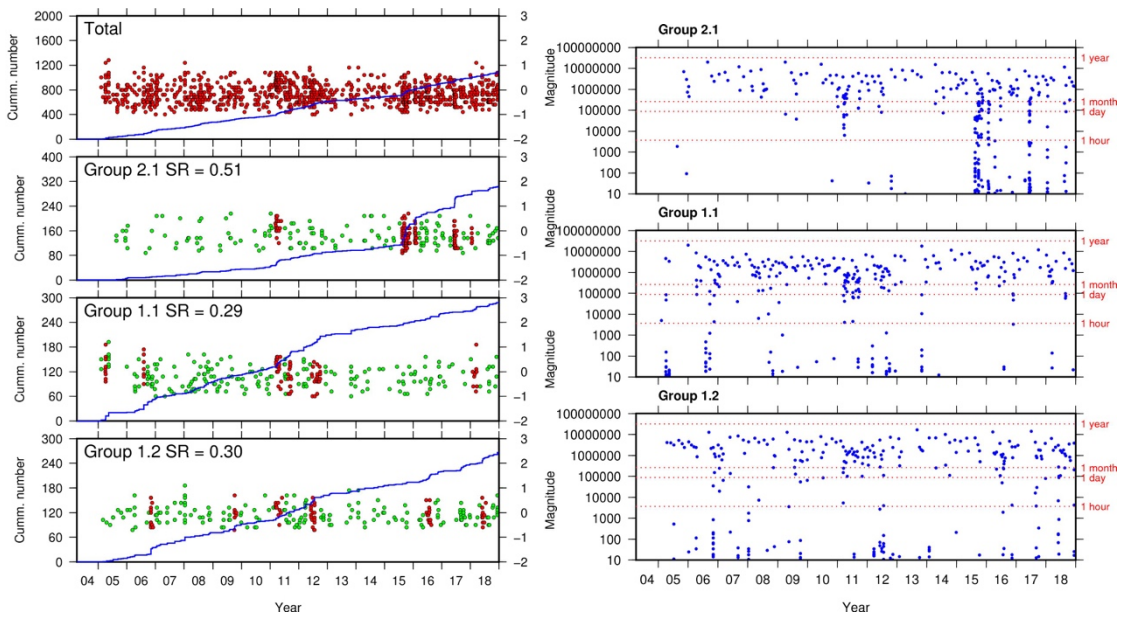

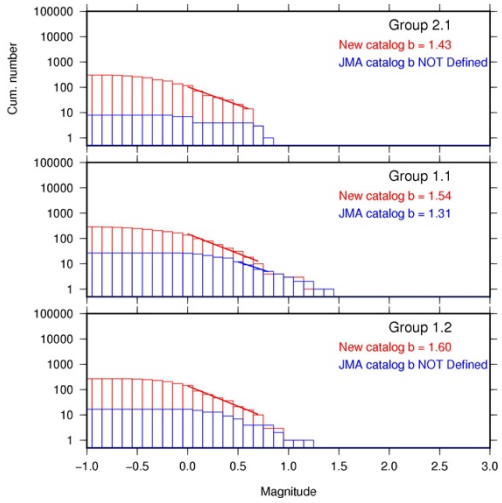

10.1.33. Nasu

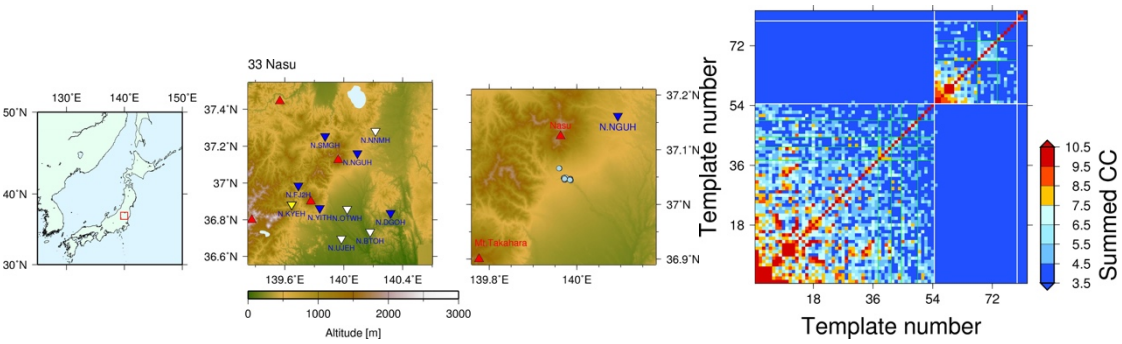
33 Nasu
Altitude [m]
Template number
Summed CC

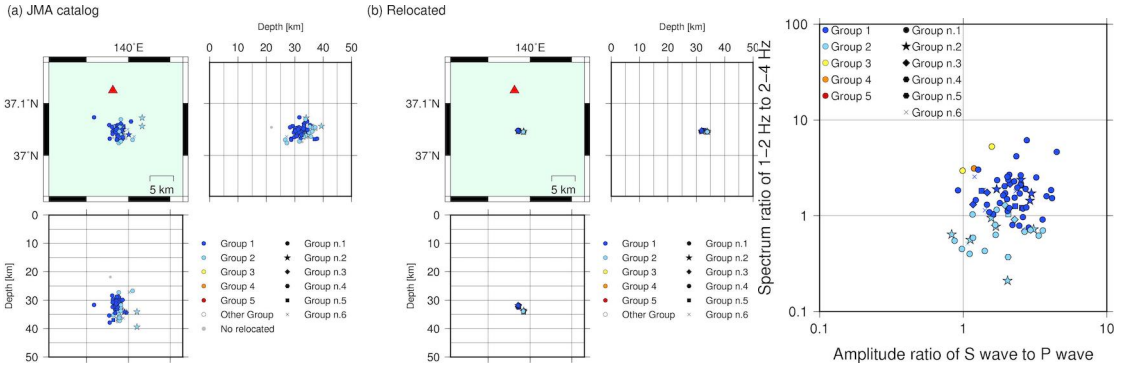
(a) JMA catalog
(b) Relocated
Depth [km]
Group 1
Group 2
Group 3
Group 4
Group 5
Other Group
No relocated
Spectrum ratio of 1–2 Hz to 2–4 Hz
Amplitude ratio of S wave to P wave

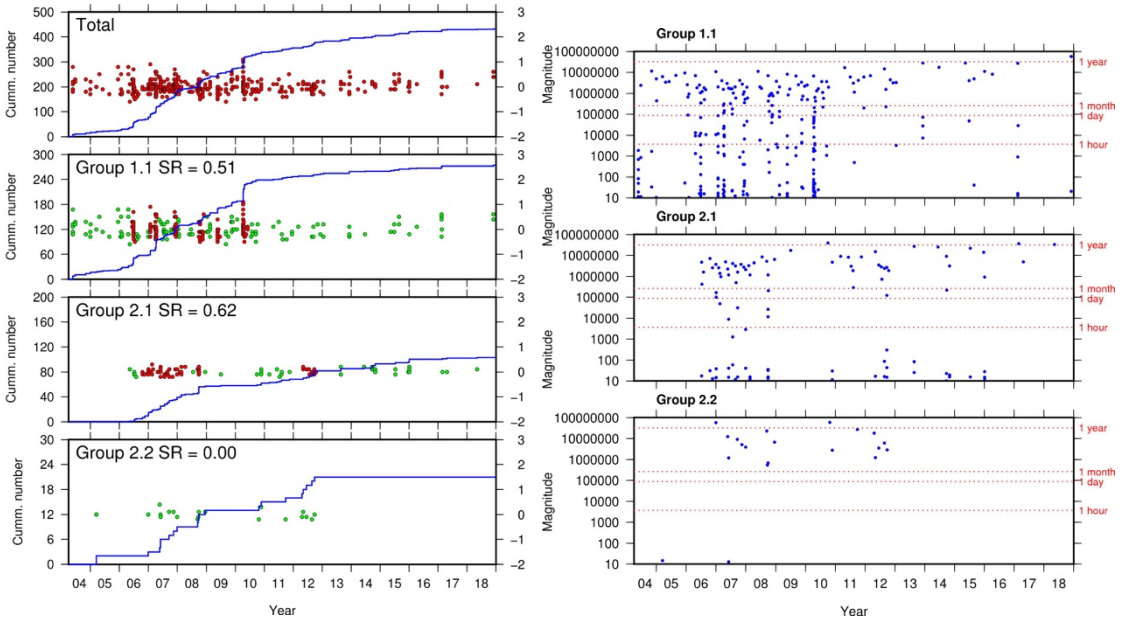
Total
Group 1.1 SR = 0.51
Group 2.1 SR = 0.62
Group 2.2 SR = 0.00
Cumm. number
Year
Group 1.1
Group 2.1
Group 2.2
Magnitude
1 year
1 month
1 day
1 hour

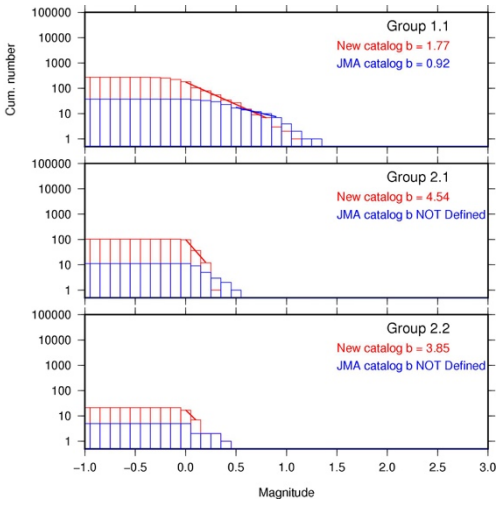
Group 1.1
New catalog b = 1.77
JMA catalog b = 0.92
Group 2.1
New catalog b = 4.54
JMA catalog b NOT Defined
Group 2.2
New catalog b = 3.85
JMA catalog b NOT Defined
Cum. number
Magnitude

10.1.34. Mt.Takahara

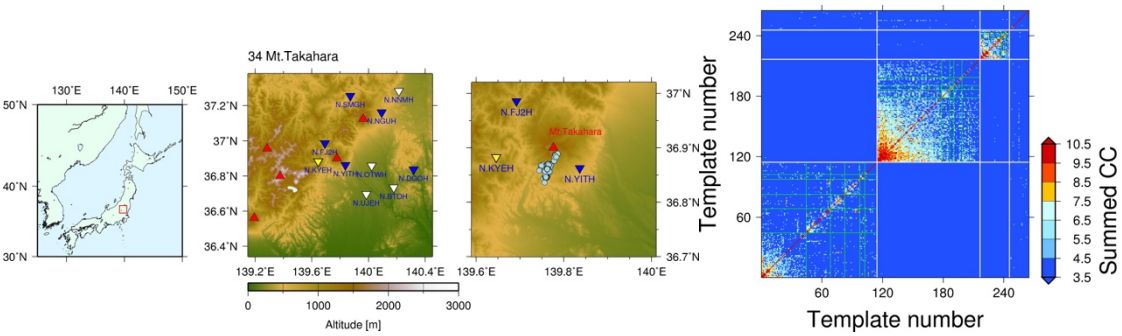

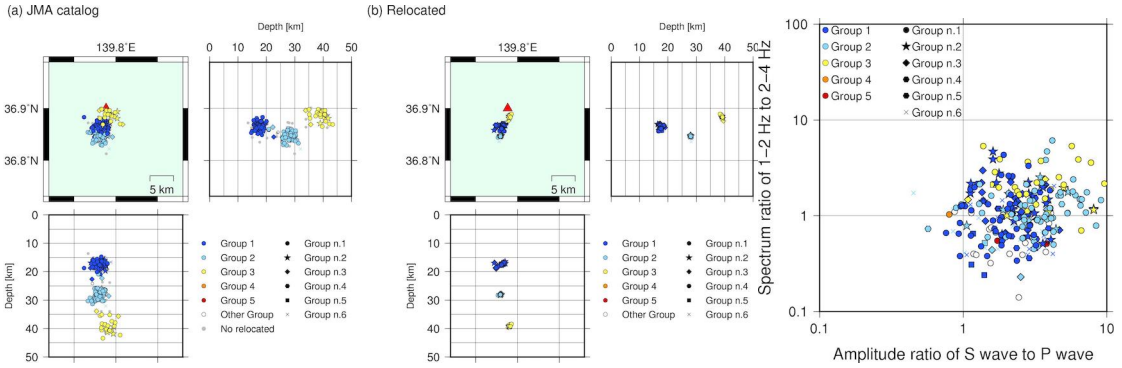

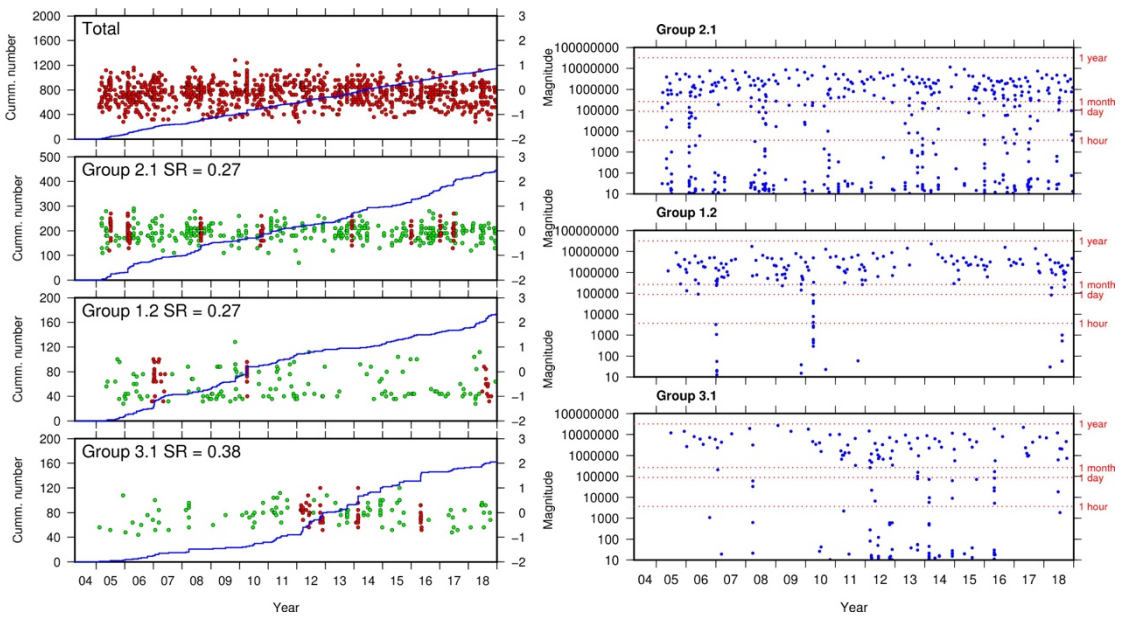

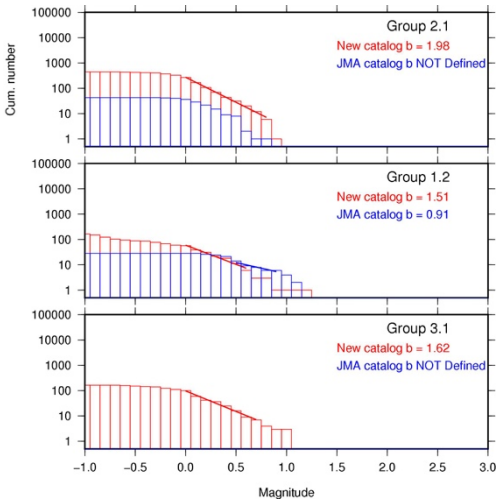

10.1.35. Nikko

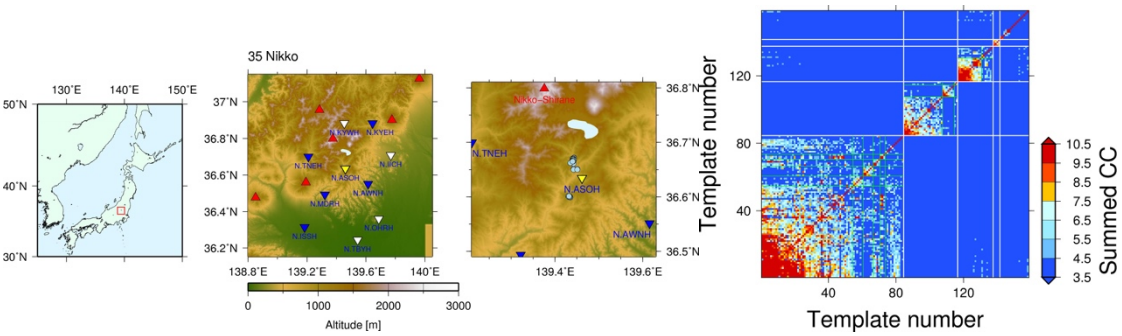
35 Nikko
Altitude [m]
Template number
Summed CC

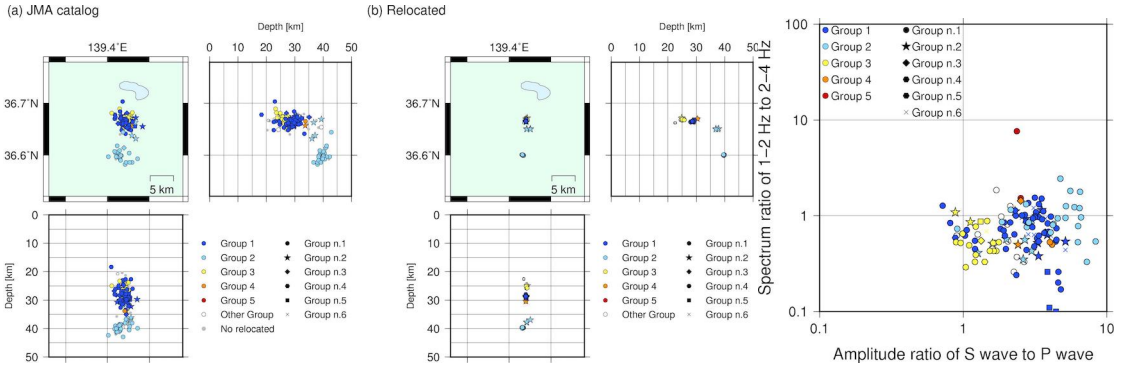
(a) JMA catalog
(b) Relocated
Depth [km]
5 km
Group 1
Group 2
Group 3
Group 4
Group 5
Other Group
No relocated
Group n.1
Group n.2
Group n.3
Group n.4
Group n.5
Group n.6
Spectrum ratio of 1–2 Hz to 2–4 Hz
Amplitude ratio of S wave to P wave

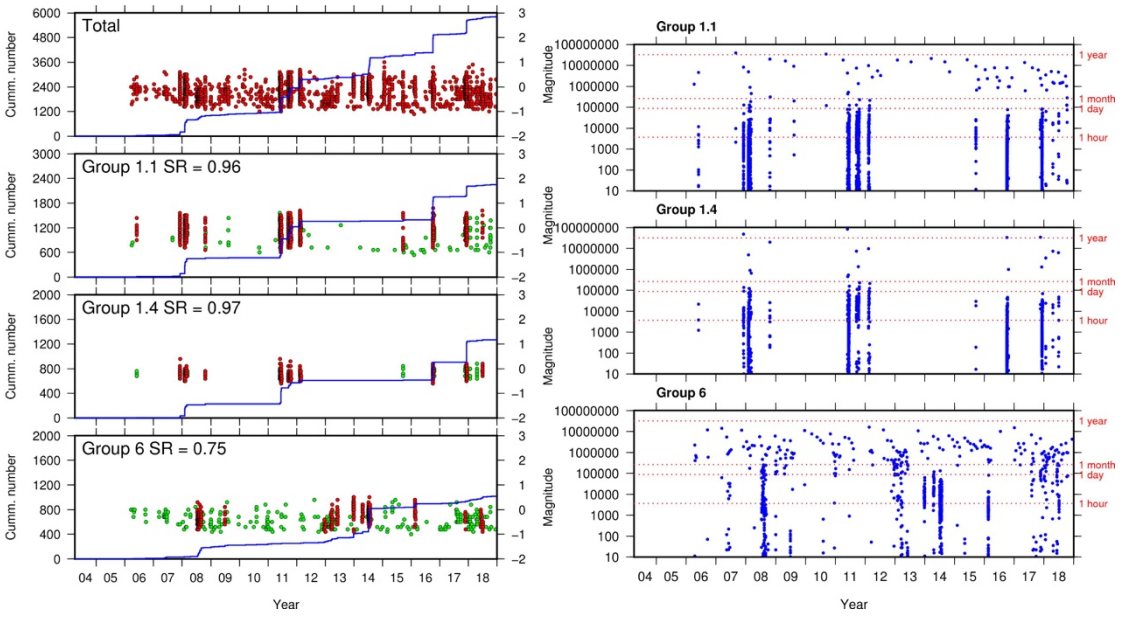
Total
Group 1.1 SR = 0.96
Group 1.4 SR = 0.97
Group 6 SR = 0.75
Cumm. number
Year
Group 1.1
Group 1.4
Group 6
Magnitude
1 year
1 month
1 day
1 hour

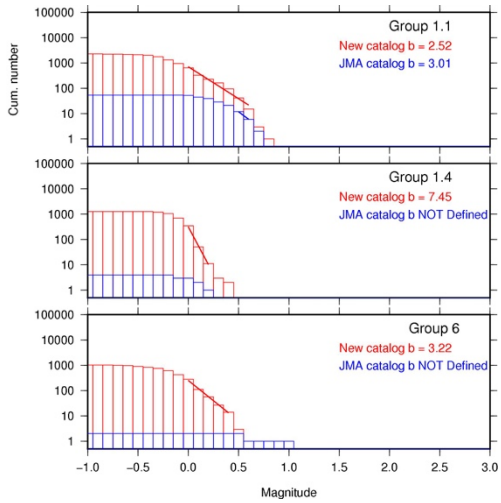
Group 1.1
New catalog b = 2.52
JMA catalog b = 3.01
Group 1.4
New catalog b = 7.45
JMA catalog b NOT Defined
Group 6
New catalog b = 3.22
JMA catalog b NOT Defined
Cum. number
Magnitude

10.1.36. Kusatsu-Shirane

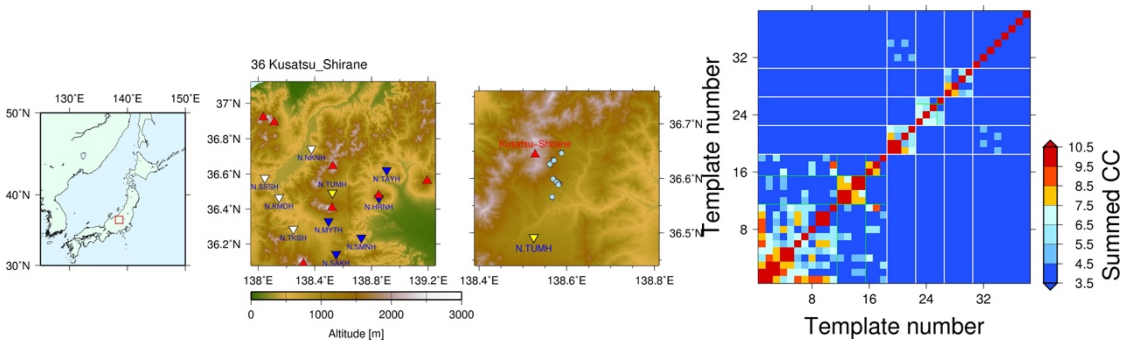

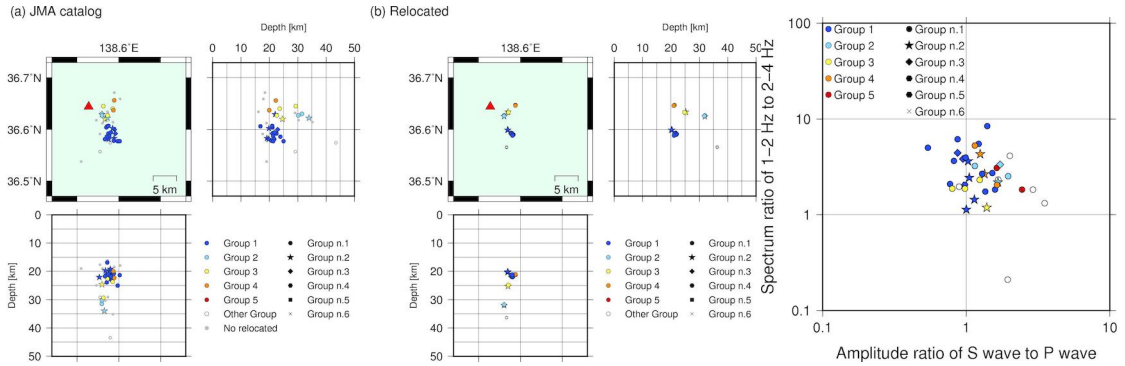

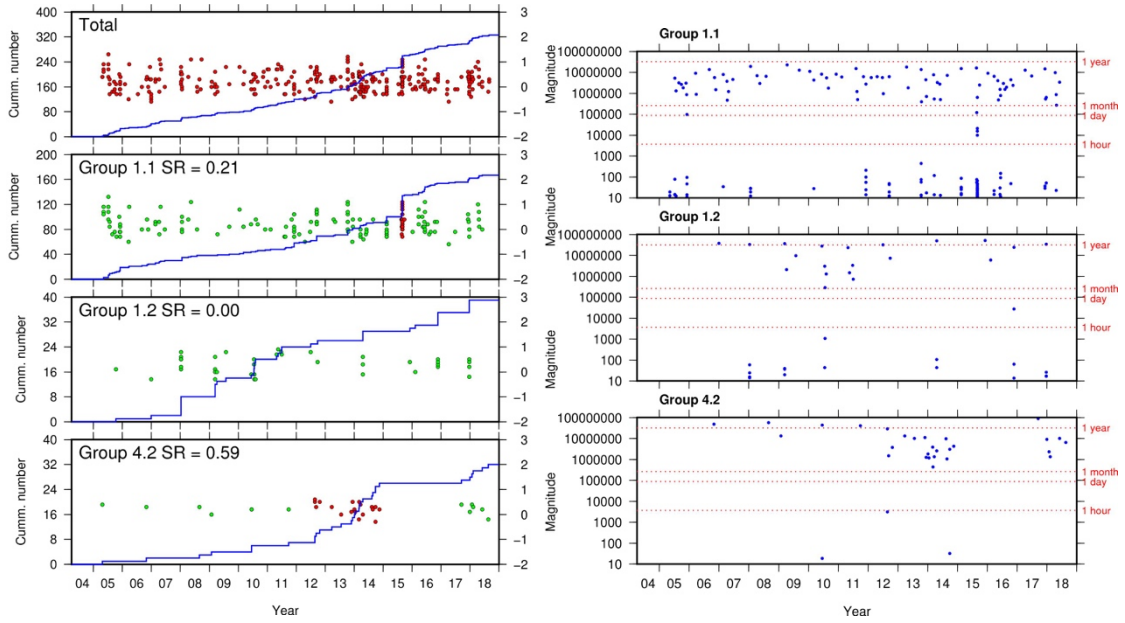

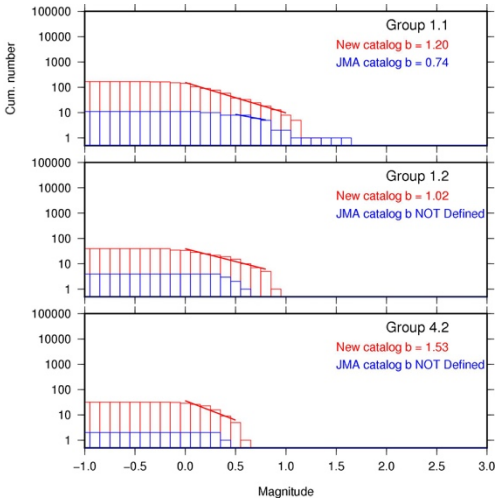

10.1.37. Hakone

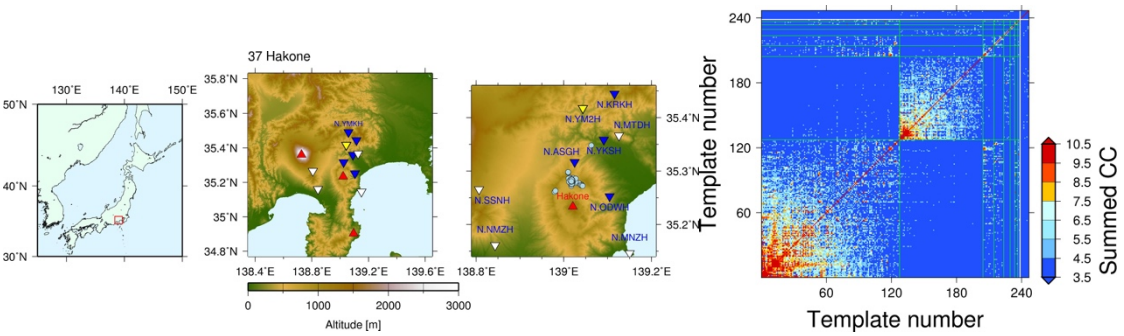

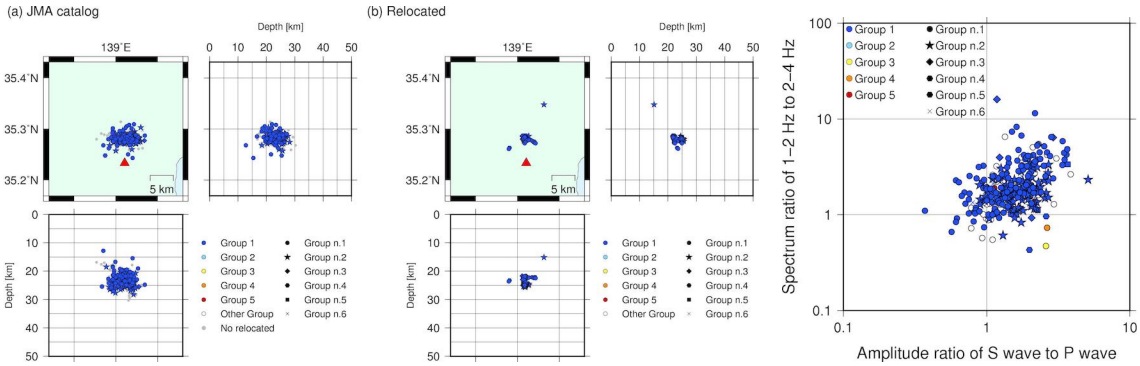

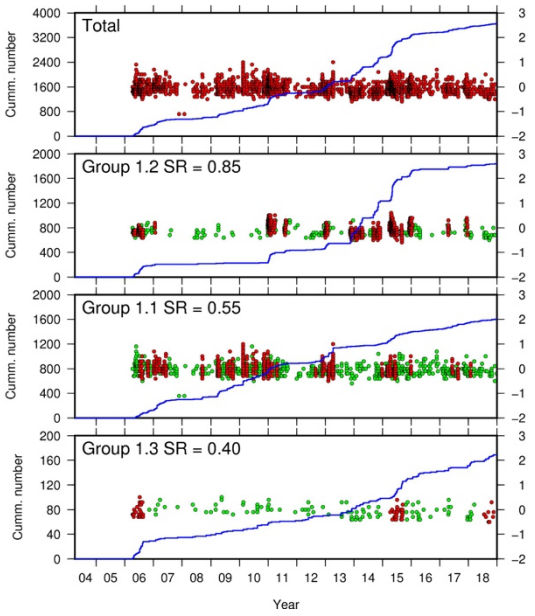

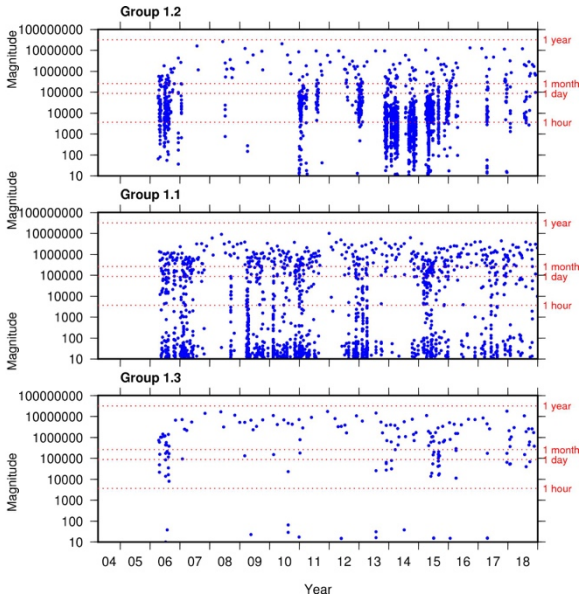

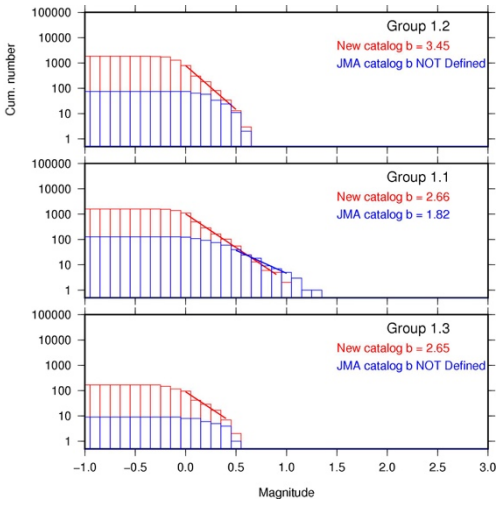

10.1.38. Fuji

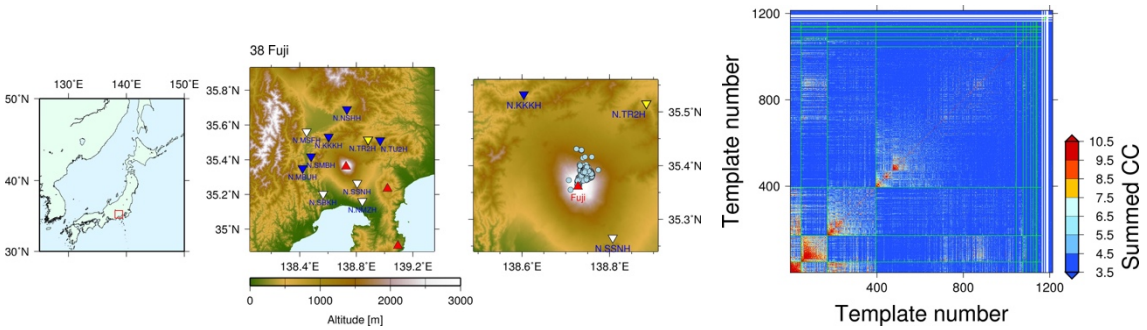
38 Fuji
Altitude [m]
Template number
Summed CC

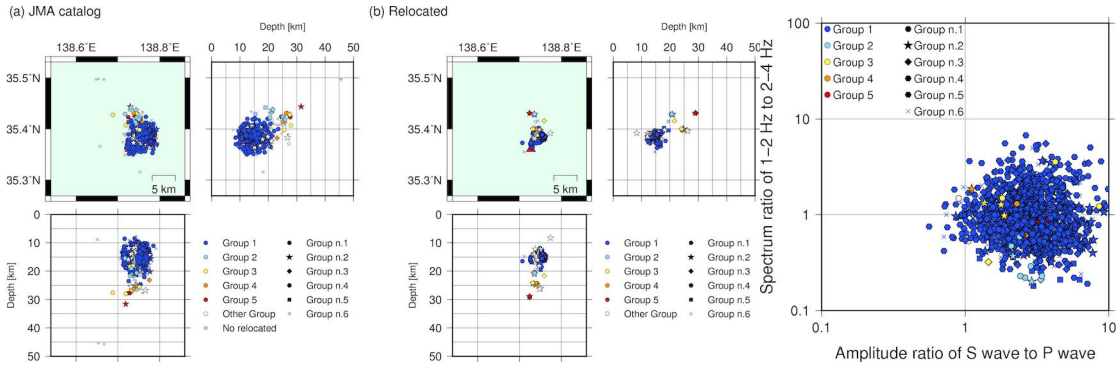
(a) JMA catalog
(b) Relocated
Depth [km]
Group 1
Group 2
Group 3
Group 4
Group 5
Other Group
No relocated
Spectrum ratio of 1–2 Hz to 2–4 Hz
Amplitude ratio of S wave to P wave

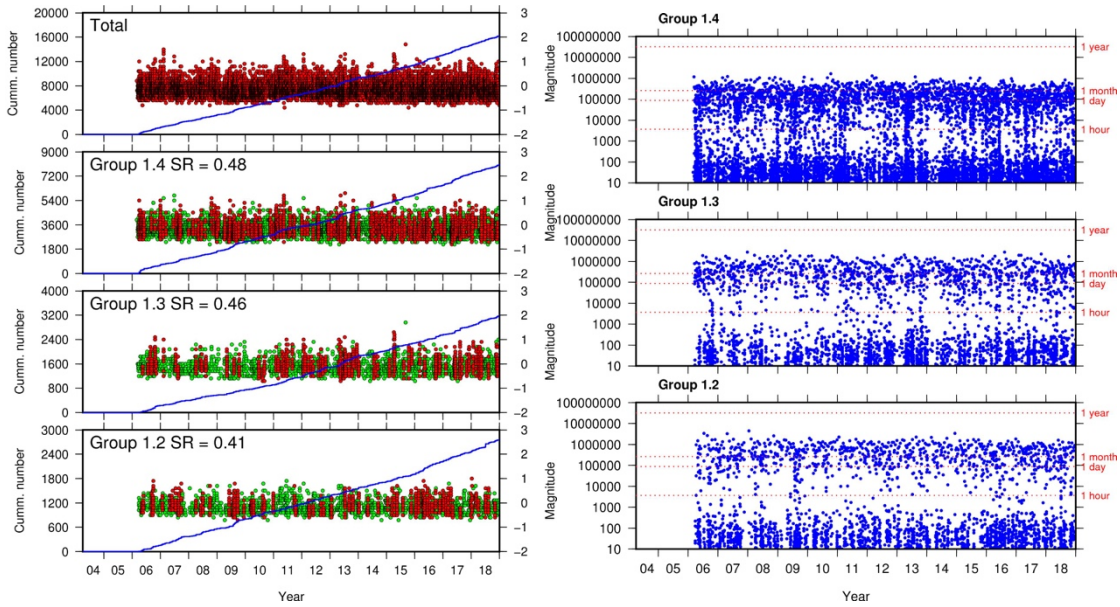
Total
Group 1.4 SR = 0.48
Group 1.3 SR = 0.46
Group 1.2 SR = 0.41
Cumm. number
Year
Group 1.4
Group 1.3
Group 1.2
Magnitude
1 year
1 month
1 day
1 hour

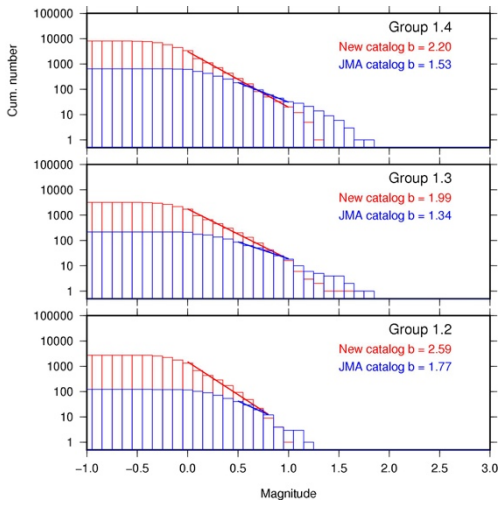
Group 1.4
New catalog b = 2.20
JMA catalog b = 1.53
Group 1.3
New catalog b = 1.99
JMA catalog b = 1.34
Group 1.2
New catalog b = 2.59
JMA catalog b = 1.77
Cum. number
Magnitude

10.1.39. Myoko

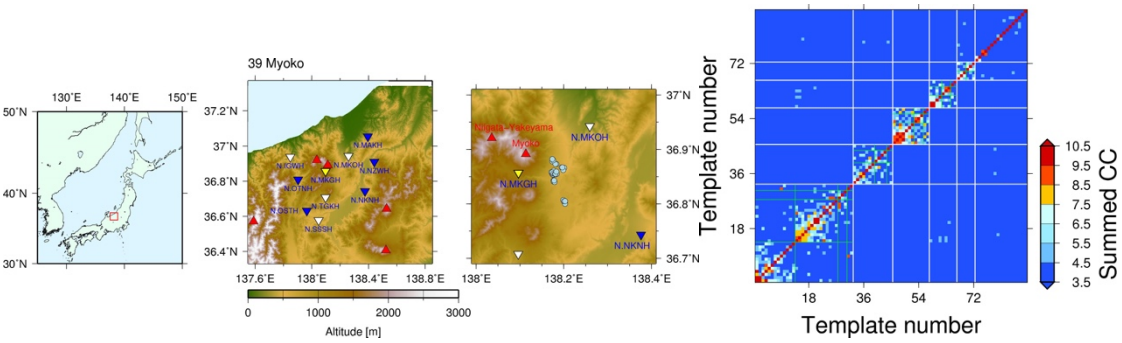
39 Myoko
Altitude [m]
Template number
Summed CC

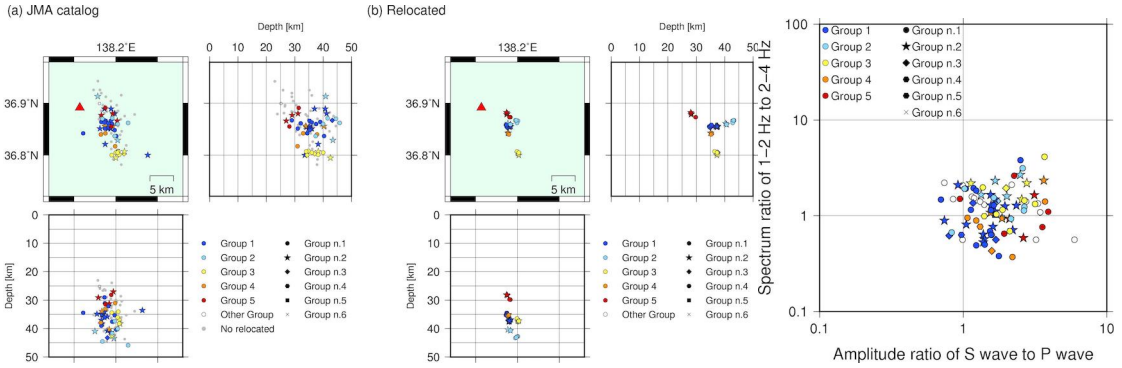
(a) JMA catalog
(b) Relocated
Depth [km]
5 km
Group 1
Group 2
Group 3
Group 4
Group 5
Other Group
No relocated
Group n.1
Group n.2
Group n.3
Group n.4
Group n.5
Group n.6
Spectrum ratio of 1–2 Hz to 2–4 Hz
Amplitude ratio of S wave to P wave

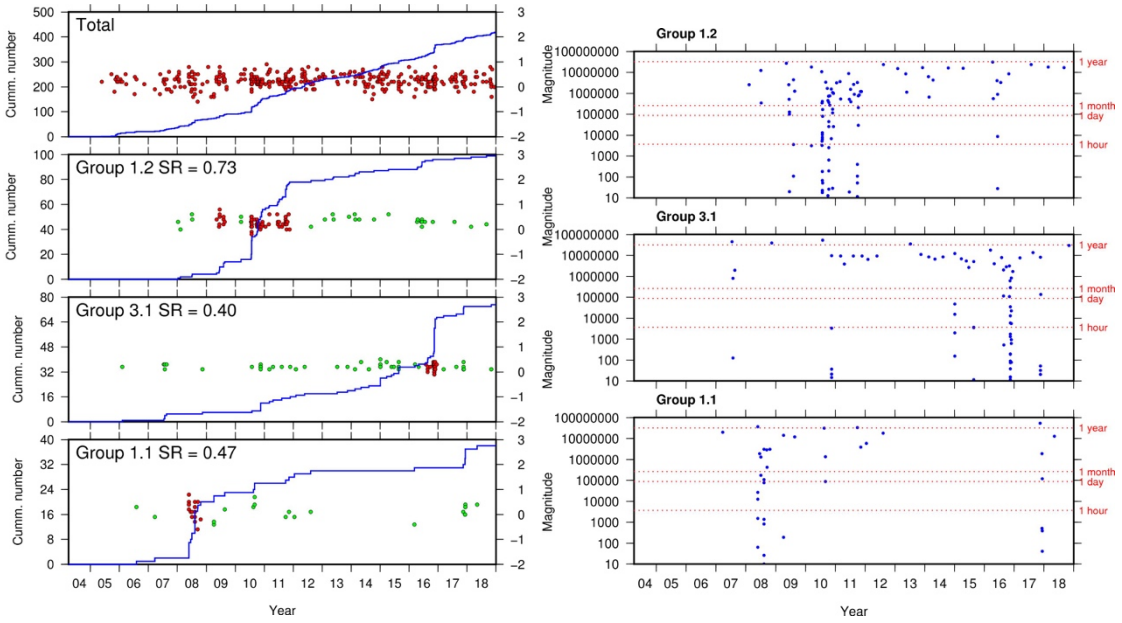
Total
Group 1.2 SR = 0.73
Group 3.1 SR = 0.40
Group 1.1 SR = 0.47
Cumm. number
Year
Group 1.2
Group 3.1
Group 1.1
Magnitude
1 year
1 month
1 day
1 hour

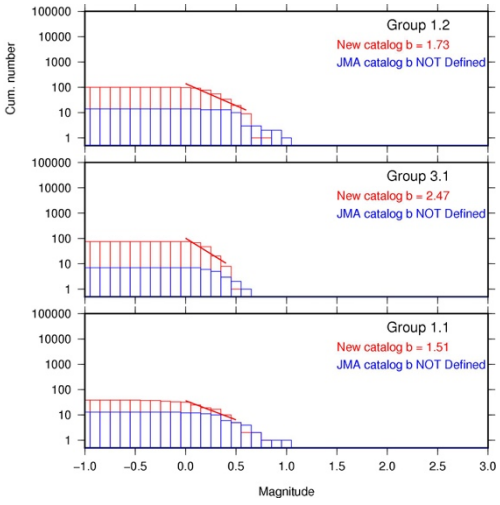
Group 1.2
New catalog b = 1.73
JMA catalog b NOT Defined
Group 3.1
New catalog b = 2.47
JMA catalog b NOT Defined
Group 1.1
New catalog b = 1.51
JMA catalog b NOT Defined
Cum. number
Magnitude

10.1.40. Shirouma

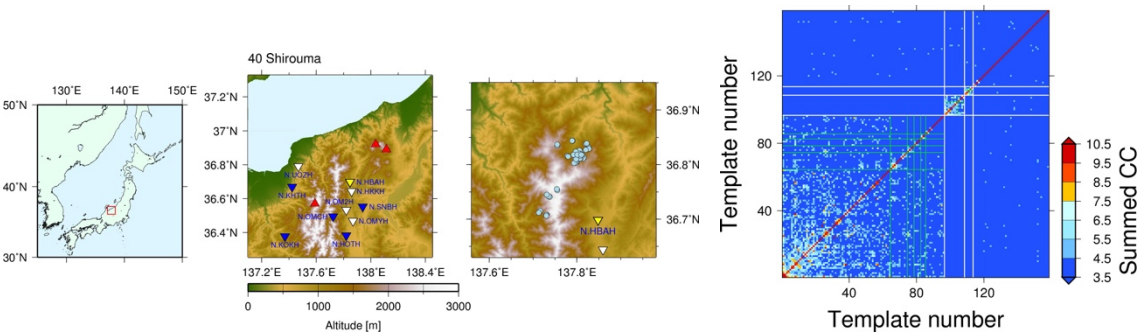

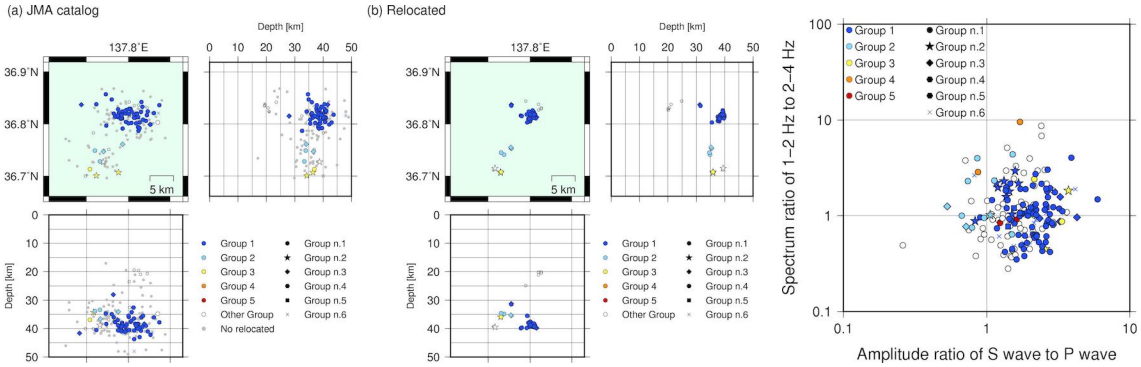

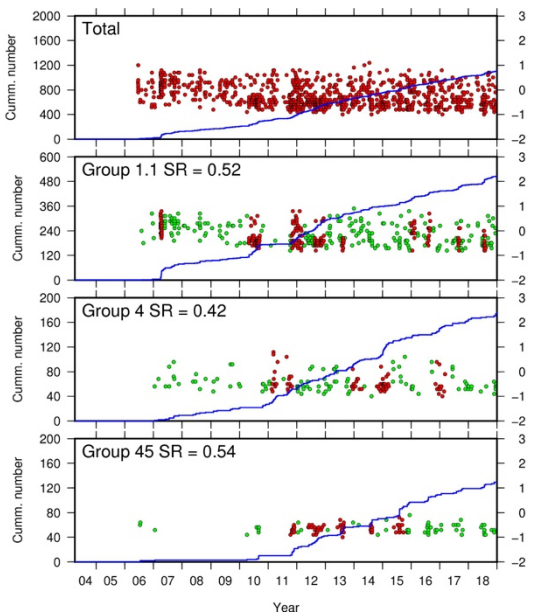

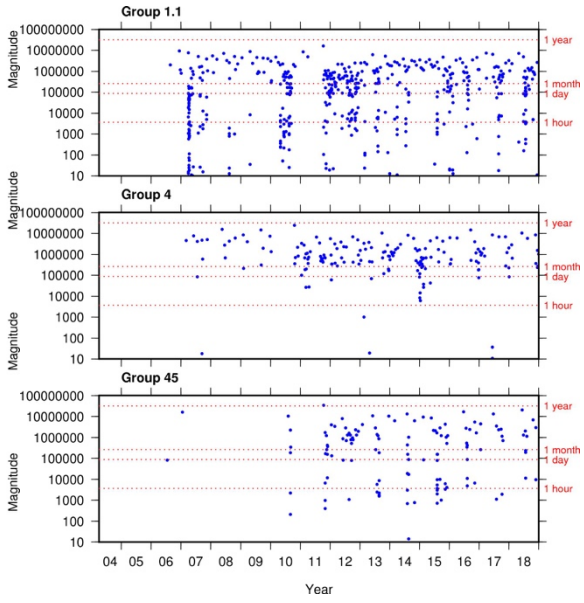

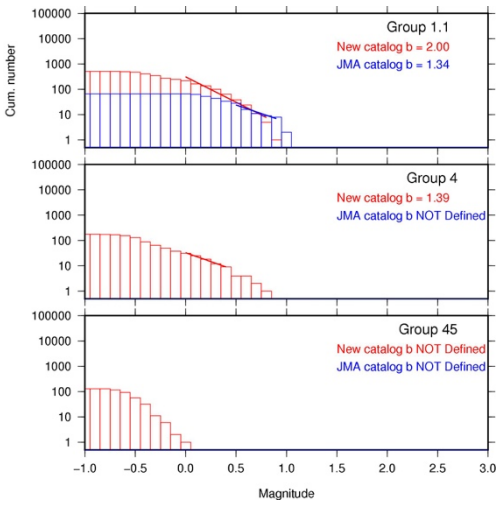

10.1.41. Tateyama

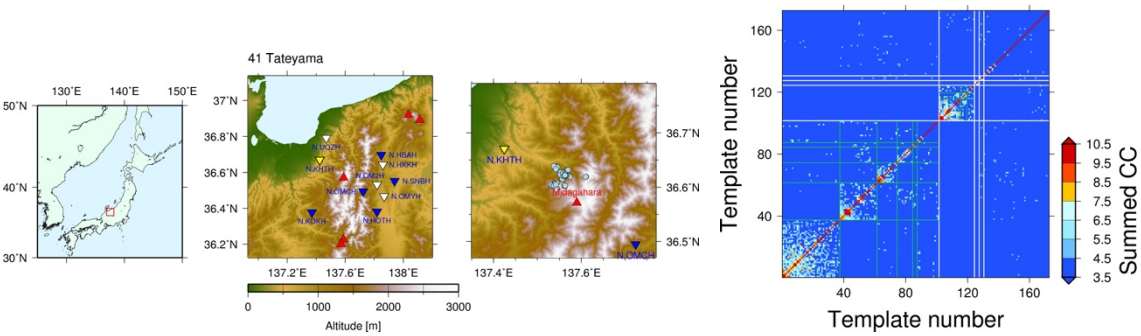

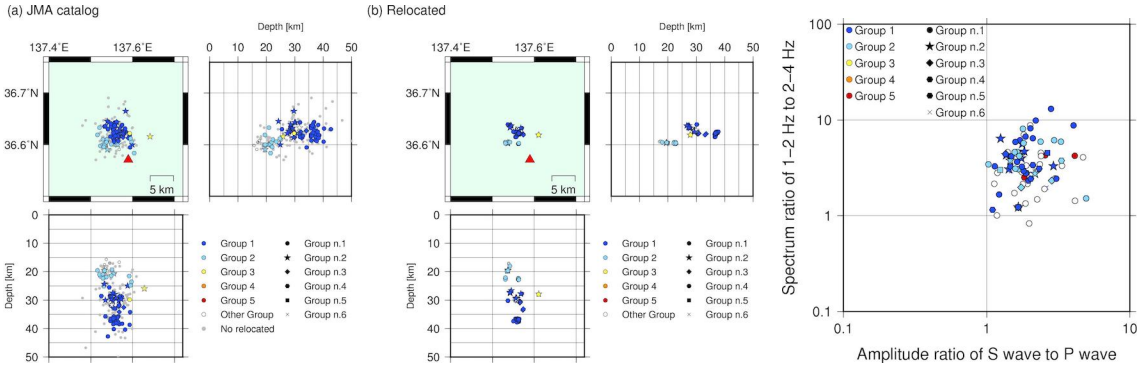

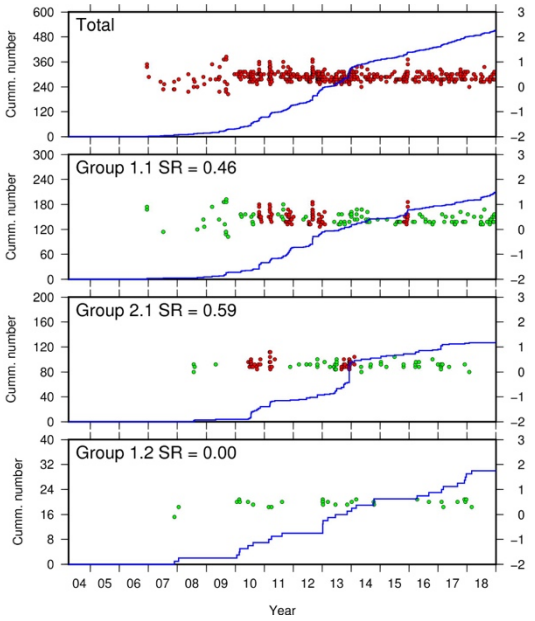

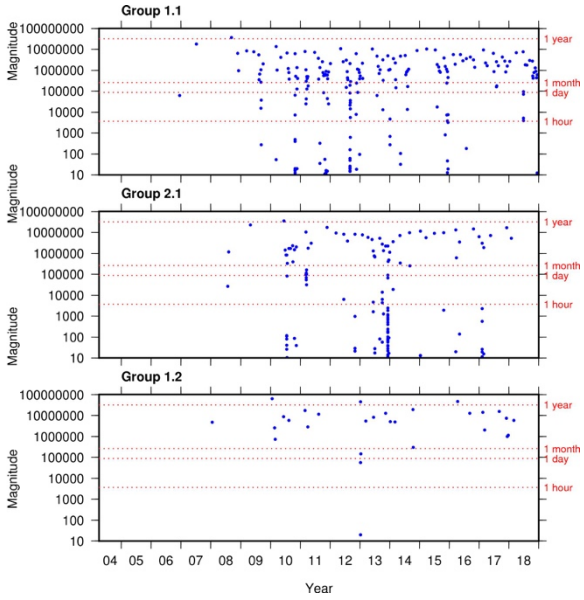

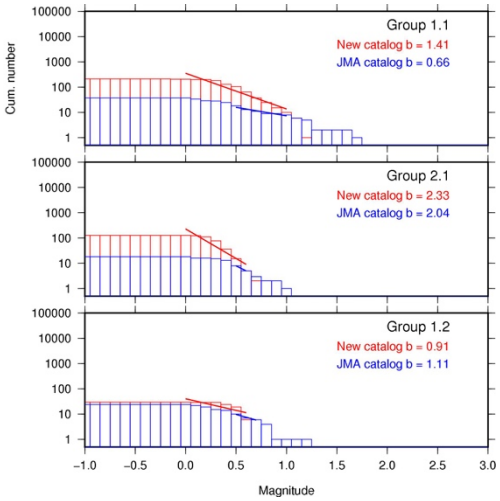

10.1.42. Washiba-Kumonotaira

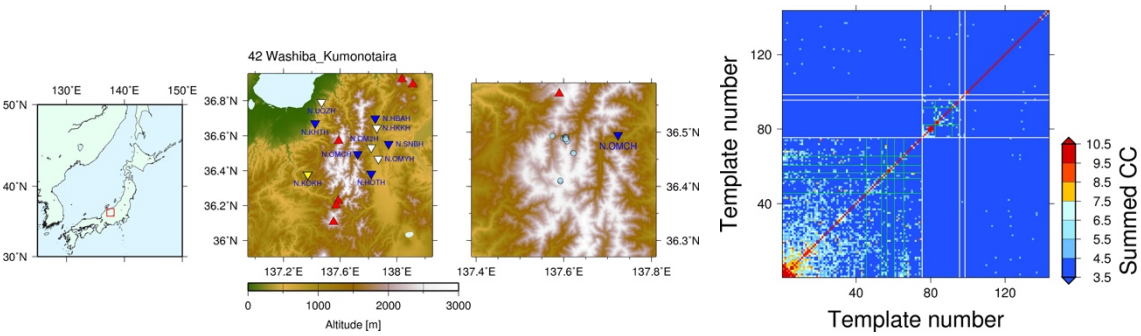

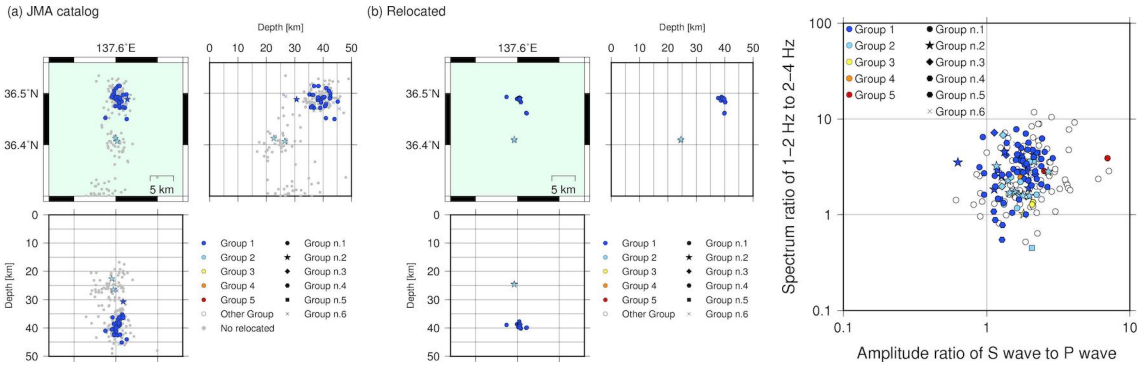

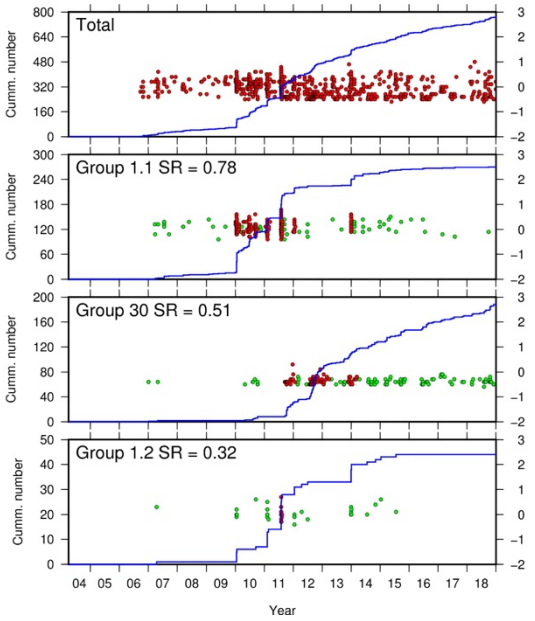

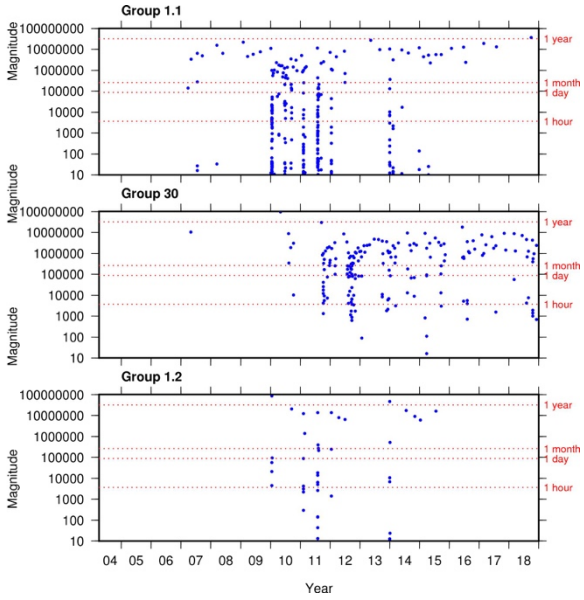

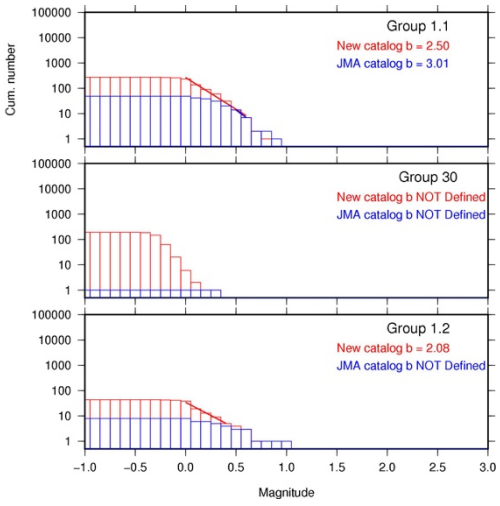

10.1.43. Yakedake

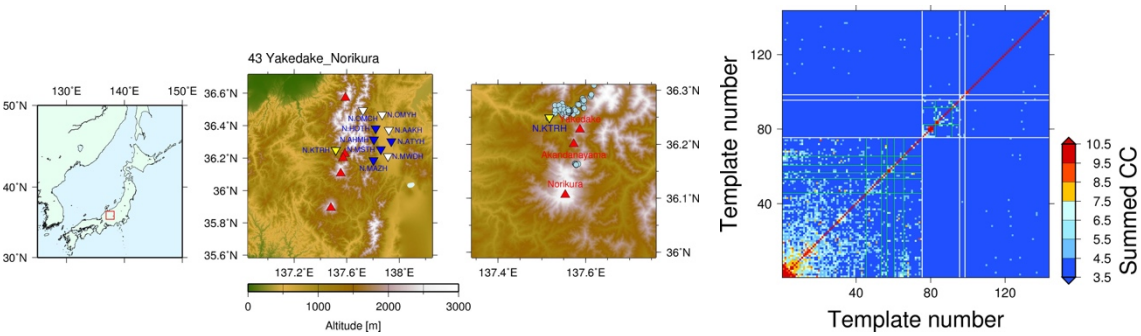

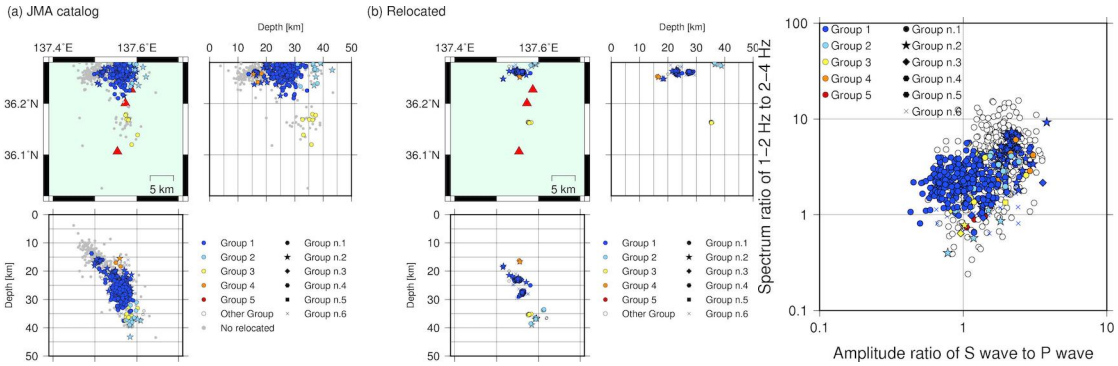

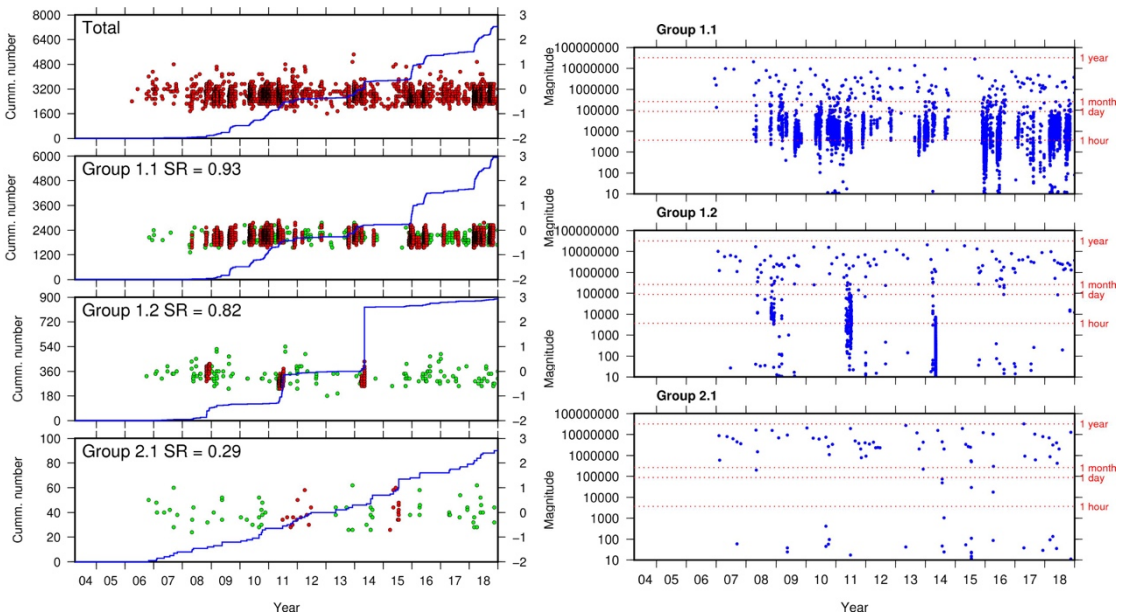

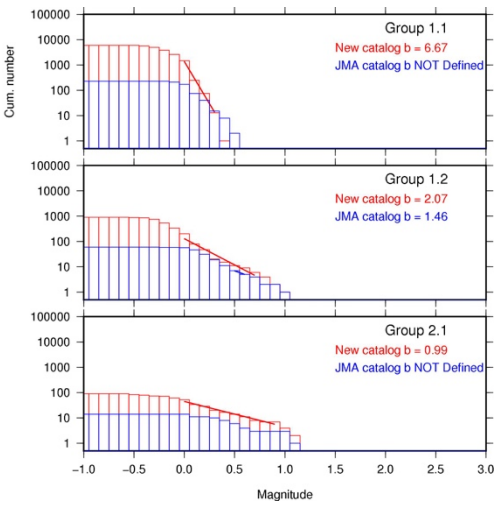

10.1.44. Ontake

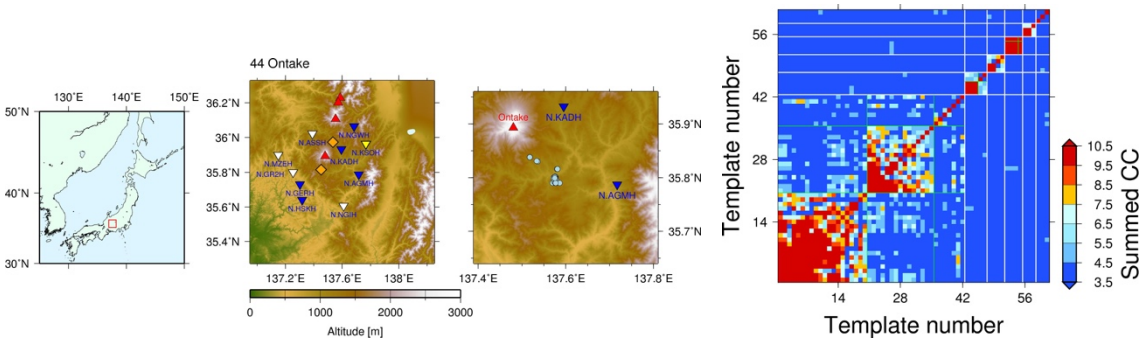

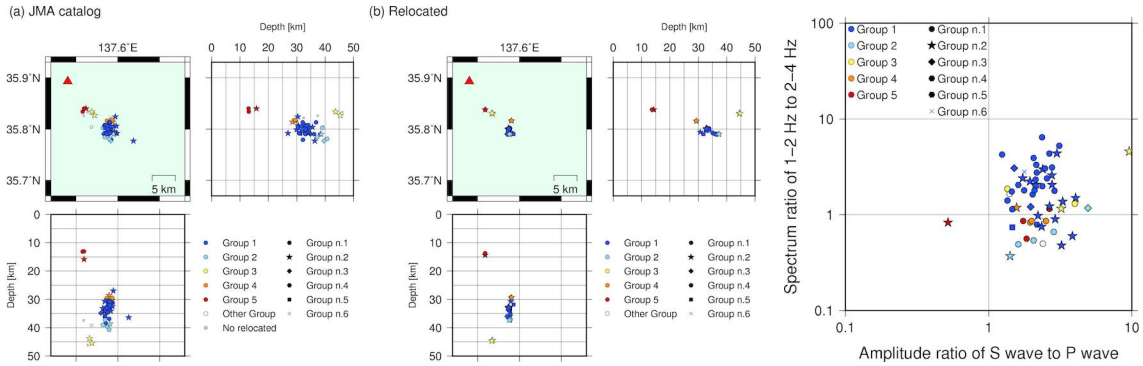

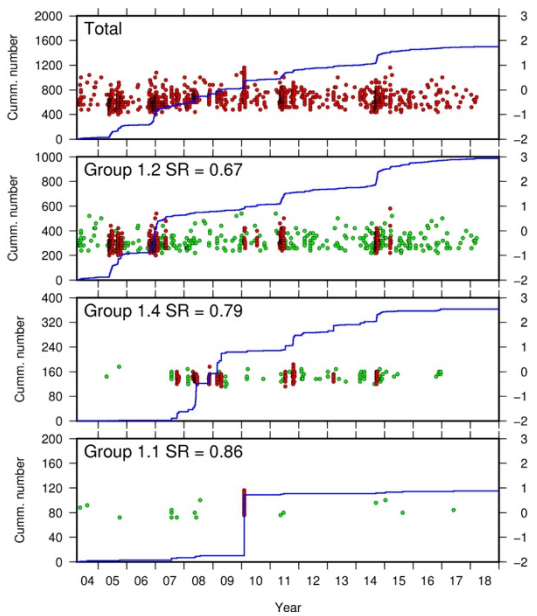

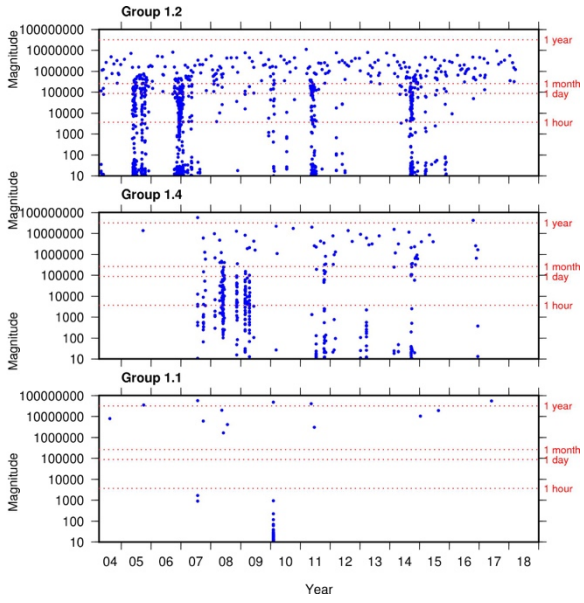

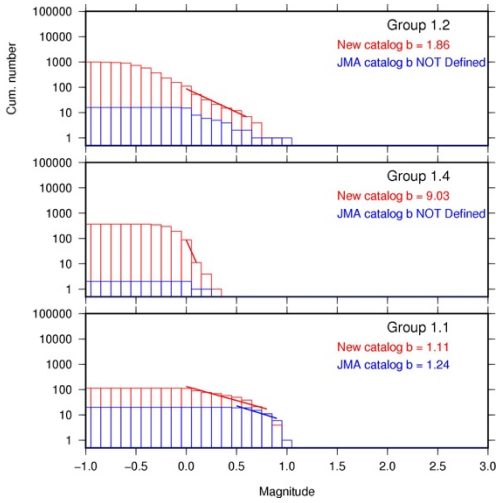

10.1.45. Tanba

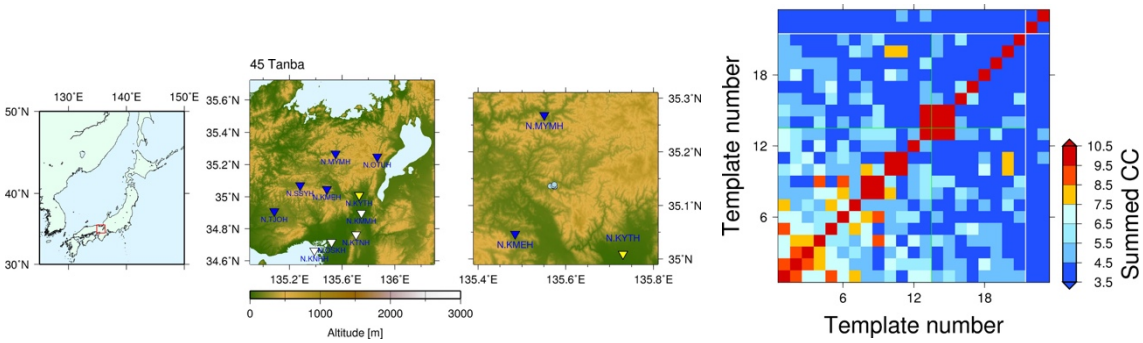
45 Tanba
Altitude [m]
Template number
Summed CC

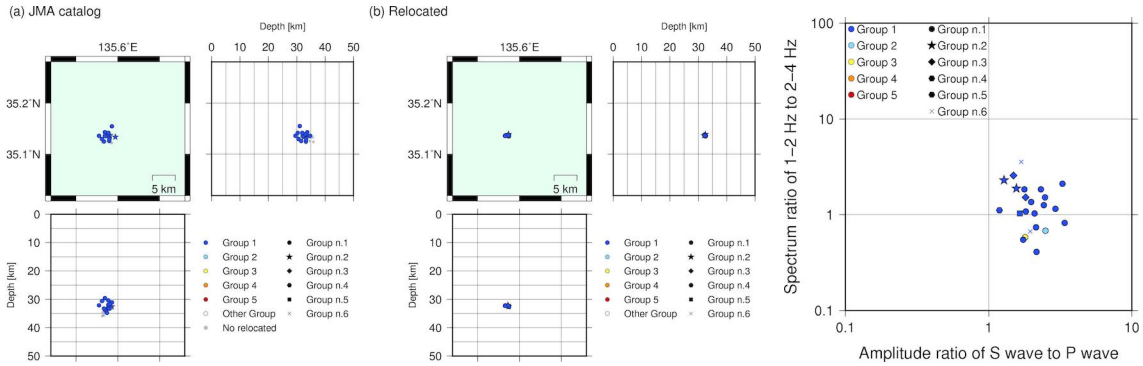
(a) JMA catalog
(b) Relocated
Depth [km]
5 km
Group 1
Group 2
Group 3
Group 4
Group 5
Other Group
No relocated
Group n.1
Group n.2
Group n.3
Group n.4
Group n.5
Group n.6
Spectrum ratio of 1–2 Hz to 2–4 Hz
Amplitude ratio of S wave to P wave

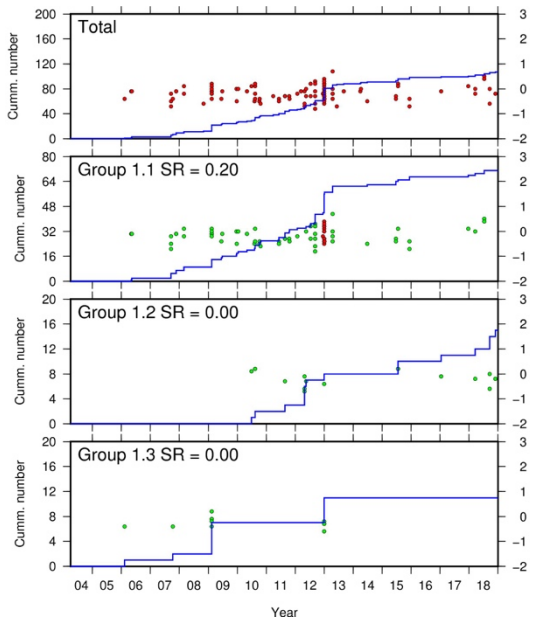
Total
Group 1.1 SR = 0.20
Group 1.2 SR = 0.00
Group 1.3 SR = 0.00
Cumm. number
Year

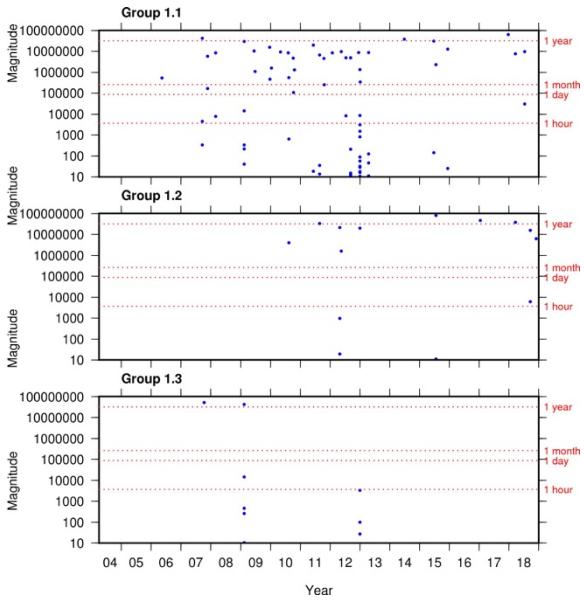
Group 1.1
Group 1.2
Group 1.3
Magnitude
1 year
1 month
1 day
1 hour
Year

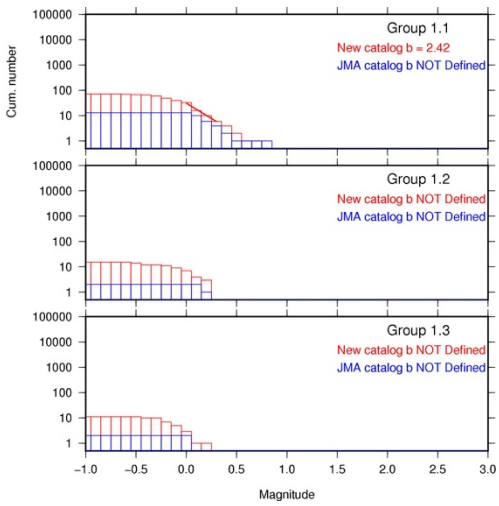
Group 1.1
New catalog b = 2.42
JMA catalog b NOT Defined
Group 1.2
New catalog b NOT Defined
JMA catalog b NOT Defined
Group 1.3
New catalog b NOT Defined
JMA catalog b NOT Defined
Cum. number
Magnitude

10.1.46. East-Shimane

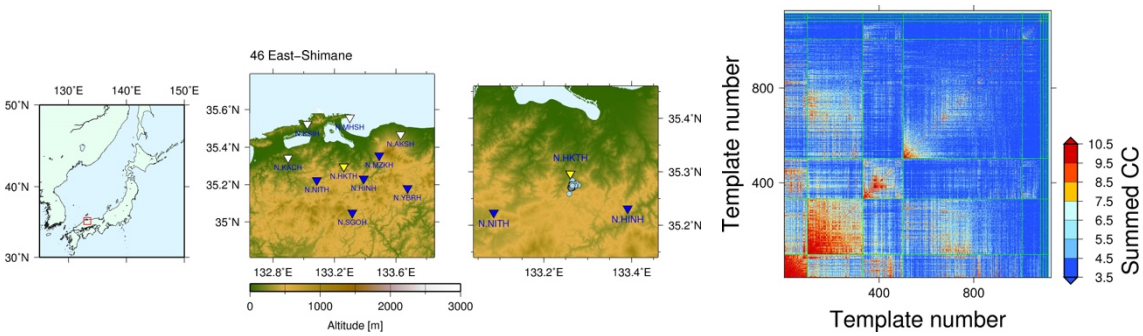

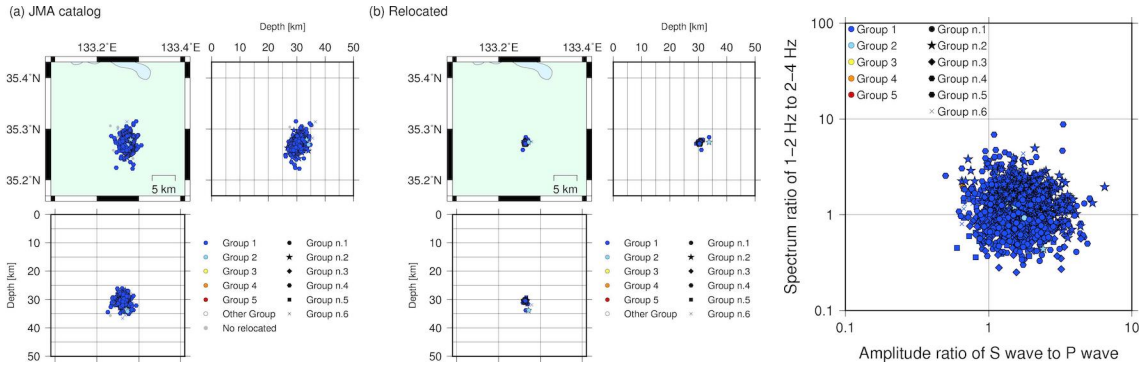

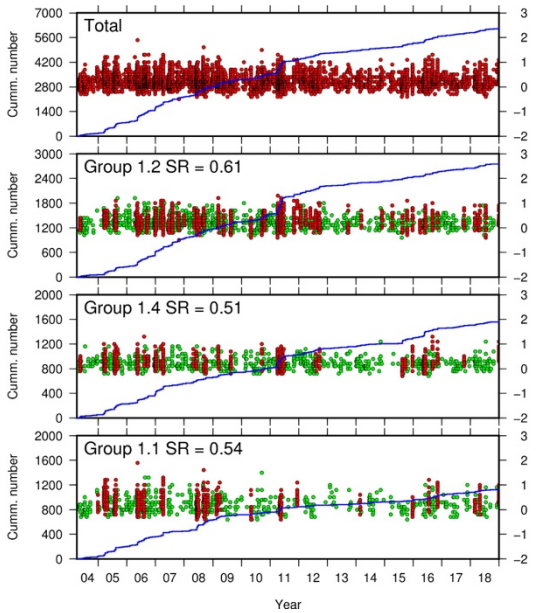

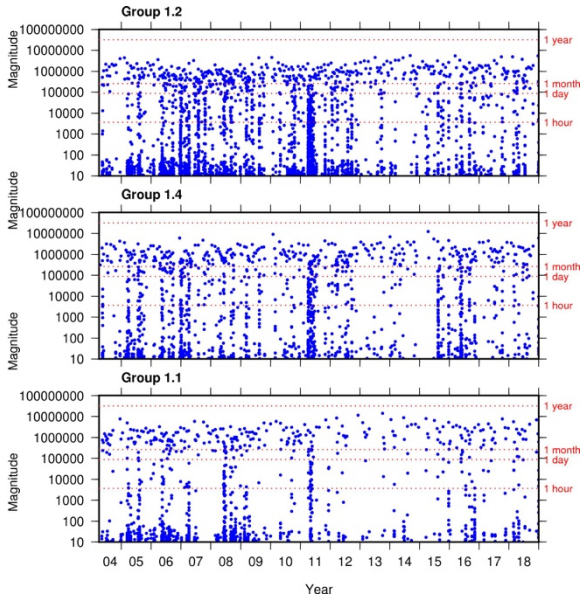

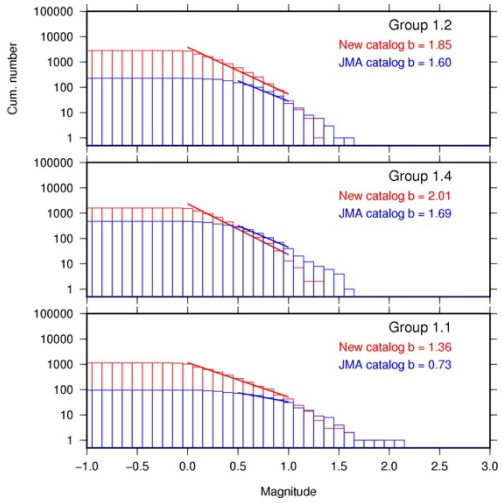

10.1.47. Beppu

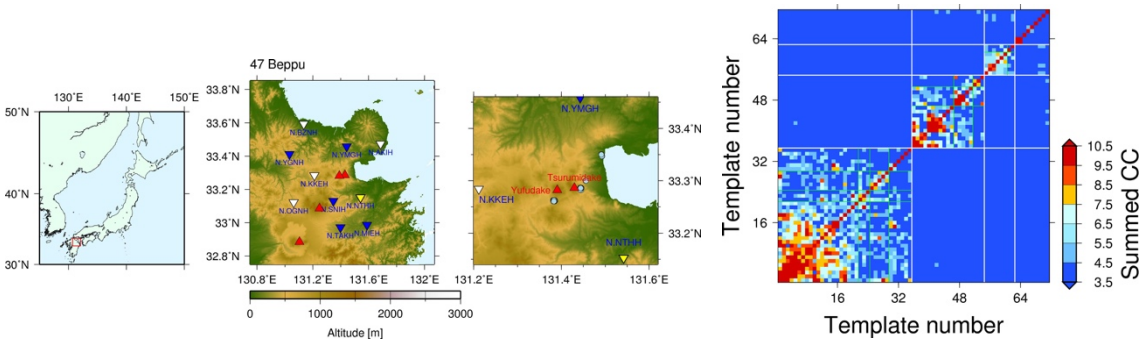
47 Beppu
Altitude [m]
Template number
Summed CC

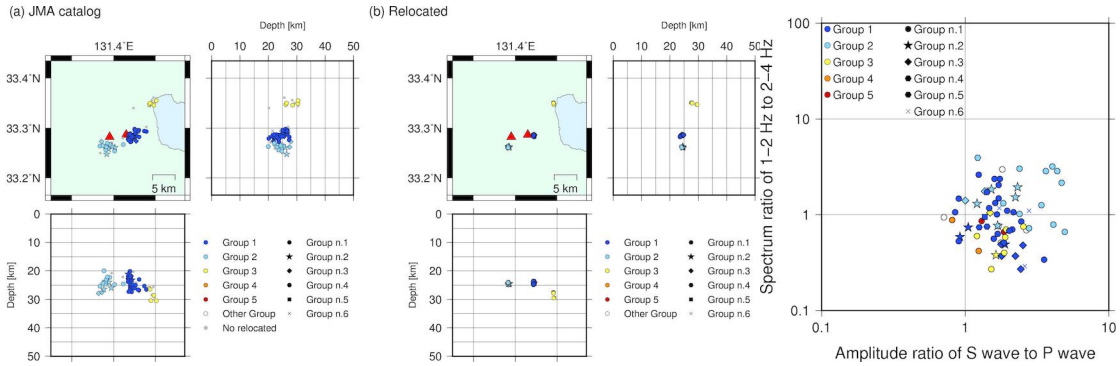
(a) JMA catalog
(b) Relocated
Depth [km]
5 km
Group 1
Group 2
Group 3
Group 4
Group 5
Other Group
No relocated
Group n.1
Group n.2
Group n.3
Group n.4
Group n.5
Group n.6
Spectrum ratio of 1–2 Hz to 2–4 Hz
Amplitude ratio of S wave to P wave

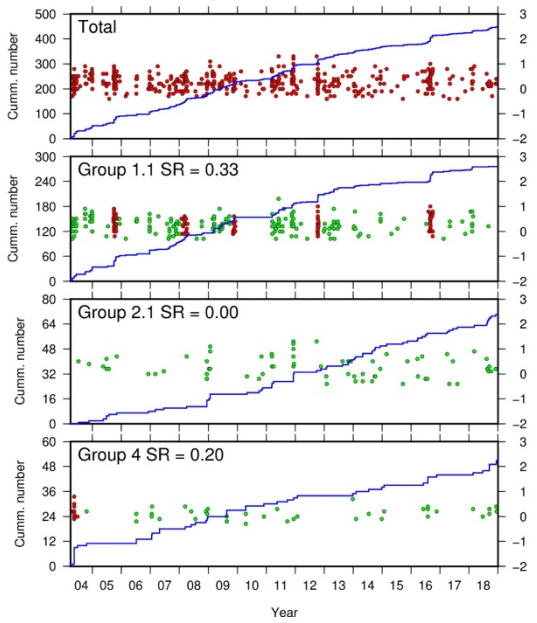
Total
Group 1.1 SR = 0.33
Group 2.1 SR = 0.00
Group 4 SR = 0.20
Cumm. number
Year

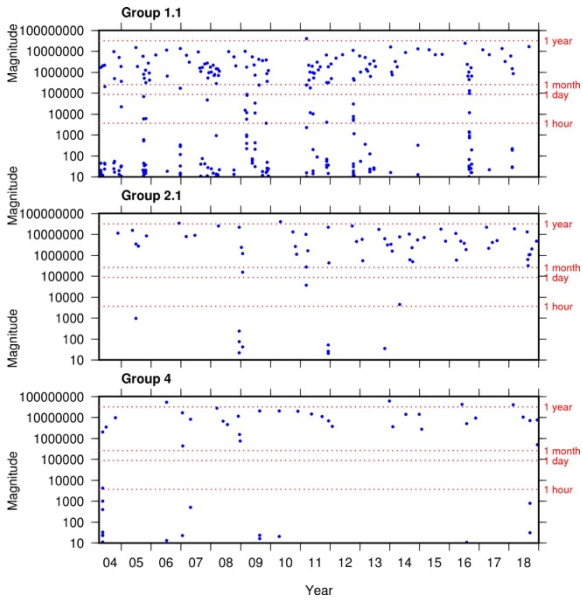
Group 1.1
Group 2.1
Group 4
Magnitude
1 year
1 month
1 day
1 hour
Year

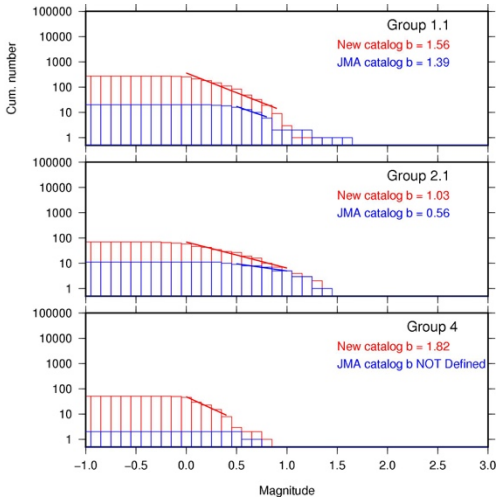
Group 1.1
New catalog b = 1.56
JMA catalog b = 1.39
Group 2.1
New catalog b = 1.03
JMA catalog b = 0.56
Group 4
New catalog b = 1.82
JMA catalog b NOT Defined
Cum. number
Magnitude

10.1.48. Kuju

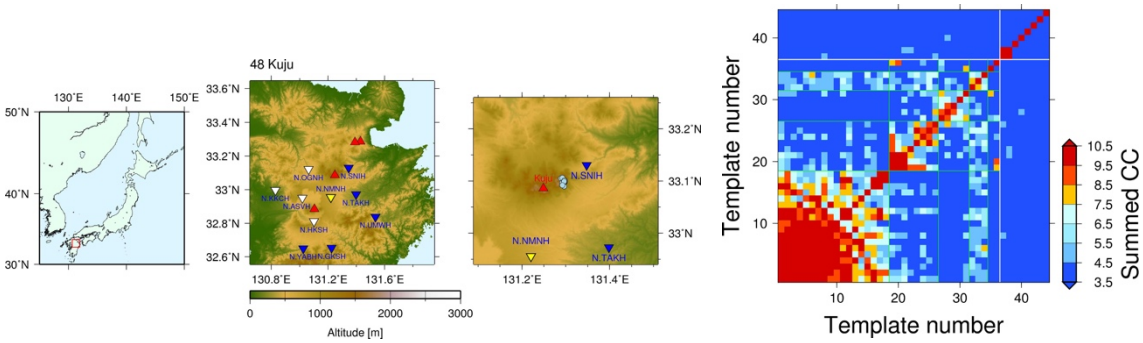
48 Kuju
Kuju
N.SNIH
N.NMNH
N.TAKH
Altitude [m]
Template number
Summed CC

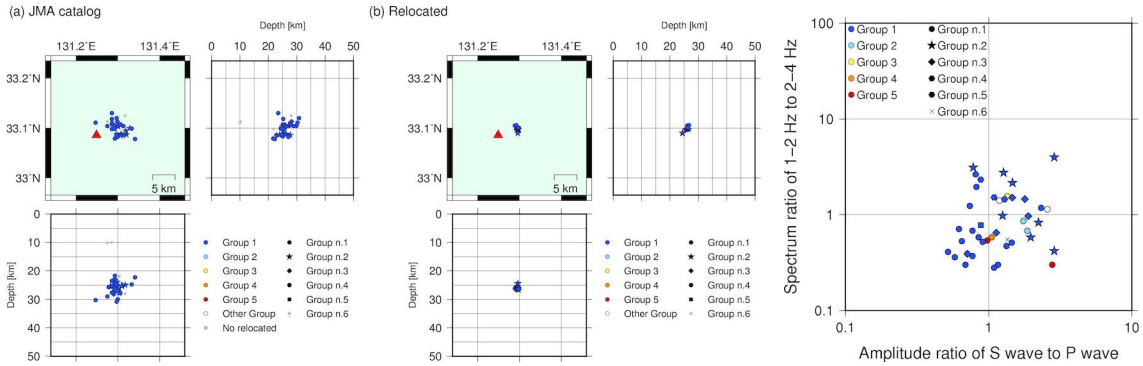
(a) JMA catalog
(b) Relocated
Depth [km]
5 km
Group 1
Group 2
Group 3
Group 4
Group 5
Other Group
No relocated
Group n.1
Group n.2
Group n.3
Group n.4
Group n.5
Group n.6
Spectrum ratio of 1–2 Hz to 2–4 Hz
Amplitude ratio of S wave to P wave

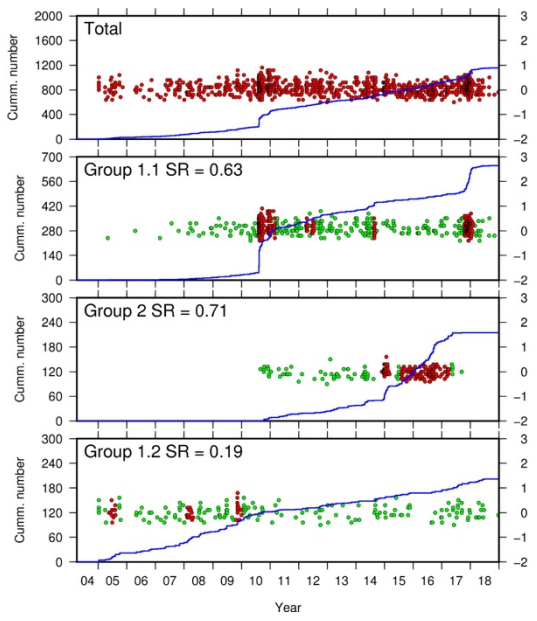
Total
Group 1.1 SR = 0.63
Group 2 SR = 0.71
Group 1.2 SR = 0.19
Cumm. number
Year

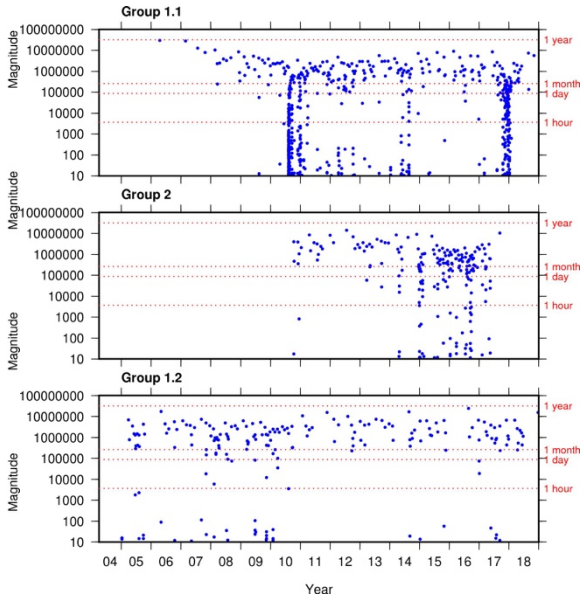
Group 1.1
Group 2
Group 1.2
Magnitude
1 year
1 month
1 day
1 hour
Year

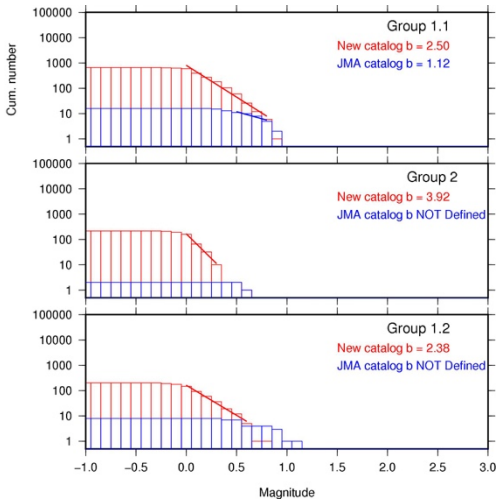
Group 1.1
New catalog b = 2.50
JMA catalog b = 1.12
Group 2
New catalog b = 3.92
JMA catalog b NOT Defined
Group 1.2
New catalog b = 2.38
JMA catalog b NOT Defined
Cum. number
Magnitude

10.1.49. Aso

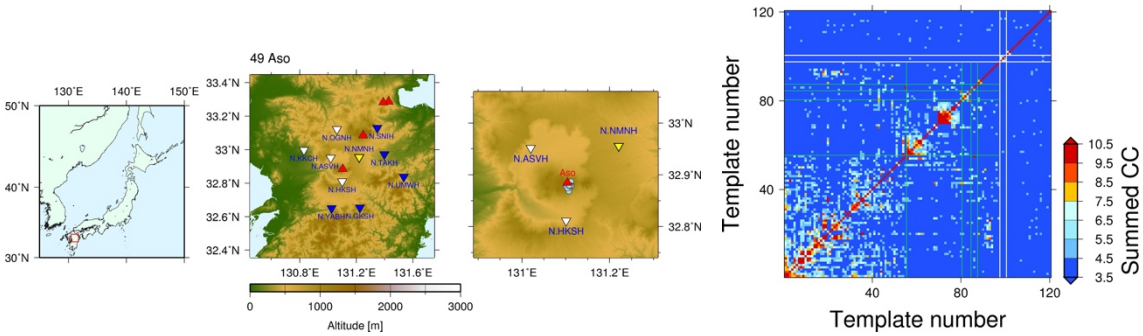
49 Aso
Altitude [m]
Template number
Summed CC

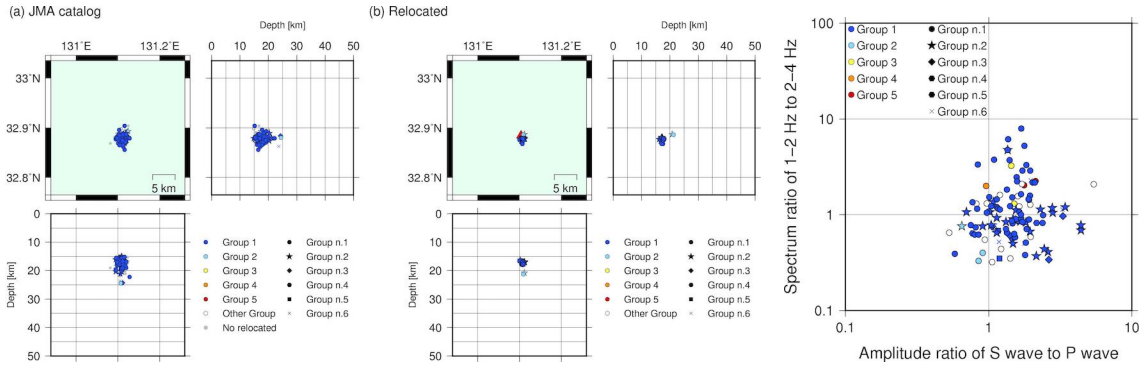
(a) JMA catalog
(b) Relocated
Depth [km]
Group 1
Group 2
Group 3
Group 4
Group 5
Other Group
No relocated
Group n.1
Group n.2
Group n.3
Group n.4
Group n.5
Group n.6
Spectrum ratio of 1–2 Hz to 2–4 Hz
Amplitude ratio of S wave to P wave

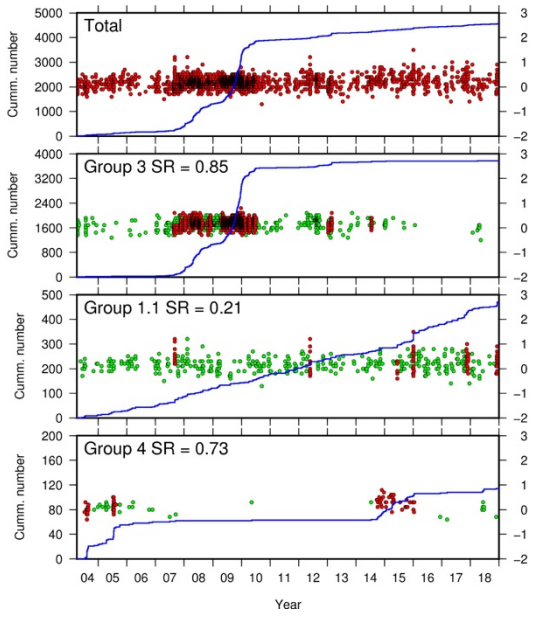
Total
Group 3 SR = 0.85
Group 1.1 SR = 0.21
Group 4 SR = 0.73
Cumm. number
Year

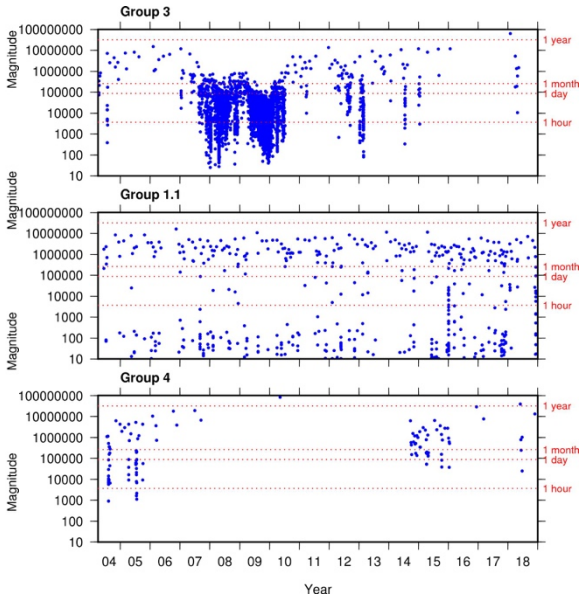
Group 3
Group 1.1
Group 4
Magnitude
1 year
1 month
1 day
1 hour
Year

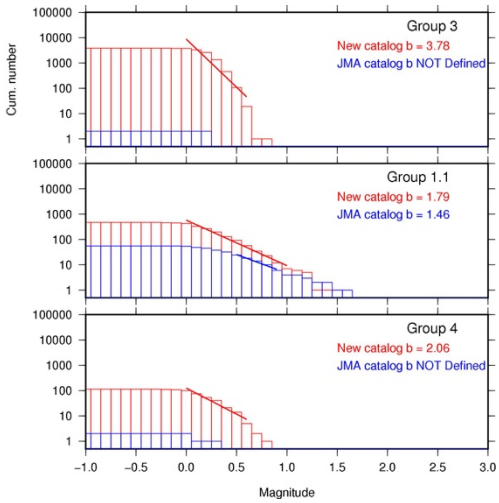
Group 3
New catalog b = 3.78
JMA catalog b NOT Defined
Group 1.1
New catalog b = 1.79
JMA catalog b = 1.46
Group 4
New catalog b = 2.06
JMA catalog b NOT Defined
Cum. number
Magnitude

10.1.50. Kirishima

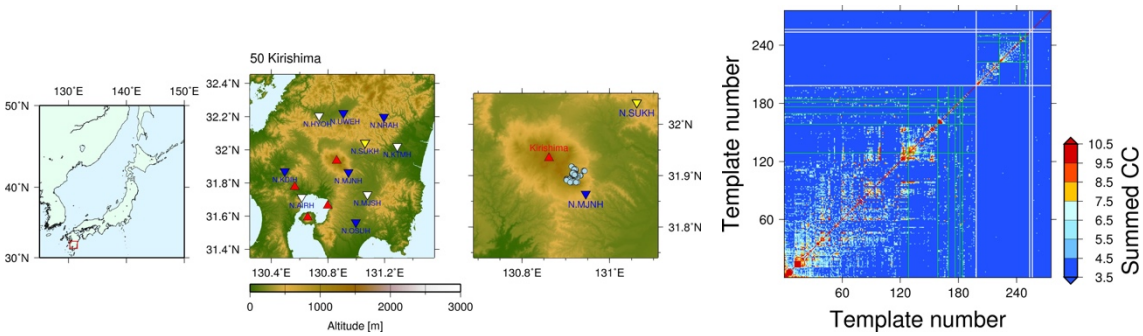

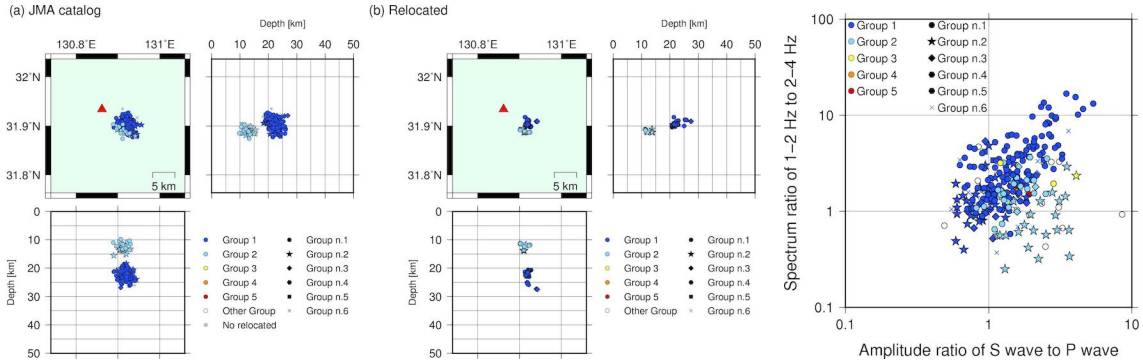

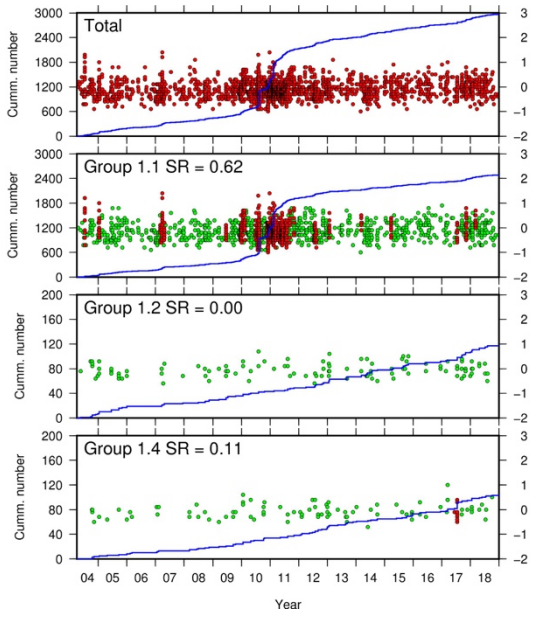

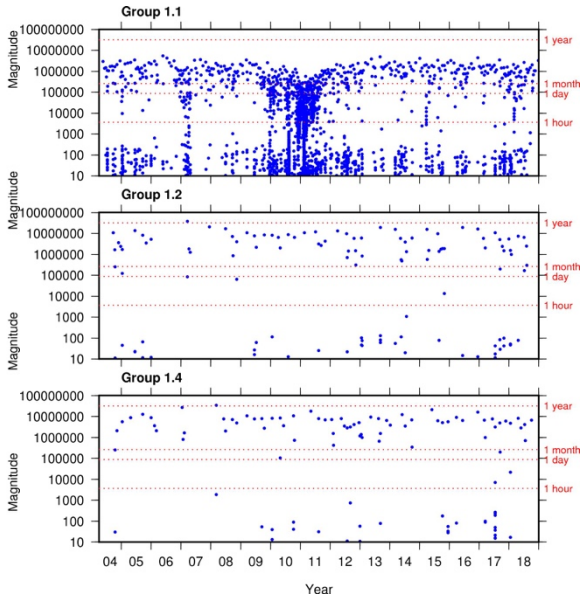

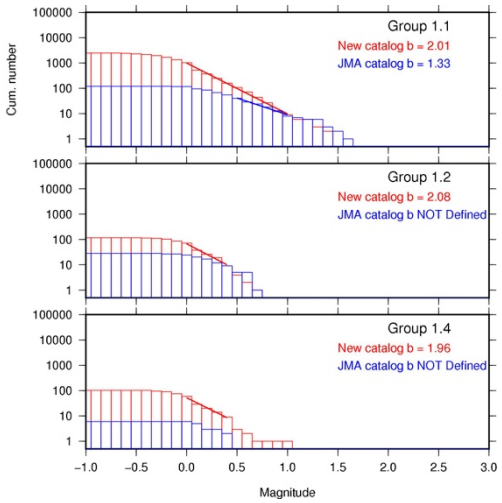

10.1.51. Sakurajima

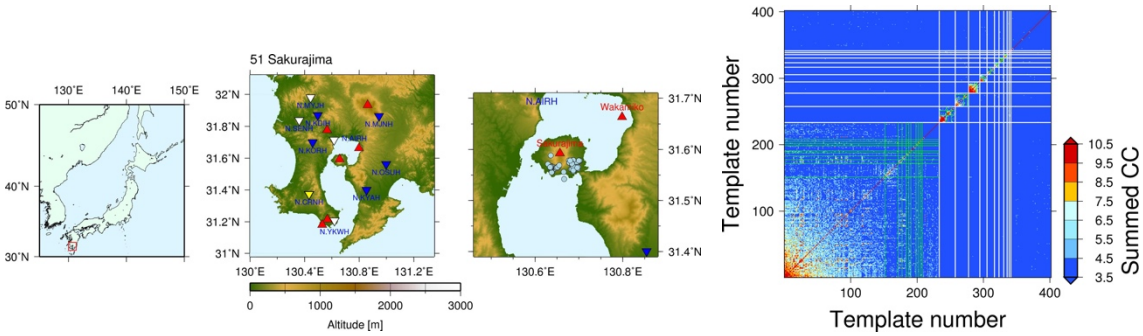

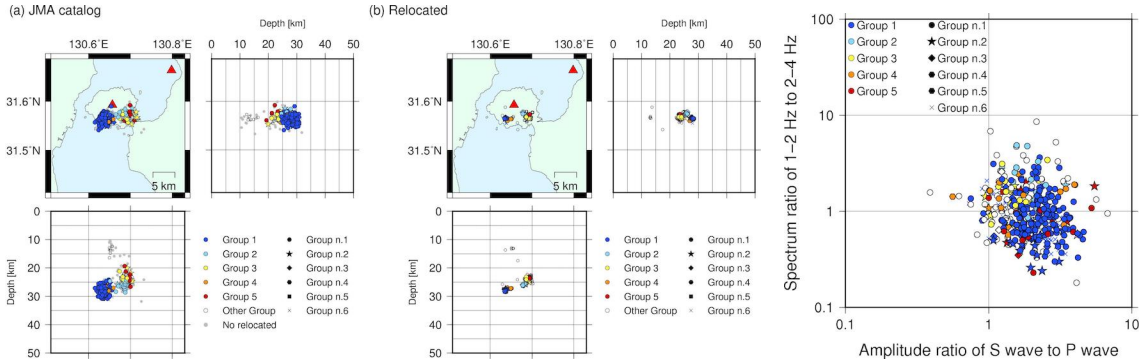

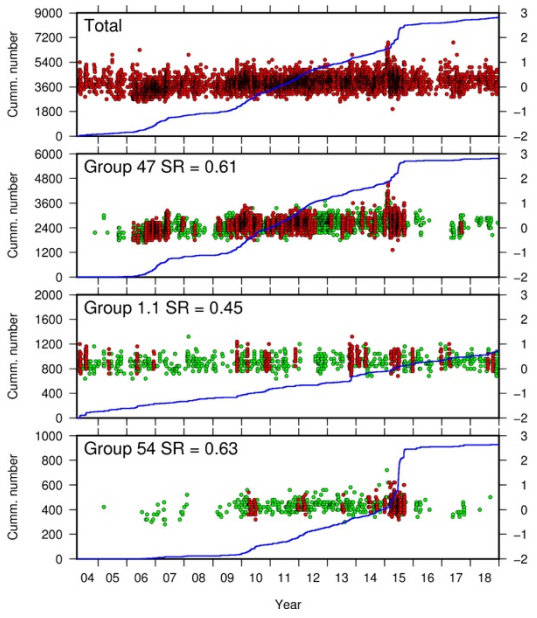

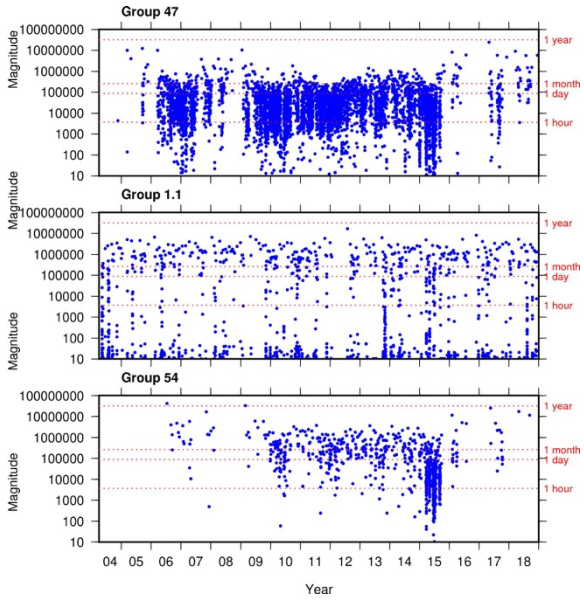

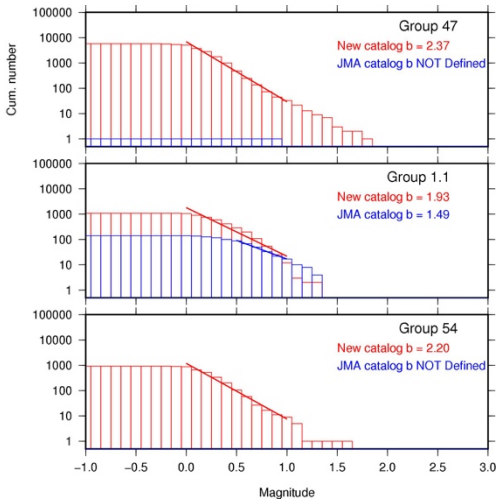

10.1.52. Kaimon

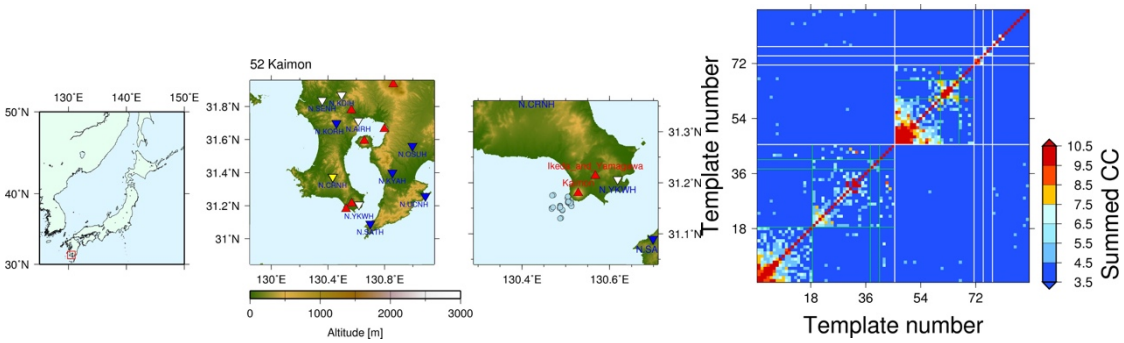

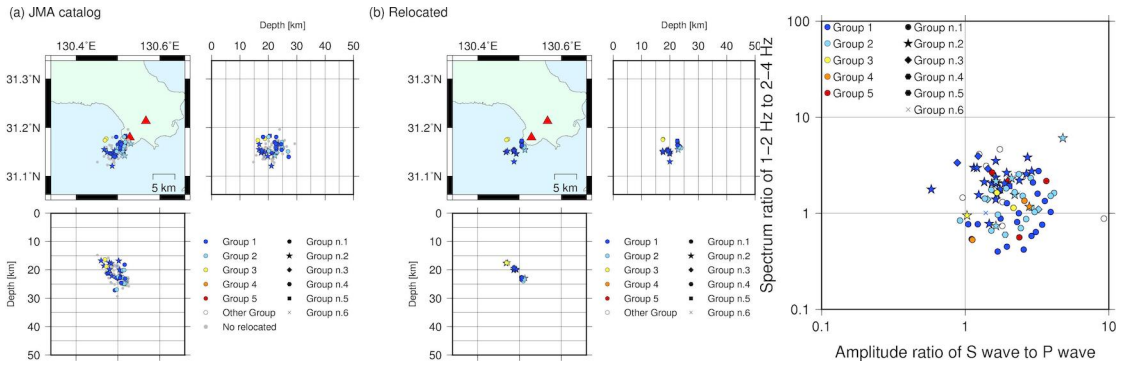

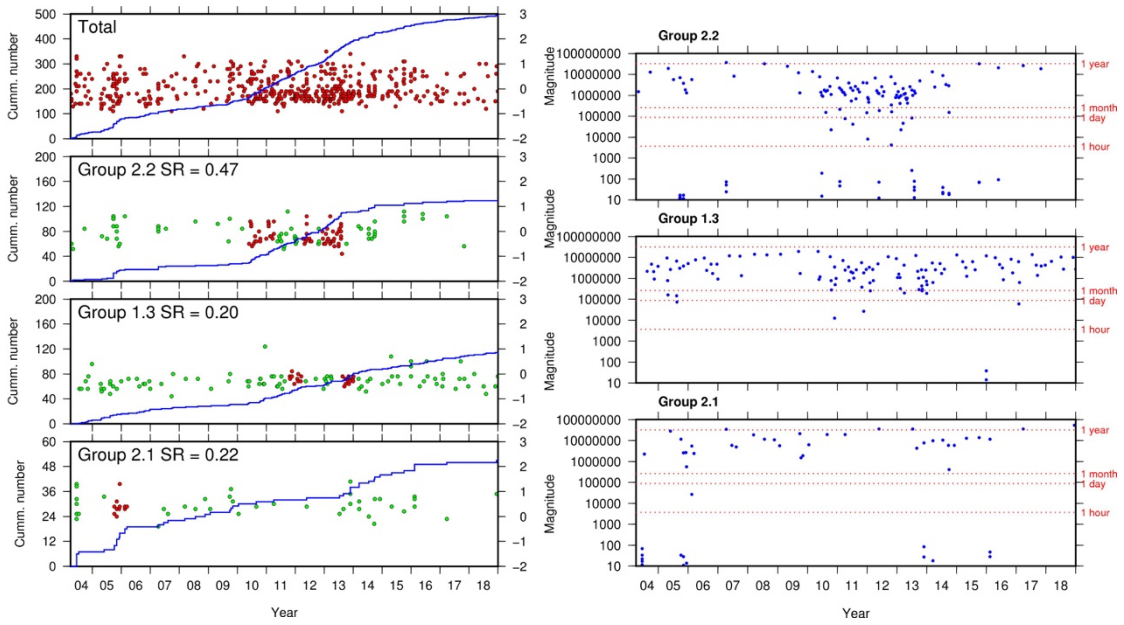

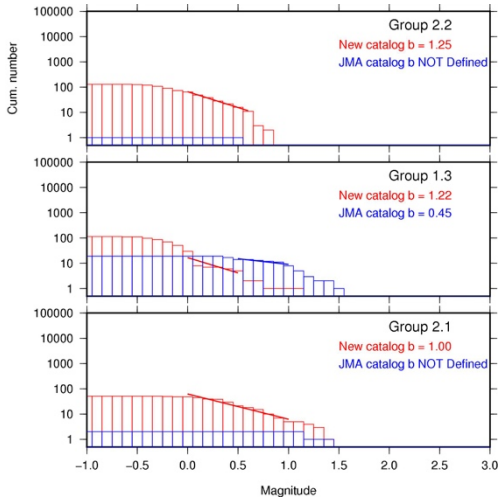

10.2. Jackknife test of network correlation coefficient method

In this section, in order to test the resolution of the results of network correlation coefficient (NCC) method, jackknife test was applied. I tried 10 samples in which a station was removed from 10 stations used for NCC method. Therefore, nine stations were used to relocate the hypocenters in each sample.

10.2.1. Jackknife test in Hijiori

In Chapter 3, the distribution of DLF earthquakes concentrated in some small clusters with depth interval of approximately 5 km was shown (Figure 10.1). In each sample of the jackknife test, the same characteristic distribution of DLF earthquakes was also seen (Figure 10.2). The error of the hypocenters of DLF earthquakes are mostly less than 1 km (Figure 10.3–Figure 10.6). Errors of Longitude and Latitude are mostly less than 0.005 degree and errors of depths are mostly less than 0.5 km.

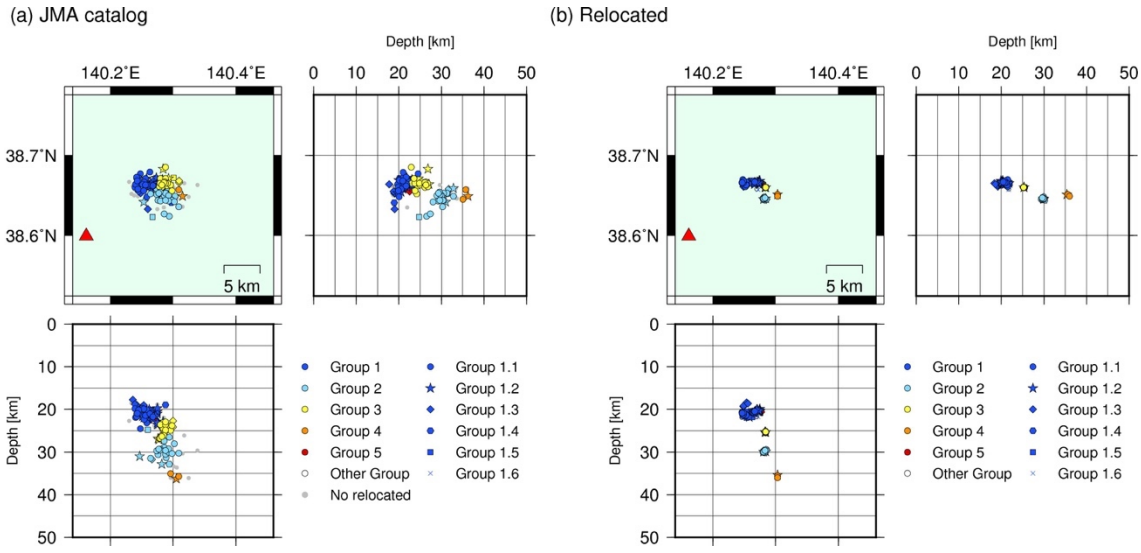

Figure 10.1 Same figure as Figure 3.1.

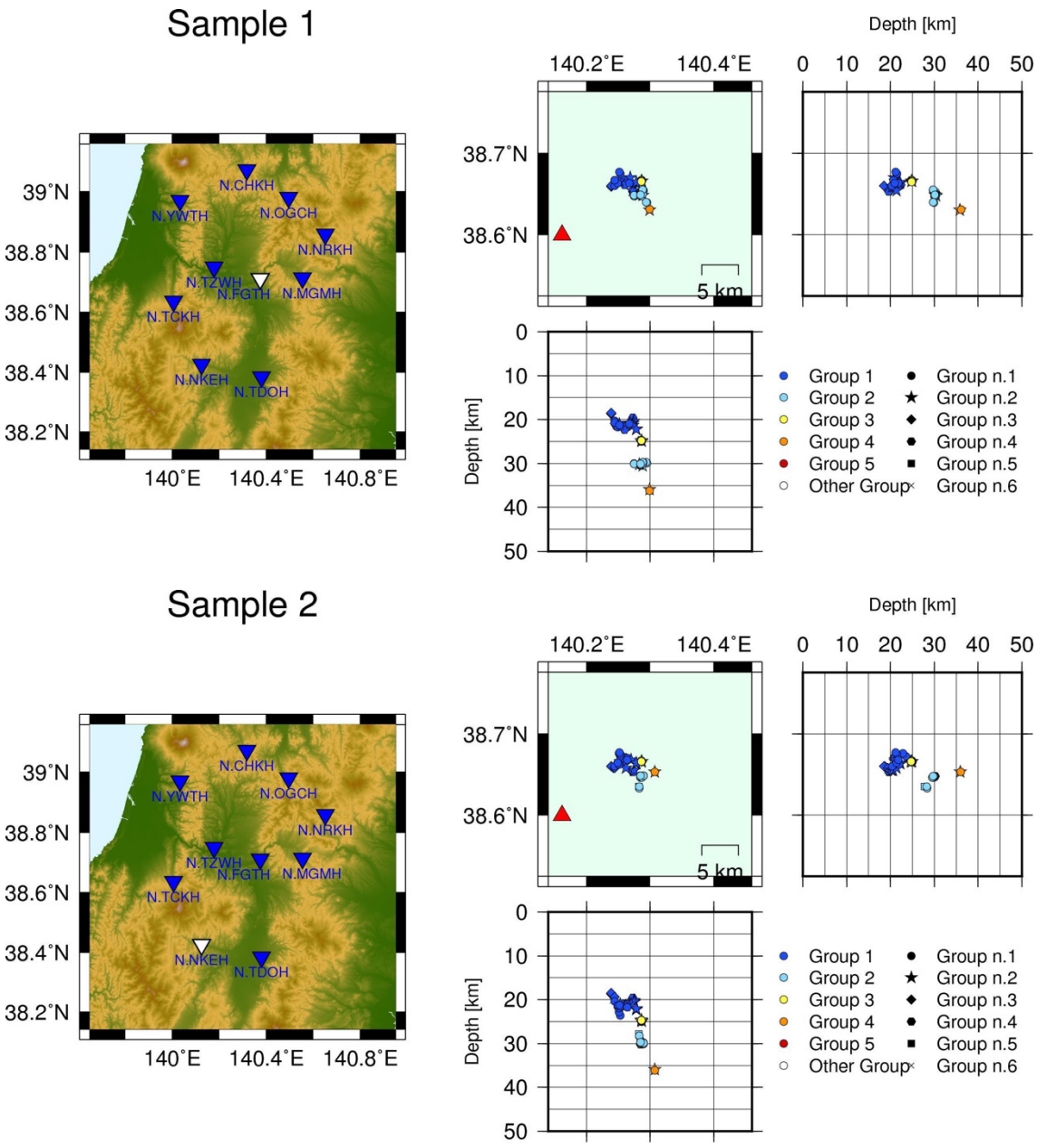

Figure 10.2 Results of jackknife test in Hijiori. Left figure shows the distribution of observation stations. Blue inverted triangles show the location of stations used for relocation and white triangle shows the location of a station removed from the test. Right figure shows the hypocentral distributions.

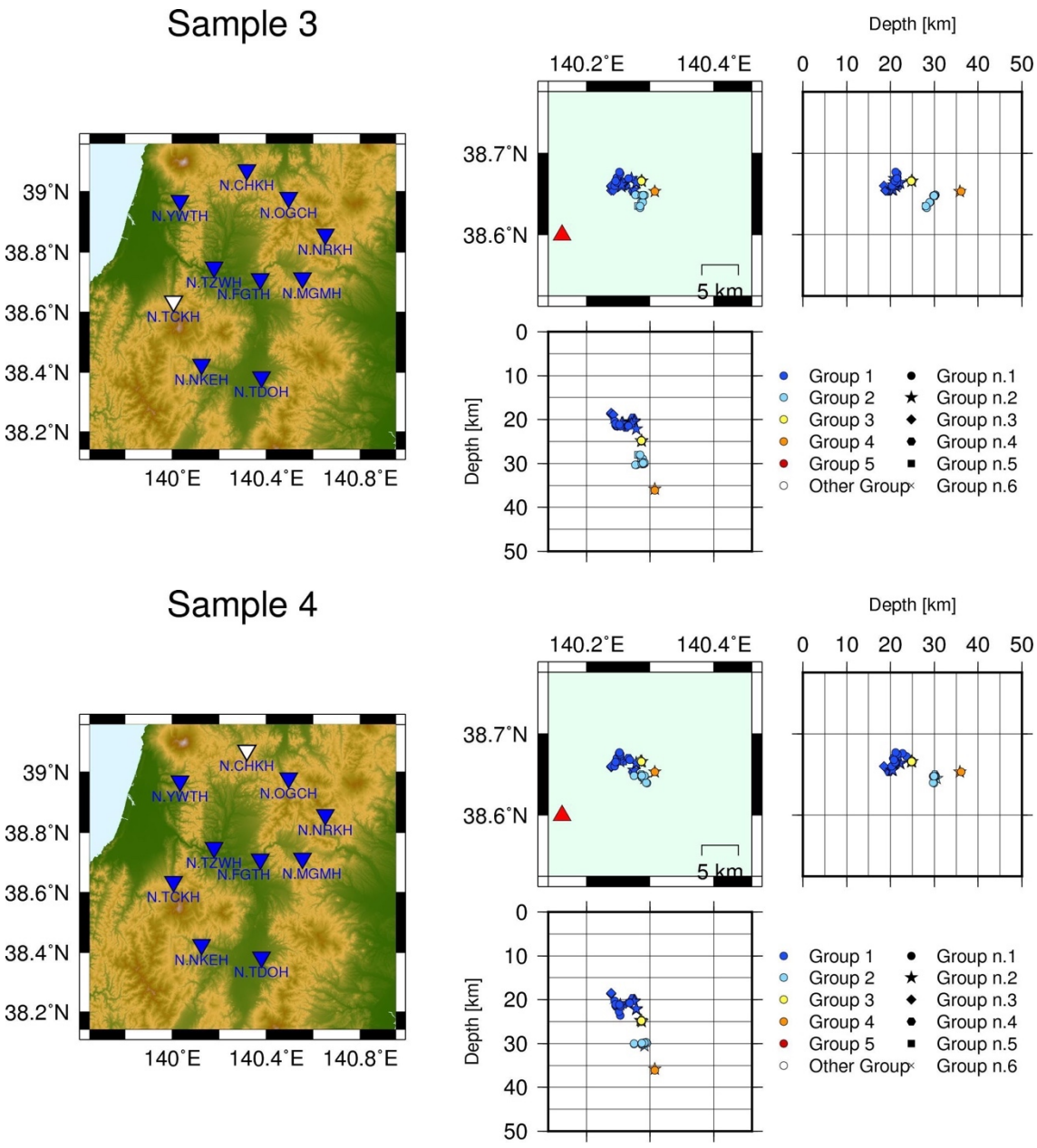

Figure 10.2 Continued.

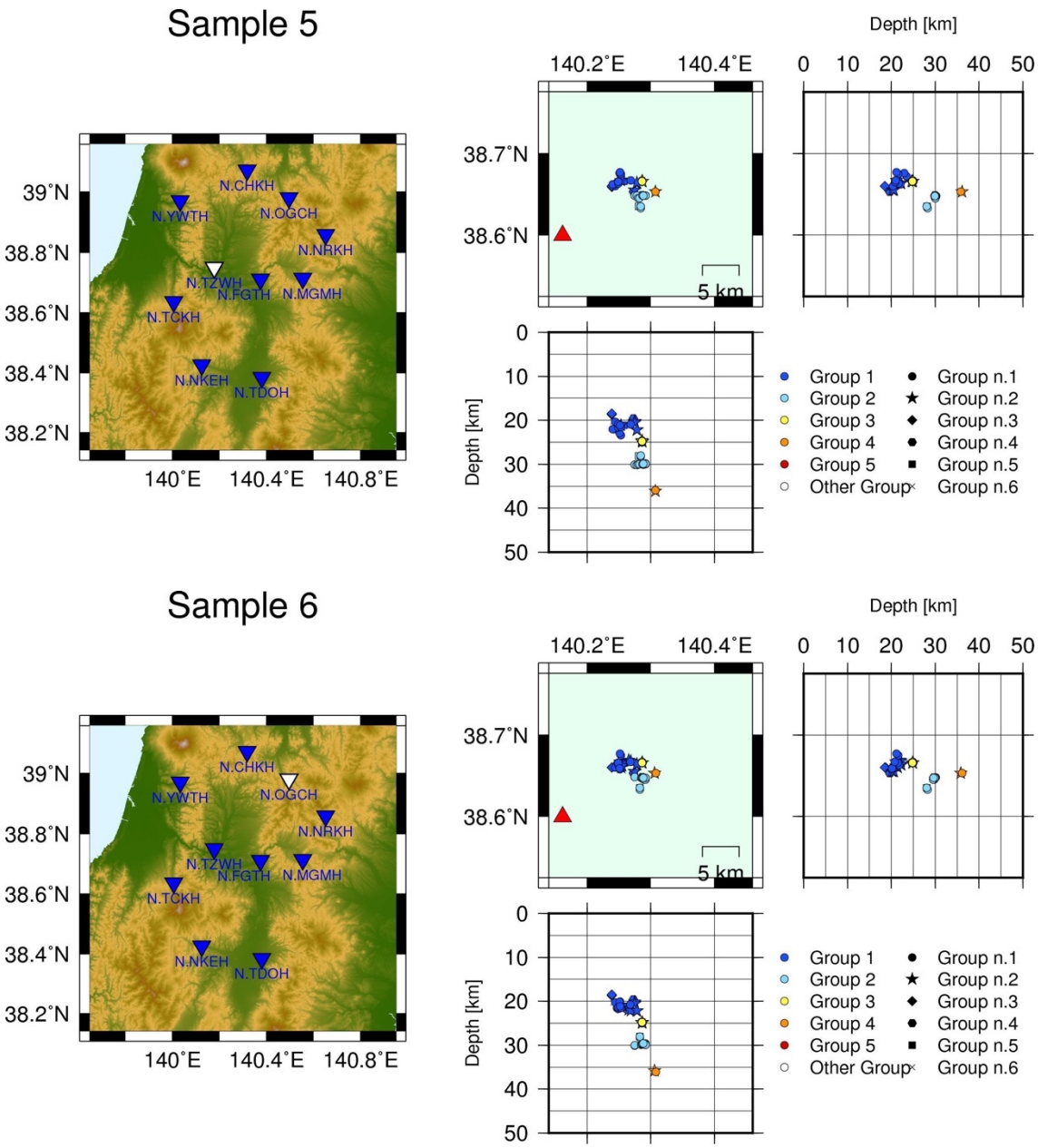

Figure 10.2 Continued.

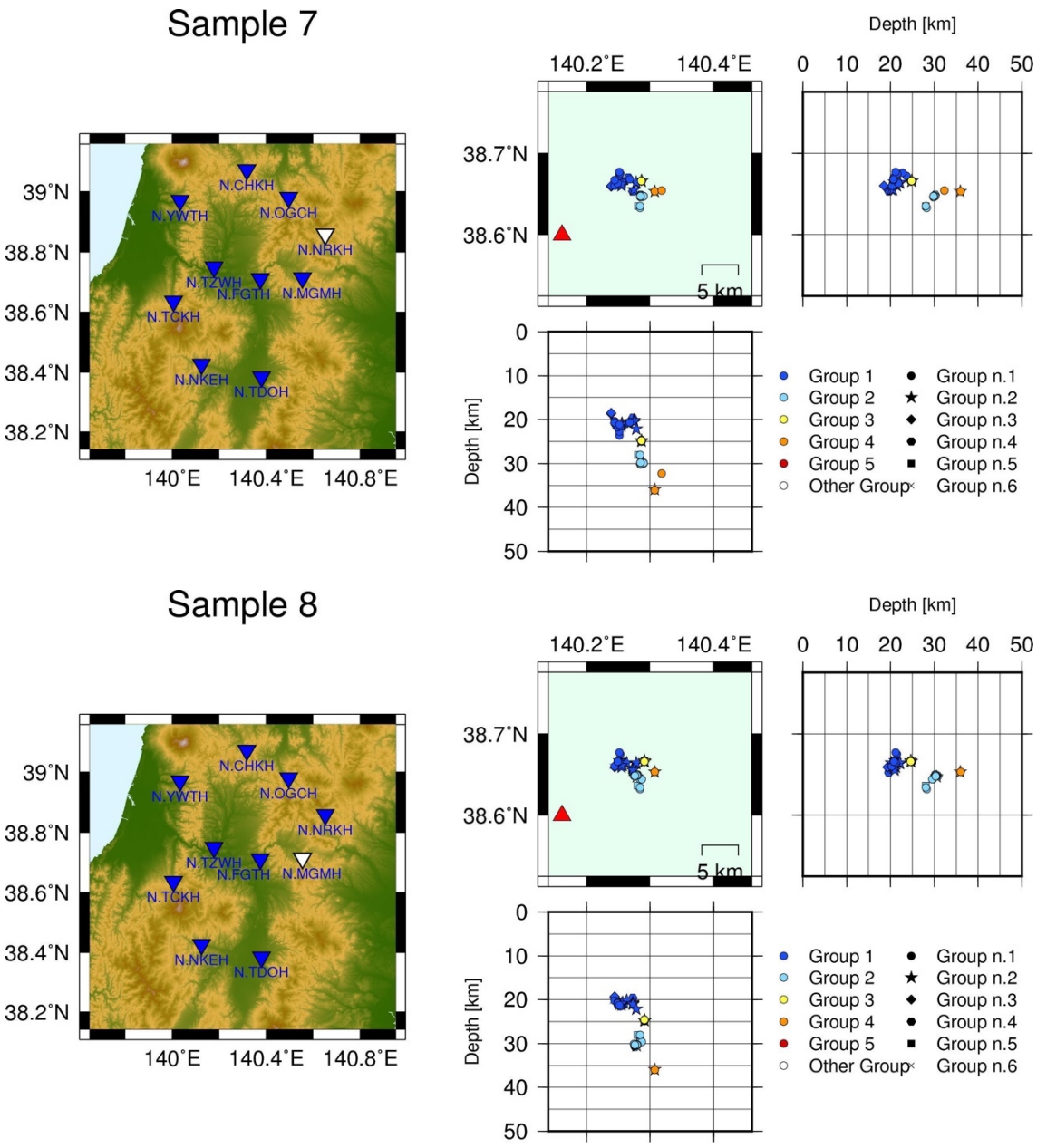

Figure 10.2 Continued.

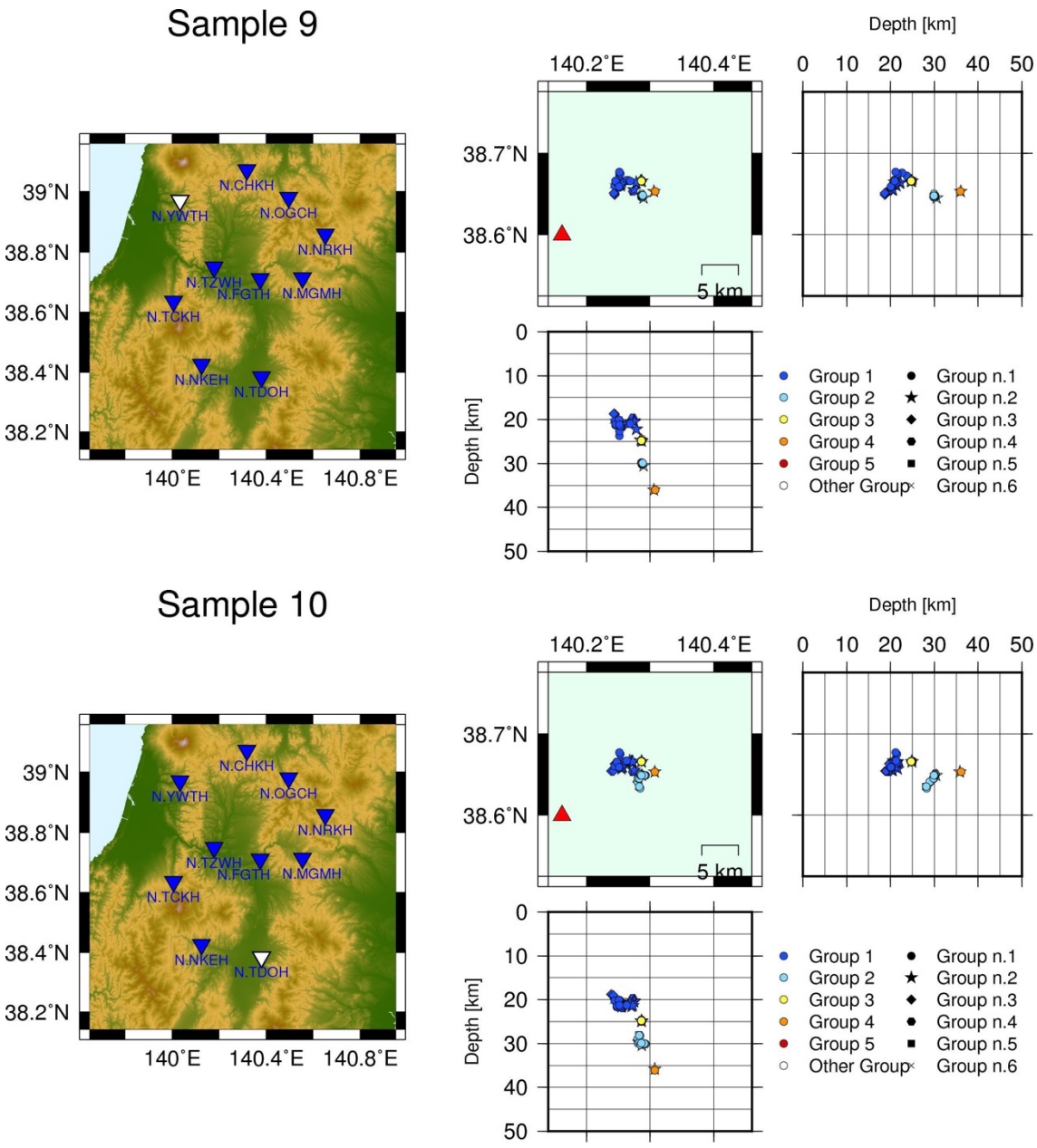

Figure 10.2 Continued.

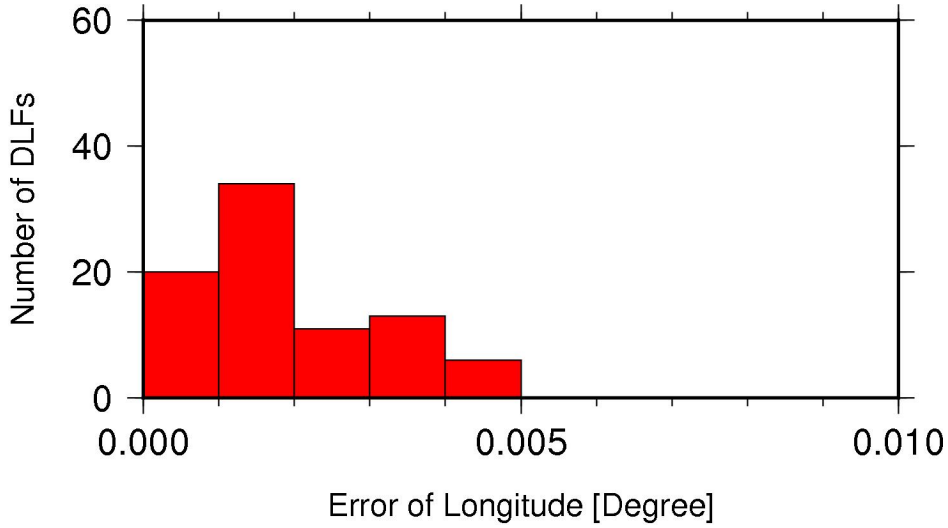

Figure 10.3 Error of Longitude of each DLF earthquake in jackknife test in Hijiori. DLF earthquakes which were relocated in more than three samples were used. Total number of the DLF earthquakes is 84.

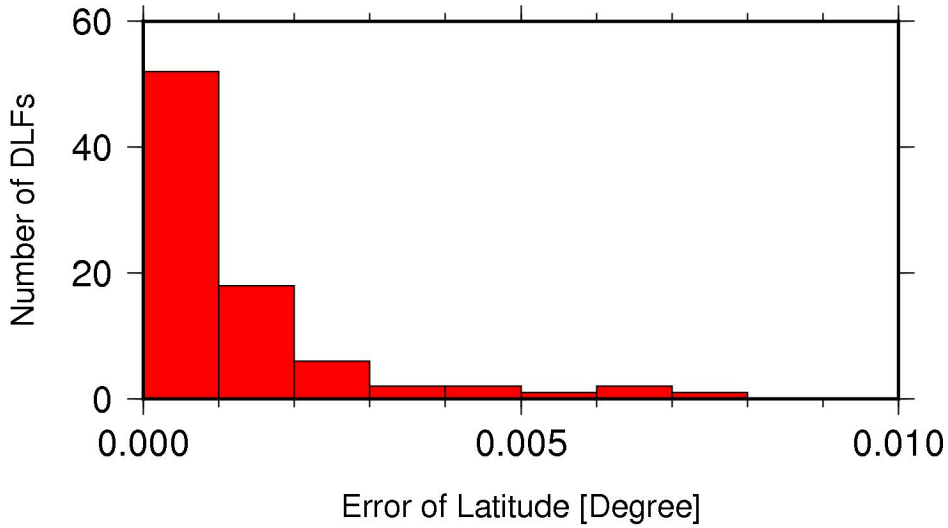

Figure 10.4 Error of Latitude of each DLF earthquake in jackknife test in Hijiori.

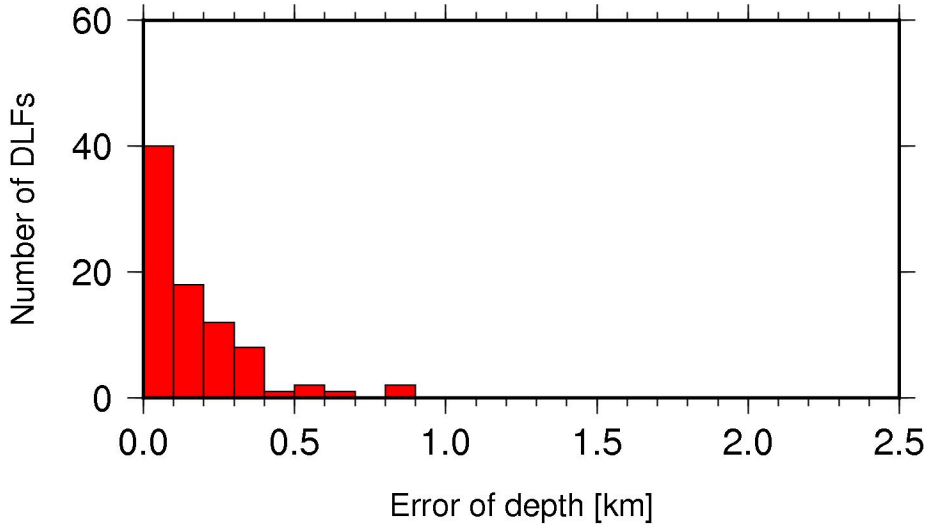

Figure 10.5 Error of depth of each DLF earthquake in jackknife test in Hijiori.

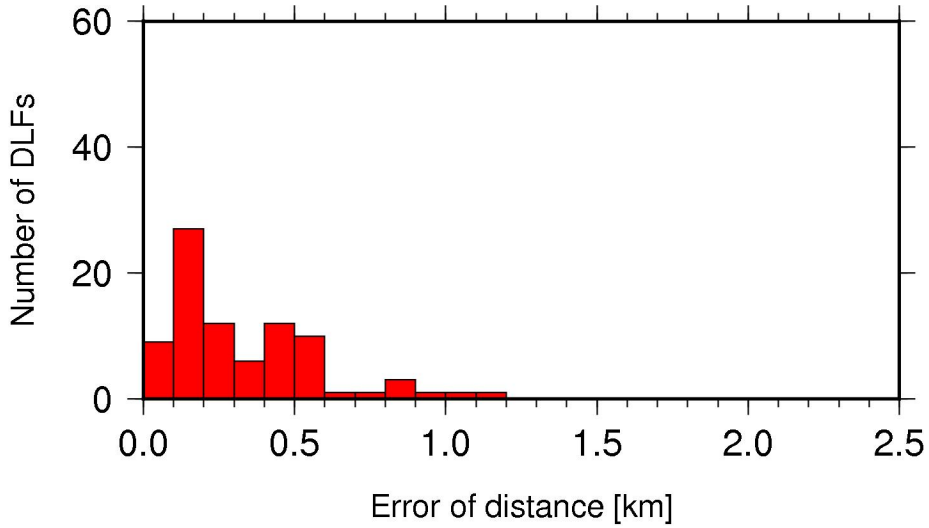

Figure 10.6 Error of three-dimensional distance of each DLF earthquake in jackknife test in Hijiori.

10.2.2. Jackknife test in Kirishima

In Chapter 4, type A2 DLF earthquakes were located at deeper than other type of DLF earthquakes. In Jackknife test, although the distribution of DLF earthquakes is slightly different, the characteristic that type A2 DLF earthquakes are deeper than other type of DLF earthquakes is confirmed (Figure 10.8). The errors of the hypocenters of DLF earthquakes are mostly less than 1 km (Figure 10.9–Figure 10.12). Errors of Longitude and Latitude are mostly less than 0.005 degree and errors of depths are mostly less than 1 km.

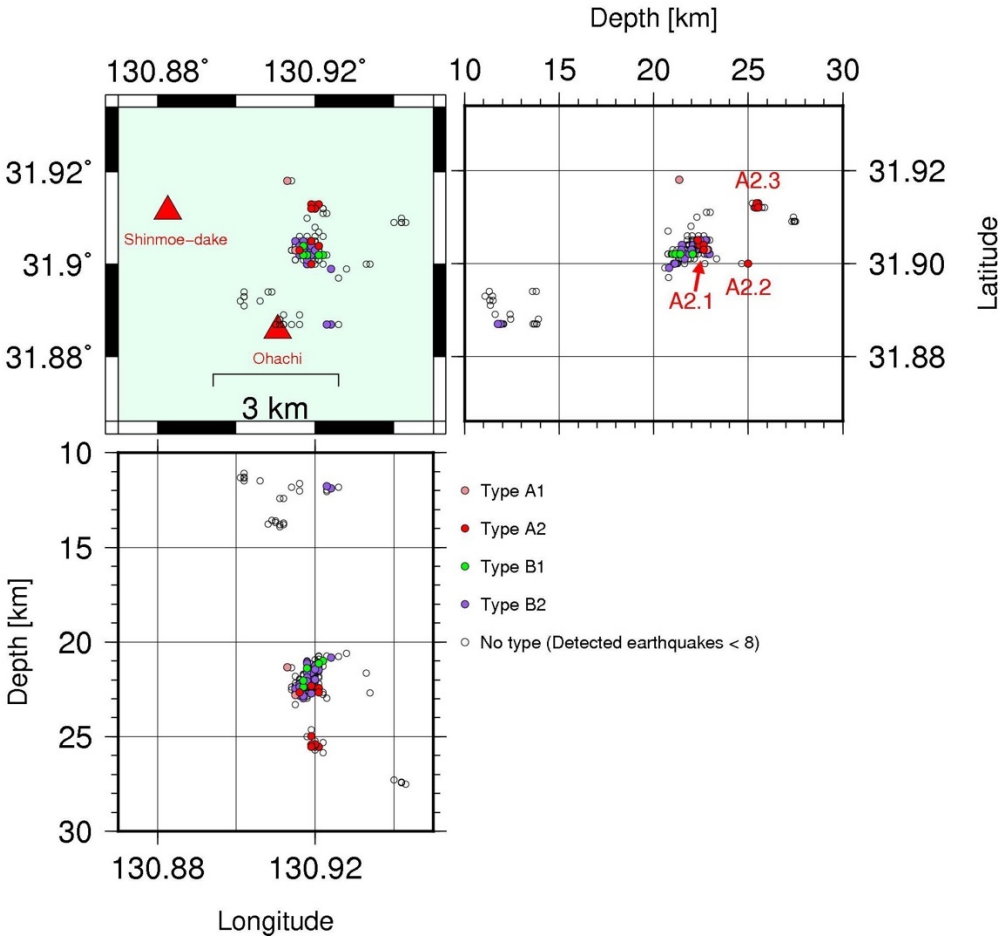

Figure 10.7 Same figure as Figure 4.10.

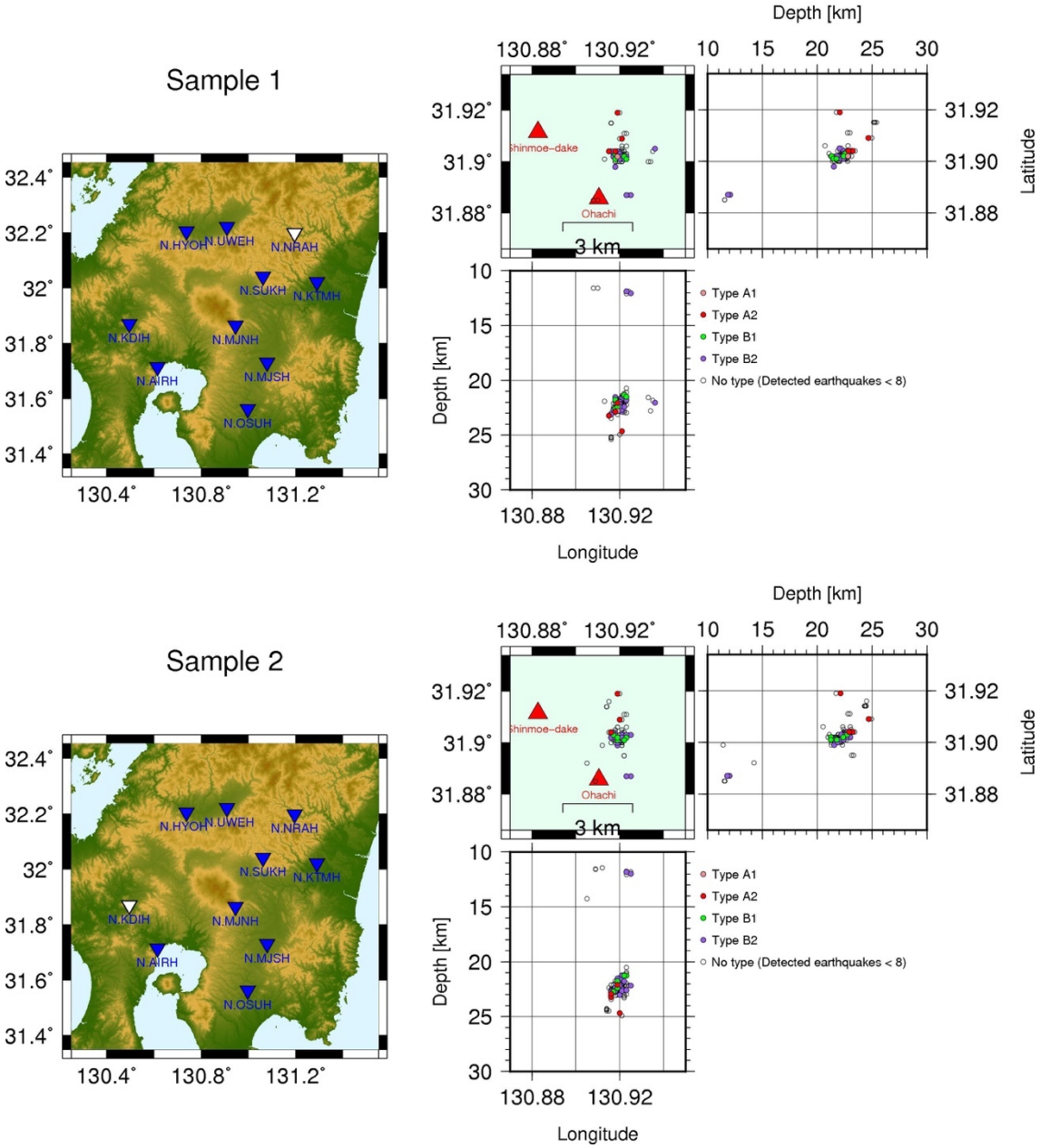

Figure 10.8 Results of jackknife test in Kirishima. Left figure is same as left figure of Figure 10.2 but in Kirishima. Right figure shows the hypocentral distribution of each type DLF earthquakes (see Chapter 4).

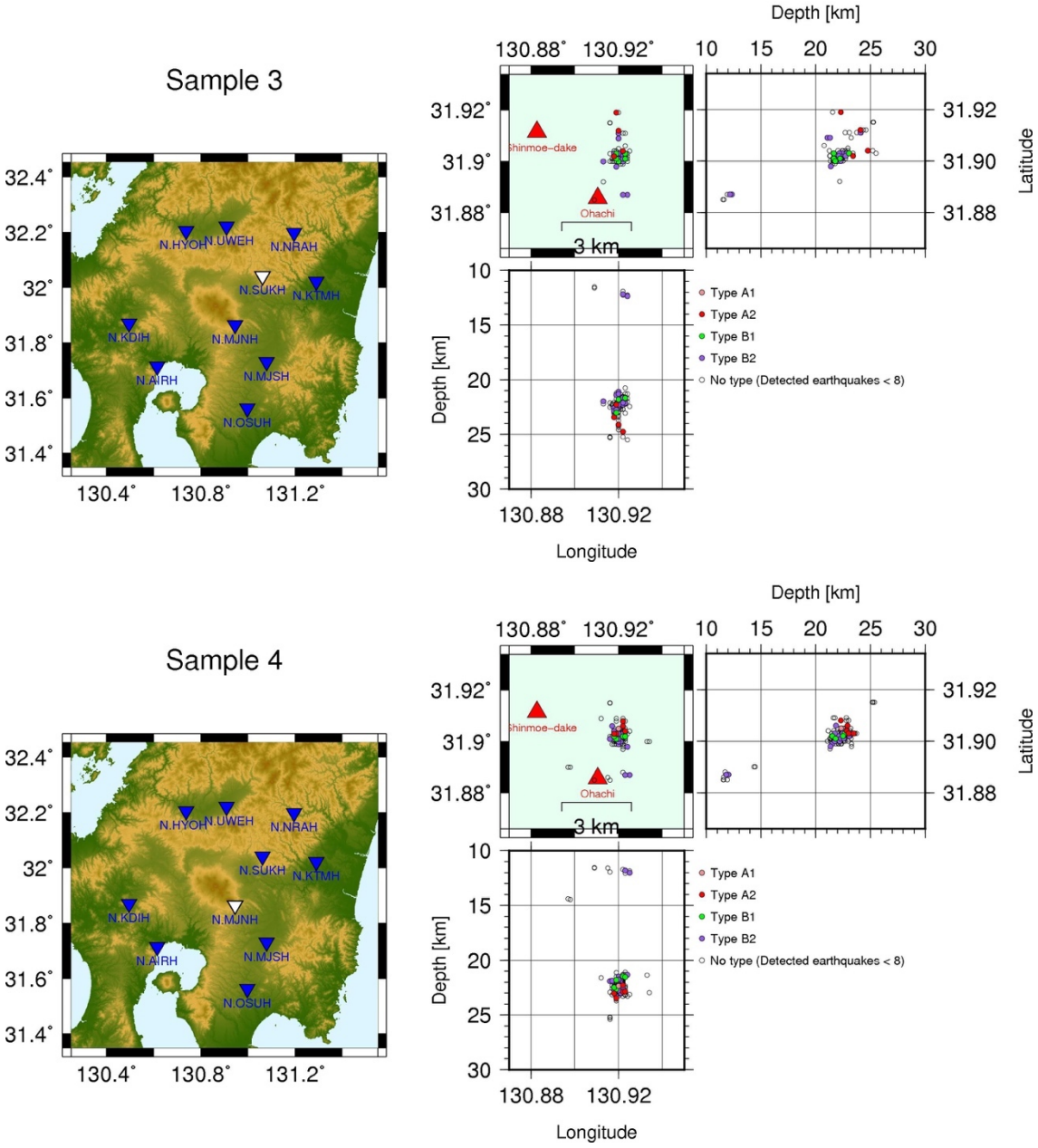

Figure 10.8 continued.

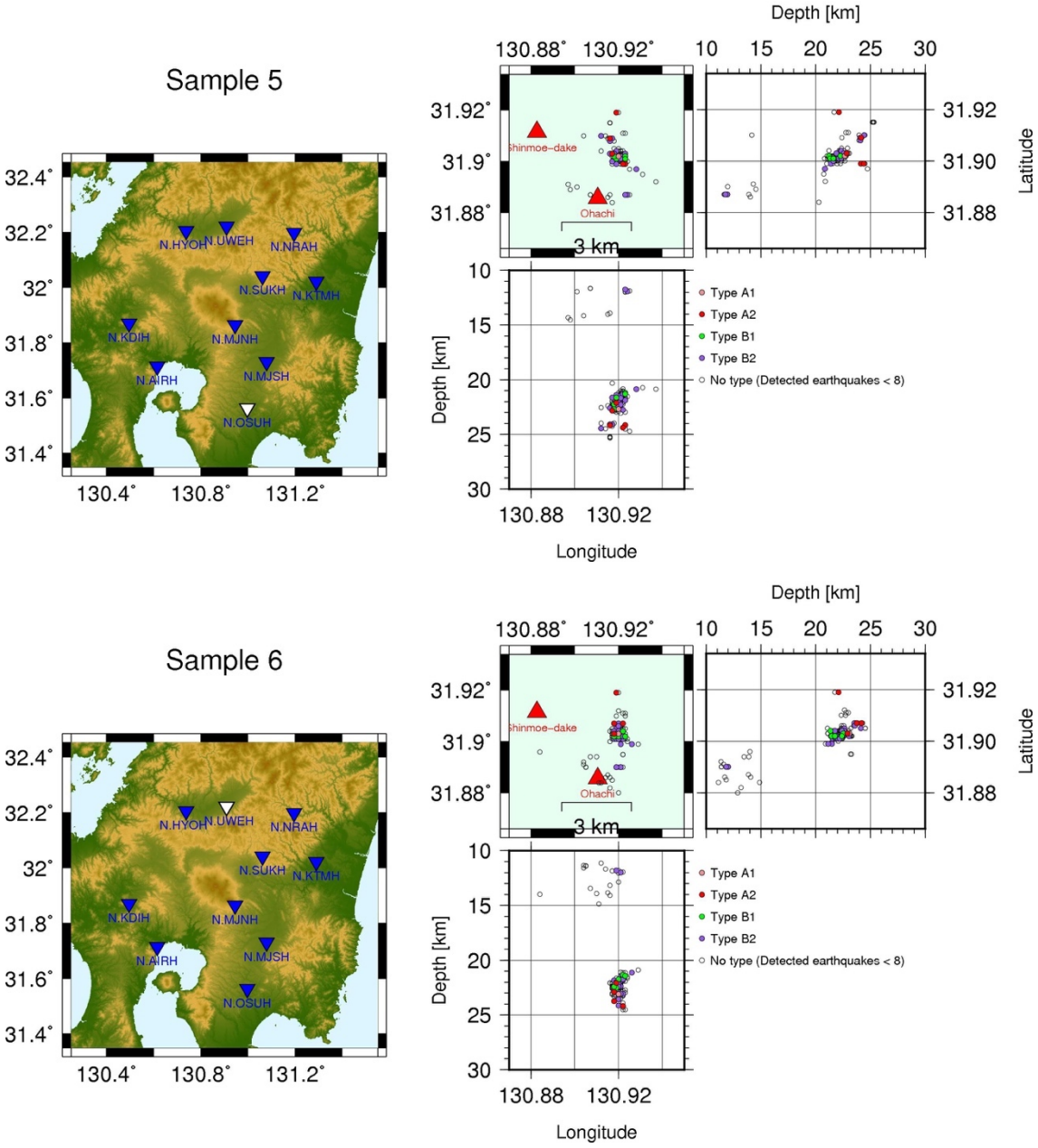

Figure 10.8 continued.

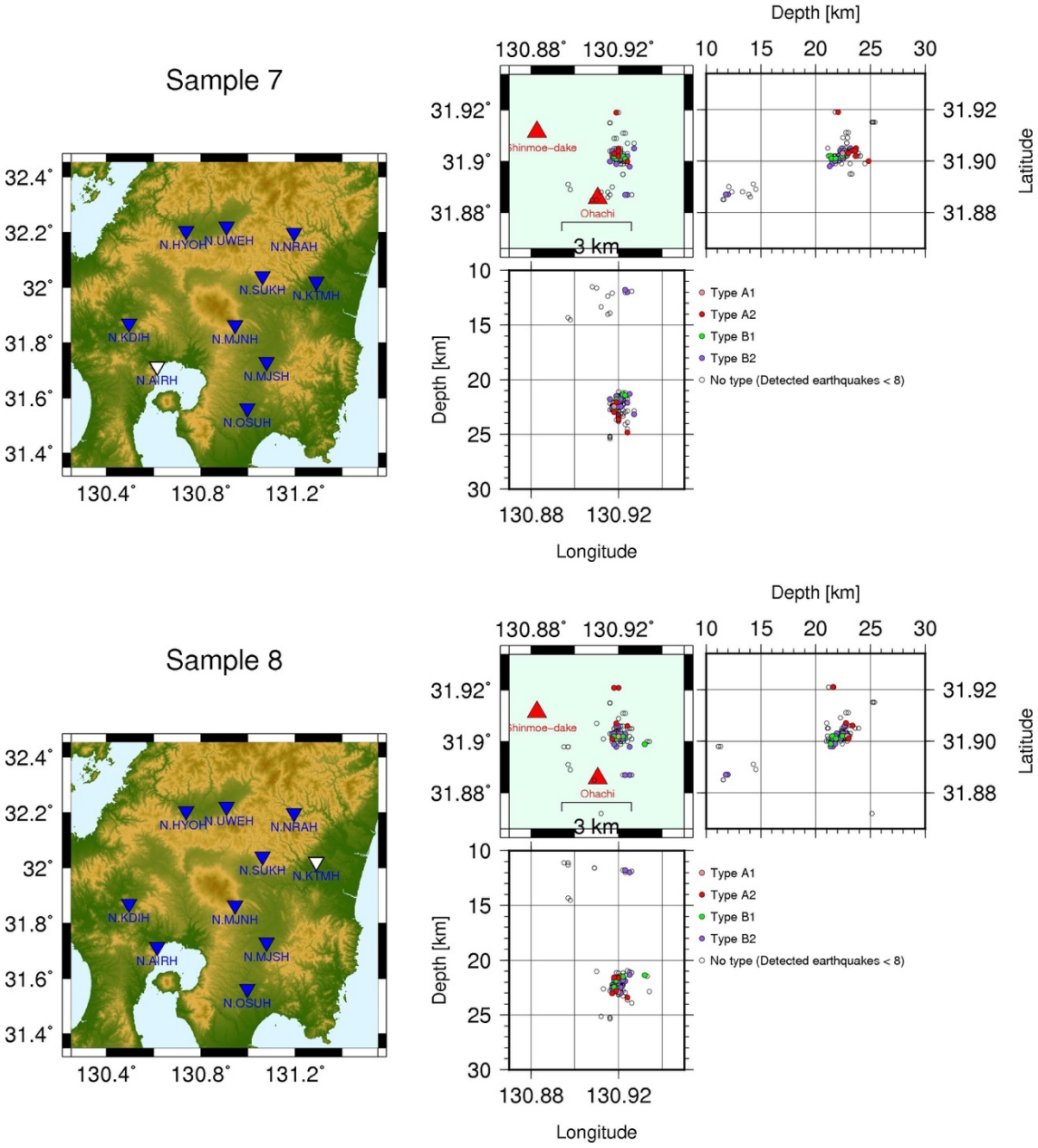

Figure 10.8 continued.

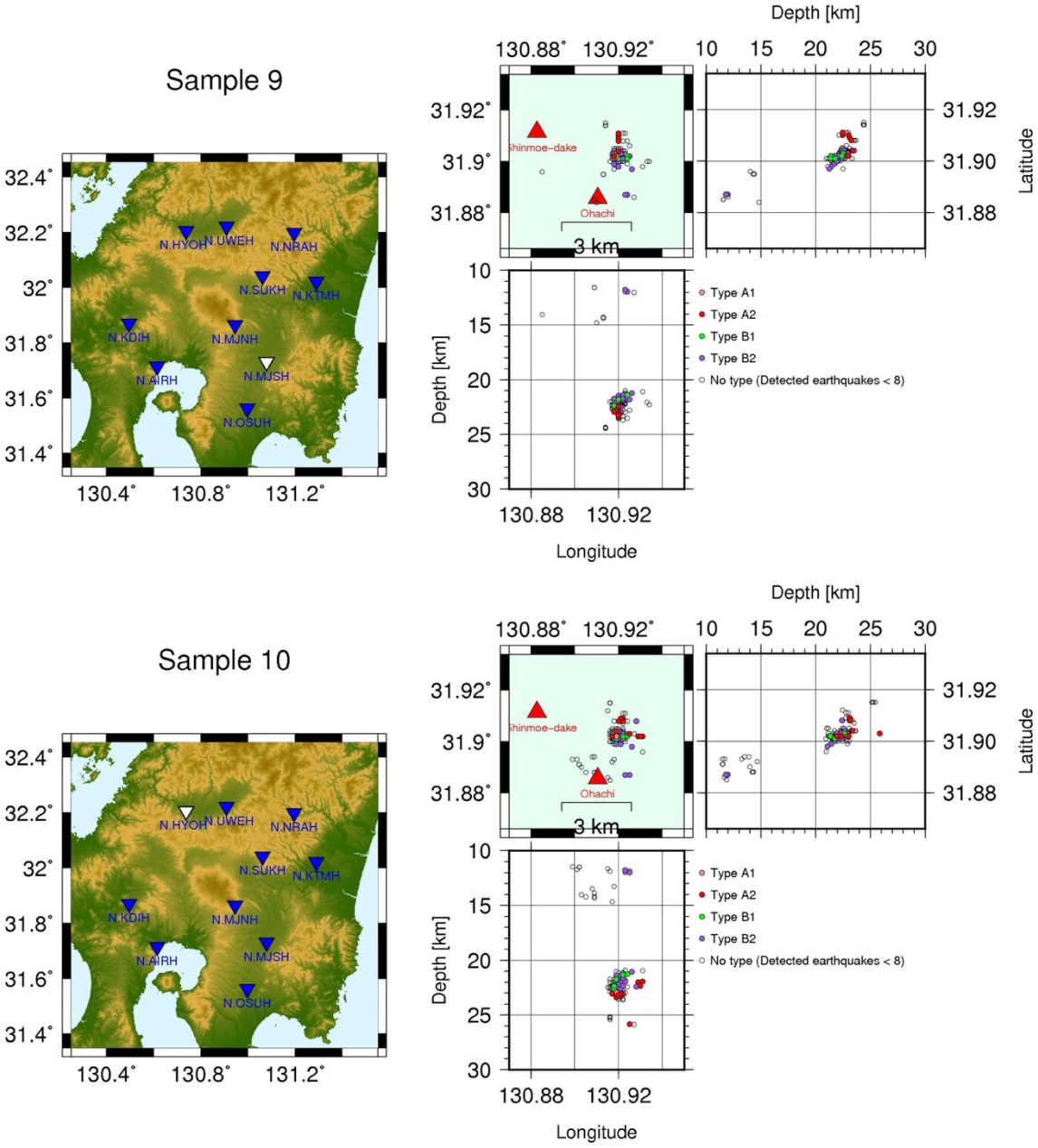

Figure 10.8 continued.

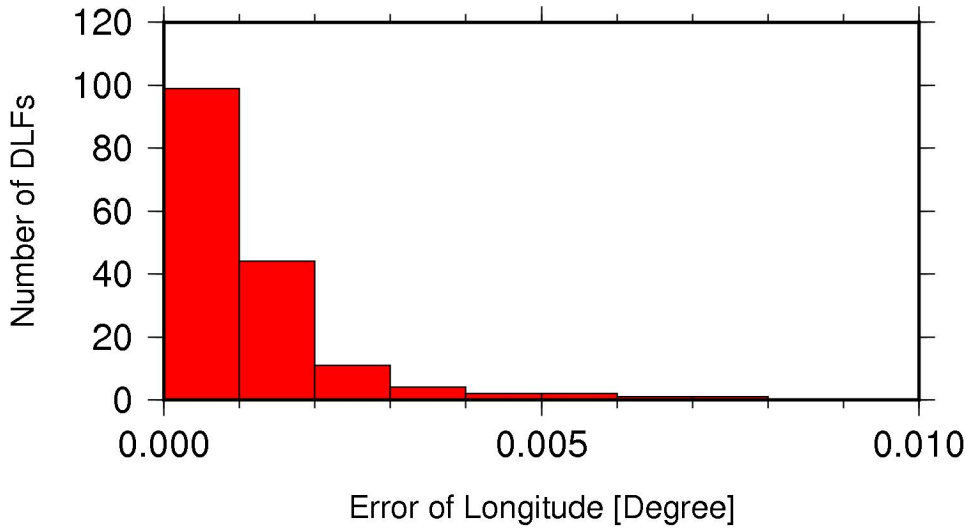

Figure 10.9 Error of Longitude of each DLF earthquake in jackknife test in Kirishima. DLF earthquakes which were relocated more than three samples were used. Total number of the DLF earthquakes is 164.

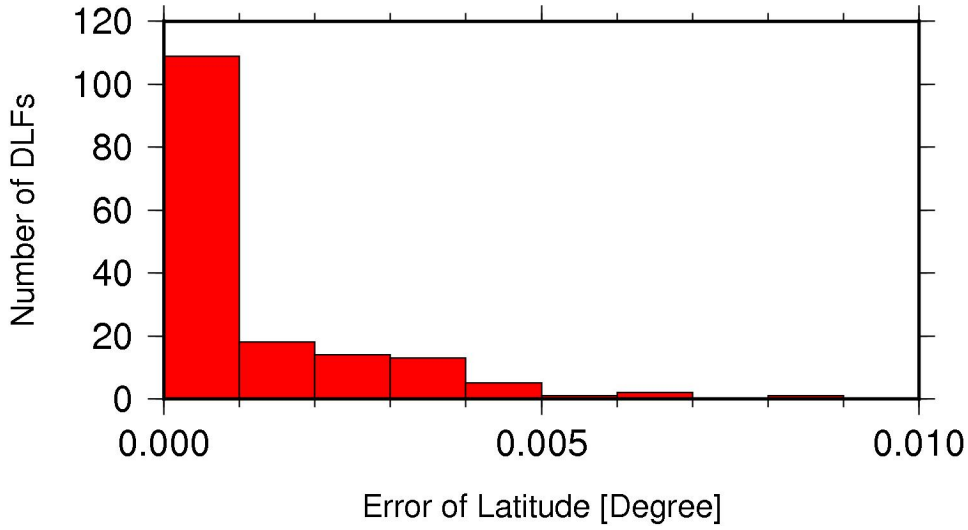

Figure 10.10 Error of Latitude of each DLF earthquake in jackknife test in Kirishima.

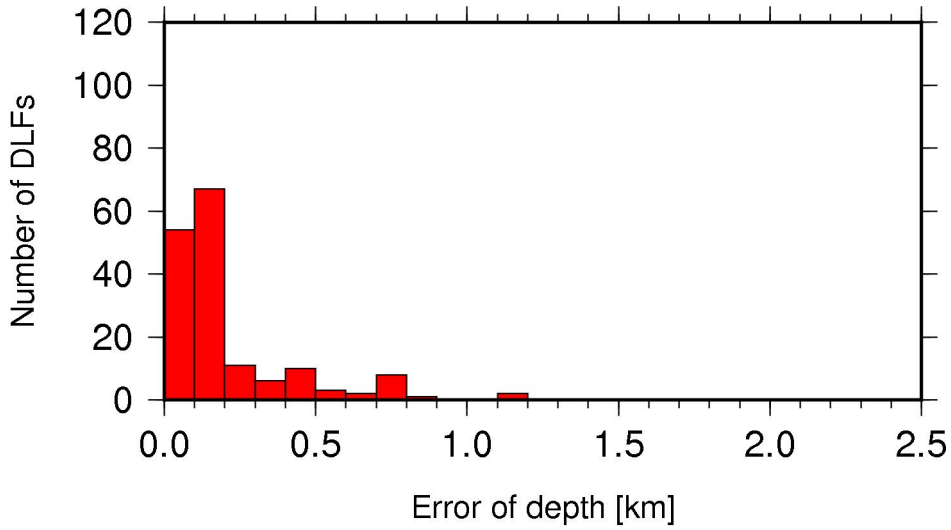

Figure 10.11 Error of depth of each DLF earthquake in jackknife test in Kirishima.

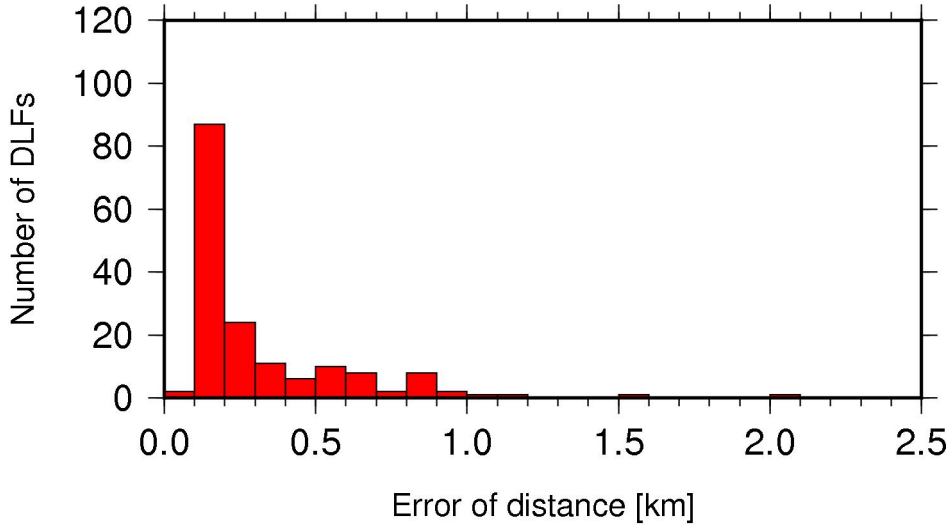

Figure 10.12 Error of three-dimensional distance of each DLF earthquake in jackknife test in Kirishima.

10.3. Verification of detection based on matched filter technique

In this study, I detected DLF earthquakes based on matched filter technique. In Chapter 2, I used 5-seconds time-window to calculate correlation coefficient using equation (2.8).

$$\mathrm{Summed\_CC}(t)=\sum_{i,j}\frac{\sum_{\tau=-2.5\mathrm{s}}^{\tau=2.5s}u_{i,j}\left(t+t_1(i,j)+\tau\right)v_{i,j}\left(t_1(i,j)+\tau\right)}{\sqrt{\left(\sum_{\tau=-2.5\mathrm{s}}^{\tau=2.5s}{u_{i,j}}^2\left(t+t_1(i,j)+\tau\right)\right)\left(\sum_{\tau=-2.5\mathrm{s}}^{\tau=2.5s}{v_{i,j}}^2\left(t_1(i,j)+\tau\right)\right)}} \quad \cdots (2.8)$$

In Chapter 4 and 5, some DLF earthquakes have long duration. For example, type A2 DLF earthquakes in Kirishima volcano has low dominant frequency and long duration. Then, I tried to detect using 10-seconds time-window based on equation (10.1) in Kirishima between 2010 and 2011.

$$\mathrm{Summed\_CC}(t)=\sum_{i,j}\frac{\sum_{\tau=-2.5\mathrm{s}}^{\tau=7.5s}u_{i,j}\left(t+t_1(i,j)+\tau\right)v_{i,j}\left(t_1(i,j)+\tau\right)}{\sqrt{\left(\sum_{\tau=-2.5\mathrm{s}}^{\tau=7.5s}{u_{i,j}}^2\left(t+t_1(i,j)+\tau\right)\right)\left(\sum_{\tau=-2.5\mathrm{s}}^{\tau=7.5s}{v_{i,j}}^2\left(t_1(i,j)+\tau\right)\right)}} \quad \cdots (10.1)$$

The result of detection is almost same as original result (Figure 10.13). Therefore, length of time-window in matched filter technique may not affect the results so much. However, in December 2010, more DLF earthquakes were observed when the 10 seconds time-window was used. Many DLF earthquakes with long durations might occur in the period.

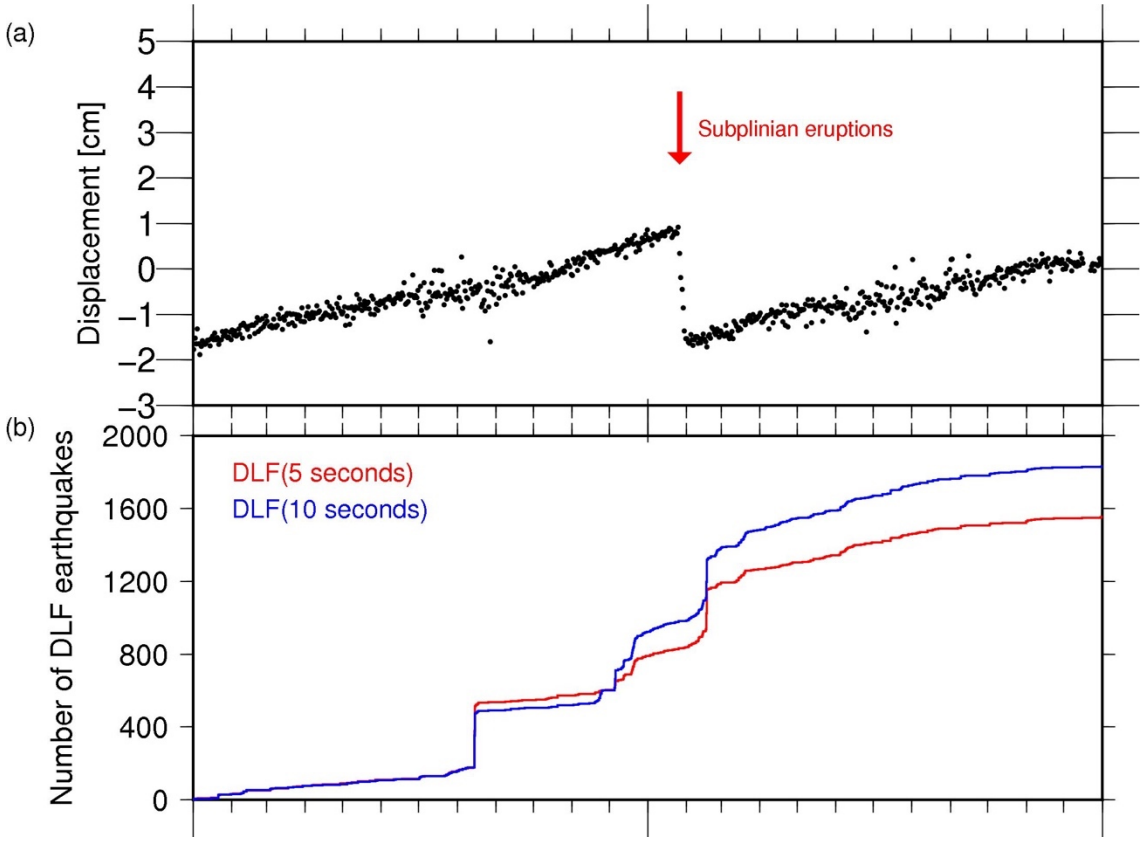

Figure 10.13 Comparison the results of detection using 5-seconds time window and 10-seconds time window.